

**INVESTIGATION ON ELEVATED
TEMPERATURE ADHESIVE WEAR
BEHAVIOR OF MICROWAVE FUSED
THERMAL SPRAY TRIBALLOY
COMPOSITE COATINGS**

Thesis

Submitted in partial fulfillment of the requirements for the degree of

DOCTOR OF PHILOSOPHY

by

DURGA PRASAD C



**DEPARTMENT OF MECHANICAL ENGINEERING
NATIONAL INSTITUTE OF TECHNOLOGY KARNATAKA
SURATHKAL, MANGALORE – 575025
APRIL, 2019**

DECLARATION

I hereby declare that the Research Thesis entitled “**INVESTIGATION ON ELEVATED TEMPERATURE ADHESIVE WEAR BEHAVIOR OF MICROWAVE FUSED THERMAL SPRAY TRIBALLOY COMPOSITE COATINGS**” which is being submitted to the **National Institute of Technology Karnataka, Surathkal** in partial fulfillment of the requirements for the award of the Degree of **Doctor of Philosophy in Mechanical Engineering** is a *bonafide report of the research work carried out by me*. The material contained in this Research Thesis has not been submitted to any other Universities or Institutes for the award of any degree.

Register Number : **165049ME16F03**

Name of the Research Scholar : **DURGA PRASAD C**

Signature of the Research Scholar:

Department of Mechanical Engineering

Place: NITK-Surathkal

Date:

CERTIFICATE

This is to certify that the Research Thesis entitled “**INVESTIGATION ON ELEVATED TEMPERATURE ADHESIVE WEAR BEHAVIOR OF MICROWAVE FUSED THERMAL SPRAY TRIBALLOY COMPOSITE COATINGS**” submitted by **Mr. DURGA PRASAD C (Register Number: 165049ME16F03)** as the record of the research work carried out by him, *is accepted as the Research Thesis submission* in partial fulfillment of the requirements for the award of the Degree of **Doctor of Philosophy**.

Research Guides

Dr. SHARNAPPA JOLADARASHI

Assistant Professor

Department of Mechanical

Engineering, NITK, Surathkal

Dr. RAMESH M R

Associate Professor

Department of Mechanical

Engineering, NITK, Surathkal

Chairman-DRPC

Date:

ACKNOWLEDGEMENTS

The author has great privilege and pride to express my immense sense of gratitude to **Dr. Sharnappa Joladarashi**, Assistant Professor, and **Dr. Ramesh M R**, Associate Professor, Department of Mechanical Engineering, National Institute of Technology Karnataka, Surathkal for their valuable guidance, inspiration, unwavering moral support, constructive criticism, and painstaking efforts during the course of this work. They provide me much more than just an education.

I wish to record my deep sense of gratitude to **Prof. Shrikantha S Rao**, The Head, Department of Mechanical Engineering and all the faculty members, technical and administrative staffs of the Mechanical Engineering, National Institute of Technology Karnataka, Surathkal for their help, as and when needed.

I highly thankful to my Research Progress Assessment Committee members **Dr. Mohammad Rizwanur Rahman**, Dept. of Metallurgical and Materials Engineering and **Dr. Ranjith M**, Dept. of Mechanical Engineering, for their valuable inputs.

I wish to record my deep sense of gratitude to **Mr. Channabasappa B H**, Hognas, Private Limited, Belgium, for supplying of CoMoCSi (Tribaloy T400) powder. **Mr. Raghavendra K**, AUM Techno Spray, Private Limited, Bengaluru, for his support and interaction in High-velocity oxy-fuel (HVOF) and Flame spray facility. **Dr. Srinath M S**, Dept. of Industrial Production and Engineering, Malnad College of Engineering, Hassan, for his support and interaction in extending Microwave oven facility. I wish to register my sincere thanks to **High Tech Ceramics**, Chennai, India, for providing High Energy Ball Milling (HEBM) facility.

I wish to thank my seniors of Tribology Laboratory, Dr. Gajanan Anne, Dr. Mahantayya Mathapati, Mr. Nithin H S, Mr. Veeresh Nayak, for their constant help and encouragement during the entire process of this research work. Author also wishes to thank all friends especially to Mr. Rahul, Mr. Shashank M, Mr. Pradeep V Badiger, Mr. Bhaskar M, Mr. Harish Yadav, Mr. Sachin B, Mr. Anjan B, Mr. Brijesh, Mr. Srikumar Biradar, Mr. Syam Narayan, Mr. Vinay Varghese, Mr. Vijay Kumar, and all the research scholars of Dept. of Mechanical Engineering for their everlasting support.

Finally, I thank my parents **Sri Channabasavaiah** and **Smt Indira**, my brother **Bharath C**, and my wife **Swathi D S** for their inspiration and love that accompanies me all the time. A special note of thanks to all my relatives and well-wishers for their constant help, encouragement, and understanding.

(DURGA PRASAD C)

ABSTRACT

Metallic materials that operate under high speed, high temperature and harsh chemical environments are prone to wear and corrosion degradation. This leads to the failure of metallic components and results in huge economic loss to industries. The amorphous alloy or metallic glasses exhibit superior properties like high hardness, good wear, and corrosion resistance. Metallic glasses eliminate an ordered crystalline structure, hinders plastic deformation. The Co-based amorphous alloy is the best example of bulk metallic glassy structure alloy and presence of primary intermetallic laves phase's exhibits good mechanical as well as chemical properties. This is mostly employed as coatings because they are too brittle to be used in bulk form. Co-based metallic glass coating depositing on metallic materials could positively eliminate the failure of the working component caused by serious wear and erosion issues.

In the present study, CoMoCrSi superalloy powder (Tribaloy-T400) comprising of a primary intermetallic laves phase of Co-rich solid solution has shown better mechanical and tribological properties. Processing of CoMoCrSi feedstock powder is carried out through a high-energy ball milling (HEBM) technique to obtain a higher volume fraction of intermetallic laves phases. The hard phases of 30% Cr₃C₂, WC-CrC-Ni and WC-12Co are reinforced into milled CoMoCrSi feedstock. The four different feedstock powders CoMoCrSi, CoMoCrSi+30%Cr₃C₂, CoMoCrSi+30%WC-CrC-Ni and CoMoCrSi+30%WC-12Co are sprayed on pure titanium grade-15 substrate using High-Velocity-Oxy-Fuel (HVOF) and flame spray methods. The as-sprayed coatings are subjected to post heat treatment to refine their metallurgical and mechanical properties using microwave hybrid heating technique. Characterization of feedstock, as-sprayed and microwave fused coatings is done by using Scanning Electron Microscopy (SEM), Energy dispersive spectroscopy (EDS) and X-ray Diffraction (XRD). Porosity, surface roughness, microhardness, and adhesion strength of as-sprayed and fused coatings are evaluated. The substrate, as-sprayed and microwave fused coatings are subjected to elevated temperature sliding wear test against alumina disc under dry conditions. The test is carried out at 200°C, 400°C, and 600°C temperatures for 10 N and 20 N normal loads. Microwave fused coatings exhibit higher wear resistance than the as-sprayed coatings and substrate. The hard intermetallic

laves phases which are amorphous (bulk metallic glass) in nature strengthen the coatings at high temperatures. $\text{Co}_3\text{Mo}_2\text{Si}$, Co_7Mo_6 , Mo_3Si , Co_3Mo , and Co_2Mo_3 are the intermetallic laves phases generated in CoMoCrSi feedstock during HEBM process. The coatings produced from HVOF and flame spray process exhibits heterogeneous structure by showing cracks and pores, also cohesive strength between splats is low. The microhardness and adhesion strength of as-sprayed coatings is lower than fused coatings. Microwave fused coatings exhibit homogeneous structure with less porosity, and surface roughness. The post-treated coatings reveals the inter-diffusion of atoms near substrate-coating interface region, these results in formation of metallurgical bonding leads to increase in microhardness and adhesion strength. The as-sprayed coatings exhibits higher wear rate and coefficient of friction due to lower microhardness. The worn surface of as-sprayed coatings reveals detachment of splats with severe deformation results in adhesive wear mechanism. Microwave fused coatings exhibits lower wear rate and coefficient of friction due to higher microhardness obtained from intermetallic laves phases and also formation of homogeneous structure. The fused coatings exhibits tribo-oxide layers during sliding action which is the main phenomenon for improving the wear resistance of the fused composite coatings. CoMoCrSi+WC-12Co composite coating showed better mechanical and tribological properties compared to other types of coatings.

Keywords: Tribology; Intermetallic laves phase; High energy ball milling; HVOF; Flame spray Microwave hybrid heating; Wear.

TABLE OF CONTENTS

Declaration	
Certificate	
Acknowledgement	
ABSTRACT	
TABLE OF CONTENTS	i
LIST OF FIGURES	ix
LIST OF TABLES	xviii
ABBREVIATIONS	xx
CHAPTER 1 INTRODUCTION	1
1.1 OBJECTIVES OF THE PRESENT INVESTIGATION	6
1.2 THESIS OUTLINE	7
CHAPTER 2 LITERATURE REVIEW	9
2.1 THERMAL SPRAY PROCESS	9
2.1.1 High Velocity Oxy Fuel Process	10
2.1.2 Flame Spray Process	11
2.2 POST COATING TREATMENT	11
2.2.1 Microwave Processing of Materials	13
2.2.2 Difference between Conventional heating and Microwave Heating	13
2.3 SLIDING WEAR	17
2.3.1 Wear Mechanisms and Modes	17
2.3.2 Role of Coatings in Elevated Temperature Wear Environments	20
2.4 COBALT BASED COATINGS	23
2.5 FORMULATION OF PROBLEM	26

CHAPTER 3 EXPERIMENTAL PROCEDURES AND	
MATERIALS	27
3.1 SUBSTRATE MATERIAL	27
3.2 COATING POWDERS	27
3.3 PREPARATION OF COATING FEEDSTOCK	28
3.3.1 High Energy Ball Milling of CoMoCrSi powder	28
3.3.2 Processing of Composite Feedstock	29
3.4 COATING TECHNIQUES	30
3.4.1 High Velocity Oxy Fuel Spraying	30
3.4.2 Flame Spraying	31
3.5 FUSING OF AS-SPRAYED COATINGS	32
3.5.1 Experimental Setup	32
3.5.2 Microwave Hybrid Heating	33
3.6 CHARACTERISATION OF FEEDSTOCK, AS-SPRAYED	
COATINGS AND FUSED COATINGS	34
3.6.1 Samples Preparation for Cross Sectional Analysis	34
3.6.2 Metallographic Studies	34
3.6.3 X-Ray Diffraction (XRD) analysis	34
3.6.4 Particle Size Analysis	35
3.6.5 Measurement of As-sprayed and Fused Coatings Thickness	35
3.6.6 Porosity Analysis	35
3.6.7 Microhardness Measurement	35
3.6.8 Adhesion Strength Test	35
3.7 ELEVATED TEMPERATURE SLIDING WEAR STUDIES	36
3.7.1 Experimental Setup	36
3.7.2 Wear rate calculations	37

**CHAPTER 4 CHARACTERISATION OF FEEDSTOCK AND
COATINGS**

	39
4.1 MORPHOLOGY OF COATING POWDERS	39
4.2 COATING PARTICLE SIZE ANALYSIS	41
4.3 XRD STUDIES OF COATING POWDERS	42
4.3.1 Milled Coating Powder	42
4.3.2 Composite Coating Powder	43
4.4 MEASUREMENT OF COATINGS THICKNESS	44
4.5 HVOF SPRAYED AND MICROWAVE FUSED CoMoCrSi COATINGS	45
4.5.1 Surface SEM and EDS Analysis	45
4.5.2 Cross Sectional Microstructure and Elemental Mapping	46
4.5.3 X-Ray Diffraction Studies	49
4.6 HVOF SPRAYED AND MICROWAVE FUSED CoMoCrSi+Cr₃C₂ COMPOSITE COATINGS	50
4.6.1 Surface SEM and EDS Analysis	50
4.6.2 Cross Sectional Microstructure and Elemental Mapping	51
4.6.3 X-Ray Diffraction Studies	54
4.7 HVOF SPRAYED AND MICROWAVE FUSED CoMoCrSi+WC-CrC-Ni COMPOSITE COATINGS	55
4.7.1 Surface SEM and EDS Analysis	55
4.7.2 Cross Sectional Microstructure and Elemental Mapping	56
4.7.3 X-Ray Diffraction Studies	59
4.8 HVOF SPRAYED AND MICROWAVE FUSED CoMoCrSi+WC-12Co COMPOSITE COATINGS	60
4.8.1 Surface SEM and EDS Analysis	60
4.8.2 Cross Sectional Microstructure and Elemental Mapping	61
4.8.3 X-Ray Diffraction Studies	64

4.9	FLAME SPRAYED AND MICROWAVE FUSED	
	CoMoCrSi COATINGS	65
4.9.1	Surface SEM and EDS Analysis	65
4.9.2	Cross Sectional Microstructure and Elemental Mapping	67
4.9.3	X-Ray Diffraction Studies	69
4.10	FLAME SPRAYED AND MICROWAVE FUSED	
	CoMoCrSi+Cr₃C₂ COMPOSITE COATINGS	70
4.10.1	Surface SEM and EDS Analysis	70
4.10.2	Cross Sectional Microstructure and Elemental Mapping	71
4.10.3	X-Ray Diffraction Studies	74
4.11	FLAME SPRAYED AND MICROWAVE FUSED	
	CoMoCrSi+WC-CrC-Ni COMPOSITE COATINGS	75
4.11.1	Surface SEM and EDS Analysis	75
4.11.2	Cross Sectional Microstructure and Elemental Mapping	77
4.11.3	X-Ray Diffraction Studies	79
4.12	FLAME SPRAYED AND MICROWAVE FUSED	
	CoMoCrSi+WC-12Co COMPOSITE COATINGS	81
4.12.1	Surface SEM and EDS Analysis	81
4.12.2	Cross Sectional Microstructure and Elemental Mapping	82
4.12.3	X-Ray Diffraction Studies	84
4.13	POROSITY OF AS-SPRAYED AND FUSED COATINGS	85
4.13.1	HVOF Sprayed and Microwave Fused Coatings	85
4.13.2	Flame Sprayed and Microwave Fused Coatings	86
4.14	MICROHARDNESS OF COATINGS	87
4.14.1	HVOF Sprayed and Microwave Fused Coatings	87
4.14.2	Flame Sprayed and Microwave Fused Coatings	89
4.15	ADHESION STRENGTH OF COATINGS	90
4.15.1	HVOF Sprayed Coatings	90
4.15.2	Microwave Fused HVOF Coatings	91

4.15.3	Flame Sprayed Coatings	93
4.15.4	Microwave Fused Flame Spray Coatings	94
4.16	SUMMARY	95
CHAPTER 5 WEAR STUDIES		101
5.1	WEAR STUDIES ON HVOF SPRAYED AND MICROWAVE FUSED CoMoCrSi COATINGS	101
5.1.1	Volume loss and Wear rate of Coatings	101
5.1.2	Coefficient of Friction	104
5.1.3	X-Ray Diffraction analysis of Fused Coatings	106
5.1.4	Worn Surface SEM and EDS analysis	107
5.2	WEAR STUDIES ON HVOF SPRAYED AND MICROWAVE FUSED CoMoCrSi+Cr₃C₂ COMPOSITE COATINGS	112
5.2.1	Volume loss and Wear rate of Coatings	112
5.2.2	Coefficient of Friction	115
5.2.3	X-Ray Diffraction analysis of Fused Coatings	117
5.2.4	Worn Surface SEM and EDS analysis	118
5.3	WEAR STUDIES ON HVOF SPRAYED AND MICROWAVE FUSED CoMoCrSi+WC-CrC-Ni COMPOSITE COATINGS	
5.3.1	Volume loss and Wear rate of Coatings	123
5.3.2	Coefficient of Friction	126
5.3.3	X-Ray Diffraction analysis of Fused Coatings	128
5.3.4	Worn Surface SEM and EDS analysis	129
5.4	WEAR STUDIES ON HVOF SPRAYED AND MICROWAVE FUSED CoMoCrSi+WC-12Co COMPOSITE COATINGS	133
5.4.1	Volume loss and Wear rate of Coatings	133
5.4.2	Coefficient of Friction	137
5.4.3	X-Ray Diffraction analysis of Fused Coatings	139
5.4.4	Worn Surface SEM and EDS analysis	139

5.5	COMPARATIVE DISCUSSION OF HVOF SPRAYED AND FUSED COATINGS SUBJECTED TO WEAR	144
5.6	WEAR STUDIES ON FLAME SPRAYED AND MICROWAVE FUSED CoMoCrSi COATINGS	148
5.6.1	Volume loss and Wear rate of Coatings	148
5.6.2	Coefficient of Friction	151
5.6.3	X-Ray Diffraction analysis of Fused Coatings	153
5.6.4	Worn Surface SEM and EDS analysis	154
5.7	WEAR STUDIES ON FLAME SPRAYED AND MICROWAVE FUSED CoMoCrSi+Cr₃C₂ COMPOSITE COATINGS	157
5.7.1	Volume loss and Wear rate of Coatings	157
5.7.2	Coefficient of Friction	160
5.7.3	X-Ray Diffraction analysis of Fused Coatings	162
5.7.4	Worn Surface SEM and EDS analysis	163
5.8	WEAR STUDIES ON FLAME SPRAYED AND MICROWAVE FUSED CoMoCrSi+WC-CrC-Ni COMPOSITE COATING	166
5.8.1	Volume loss and Wear rate of Coatings	166
5.8.2	Coefficient of Friction	169
5.8.3	X-Ray Diffraction analysis of Fused Coatings	171
5.8.4	Worn Surface SEM and EDS analysis	171
5.9	WEAR STUDIES ON FLAME SPRAYED AND MICROWAVE FUSED CoMoCrSi+WC-12Co COMPOSITE COATINGS	175
5.9.1	Volume loss and Wear rate of Coatings	175
5.9.2	Coefficient of Friction	178
5.9.3	X-Ray Diffraction analysis of Fused Coatings	180
5.9.4	Worn Surface SEM and EDS analysis	180

5.10	COMPARATIVE DISCUSSION OF FLAME SPRAYED AND FUSED COATINGS SUBJECTED TO WEAR	184
5.11	WEAR STUDIES ON SUBSTRATE	187
5.11.1	Volume loss and Wear rate of Substrate	187
5.11.2	Coefficient of Friction	188
5.11.3	Worn Surface SEM Micrographs	190
5.12	SUMMARY	191
CHAPTER 6 CONCLUSIONS		193
SCOPE OF FUTURE WORK		196
REFERENCES		197
LIST OF PUBLICATIONS		207
BIO-DATA		209

LIST OF FIGURES

Figure 1.1 Microwave material interactions	04
Figure 2.1 Principle of thermal spray coating (Metco 2014)	10
Figure 2.2 Graphical representation of conventional and microwave heating	13
Figure 2.3 Microwave processing of bulk metallic materials	14
Figure 2.4 Research trends in microwave processing of metal-based materials	15
Figure 2.5 Macro mechanical contact conditions for different mechanisms which influence friction when a hard spherical slider moves on a coated flat surface	18
Figure 3.1 High energy ball milling facility	29
Figure 3.2 HVOF spray schematic (Yi Ding, 2009) and Experimental set up	30
Figure 3.3 Flame spray schematic (Tucker, 1994) and Experimental set up	31
Figure 3.4 Domestic microwave oven set up	32
Figure 3.5 Graphical representation of microwave hybrid heating	33
Figure 3.6 (a) Pin-on-disc experimental set up (b) graphical representation of wear test setup	36
Figure 4.1 SEM morphology of coating powders before HEBM process (a) CoMoCrSi (b) Cr ₃ C ₂ (c) WC-CrC-Ni (d) WC-12Co	40
Figure 4.2 (a-d) typical morphology of powder subjected to HEBM operation	40
Figure 4.3 Morphology of CoMoCrSi powder milled for (a) 2 hr, (b) 3 hr (c) 4 hr and (d) 5 hr	41
Figure 4.4 XRD pattern of milled CoMoCrSi powder at different milling time	42
Figure 4.5 XRD pattern of CoMoCrSi+Cr ₃ C ₂ composite feedstock	43
Figure 4.6 XRD patterns of (a) CoMoCrSi+WC-CrC-Ni (b) CoMoCrSi+WC-12Co composite feedstock	44
Figure 4.7 HVOF spray CoMoCrSi coating (a) SEM surface morphology and (b) EDS Analysis	46
Figure 4.8 Fused CoMoCrSi coating (a) SEM surface morphology and (b) EDS analysis	46
Figure 4.9 SEM micrographs along the cross-section of CoMoCrSi coatings (a) HVOF sprayed (b) microwave fused	47

Figure 4.10 Elemental X-ray mapping of HVOF sprayed CoMoCrSi coating	48
Figure 4.11 Elemental X-ray mapping of microwave fused CoMoCrSi coating	48
Figure 4.12 XRD patterns of CoMoCrSi coatings (a) HVOF sprayed (b) microwave Fused	49
Figure 4.13 HVOF spray CoMoCrSi+Cr ₂ C ₃ composite coating (a) SEM surface morphology and (b) EDS analysis	51
Figure 4.14 SEM surface micrograph of microwave fused CoMoCrSi+Cr ₂ C ₃ composite Coating	51
Figure 4.15 SEM micrographs along the cross-section of CoMoCrSi+Cr ₃ C ₂ coatings (a) HVOF sprayed (b) Microwave fused	52
Figure 4.16 Elemental X-ray mapping of HVOF sprayed CoMoCrSi+Cr ₃ C ₂ composite Coating	53
Figure 4.17 Elemental X-ray mapping of microwave fused CoMoCrSi+Cr ₃ C ₂ composite Coating	54
Figure 4.18 XRD patterns of as CoMoCrSi+Cr ₃ C ₂ (a) feedstock (b) HVOF sprayed and (c) Microwave fused	55
Figure 4.19 SEM micrograph taken on CoMoCrSi+WC-CrC-Ni composite coating surface (a) HVOF sprayed (b) Microwave fused the coating	56
Figure 4.20 SEM micrograph of CoMoCrSi+WC-CrC-Ni composite coating along cross-section (a) HVOF sprayed (b) Microwave fused coating	56
Figure 4.21 Elemental X-ray mapping of HVOF sprayed CoMoCrSi+WC-CrC-Ni composite coating	57
Figure 4.22 Elemental X-ray mapping of microwave fused CoMoCrSi+WC-CrC-Ni composite coating	58
Figure 4.23 XRD pattern of CoMoCrSi+WC-CrC-Ni composite coatings (a) HVOF sprayed (b) Microwave fused	60
Figure 4.24 SEM micrograph of CoMoCrSi+WC-12Co composite coating surface (a) HVOF sprayed (b) Microwave fused coating	61
Figure 4.25 SEM micrograph of CoMoCrSi+WC-12Co composite coating along cross-section (a) HVOF sprayed (b) Microwave fused coating	62

Figure 4.26 Elemental X-ray mapping of HVOF sprayed CoMoCrSi+WC-12Co composite coating	63
Figure 4.27 Elemental X-ray mapping of microwave fused CoMoCrSi+WC-12Co composite coating	64
Figure 4.28 XRD pattern of CoMoCrSi+WC-12Co composite coatings (a) HVOF sprayed (b) Microwave fused	65
Figure 4.29 Flame sprayed CoMoCrSi coating (a) SEM surface morphology (b) EDS analysis	66
Figure 4.30 Microwave fused CoMoCrSi coating (Flame sprayed) (a) SEM surface Morphology (b) EDS analysis	66
Figure 4.31 SEM micrograph of CoMoCrSi coating along cross-section (a) Flame sprayed (b) Microwave fused coating	67
Figure 4.32 Elemental X-ray mapping of flame sprayed CoMoCrSi coating	68
Figure 4.33 Elemental X-ray mapping of microwave fused CoMoCrSi coating	69
Figure 4.34 XRD patterns of (a) feedstock and flame sprayed CoMoCrSi coatings (b) As-sprayed (c) Microwave fused	70
Figure 4.35 Flame sprayed CoMoCrSi+Cr ₃ C ₂ composite coating (a) SEM surface morphology (b) EDS analysis	71
Figure 4.36 Microwave fused CoMoCrSi+Cr ₃ C ₂ composite coating (a) SEM surface morphology (b) EDS analysis	71
Figure 4.37 SEM micrograph of CoMoCrSi+Cr ₃ C ₂ composite coating along cross-section (a) Flame sprayed (b) Microwave fused coating	72
Figure 4.38 Elemental X-ray mapping of flame sprayed CoMoCrSi+Cr ₃ C ₂ composite Coating	73
Figure 4.39 Elemental X-ray mapping of microwave fused CoMoCrSi+Cr ₃ C ₂ composite coating	74
Figure 4.40 XRD patterns of CoMoCrSi+Cr ₃ C ₂ composite coating (a) feedstock (b) flame sprayed (c) Microwave fused	75
Figure 4.41 Flame sprayed CoMoCrSi+WC-CrC-Ni composite coating (a) SEM surface morphology (b) EDS analysis	76

Figure 4.42 Microwave fused CoMoCrSi+WC-CrC-Ni composite coating (a) SEM surface morphology (b) EDS analysis	76
Figure 4.43 SEM micrograph of CoMoCrSi+WC-CrC-Ni composite coating along cross-section(a) Flame sprayed (b) Microwave fused the coating	77
Figure 4.44 Elemental X-ray mapping of flame sprayed CoMoCrSi+WC-CrC-Ni composite coating	78
Figure 4.45 Elemental X-ray mapping of microwave fused CoMoCrSi+WC-CrC-Ni composite coating	79
Figure 4.46 XRD patterns of CoMoCrSi+WC-CrC-Ni composite coatings (a) flame sprayed (b) Microwave fused	80
Figure 4.47 Flame sprayed CoMoCrSi+WC-12Co composite coating (a) SEM surface morphology (b) EDS analysis	81
Figure 4.48 Microwave fused CoMoCrSi+WC-12Co composite coating (a) SEM surface morphology (b) EDS analysis	82
Figure 4.49 SEM micrograph of CoMoCrSi+WC-12Co composite coating along cross-section (a) Flame sprayed (b) Microwave fused coating	82
Figure 4.50 Elemental X-ray mapping of flame sprayed CoMoCrSi+WC-12Co composite coating	83
Figure 4.51 Elemental X-ray mapping of microwave fused CoMoCrSi+WC-12Co composite coating	84
Figure 4.52 XRD patterns of CoMoCrSi+WC-12Co composite coatings (a) flame sprayed (b) Microwave fused	85
Figure 4.53 Bar chart showing average microhardness of HVOF sprayed and Microwave fused coating	88
Figure 4.54 Bar chart showing average microhardness of flame sprayed and Microwave fused coating	90
Figure 4.55 Macrograph of fractured surface of HVOF sprayed coatings during adhesion test samples (a) CoMoCrSi (b) CoMoCrSi+Cr ₃ C ₂ (c) CoMoCrSi+WC-CrC-Ni (d) CoMoCrSi+WC-12Co	91

Figure 4.56 Macrograph of fractured surface of microwave fused HVOF sprayed coatings subjected to adhesion test (a) CoMoCrSi (b) CoMoCrSi+Cr ₃ C ₂ (c) CoMoCrSi+WC-CrC-Ni (d) CoMoCrSi+WC-12Co	92
Figure 4.57 Macrograph of fractured surface of flame sprayed coatings subjected to adhesion test (a) CoMoCrSi (b) CoMoCrSi+Cr ₃ C ₂ (c) CoMoCrSi+WC-CrC-Ni (d) CoMoCrSi+WC-12Co	93
Figure 4.58 Macrograph of fractured surface of microwave fused flame sprayed coatings subjected to adhesion test (a) CoMoCrSi (b) CoMoCrSi+Cr ₃ C ₂ (c) CoMoCrSi+WC-CrC-Ni (d) CoMoCrSi+WC-12Co	94
Figure 5.1 Wear volume loss of HVOF sprayed and microwave fused CoMoCrSi coatings with respect to temperature (a) 10 N, (b) 20 N	102
Figure 5.2 Wear rate plots of HVOF sprayed and microwave fused CoMoCrSi coatings (a) 10 N, (b) 20 N	103
Figure 5.3 Wear rate coefficient k plot of HVOF sprayed and fused CoMoCrSi coating	104
Figure 5.4 Friction coefficient of HVOF sprayed and microwave fused CoMoCrSi coatings with respect to sliding distance (a) 10 N, (b) 20 N	105
Figure 5.5 XRD pattern of CoMoCrSi fused coating worn surfaces at all test temperature	106
Figure 5.6 Morphology of HVOF sprayed CoMoCrSi coating worn surface (a-c) under 10 N and (d-f) under 20 N at temperatures of 200 °C, 400°C, 600°C	108
Figure 5.7 Morphology of microwave fused CoMoCrSi coating worn surface (a-c) under 10 N and (d-f) under 20 N at temperatures of 200 °C, 400°C, 600°C	109
Figure 5.8 Wear volume loss of HVOF sprayed and microwave fused CoMoCrSi+Cr ₃ C ₂ composite coatings with respect to temperature (a) 10 N, (b) 20 N	113
Figure 5.9 Wear rate plots of HVOF sprayed and microwave fused CoMoCrSi+Cr ₃ C ₂ composite coatings (a) 10 N, (b) 20 N	114
Figure 5.10 Wear rate coefficient k plot of HVOF sprayed and fused CoMoCrSi+Cr ₃ C ₂ composite coating	115
Figure 5.11 Friction coefficient of HVOF sprayed and microwave fused CoMoCrSi+Cr ₃ C ₂ composite coatings with respect to sliding distance (a) 10 N, (b) 20 N	116
Figure 5.12 XRD pattern of fused CoMoCrSi+Cr ₃ C ₂ composite coating worn surfaces at all test temperatures	117

Figure 5.13 Morphology of HVOF sprayed CoMoCrSi+Cr ₃ C ₂ composite coating worn surfaces (a-c) under 10 N and (d-f) under 20 N at temperatures of 200 °C, 400°C, 600°C	120
Figure 5.14 Morphology of microwave fused CoMoCrSi+Cr ₃ C ₂ composite coating worn surface (a-c) under 10 N and (d-f) under 20 N at temperatures of 200 °C, 400°C, 600°C	121
Figure 5.15 Wear volume loss of HVOF sprayed and microwave fused CoMoCrSi+WC-CrC-Ni composite coatings with respect to temperature at loads of (a) 10 N (b) 20N	124
Figure 5.16 Wear rate plots of HVOF sprayed and microwave fused CoMoCrSi+WC-CrC-Ni composite coatings (a) 10 N, (b) 20 N	125
Figure 5.17 Wear rate coefficient k plot of HVOF sprayed and fused CoMoCrSi+WC-CrC-Ni composite coating	126
Figure 5.18 Friction coefficient of HVOF sprayed and microwave fused CoMoCrSi+WC-CrC-Ni composite coatings with respect to sliding distance (a) 10 N, (b) 20 N	127
Figure 5.19 XRD pattern of fused CoMoCrSi+WC-CrC-Ni composite coating worn surfaces at all test temperatures	128
Figure 5.20 Morphology of HVOF sprayed CoMoCrSi+WC-CrC-Ni composite coating worn surfaces (a-c) under 10 N and (d-f) under 20 N at temperatures of 200 °C, 400°C, 600°C	130
Figure 5.21 Morphology of microwave fused CoMoCrSi+WC-CrC-Ni composite coating worn surfaces (a-c) under 10 N and (d-f) under 20 N at temperatures of 200 °C, 400°C, 600°C	132
Figure 5.22 Wear volume loss of HVOF sprayed and microwave fused CoMoCrSi+WC-12Co composite coatings with respect to temperature (a) 10 N, (b) 20 N	134
Figure 5.23 Wear rate plots of HVOF sprayed and microwave fused CoMoCrSi+WC-12Co composite coatings (a) 10 N, (b) 20 N	135
Figure 5.24 Wear rate coefficient k plot of HVOF sprayed and fused CoMoCrSi+WC-12Co composite coating	136
Figure 5.25 Friction coefficient of HVOF sprayed and microwave fused CoMoCrSi+WC-12Co composite coatings with respect to sliding distance (a) 10 N, (b) 20 N	138

Figure 5.26 XRD pattern of fused CoMoCrSi+WC-12Co composite coating worn surfaces at all test temperatures	139
Figure 5.27 Morphology of HVOF sprayed CoMoCrSi+WC-12Co composite coating worn surfaces (a-c) under 10 N and (d-f) under 20 N at temperatures of 200 °C, 400°C, 600°C	141
Figure 5.28 Morphology of microwave fused CoMoCrSi+WC-12Co composite coating worn surfaces (a-c) under 10 N and (d-f) under 20 N at temperatures of 200 °C, 400°C, 600°C	142
Figure 5.29 Wear volume loss of HVOF sprayed and microwave fused of four different coatings with respect to temperature (a) 10 N, (b) 20 N	146
Figure 5.30 Wear rate plots of HVOF sprayed and microwave fused of four different coatings with respect to temperature (a) 10 N, (b) 20 N	147
Figure 5.31 Wear volume loss of flame sprayed and microwave fused CoMoCrSi coatings with respect to temperature (a) 10 N, (b) 20 N	149
Figure 5.32 Wear rate plots of flame sprayed and microwave fused CoMoCrSi coatings (a) 10 N, (b) 20 N	150
Figure 5.33 Wear rate coefficient k plot of flame sprayed and fused CoMoCrSi coating	151
Figure 5.34 Friction coefficient of flame sprayed and microwave fused CoMoCrSi coatings with respect to sliding distance (a) 10 N, (b) 20 N	152
Figure 5.35 XRD pattern of microwave fused flame sprayed CoMoCrSi coating worn surfaces at all test temperatures	153
Figure 5.36 Morphology of flame sprayed CoMoCrSi coating worn surfaces (a-c) under 10 N and (d-f) under 20 N at temperatures of 200 °C, 400°C, 600°C	155
Figure 5.37 Morphology of microwave fused flame sprayed CoMoCrSi coating worn surfaces (a-c) under 10 N and (d-f) under 20 N at temperatures of 200 °C, 400°C, 600°C	156
Figure 5.38 Wear volume loss of flame sprayed and microwave fused CoMoCrSi+Cr ₃ C ₂ composite coatings with respect to temperature (a) 10 N, (b) 20 N	158
Figure 5.39 Wear rate plots of flame sprayed and microwave fused CoMoCrSi+Cr ₃ C ₂ composite coatings with respect to temperature (a) 10 N, (b) 20 N	159
Figure 5.40 Wear rate coefficient k plot of flame sprayed and fused CoMoCrSi+Cr ₃ C ₂ composite coatings	160
Figure 5.41 Friction coefficient of flame sprayed and microwave fused CoMoCrSi+Cr ₃ C ₂ composite coatings with respect to sliding distance (a) 10 N, (b) 20 N	161

Figure 5.42 XRD pattern of microwave fused flame sprayed CoMoCrSi+Cr ₃ C ₂ composite coatings worn surfaces at all test temperatures	162
Figure 5.43 Morphology of flame sprayed CoMoCrSi+Cr ₃ C ₂ composite coating worn surfaces (a-c) under 10 N and (d-f) under 20 N at temperatures of 200°C, 400°C, 600°C	164
Figure 5.44 Morphology of microwave fused flame sprayed CoMoCrSi+Cr ₃ C ₂ composite coating worn surfaces (a-c) under 10 N and (d-f) under 20 N at temperatures of 200°C, 400°C, 600°C	165
Figure 5.45 Wear volume loss of flame sprayed and microwave fused CoMoCrSi+WC-CrC-Ni composite coatings with respect to temperature (a) 10 N, (b) 20 N	167
Figure 5.46 Wear rate plots of flame sprayed and microwave fused CoMoCrSi+WC-CrC-Ni composite coatings with respect to temperature (a) 10 N, (b) 20 N	168
Figure 5.47 Wear rate coefficient k plot of flame sprayed and fused CoMoCrSi+WC-CrC-Ni composite coatings	169
Figure 5.48 Friction coefficient of flame sprayed and microwave fused CoMoCrSi+WC-CrC-Ni composite coatings with respect to sliding distance (a) 10 N, (b) 20 N	170
Figure 5.49 XRD pattern of microwave fused flame sprayed CoMoCrSi+WC-CrC-Ni composite coatings worn surfaces at all test temperatures	171
Figure 5.50 Morphology of flame sprayed CoMoCrSi+WC-CrC-Ni composite coating worn surfaces (a-c) under 10 N and (d-f) under 20 N at temperatures of 200°C, 400°C, 600°C	173
Figure 5.51 Morphology of microwave fused flame sprayed CoMoCrSi+WC-CrC-Ni composite coating worn surfaces (a-c) under 10 N and (d-f) under 20 N at temperatures of 200°C, 400°C, 600°C	174
Figure 5.52 Wear volume loss of flame sprayed and microwave fused CoMoCrSi+WC-12Co composite coatings with respect to temperature (a) 10 N, (b) 20 N	176
Figure 5.53 Wear rate plots of flame sprayed and microwave fused CoMoCrSi+WC-12Co composite coatings with respect to temperature (a) 10 N, (b) 20 N	177
Figure 5.54 Wear rate coefficient k plot of flame sprayed and fused CoMoCrSi+WC-12Co composite coatings	178
Figure 5.55 Friction coefficient of flame sprayed and microwave fused CoMoCrSi+WC-12Co composite coatings with respect to sliding distance (a) 10 N, (b) 20 N	179
Figure 5.56 XRD pattern of microwave fused flame sprayed CoMoCrSi+WC-12Co	

composite coatings worn surfaces at all test temperatures	180
Figure 5.57 Morphology of flame sprayed CoMoCrSi+WC-12Co composite coating worn surfaces (a-c) under 10 N and (d-f) under 20 N at temperatures of 200°C, 400°C, 600°C	182
Figure 5.58 Morphology of microwave fused flame sprayed CoMoCrSi+WC-12Co composite coating worn surfaces (a-c) under 10 N and (d-f) under 20 N at temperatures of 200°C, 400°C, 600°C	183
Figure 5.59 Wear volume loss of flame sprayed and microwave fused of four different coatings with respect to temperature (a) 10 N, (b) 20 N	185
Figure 5.60 Wear rate plots of flame sprayed and microwave fused of four different coatings with respect to temperature (a) 10 N, (b) 20 N	186
Figure 5.61 Wear volume loss of substrate with respect to temperature (a) 10 N, (b) 20 N	187
Figure 5.62 Wear rate plots of substrate with respect to temperature (a) 10 N, (b) 20 N	188
Figure 5.63 Friction coefficient of substrate with respect to sliding distance (a) 10 N, (b) 20 N	189
Figure 5.64 Morphology of substrate worn surfaces (a-c) under 10 N and (d-f) under 20 N at temperatures of 200°C, 400°C, 600°C	190

LIST OF TABLES

Table 3.1: Chemical composition (wt. %) of substrate Pure Titanium grade-2	27
Table 3.2: Chemical composition and particle size of coating feedstock	28
Table 3.3: HVOF process parameters	31
Table 3.4: Flame spray parameters	32
Table 4.1: CoMoCrSi particle size distribution and density at different milling time	42
Table 4.2: Average coatings thickness	45
Table 4.3 EDS results of microwave fused CoMoCrSi+Cr ₃ C ₂ composite coating for selected points representing in Figure 4.15 (b)	52
Table 4.4 EDS results of microwave fused CoMoCrSi+WC-CrC-Ni composite coating with respect to points marked in Figure 4.20 (b)	59
Table 4.5 EDS results of microwave fused CoMoCrSi+WC-12Co composite coating with respect to points marked in (Figure 4.25b)	62
Table 4.6: Average porosity of the coatings	86
Table 4.7: Average Microhardness of HVOF sprayed and Microwave fused coatings	88
Table 4.8: Average Microhardness of Flame sprayed and Microwave fused coatings	89
Table 4.9: Adhesion strength of HVOF sprayed and Microwave fused coatings	92
Table 4.10: Adhesion strength of Flame sprayed and Microwave fused coatings	94
Table 5.1: EDS results of HVOF sprayed CoMoCrSi coating worn surfaces at selected points shown in Figure 5.6	111
Table 5.2: EDS results of fused CoMoCrSi coating worn surfaces at selected points shown in Figure 5.7	111
Table 5.3 EDS results of HVOF sprayed CoMoCrSi+Cr ₃ C ₂ composite coating worn surfaces at selected points shown in Figure 5.13	122
Table 5.4 EDS results of fused CoMoCrSi+Cr ₃ C ₂ composite coating worn surfaces at selected points shown in Figure 5.14	122
Table 5.5: EDS analysis of HVOF sprayed CoMoCrSi+WC-CrC-Ni composite coating worn surfaces on points marked in Figure 5.20	131
Table 5.6: EDS analysis of fused CoMoCrSi+WC-CrC-Ni composite coating worn	

surfaces on points marked in Figure 5.21	133
Table 5.7: EDS analysis of HVOF sprayed CoMoCrSi+WC-12Co composite coating worn surfaces on points marked in Figure 5.27	143
Table 5.8: EDS analysis of fused CoMoCrSi+WC-12Co composite coating worn surfaces on points marked in Figure 5.28	143

ABBREVIATIONS

HVOF	: High Velocity Oxy Fuel
FS	: Flame Spray
HEBM	: High Energy Ball Milling
MHH	: Microwave Hybrid Heating
MWF	: Microwave Fused
COF	: Coefficient of Friction
SEM	: Scanning Electron Microscope
EDS	: Energy Dispersive Spectroscopy
BSE	: Back Scattered Electron
XRD	: X-ray Diffraction
lpm	: Liters per Minute
UTS	: Ultimate Tensile Strength
hr	: Hour
Min	: Minute
Bal	: Balance
Wt%	: Weight Percentage
H _v	: Vickers Hardness
Psi	: Pounds per square inch
FCC	: Face-Centered Cubic
HCP	: Hexagonal Closely Packed

CHAPTER 1

INTRODUCTION

In the modern era of industrialization, there is ever increasing demand for research in new materials for strength and economy of use. The metals and their alloys like Steel, Titanium, Tungsten and, Inconel are some among the top of that list. Unlike other metals, Titanium has a remarkable combination of versatile properties (Schneider et al., 2014). The properties, like high specific strength, good corrosion resistance, non-magnetic properties provide it with a competitive advantage in many applications. Titanium is almost half as dense as steel and has equal in strength when put alongside to ship-building or structural steel (Gorynin, 1999). It has very good corrosion resistance property, the quality that is helpful in bringing down the recurrent maintenance and cost in spite of the high initial cost. This makes it a plausible replacement for steel and an obvious choice in marine research and applications (Zhou et al., 2007).

Titanium finds its applications in aircraft, space industry, chemical field, and ship-building corporations because of the above properties. It was also proved that when different piping materials were used for fleet ships, the lifetime has been restricted (Miller and Holladay, 1959). The service life of steel and copper-nickel based alloy piping is 1.2-2 and 6-8 years respectively, due to corrosion damage (Bemporad et al., 2007). Titanium can much better in marine applications like hulls, pressure vessels, deepwater risers, supply piping, pumps, filters etc as reported by Bemporad et al., (2008). The researcher Lin et al., (2016) reported that titanium and its alloys can also be vastly used in steam generators for icebreakers, structural members in offshore hydrocarbon extraction units, equipment exposed to high concentration solutions of chlorine and fluorine (offshore extracts).

The surfaces of titanium and most of its alloys have relatively poor wear resistance and also it is prone to oxidation and oxygen-induced embrittlement at temperatures above 600° C (Khun et al., 2016). All materials do wear to some extent and usual solution to minimize that is the proper configuration of mating surfaces or wise choice of lubricants (Peat et al., 2016). In metals, wear usually occurs by plastic displacement and detachment of the surface

particles. Wear rate is affected by many factors such as, the type of loading, type of motion and temperature. Loading may be of static, dynamic, impact and motion may be of sliding, rolling etc., depending on the system different wear types and wear mechanisms can be found (Bolelli, and Lusvarghi, 2007).

In most of the countries, the cost of material loss caused due to wear accounts for about 4% of their gross internal product (GIP). For instance, in the United States alone it is seen that the wear and corrosion of spare parts cost around 22 billion Euros per year. Besides this, an indirect cost involved in the production stops, scrap management, maintenance, adds up to the cost of material and thereby increases the cost of the material. To overcome these tribological problems, the demand for new alternatives has increased in recent times (Bhupinder et al., 2018).

Modification of the surface is the most cost-effective and potential method in order to improve the service life of bulk metal components because wear only occurs at the surface. Some of the surface modification techniques have shown the most productive solutions for the wear problems. For example, plasma nitriding, chemical vapor deposition, physical vapor deposition, thermal spraying, laser cladding, and hardening have been developed to improve the wear resistance of the surface of the component (Ding et al., 2017). Research work till date has shown that the most effective method of wear reduction is by modification of surface by deposition of protective metallic or conversion coatings than by alloying (Fang et al., 2009), (Houdkova et al., 2014). Nowadays, surface modification is mainly done by depositing the coating materials, usually hard and corrosion resistant materials on the surface of ductile materials that are prone to corrosion and wear attack. In these surface coating technologies, the properties of the deposited coatings are quite different from that of the substrate materials. This approach also enables the use of economical materials for the components which also results in better properties by modifying the surface of the substrate. They involve dry and wet processes that can be divided into two groups according to the thickness of the coating. The coatings with thicknesses below 0.01 to 9 microns are called thin coatings, while those with thicknesses over 10 to 1000 and above microns are called thick coatings (Ramesh et al., 2010).

Thermal spray coatings belong to the surface modification techniques, in which the coating material is applied onto the surface so as to obtain thick wear resistant surfaces. It improves

the service life of materials and enhances the performance of the components, by adding functionality to the surfaces. The feedstock which is generally a powder or a wire form is subjected to heat and allowed on to the substrate material with high velocity. The coating is built upon the substrate surface in multiple layers until the required thickness is obtained, which usually falls in the range of 50-1000 μm . One major advantage with thermal coatings is that variety of materials, ranging from soft plastics to hard refractory materials can be easily processed to produce coatings for multiple applications, e.g. corrosion resistant coatings for offshore applications, wear resistant coatings in mining, thermal barrier coatings in the aviation industry. This is the reason for its growth around worldwide, accounting for several billion dollars of investment since its discovery. The versatility of the process makes it suitable for use against wear, high-temperature environments, corrosion, repair and restoration of parts. Various spraying methods are categorized on the basis of the source of energy like plasma arc spray; High-velocity oxy-fuel (HVOF) spray, flame spray, and electric arc spray (Davies, 2004).

The HVOF and flame spray coating process is one of the basic and conventional methods among the thermal spray processes have existed from more than 10 decades. It is a low-cost process, because of hardware simplicity and also has high production rates and process rapidity in the coating to improve tribological and corrosion properties (Gisario et al., 2015), (Torres et al., 2013).

However, even using state-of-the-art technology for coating systems, it is not possible to achieve defect-free thermal spray coatings. When the HVOF process is conducted under room temperature, the air will easily entrap into the coating region. This creates possible defects like pores, voids originating from the spraying process that is found at the splat boundaries through which the coatings are mainly affected by wear and corrosive environment (KhamenehAsl et al., 2006), (Picas e al., 2015). Unmelted particles or partially melted particles can be observed in the HVOF-deposited process because of very high-velocity molten particles which also makes the route to cause residual stresses in the coating as reported by Pukasiewicz et al., (2017) and Matikainen et al., (2017). In order to produce quality coatings, thermal spray process should be conducted under vacuum or inert conditions so that there is no provision of air entering into the coating; this route is very

expensive for production of coatings (Utu and Marginean, 2017). This can be achieved by using high energy heating sources like electron beam welding, laser processing, or conventional furnace heat treatment (Wang et al., 2009), (Guo et al., 1995). Laser technique and electron beam welding process cause several drawbacks, such as high processing cost and high maintenance cost. Also due to the rapid cooling rate, chances of formation of cracks during solidification and high thermal distortion of the base material can be observed; whereas conventional heat-treating methods require less cost but high processing time (Gupta and Sharma, 2011) and (Srinath et al., 2011). The focus is on an emerging technology called “Microwave hybrid heating process”. There are fewer publications available on microwave processing of cladding and joining of materials (Hebbale and Srinath, 2017), (Zafar and Sharma, 2014) and (Bhattacharya and Basak, 2016).

Microwave energy has been used in various applications for more than four decades, including communication, food processing, medical therapy, polymers, etc. In recent years, microwave processing of materials has emerged as one of the advanced and fastest material processing techniques. Microwaves interact cause heating through the following two mechanisms:

- Microwaves interact with materials selectively
- Microwave interaction depends on the dielectric properties of the irradiated material, the higher the dielectric loss factor, higher is the interaction

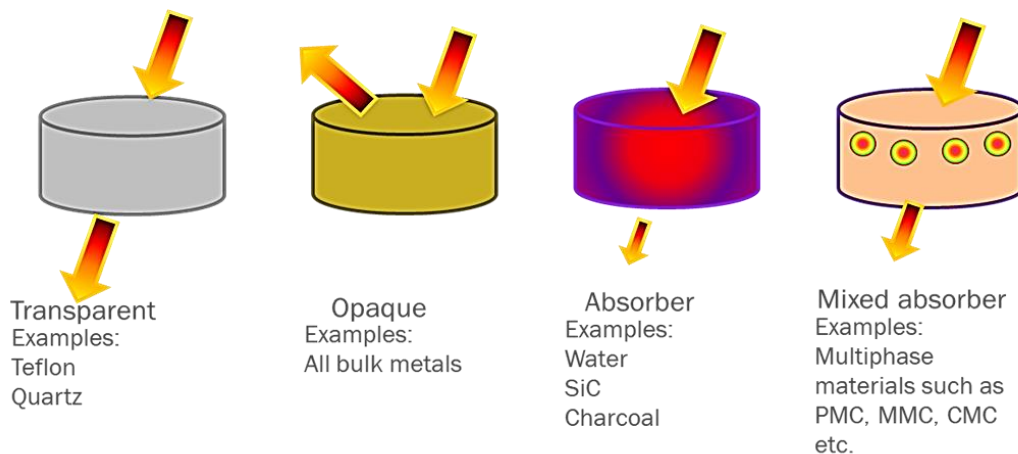


Figure 1.1 Microwave material interactions

The above Figure 1.1 demonstrates the microwave interaction with different materials used. If the material is transparent like Teflon or quartz, microwaves are not getting absorbed by these materials; it passes through it without heat transfer. On the other hand, if the material is bulk or made by multiphase materials like PMC, MMC, and CMC, due to its lower dielectric property heat transfer is difficult by microwaves. In order to achieve a proper heat transfer from microwaves, silicon carbide and charcoal are the best materials in absorbing microwaves with 99% efficiency (Bhattacharya and Basak, 2016).

The important significances of microwave processing are as follows:

- Potential to heat large sections uniformly
- Improved product quality
- Reduced cycle time
- Precise temperature control
- Environmentally clean
- Selective heating
- Rapid heating
- Reduced power consumption

A wide range of coating materials is available like metals, cermets, and ceramics. Cermets based HVOF coatings like WC-12Co, Cr₃C₂-NiCr are the general (established) coating which is used in practice from many years since they are very hard and tough. Cermet powders are often more expensive than metallic ones and are difficult to grind and polish. Use of metallic alloys with good high-temperature strength is advisable in hot environments (Zhang et al., 2014). The unique combination of cobalt-based CoMoCrSi (Tribaloy) provides high strength, toughness, hardness, superior wear and corrosion resistance from room temperature up to 800 °C, relating to existing traditional crystalline metallic materials (Bolelli and Lusvardi, 2006), (Cho et al., 2009). Few studies that explore CoMoCrSi suggest precipitation strengthening and processing of CoMoCrSi to obtain a higher fraction of hard intermetallic laves phases. This hard intermetallic laves phases, which are in the form of the amorphous microstructure (metallic glass nature) that enhances the high-temperature strength of the CoMoCrSi coating (Bolelli and Lusvardi, 2007), (Gao et al., 2010). The reinforcement of

hard phase carbides to CoMoCrSi can improve the mechanical properties and provides high-temperature sliding wear resistance. The major focus in the available literature on hard phase reinforced NiCrSiB based composite coatings includes phase evolution and tribological properties. There is a need and great demand to evaluate the performance of CoMoCrSi composite coatings in elevated temperature sliding wear environment. The present investigation aims to study the elevated temperature wear behavior of these coatings.

1.1 OBJECTIVES OF THE PRESENT INVESTIGATION

The specific objectives of the present investigation are as follows:

1. To process the CoMoCrSi feedstock to obtain higher fraction of intermetallics laves phase using High energy ball milling technique.
2. To formulate the CoMoCrSi feedstock by reinforcing chromium carbide, tungsten carbide-chromium carbide-nickel and tungsten carbide-cobalt with an improving resistance to wear.
3. To develop CoMoCrSi coatings by using High-velocity oxy-fuel (HVOF) and Flame spray methods on pure titanium grade-2 substrate.
4. To fusing of as-sprayed coatings and induce carbon into coatings through graphite sheet using microwave hybrid heating process.
5. To characterize the as-sprayed and microwave fused coatings with respect to microstructure studies, phase analysis, microhardness, and adhesion strength.
6. To investigate the sliding wear behavior of as-sprayed and microwave fused coatings at elevated temperature using a pin on disc apparatus.

1.2 THESIS OUTLINE

The whole study has been presented in 6 chapters.

Chapter-1 contains introductory remarks on wear problems, its disastrous consequences and prevention methods, and the methods used in present research.

Chapter-2 presents a critical review of the published literature relevant to the present study. A comprehensive review of the existing literature on elevated temperature wear, its characteristics, and mechanism. Various aspects for the control of this degradation by protective coatings through HVOF and flame spray process. Post heat treatment of thermally sprayed coatings and its effect on the wear performance. Also highlights the scope of processing of feedstock by milling and reinforcement of hard carbides in coatings and objectives of the present study.

Chapter-3 contains a description of experimental procedures and materials adopted for feedstock processing, deposition of coatings, fusing of as-sprayed coatings, characterization methodologies of coatings and wear studies,

Chapter 4 describes the characterization results of feedstock before and after milling and characterization of different coatings deposited by HVOF and Flame spray techniques. The post heat treatment of as-sprayed coatings by Microwave hybrid heating has been characterized. The characterization has been done using SEM/EDS studies, evaluation of porosity, microhardness, and adhesion strength have been reported and discussed with respect to the present literature.

Chapter 5 deals with the sliding wear behavior of substrate, HVOF sprayed, flame sprayed and microwave fused coatings at different temperatures i.e. 200 °C, 400 °C and 600 °C under dry conditions for 10 N and 20 N normal loads. The coefficient of friction of tested samples is calculated and also the wear rate is calculated by the volume loss method. The wear out samples is analyzed using XRD and SEM/EDS techniques. The computed results have been compiled to provide the comparative performance of the coatings.

Chapter 6 The major conclusions resulting from the current investigations are listed.

CHAPTER 2

LITERATURE REVIEW

This chapter comprises a broad review of the literature related to the thermal spray process such as HVOF and flame sprayed coatings. The studies related to post-treatment of coatings have been reviewed. High-temperature sliding wear and role of metallic and composite coatings in restricting the degradation has been described in detail.

2.1 THERMAL SPRAY PROCESS

In the last decades, technology in coating process has been improved. Thermal spray coating process is one of the most flexible and versatile techniques for spraying feedstock powders to improve the substrate surface properties such as wear and corrosion resistance. Thermal spray process which is used to produce high-quality coating by a combination of high temperature, high energy heat source, an inert spraying medium, and high-velocity particles. This spray technique is generally used for spraying of molten material onto a surface so as to provide a coating. In this, the material in the form of powder is initially heated to a high temperature by using flame and this hot material impinges on the substrate surface to develop a coating. In this technique, the substrate temperature can be maintained minimum so as to avoid metallurgical changes and distortion of the base material. The main advantage of this technique is that it can be used for spraying very high melting point materials such as tungsten and ceramics like zirconium (Bunshah, 1994). The principle of thermal spraying coating is shown in Figure 2.1.

Most commonly used coatings materials are carbides, cermets, and ceramics. Meanwhile, researchers had been trying to use the polymers as a coating material. Initially, in thermal methods, the coating materials used are in the form of powder, or wire shape is heated usually to a molten state and projected onto a receiving surface, known as a substrate. The use of thermal spraying ranges across many manufacturing processes, from the automotive industry to the space exploration industry. Any material which, can be thermally sprayed which includes metallic and non-metallic materials (metals, alloys, ceramics, cermets, and polymers) can be deposited by thermal spraying techniques (Davis, 2004, Tucker, 2013).

Thermal spraying uses two principal energy sources, the chemical energy of the combusting gases that power the flame spray torches (e.g. HVOF spraying), and electric currents providing energy for the plasma (e.g. Atmospheric Plasma spraying). Generally, these coatings appear to be chosen on the basis of their good high-temperature oxidation resistance and are mainly alloys containing high quantities of nickel and/or chromium. While it has been reported that uniformly deposited and coherent metallic coatings can provide wear protection, only a few systematic experimentations have been undertaken to quantify the erosion performance of these materials (Miguel 2003 and Hoop et al. 1999).

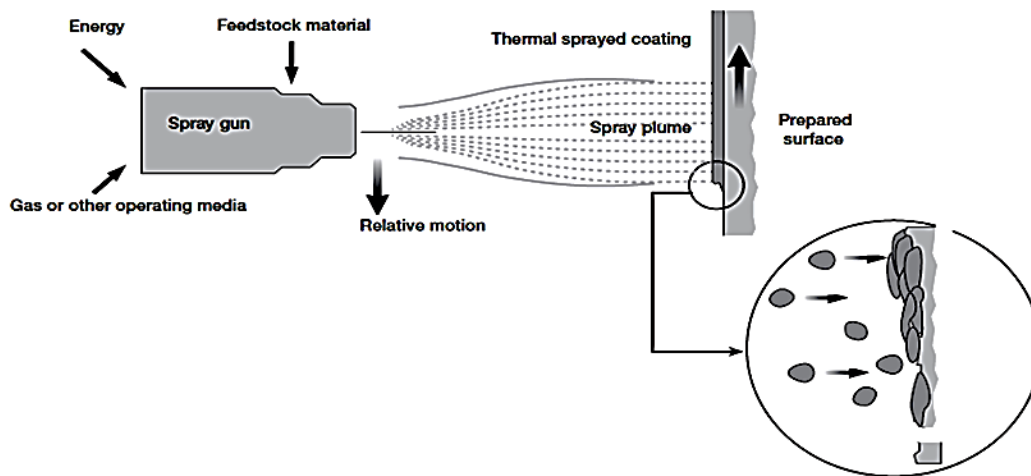


Figure 2.1 Principle of thermal spray coating (Metco 2014)

2.1.1 High-Velocity Oxy-Fuel Spray Process

HVOF spray technique is one of the best techniques for producing tribological coatings for a variety of applications, including sliding wear resistance, dry lubrication condition, and wear resistance at elevated temperatures. A particular coating material is eligible in HVOF spraying, only when it has a stable liquid phase before decomposition. HVOF employs the increase of velocity of powder material to various times the speed of sound. Coated is started once the flame temperature reaches around 3000°C (Thorpe and Richter, 1992). The force of the flame will be around 1000km/hr. The enormous shock energy coalesces the powder materials to the surface of the parts to produce a very tough coating (Gartner et al., 2006). It combines both the thermal and kinetic energies in a much effective fashion, thus they possess

excellent cohesion between adjacent lamellae, very good adhesion between coating and substrate materials (Davis, 2004, Tucker, 2013).

2.1.2 Flame Spray Process

Flame spray coating process is one of the basic and conventional methods among the thermal spray processes that have been existing from more than 10 decades (Sharma, 2014). It is a process with a low cost because of hardware simplicity and also has high production rates and process rapidity (Cano et al., 2006), (Li et al., 2002). It is easily adopted and integrated into both small and large scale industries (Harsha et al., 2007). The flame temperature in the process is dependent on the oxygen-to-fuel ratio and pressure, which effects particle melting, porosity and adhesion strength (Gonzalez et al., 2007). As the temperatures produced are low the powder may be propelled on to substrate in the molten or semi-molten state causing inclusions in coatings. Regardless of the shortcomings, the flame spray process is extensively and commercially used the technique for low melting point materials at higher spray rates (Torres et al., 2013). The temperatures and velocity of particles are low which leads to porosity, low adhesion strength, and inclusions. The adhesion strength of coating produced from flame spraying is relatively low with values ranging from 11–23 MPa (Navas et al., 2006). A coating produced from a typical as-flame spray technique exhibits a porosity of 10-20% which can be reduced to 0.3-5% by fusing because of conversion of mechanical bonds to metallurgical bonds due to fusing (Uyulgan et al., 2007), (Soveja et al., 2011).

2.2 POST COATING TREATMENT

Dejun et al., (2017) studied the influence of laser heat treatment of HVOF sprayed WC-12Co coatings subjected to wear under dry and lubricated conditions. The laser treated coatings exhibited higher adhesion strength than as-sprayed coating and also obtained lower surface roughness. The COF of dry and lubricated conditions are 0.069, and 0.052 respectively for 80 N normal load which is lower than as-sprayed coating results. The wear out samples of as-sprayed coating showed surface crack followed by fatigue failure results in abrasive wear. In case of laser treated coatings presented irregular cavities due to the spalling effect of hard surface restricts the further material loss.

Gisario et al., (2015) reported the laser post heat treatment of WC-Co/NiCr coating sprayed by HVOF process on AA 6082 T6 aluminium substrate. Results showed that laser treated

coating having a dense structure with higher microhardness, lower porosity, and surface roughness. This is achieved due to the finer structure of coatings like dendrite-like branches made by laser processing. Re-precipitation of carbides have been observed during coating post-treatment, this is the main reason for the improvement in microhardness,

Gonzalez et al., (2007) investigated the NiCrBSi coatings deposited on cast iron by flame spray and further, it is subsequently remelted by using laser and flame spray techniques. The as-sprayed coatings showed a poor bond strength, high porosity, and surface roughness. Both treated coatings are subjected to different characterization methods and sliding wear test. Results of laser treated coatings exhibited pore-free microstructure, a high adhesion strength to the substrate. In the case of flame spray, remelted coatings showed similar results but the values of microhardness are slightly higher than laser due to compressive stresses built. Also due to the high power of laser substrate distortion have noticed. The treated coatings significantly enhanced the wear resistance with no significant changes have observed in its results than as-sprayed coating and substrate.

Kong et al., (2017) examined the high temperature wear resistance of NiCrBSi coatings sprayed by HVOF on H13 mould steel, and remelted by using laser technology. The results of sliding wear of laser remelted coatings exhibited lower COF of 0.34, 0.47, and 0.36 under normal loads of 4 N, 8 N and 12 N respectively. The COF values are significantly decreased compared to as-sprayed coating due to higher microhardness and homogeneous structure. At 600°C temperature Ni, Cr, Fe subjected to oxidation results in the formation of stable oxides which improves the wear resistance.

As observed from available literature on post heat treatment of thermally sprayed coatings, it is proved to more effective to enhance the coating properties, but due to application of high power like laser process it causes serious distortion of substrate leads to change in its bulk properties and also optimizing the parameters is necessary to achieve the required output. In this regard, without optimization of process parameters with rapid processing and no significant changes of the substrate during processing is done by a technology called Microwave processing of materials. The major research finding based on microwave heating is discussed.

2.2.1 Microwave Processing of Materials

The processing of materials technology has been advanced a lot in recent years with a reduction in processing cost and time. Microwave heating process is one of the cost-effective and rapid processing technique. It is easily available, simple to operate, reduces power consumption.

In microwave processing, energy is supplied by an electromagnetic field directly to the material. This results in rapid heating throughout the material thickness with reduced thermal gradients. Volumetric heating can also reduce processing times and save energy. The microwave field and the dielectric response of a material govern its ability to heat with microwave energy. Microwave processing technique should be widely acceptable for all types of materials including metal matrix composites, ceramics, alloys, and fiber reinforced plastics (Mishra and Sharma, 2016). Microwave materials processing is emerging as a novel processing technology which is applicable to a wide variety of materials system including processing of MMC, FRP, alloys, ceramics, metals, powder metallurgy, material joining, coatings, and claddings (Lingappa et al., 2017).

2.2.2 Difference between Conventional Heating and Microwave Heating

In comparison to the conventional processes, microwave processing of materials offers better mechanical properties with reduced defects. The graphical representation of the difference between conventional heating and microwave heating is shown in Figure 2.2.

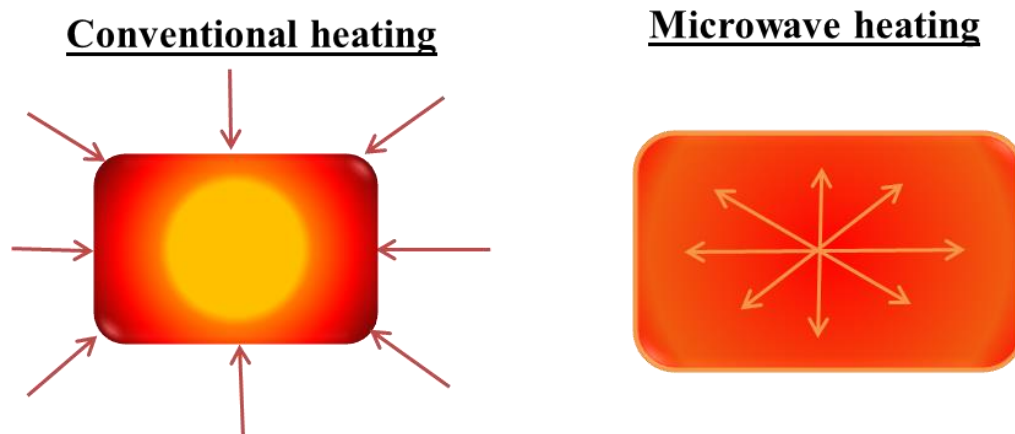


Figure 2.2 Graphical representation of conventional and microwave heating

During conventional heating, outside to inside heat transfer will take place, this leads to layer by layer heating of the component, which causes thermal gradient formation and results in the non-uniform microstructure. Whereas in case of microwave heating, inside to outside heating will take place, this provides the molecular level heating of the component, which reduces thermal gradients, results in uniform microstructure (Gupta, 2007).

The schematic representation of microwave processing of bulk metallic materials is shown in Figure 2.3. Microwaves are known to be reflected by metallic materials owing to the lower skin depth. Skin depth refers to the distance from the surface up to which microwaves penetrate into the material. Microwaves couple with metallic materials only at an elevated temperature, depending upon the characteristics of the material being processed. Such difficulty can be overcome by Microwave Hybrid Heating (MHH) (Srinath et al., 2011). There are some studies existed on cladding developed by using microwave hybrid heating and performed different tribological tests. The description of available literature on microwave processing is discussed as follows.

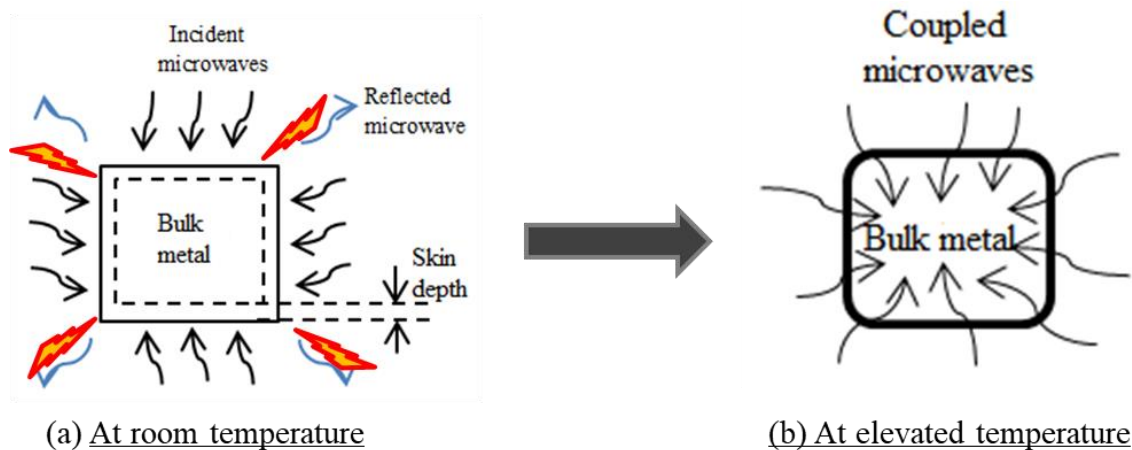


Figure 2.3 Microwave processing of bulk metallic materials

Sharma and Gupta, (2010) studied that microwave processing is an advanced novel technology, where the processing time is very rapid comparable with laser processes, thermal distortion of substrate is less, formation of residual stresses is low, high deposition rate, volumetric heating, and microwave clad microstructure exhibits almost zero interfacial

cracks, with least porosity and excellent metallurgical bonding with base metal and cost-effective process for present industrial issues with satisfying all the demands.

Gupta and Sharma, (2011) reported the formation of 2 mm thick WC-10Co-2Ni clad by microwave hybrid heating technique. The substrate metal used was austenitic stainless steel. The coating powder was treated with 2.45GHz frequency microwave at 900W power, for a period of 360 seconds. On characterization using SEM, good metallurgical bonding was noticed and cracks were not found. The developed clad had low porosity and high hardness.

Srinath et al., (2011) successfully investigated the joining of very high thermal conductivity materials like copper with a thickness of 0.5mm by using domestic microwave applicator. Results showed that clads have a uniform microstructure with excellent metallurgical bonding at the joint area having good hardness and least porosity of 0.92 %.

Gupta et al., (2014) reported the developments in the field of microwave processing and described the industrial applications of microwave processing of materials technique.

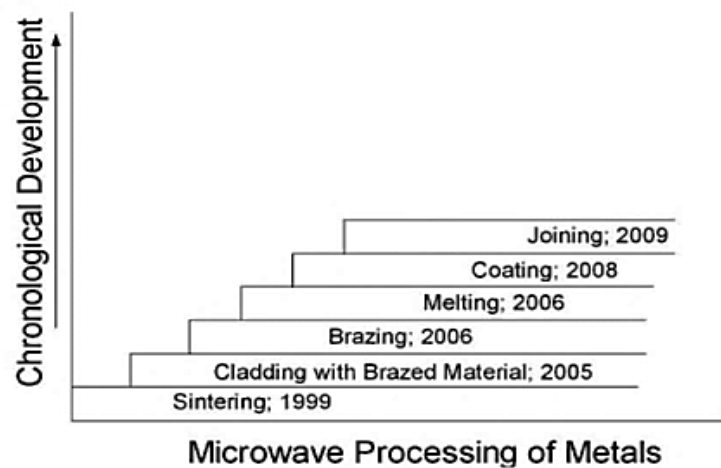


Figure 2.4 Research trends in microwave processing of metal-based materials

- Dielectric loss is the loss of energy, accompanied by heating, from a dielectric material in a varying electric field. The dielectric loss factor decides if the material is able to convert electromagnetic energy into heat energy.
- The skin depth of a material is the depth below the surface at which the value of microwave power becomes approximately 36% of the value at the surface, at a

particular frequency. This provides an idea as to how much depth of bulk material can be treated by microwave heating.

Zafar and Sharma, (2014) investigated the WC-12Co microwave clad on AISI 304 stainless steel and tested for mechanical and metallurgical properties, developed clad shows uniform distribution, indicates no presence of voids with least porosity of 0.98%. Influence of microwave hybrid heating developed clad shows very high hardness because of the presence of various carbides and excellent metallurgical bonding with the substrate.

Hebbale and Srinath, (2016) studied the microstructure of nickel-based clads through microwave irradiation on SS-304 substrate. Further various complex metal carbides and intermetallic are formed which could be the reason for the increase in hardness value.

Hebbale and Srinath, (2017) developed the cladding of cobalt on the substrate AISI 420 steel through microwave irradiation oven and tested for erosive wear behavior. The developed cladding has better metallurgical bonding with the substrate which confirms diffusion of elements and enhanced the hardness and wear resistance. Hard facing cobalt base superalloy powders are used as a material to develop a coating for many functional applications. The presence of primary intermetallic laves phases in cobalt-rich solid solution provides higher hardness and exhibits very high wear resistance.

Upadhyaya et al., (2012) have conducted a comparative study by heating W-Ni-Fe alloy in a conventional furnace as well as in a microwave furnace. The study in the conventional furnace was conducted at 1500°C while the microwave furnace worked at 2.45GHz. The authors observed that process time reduced by almost 75%, grain coarsening of W reduced and less formation of intermetallic phase in the microwave sintered compacts.

Prasad et al., (2015) developed a 500 microns thick cladding of Ni/Li₂O₃ composite on AISI 1040 steel substrate. They used microwave irradiation at a 2.45GHz frequency and 900W power. A dense, homogenous cladding was formed, as observed in the images produced by SEM. Owing to the presence of oxygen, an iron oxide layer was formed, which helps to a couple of microwaves. The microhardness test showed high hardness, which may be caused by nickel present in powder.

There are few significant kinds of literature available on the factors affecting microwave fusing of thermally sprayed coatings and inducing of carbon into coatings to obtain carbides for enhancing wear resistance (Prasad et al., 2018).

2.3 SLIDING WEAR

A simple and valuable definition of wear is “damage to a solid surface, generally involving progressive loss of material, due to relative motion between that surface and a contacting substance or substances” This definition, purposely, does not mention the mechanisms by which the wear takes place. This could be purely mechanical involving plastic deformation or brittle fracture, or it may include important chemical aspects, for instance, oxidation of a metal or hydration of a ceramic. In many applied cases, both chemical and mechanical processes play a role (Stachowiak, 2006).

2.3.1 Wear mechanisms and modes

In order to understand the tribological process in contact with solid bodies during relative motion is very difficult. Since the process combines wear, friction, and material deformation simultaneously at different working conditions. To achieve the controlled wear and friction conditions, it is necessary to analyze the properties of two contacting solid parts which involves different tribological mechanisms. In engineering design, eight different wear design rules have been introduced for selecting base materials (substrate), coating materials, and surface treatments approach made by (Matthews et al., 1993), and (Franklin and Dijkman, 1995).

In the case of coated components, when it is in contact between two surfaces four important parameters can be defined to restrict the tribological behavior. The influenced parameters are as follows:

- Coating-to-substrate hardness relationship,
- The thickness of the coating,
- Surface roughness, and
- Size and hardness of any debris in the contact which may originate from external sources or be produced by the surface wear interactions themselves.

The combinations of these four parameters result in several contact conditions characterized by specific tribological contact mechanisms. Figure 2.5 shows, schematically, 12 such very typical tribological contacts, with different mechanisms influencing friction, when a hard spherical slider moves on a coated flat surface (Holmberg, 1992). The corresponding wear mechanisms have been described in a similar way. The coating hardness and its bond with the substrate is the chief parameter. It is well known to develop soft and hard coating individually over the substrate. Soft coatings mainly used to decrease the friction owing to the work of Bowden and Tabor, (1950), whereas some of the soft coatings such as Ag and Au have subjected to wear, these coatings exhibited cracking in subsurface layer with forming higher tensile stresses and results in severe wear (Spalvins and Sliney, 1994). A hard coating on a softer substrate can decrease friction and wear by preventing ploughing both on a macro scale and a micro scale (Voevodin et al., 1995), (Voevodin et al., 1996). The hard coatings generally produce residual compressive stresses which avoid tensile forces occurring. Further decreases in friction and wear can be achieved by improving the load support that is by increasing the hardness of the substrate to inhibit deflections and ploughing due to counterpart load.

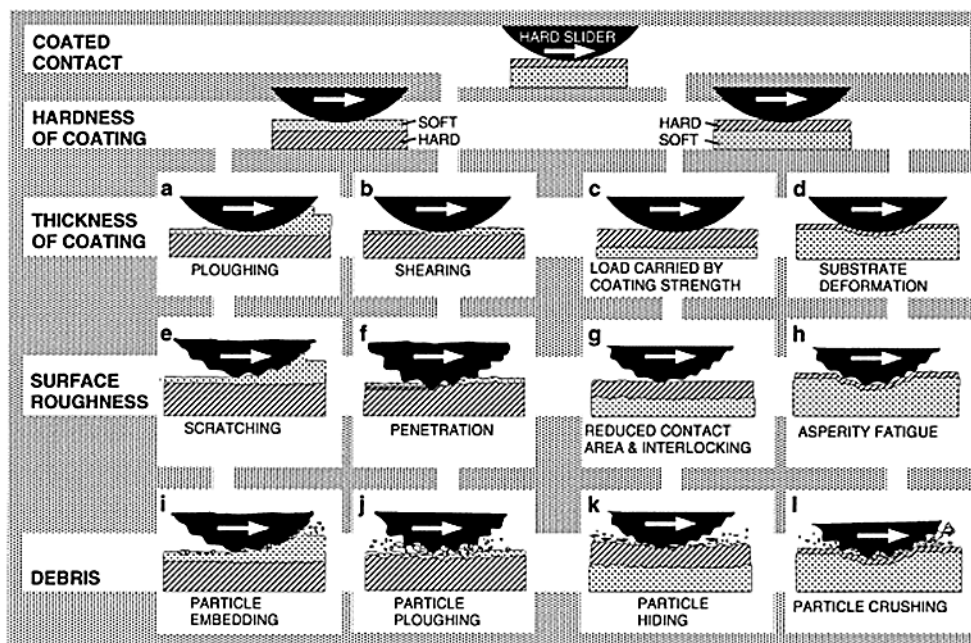


Figure 2.5 Macro mechanical contact conditions for different mechanisms which influence friction when a hard spherical slider moves on a coated flat surface (Holmberg et al., 2000)

For soft coatings the thickness of the coating influences the ploughing component of friction, while for rough surfaces it affects the degree of asperity penetration through the coating into the substrate as shown in (a), (b), (e) and (f) in Figure 2.5 (Sherbiny and Halling, 1977), (Aubert et al., 1990) and (Holmberg et al., 2000). A thick hard coating can assist a softer substrate in carrying the load and thus decrease the contact area and the friction. Thin hard coatings on soft substrates are susceptible to coating fracture because of stresses caused by substrate deformation. Rough surfaces will reduce the real contact area, although the asperities may be subject to abrasive or fatigue wear (Hayward et al., 1992), (Guu et al., 1996) and (Holmberg et al., 2000).

Loose particles or debris are quite often present in sliding contacts. They can either originate from the surrounding environment or be generated by different wear mechanisms. Their influence on friction and wear may be considered in some contact conditions, depending on the particle diameter, coating thickness and surface roughness relationship and the particle, coating, and substrate hardness relationship. Particle embedding, entrapping, hiding and crushing represent typical contact conditions involving the influence of debris, as shown in Figure 2.5 (Holmberg, 1992), (Holmberg et al., 2000).

The wear process is by which material is removed from the contact surface. Common wear mechanisms are adhesive, abrasive, fatigue and chemical wear. In actual contact, it is very common that different wear mechanisms are acting at the same time. This depends on the contact conditions and will result in a specific type of wear. A wear mode is an organization of contact type, which is characterized by a detailed kind of movement, geometry or environment. Wear modes are including sliding wear, rolling wear, fretting, erosion, impact wear and cavitation.

a) Adhesive (sliding) wear

Asperity junctions form when asperities of one surface contact with asperities of the counter surface and they might adhere to each other. The bulk of the softer asperities are separated and the material is removed due to the relative tangential motion of the surfaces. In adhesive (sliding) wear the surface material properties, protecting surface films and contaminants, play essential roles (Holmberg and Matthews, 2009).

b) Abrasive wear

In abrasive wear, the plastic deformation takes place during asperity deformation. In contacts when one of the surfaces is significantly harder than the other, abrasive wear occurs also when hard particles are introduced between two surfaces. Asperities of the harder surface are pressed into the softer surface, this results in a plastic flow of the softer material around the hard one. Ploughing and removal of softer material take place when the harder surface moves tangentially, resulting in grooves or scratches in the surface. Depending on the degree of penetration and the geometry of the harder surface, the removal of material can take different forms, such as ploughing, wedge formation or cutting.

2.3.2 Role of Coatings in Elevated Temperature Wear Environments

The coatings serve important roles at elevated temperature wear operating conditions by forming oxide films at surface level which protects the underlying part from material loss.

Peat et al., (2016) evaluated the synergistic erosion - corrosion behavior of HVOF sprayed cermet coatings. The WC-CoCr, Cr₃C₂-NiCr and Al₂O₃ coatings selected for erosion-corrosion testing deposited on EN 10025 S355 JR steel substrate. They found that Al₂O₃ coatings provide comparably poor protection under erosion-corrosion conditions. Despite Cr₃C₂-NiCr providing substantial corrosion resistance and WC-CoCr provides enhanced wear protection over the uncoated S355 substrate.

Kumar et al., (2016) investigated the erosion behavior of WC-10Co-4Cr coating on 23-8-N nitronic steel as base metal using HVOF method. It was observed that the coated substrate was superior to cast substrate and loss of material reduces because that coating has a dense and well-bonded structure with low porosity.

Susila et al., (2016) studied the effect of optimized HVOF spray parameters on erosion wear behavior of NiCrSiB/WC-Co deposited on AISI 304 stainless steel. The optimized HVOF spray parameters were oxygen flow rate, fuel flow rate; powder feed rate and standoff distance. Results showed that due to optimization of HVOF spray parameters and NiCrSiB/WC-Co provides better erosion resistance because of the presence of hard phases of WC-Co.

Sathiyamoorthy et al., (2014) investigated the dry sliding wear behavior of SiC reinforced titania coating deposited on titanium substrate using HVOF process. The average thickness of the coating was 200-250 μ m. The wear tests were carried out as per as ASTM G99-04 using a pin on disc tribometer. After the tests, the microstructural analysis was done and coated samples exhibit excellent hardness, wear resistance compared to uncoated samples the reason being low porosity, uniform distribution of splats and no significant microcracks.

Kumari et al., (2010) examined the effect of microstructure on abrasive wear behavior of thermally sprayed WC-10Co-4Cr coatings were obtained on 4140 steel substrates. The coating microstructural parameters including WC grain size, volume fraction, and binder mean free path has been quantitatively measured, and the correlation between abrasive wear behavior of coated substrates. This study showed that binder means free path of carbides (which is a function of WC grain size and volume fraction) is a very important parameter affecting the abrasion resistance of good quality coatings (containing low porosity). The lower the binder mean free path, the higher is the abrasive wear resistance offered by the coating.

Yuan et al., (2016) tested the wear behavior of high-velocity oxy-fuel (HVOF) sprayed WC-Co coatings XRD analyses suggest a small amount of decarburization of the incorporated WC phase after the composite coating deposition. The SEM microstructure showed an even distribution of WC particles at the interfaces of WC-Co splats, indicating significantly enhanced wear resistance of the coatings.

Hou et al., (2011) developed the WC-(W, Cr) 2C-Ni and WC-17Co coatings on 1Cr18Ni9Ti stainless steel substrate through HVOF method. The as-sprayed coating subjected to the ball on disk contact type wear test at temperatures of 20°C, 700°C and 800°C. WC-17Co coating exhibited a higher wear rate at 800°C due to severe oxidation results in lower mechanical properties. WC-(W, Cr) 2C-Ni coating showed a better wear resistance at all test temperatures due to the formation of NiWO₄, CrWO₄ and Cr₂WO₆ oxides which serves as a protective shield for as-sprayed coating.

Bolelli et al., (2014) investigated the comparative wear studies of WC-(W, Cr) 2C-Ni and WC-10Co-4Cr coatings deposited on stainless steel using the HVOF process. The deposited coatings subjected to sliding wear at different temperatures of 25 °C, 400 °C, 600 °C, and 750 °C. The NiWO₄+CrWO₄ oxide is formed at 750 °C which protects the underlying surface from the counter body and drastically decreased the COF compared to WC-10Co-4Cr coating. The WC-(W, Cr) 2C-Ni coating reveals better wear resistance at all tested temperatures, WC-10Co-4Cr coating experienced severe catastrophic oxidation at 750 °C results in mild wear resistance.

Wood et al., (2010) examined the CoMoCrSi sliding bearing rig at 600 °C between 2 min and 12 h at a rotation speed of 3ms⁻¹. The stable wear protective oxide layers are formed at elevated temperatures; an increase in time, wear scars tends to cover the underlying surface and avoids damage to the surface. Co and Mo oxide films are formed at the surface through the chromium oxide layer. The formation of oxides significantly improves the wear resistance of the tested material and it withstands elevated temperatures for a longer duration hence material provides better service life at higher temperatures.

Karaoglanli et al., (2017) reported the comparative studies of wear behavior of NiCrBSi/WC (50/50), NiCr (80/20), WC/Co (88/12), WC/CoCr and Cr₃C₂/NiCr (75/25) coatings sprayed on stainless steel using HVOF process. The sliding wear test is conducted at 5 N and 15 N normal loads and varying sliding speed 10 and 20 m/s. The WC/CoCr coatings exhibited lowest COF and better wear resistance than other coatings. NiCrBSi/WC coating showed a higher wear rate and COF due to plastic deformation, pull-out of splats results in abrasion wear.

Zhang et al., (2015) studied the comparative wear behavior of WC-10Co-4Cr and Cr₃C₂-25NiCr coatings deposited on H13 steel by HVOF process. Friction test is carried out by employing a ball on disk equipment at 500 °C and 600 °C. The Cr₃C₂-25NiCr coating exhibited higher friction due to the formation of crack during the test, whereas WC-10Co-4Cr showed lower COF, and wear rate.

Uyulgan et al., (2007) investigated the wear behavior of FeCr coatings on AISI 303 plain carbon steel using a flame spray process. The as-sprayed coatings are subjected to sliding wear test under dry and acidic environments. The friction coefficients of tested coatings showed high under dry conditions than acidic environments, this is mainly caused by surface roughness of as-sprayed coatings results in an increase in static and dynamic friction under dry conditions.

2.4 COBALT BASED COATINGS

The cobalt-based superalloys can be classified into three categories such as carbide-strengthened alloys (Stellite alloys), intermetallic laves phase alloys (Tribaloy alloys) and solid solution-strengthened alloys, depending on the chemical composition, mainly the content of carbon in the alloys. Stellite alloys gain their strength and hardness primarily by combining solid-solution-strengthening with carbide precipitation. Whereas tribaloy includes more quantity of tough intermetallic laves phase is dispersed in a eutectic and is mostly depending on the difficulty of carbides than the presence of intermetallic in the cobalt-rich solid solution matrix reported by Betteridge, (1982). Halstead and Rawlings, (1984) carbon percentage in tribaloy are remained less to protect the formation of carbides in preference to laves phase. The major alloying elements in the alloys are chromium (Cr), molybdenum (Mo), carbon (C) and silicon (Si). Chromium is used to increase corrosion resistance and strengthen the solid solution in cobalt-based alloys. Halstead and Rawlings, (1985) stated as the presence of molybdenum in cobalt-based alloys is to strengthen the solid solution matrix alloys to impart wear resistance by forming laves phase. Alloys with a low carbon content offer better corrosion resistance. Silicon is an important element in tribaloy to form laves phase, thus providing wear resistance of the alloys. Solid solution-strengthened alloys are primarily designed for resisting erosion-corrosion and galling, which are enriched with Cr and Mo to provide resistance to various corrosive media. Davis, (2000) reported the major difference between stellite alloys and tribaloy alloys is that the former gains wear resistance from carbides and the latter from laves phases. C. B. Cameron et.al (1975) stated the hardness of the carbides is in the range above Vickers 2000 (Hv) and that of laves phase is around 1000 - 1300 (Hv). Halstead and Rawlings, (1985) reported laves phase is hard enough to resist wear and erosion. Therefore CoMoCrSi is mostly used to resist wear under poorly

lubricated conditions. The processing of the CoMoCrSi can result in abundant laves phases of about 35 to 70 vol. %

Bolelli and Lusvarghi, (2006) tested the tribological properties of HVOF as-sprayed conditions and thermal treatments of CoMoCrSi at 200, 400, 600°C for 1 h. Intermetallic like $\text{Co}_3\text{Mo}_2\text{Si}$, Mo_2Si , Co_7Mo_6 , Co_3Mo was found. As-sprayed coating possesses low hardness, undergoes adhesive wear against 100Cr6 steel and displays a high-friction coefficient causing relevant thermal effects. The 600°C-heat treatment increases microhardness, thus preventing adhesive wear and reducing friction also enhances the bond strength of the as-sprayed coatings.

Bolelli et al., (2006) studied the Mechanical and tribological properties of electrolytic hard chrome (EHC) and HVOF-sprayed coatings. WC-17Co, WC-10Co-4Cr, and Co-28Mo-17Cr-3Si coatings of EHC and HVOF deposited on AISI 1040 substrate. EHC coatings are very tough, in fact, no cracks, HVOF-sprayed cermet coatings are harder but less tough than EHC ones. Therefore HVOF sprayed coatings provide higher wear resistance

J. Y. Cho et al., (2009) investigated the CoMoCrSi coated on Inconel 718 substrate using the HVOF process; tested the as-sprayed coating for microhardness and porosity exhibits 560-630 Hv and 1.0-2.7% respectively. Introduction of bonding layer Ni-Cr enhances the adhesion strength of the T800 coating with the substrate and thermal shock resistance. Friction and wear behaviors have been investigated by a reciprocating sliding test at both room temperature and an elevated temperature of 538 °C. Both friction coefficients (FC) and wear traces of the coating are smaller than those of IN718 substrate at both room temperature and 538 °C.

Gao et al., (2011) investigated the tribological behavior of a tin/bronze-based reinforced into CoMoCrSi coating using the HVOF process. The tribological properties such as friction and wear resistance of the coated bushing are investigated. The testing result reveals that the bushing coated with the composite exhibits superior tribological properties to the leaded tin/bronze bushing.

Lin et al., (2016) deposited the CoMoCrSi coatings deposited on Ti-6Al-4V substrates by atmospheric plasma spray method. The higher hardness under higher temperature conditions is attributed to the precipitation of Cr₃Si phase and exhibits good wear resistance. Overall, the coatings obtained in these work showed low porosity, a high hardness, and a good thermal stability at high temperatures.

Maestracci et al., (2016) deposited the composite coatings by cold spray on alumina substrates. In these studies two and three composite coatings powders were used to deposit, i.e. blends of stainless steel 316L, copper and Tribaloy T-700 powders and stainless steel and copper are considered. Two parts coating exhibits little higher porosity 1.5% whereas three parts coating provides 0.5% porosity and also a significant improvement in hardness as well as wear resistance.

Liu et al., (2005) studied the effect of post heat treatment on mechanical and tribological properties of cobalt-based T400 and T200 Tribaloy alloys sprayed by HVOF. These two alloys were heat treated in furnace conditions. The heat-treated alloys provide higher mechanical and tribological properties due to homogenous microstructure and less porosity of the alloys.

Yao et al., (2006) stated the Tribaloy alloys are considered that microstructure can hardly be modified by subsequent heat treatment after any process like casting, coating, which makes homogenous microstructure and increases properties like hardness, wear, corrosion resistance.

Houdkova et al., (2017) investigated the microstructure and wear properties of HVOF sprayed, laser re-melted and laser clad stellite 6 coatings. During spraying and laser re-melting, the FCC-to-HCP phase transformation of the Co-based solid solution is taking place and precipitation of carbides was observed and measured the mechanical values of laser re-melting has the highest microhardness than as-sprayed coatings and laser cladding. The refined microstructure of laser remelted coatings increases hardness and wear resistance.

2.5 FORMULATION OF PROBLEM

Based on the open literature review, it is found that a lot of experimental work exists in the research area of post heat treatment of thermally sprayed coatings, but the cost of the post-treatment process and processing speed, time remains too high for commercial application. In industrial applications like marine field especially the use of thermal spray coatings is high for protecting the gas turbine parts, shrouds subjected to severe high temperature and high vibrations causing of material failure. Therefore a recent and emerging technology in a surface field called microwave process can be a promising method to resolve the issues facing in thermally sprayed coatings such as porosity, interfacial cracks, voids, un-melted particles by fusing it with less time, low cost, no distortion of substrate materials (Prasad et al., 2018). After surveying a considerable amount of literature, the following gaps in the research have been identified:

- **Processing of CoMoCrSi feedstock to obtain intermetallic:** There are few studies exist on CoMoCrSi powder to obtain intermetallic fractions, which will make their widespread application financially feasible as reported by Bolelli and Lusvarghi, (2006), and J. Y. Cho et al., (2009).
- **Formulation of CoMoCrSi coating by Thermal spray method:** Various combinations of carbide powders reinforce with CoMoCrSi to enhance surface properties strategy is yet to be applied to the industrial applications (Gao et al., 2011), Lin et al., (2016).
- **Microwave fusing and diffusion of carbon to coatings:** There are fewer publications available on microwave processing of cladding and the joining of materials. There is no significant literature on the factors affecting microwave fusing of thermally sprayed coatings and inducing of carbon into coatings (Prasad et al., 2018).
- **Elevated temperature wear behavior of Microwave fused thermally sprayed coatings:** There is no literature exists on wear behavior of microwave fused coatings.

CHAPTER 3

EXPERIMENTAL PROCEDURES AND MATERIALS

The present chapter describes experimental techniques and materials adopted for the preparation of feedstock, coatings deposition and post heat treatment, characterization of the coatings, wear studies at elevated temperature.

3.1 SUBSTRATE MATERIAL

The substrate material selected for this study is commercially available pure Titanium grade-2, which is currently used in aerospace components, marine parts like heat exchangers and pipe systems for sea, condensers, and reaction vessels processing in chemical environments, tubing and tube headers in desalinization plants, and cryogenic vessels and surgical implants. The material is procured in the plate form from Mishra Dhatu Nigam Ltd. Hyderabad, India. The as-received substrate plates of size 150 mm × 150 mm × 5 mm are cut into dimensions of 12 mm × 12 mm × 5 mm using shear cutting machine for the deposition of coatings. The actual chemical composition of the as-received substrate is analyzed with the help of spectroscopy is given in Table 3.1.

Table 3.1: Chemical composition (wt %) of substrate Pure Titanium grade-2

Type of substrate	ASTM code	Composition	C	O	N	H	Fe	Ti
Pure Titanium grade 2	B 338	Nominal	0.008	0.25	0.03	0.0015	0.30	Bal
		Actual	0.07	0.44	0.007	0.0013	0.004	Bal

3.2 COATING POWDERS

The metallic cobalt based powder like CoMoCrSi (Tribaloy T400) is selected as matrix coating feedstock. The hard facing carbides such as Cr₃C₂, WC-CrC-Ni, and WC-12Co are selected as reinforcement. These coating feedstocks are available commercially and procured from Hoganas Private Limited, Belgium. The matrix feedstock and reinforcement feedstock

is mechanically blended as per mass fraction. The chemical composition and particle size of as supplied coating feedstock are listed in Table 3.2.

Table 3.2: Chemical composition and particle size of coating feedstock

Coating powder	Chemical composition (wt %)	Particle Size
CoMoCrSi (Tribaloy T400)	Co-29.5Mo-9.5Cr-2.84Si	53 to 150µm
CoMoCrSi/ Cr ₃ C ₂	70 % (Co-29.5Mo-9.5Cr-2.84Si) / 30% (Cr ₃ C ₂)	53 to 150µm 20 to 45µm
CoMoCrSi/WC- CrC-Ni	70 % (Co-29.5Mo-9.5Cr-2.84Si) / 30% (WC-27CrC-7Ni)	53 to 150µm 20 to 45µm
CoMoCrSi/WC- Co	70 % (Co-29.5Mo-9.5Cr-2.84Si) / 30% (WC-12Co)	53 to 150µm 20 to 45µm

3.3 PREPARATION OF COATING FEEDSTOCK

3.3.1 High Energy Ball Milling of CoMoCrSi Feedstock

The as-received CoMoCrSi matrix feedstock with a particle size of 53 to 150 µm is milled by using a HEBM process. The process is carried out at High Tech Ceramics Private Limited Chennai India. To obtain the higher fraction of intermetallic laves phases and also to reduce the particle size of CoMoCrSi feedstock by using HEBM process. The experimental set up used for milling is showing in Figure 3.1. The equipment consists of a milling chamber, tungsten grinding jar, and tungsten grinding media (milling balls). The jar is connected to vertical spindle rotated by a high power motor fixed at bottom of the milling chamber. The jar is having a maximum capacity of 100 grams and milling balls are having a size of 10 mm diameter. The equipment provides a facility of variable rotating speed and milling time.

During process 100 grams of CoMoCrSi feedstock is placed into jar consisting of tungsten balls and ball to powder ratio 10:1 is maintained. The milling speed of 300 rpm kept constant and varied the milling time to 5 hr. After every one hour of milling time, the samples are collected for further analysis. The process is conducted under atmospheric conditions at room temperature.

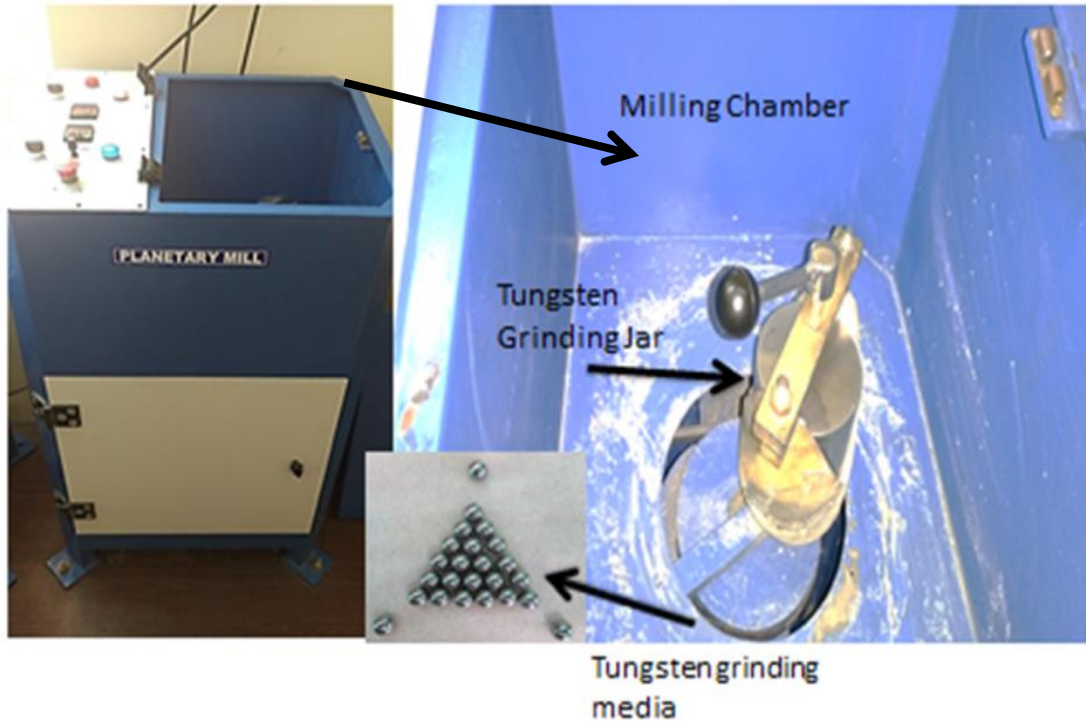


Figure 3.1 High energy ball milling facility

3.3.2 Processing of Composite Feedstock

Prior to deposition of coatings, the as-received hard facing carbides such as Cr_3C_2 , WC-CrC-Ni, and WC-12Co are reinforced individually into milled CoMoCrSi matrix feedstock and blended mechanically with a mass ratio of 70%:30%. In this study, four combinations of feedstock are prepared. The following are the prepared composite feedstock:

- a. CoMoCrSi feedstock
- b. 70 % CoMoCrSi/ 30 % Cr_3C_2
- c. 70 % CoMoCrSi/ 30 % WC-CrC-Ni
- d. 70 % CoMoCrSi/ 30 % WC-12Co

3.4 COATING TECHNIQUES

3.4.1 High-Velocity Oxy-Fuel Spraying

The feedstocks are deposited on titanium substrate through the HVOF spray process by using HIPOJET-2100 diamond jet gun equipment is shown in Figure 3.2 (Aum Techno Spray Pvt. Ltd, Bengaluru, India). The consumables used in HVOF spray process for the development of coatings are hydrogen fuel, oxygen, and nitrogen gas for combustion. These spray parameters are kept constant throughout the coating process. Substrate top surface is made rough using alumina grit blasting, cleaned with acetone and dried with high-pressure air before coating, in order to obtain better bonding between the growing coating and substrate interface.

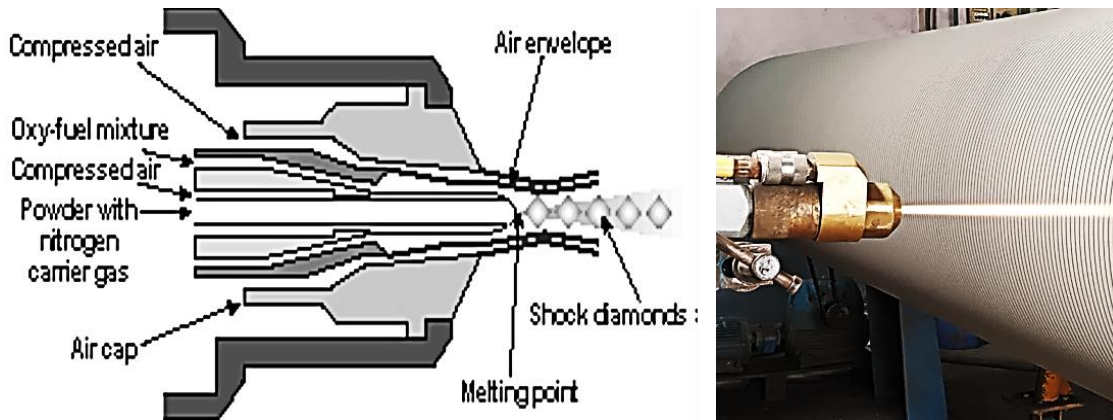


Figure 3.2 HVOF spray schematic (Yi Ding, 2009) and Experimental set up

In this study lower feed rate of powder is maintained in the HVOF coating process. The reasons are, it greatly influences particle velocity, and reduction in powder feed rate leads to a significant increase in particle velocity which increases the compressive residual stress. Higher particle velocity also helps in flattening of splats in coatings resulted in improved splat adhesion. Improved coating adhesion with increasing fuel flow and decreasing powder feed rate and standoff distance is reported previously. However higher the powder feed rate leads to the formation of tensile residual stress during cooling due to thicker layer deposition on each pass. Higher tensile residual stress produces poor splats adhesion and a decrease in coating hardness (Pukasiewicz et al., 2017), (Wang et al., 2012). Another reason is the coatings with higher the compressive residual stress leads to an increase in Vickers

microhardness and exhibits minimum porosity Murugan et al., (2014). Zhang et al., (2014) reported the effect of HVOF parameters on Fe based metallic glass coatings by maintaining the constant powder feed rate has 20 g/min. Based on the literature review spray parameters are listed in Table 3.3

Table 3.3: HVOF process parameters

Parameters	values
Oxygen (O ₂)	260 lpm
Hydrogen (H ₂)	600 lpm
Nitrogen (N ₂)	40 lpm
Powder feed rate	17 g/min
Combustion pressure	9 KPa
Spray distance	300 mm
Thickness/pass	12-15 microns

3.4.2 Flame Spraying

The prepared feedstocks are sprayed through another technique is a flame spray process using SPRAYTORCH-100 gun equipment is shown in Figure 3.3 (Aum Techno Spray Pvt. Ltd, Bengaluru, India).

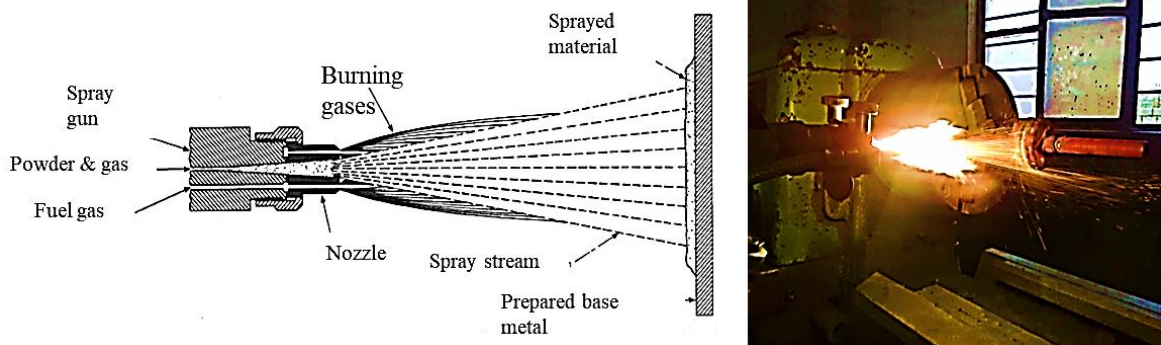


Figure 3.3 Flame spray schematic (Tucker, 1994) and Experimental set up

The oxy-acetylene used as a combustible gas which supplies heat energy to melt the feedstock. The process parameters of the flame spray system are reported in Table 3.4. The parameters are fixed constant for all the coatings. Prior to deposition of the coating, grit

blasting is performed for about 5 mins using Al_2O_3 medium on the substrate surface to create roughness. This results in enhancing bonding between coating and substrate.

Table 3.4: Flame spray parameters

Parameters	values
Oxygen flow rate	45 lpm
Fuel – acetylene	55 lpm
Powder feed rate	38 g/min
Oxygen pressure	2.1 kg/cm^2
Acetylene pressure	1.1 kg/cm^2
Spray distance	100 mm

3.5 FUSING OF AS-SPRAYED COATINGS

3.5.1 Experimental Setup

The HVOF and flame sprayed coatings are fused through the microwave hybrid heating process using a domestic microwave oven. The model of microwave equipment employed for the fusing of as-sprayed coatings (Brand: LG, Solar Dom Model No: ML-3483FRR).



Figure 3.4 Domestic microwave oven set up

The equipment mainly consists of the heating chamber which is connected to three magnetrons supplies a constant power output of 900 W. Alumina refractory blocks, glass wool, graphite sheet, and silicon carbide susceptor is used for the fusing of as-sprayed coatings. In this process power and duration for the fusing of as-sprayed coatings are kept constant. The domestic microwave oven experimental set up is shown in Figure 3.4.

3.5.2 Microwave Hybrid Heating

In order to fuse the HVOF and flame as-sprayed coatings, initially, the coated sample is positioned properly on the refractory brick; above that 1 mm thick graphite sheet (separator) having 99 % purity is placed intentionally to induce carbon. Silicon carbide (SiC) used as susceptor is placed above the graphite sheet and passes heat to coated sample by absorbing microwaves. The setup is surrounded by alumina box and it is covered with glass wool to reduce dissipation of heat. Once the setup is ready, the frequency of 2.45 GHz and 900 W of power is supplied. The SiC susceptor absorbs the high energy microwaves and supplies the same efficiency of energy to as-sprayed coating sample through a separator, which causes re-melting of as-sprayed coatings in the duration of 10 min. The remelted coating sample is allowed to cool down to atmospheric conditions gradually. The graphical representation of microwave hybrid heating is shown in Figure 3.5.

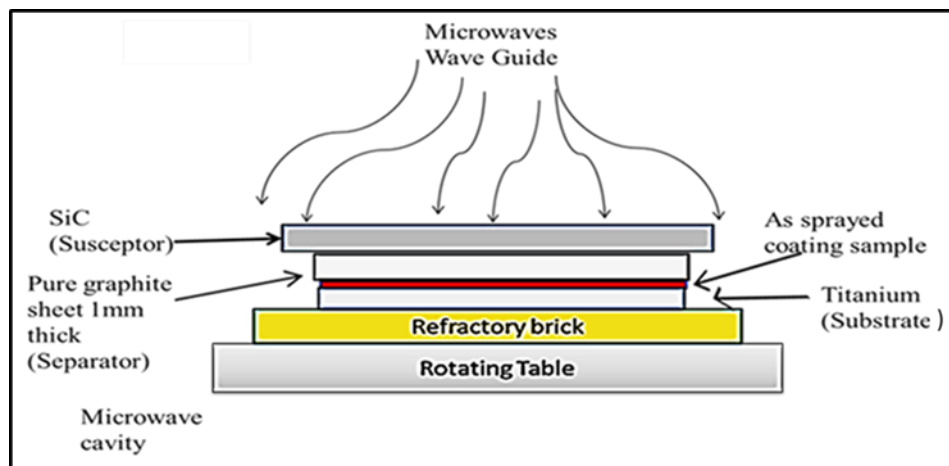


Figure 3.5 Graphical representation of microwave hybrid heating

3.6 CHARACTERISATION OF FEEDSTOCK, AS-SPRAYED COATINGS, AND FUSED COATINGS

3.6.1 Samples Preparation for Cross-Sectional Analysis

The as-sprayed and fused coating samples are cut along the cross-section with the help of metallurgical sample saw cutting machine-MS-10 (DUCOM Instruments Pvt. Ltd., Bangalore, India). The cutting speed is set to 150 rpm. The machined samples are cold mounted using acrylic powder and resin. Thereafter, the mounted samples are polished up to 2000 grit using SiC emery papers. In order to obtain a mirror finish, samples are subjected to cloth polishing by adding 0.5 μm of alumina powder suspensions. Finally, after polishing, samples are cleaned thoroughly using acetone and dried in hot air to remove any moisture.

3.6.2 Metallographic Studies

The surface morphology of feedstock, as-sprayed coatings, fused coatings and worn out samples are inspected using a scanning electron microscope. The cross-section morphology of polished as-sprayed and fused coatings samples are examined through backscattered micrographs. The elemental distributions of as-sprayed and fused coatings are studied on the surface as well as along the cross-section of coatings by employing energy dispersive spectroscopy. The SEM-EDS analysis is performed using (Model- JSM-6380LA, JEOL Japan) which is having an operating voltage of 30 kV, and maximum magnification range up to 300000.

3.6.3 X-Ray Diffraction (XRD) Analysis

X-ray diffraction analysis is carried out for feedstocks before and after the milling process, as-sprayed coatings, fused coatings and after wear tested fused coating samples. The diffraction spectrums are obtained by RIGAKU MINIFLEX-600 with CuK_α radiation and cooper filter at 20 mA under a voltage of 35 kV. The 2 degrees/minute is fixed constant for scanning speed of samples. The diffraction angle 2θ range is used and the intensities are recorded at a chart speed of 1 cm/min with $1^\circ/\text{min}$ as Goniometer speed.

3.6.4 Particle Size Analysis

Every one-hour interval of milling time, a small quantity of CoMoCrSi milled powder is collected to measure nominal particle size distributions by laser diffraction method (Cilas 1064, France) as per ASTM C1070. The density of the powder with respect to milling time is measured by the method of water immersion in accordance with standard ASTM test method designation C-135-96.

3.6.5 Measurement of As-sprayed and Fused Coatings Thickness

The thickness of as-sprayed coatings is examined during the HVOF and flame spray process using Minitest-2000 thin film thickness gauge (Elektro-Physik Koln Company, Germany, precision $\pm 1 \mu\text{m}$). The backscattered micrographs are obtained along the cross-section of as-sprayed coatings in order to validate the average thickness of as-sprayed coatings. The thickness of fused coatings is analyzed through BSE micrographs using SEM.

3.6.6 Porosity Analysis

The porosity of the as-sprayed and fused coatings are estimated along the cross-section viewed at twenty different locations of 250 X magnification using an optical microscope supported with abiovis image analyzer (ARTRAY, AT 130, Japan). The average values of porosity of 20 readings are reported.

3.6.7 Microhardness Measurement

The microhardness is assessed along the polished cross-section of as-sprayed and fused coatings using Omni-tech Vicker's tester (MVH-S-AUTO India). The test conditions used is 300 grams load applied for 10 seconds dwell time. The ten indentations are performed in different areas in a transverse direction. The mean values of measured microhardness of as-sprayed and fused coatings are reported.

3.6.8 Adhesion Strength Test

The adhesion strength of as-sprayed and fused coatings is conducted by pull off test method in according to ASTM C-633-13. FM1000 epoxy (bond strength of 10,000 psi) is used as a bonding agent. Prior to fixing of coated and uncoated counter block samples by applying

glue, grinding operation is performed on both the sample surfaces to remove any pores or voids which ensures proper distribution of glue (Cho et al., 2009). The bonded samples are cured at 150°C in the tubular furnace (Heatron Industrial Heaters, India). The test is conducted at a strain rate of 0.5 mm/min under tension mode using a Universal Testing Machine (Shimadzu hydraulic tensile machine, AG-X Plus, Japan). The ratio of maximum load to the cross-sectional area of tested samples is considered to estimate adhesion strength and mean value of four similar samples are stated.

3.7 ELEVATED TEMPERATURE SLIDING WEAR STUDIES

3.7.1 Experimental Set up

A dry sliding wear test of as-sprayed and fused coatings is conducted as per ASTM G 99-05 using a pin on disk apparatus (TR-20LE-PHM 400-CHM 600, Ducom instruments Pvt. Ltd., India). The test sample dimension of 12 × 12 × 5 mm flat surface is used. The test is conducted under a normal load of 10 and 20 N, sliding speed of 1.5 m/s and sliding distance of 3000 m is kept constant.

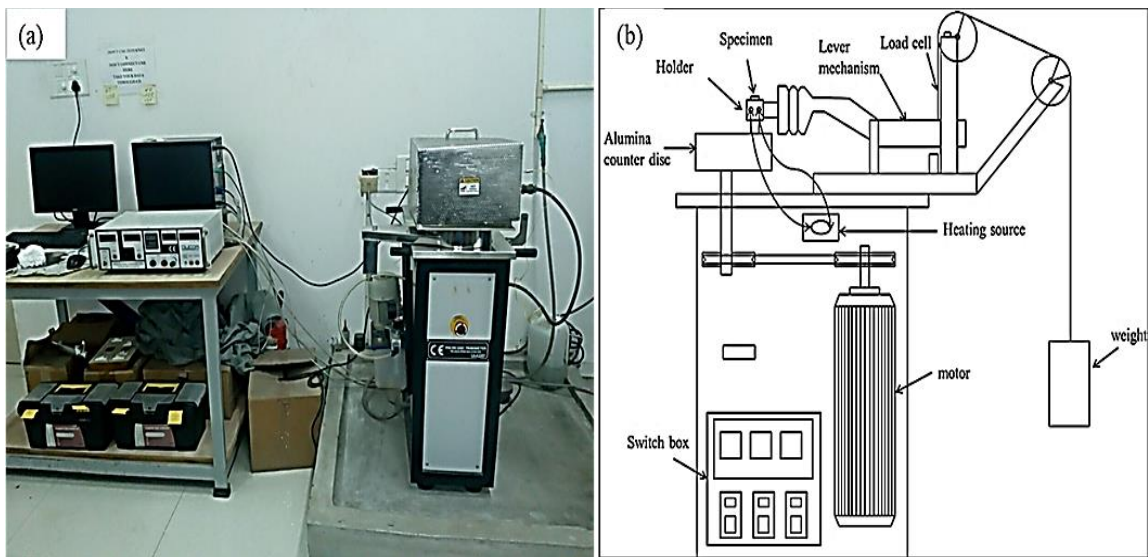


Figure 3.6 (a) Pin-on-disc experimental set up (b) graphical representation of wear test setup

The test sample is fixed rigidly in a sample holder with a specific temperature and slide against alumina counter disc. The test is conducted at temperatures of 200°C, 400°C, and 600°C. The wear debris is collected at the end of each test. Worn surfaces are examined by

SEM-EDS and phase analysis is carried out. Phase analysis of wear out fused coatings is performed by XRD technique. The pin on disc experimental setup and graphical representation of wear test setup is presented in Figure. 3.6 (a and b).

3.7.2 Wear rate Calculations

The wear rate in mm³/m of tested samples is computed by the volume loss method using equation 1.

$$W = V / (S) \dots\dots\dots (Eq 1)$$

Where ‘V’ is the wear volume loss in mm³, ‘S’ is the total sliding distance in m.

Wear volume loss in mm³ of each sample is calculated using equation 2.

$$L \times B \times H \dots\dots\dots (Eq 2)$$

Where ‘L×B’ is the total cross section area of the tested sample and ‘H’ is the height loss after the test which is obtained from computer software linked to a sliding tester.

Three tests are repeated for all the coating samples and the mean values of friction and wear rate are stated. The wear rate coefficient K in mm³/N m of tested samples is calculated using equation 3.

$$\frac{W}{LC} = k \dots\dots\dots (Eq 3)$$

Where w = wear in mm³, L = sliding length in m, C= normal load in N called Archard model. This equation is mainly used for constant sliding speed with varying load parameters (E. Fernandez et al. 2005).

CHAPTER 4

CHARACTERISATION OF FEEDSTOCK AND COATINGS

In this chapter characterization results of feedstock before and after milling are presented. The CoMoCrSi, CoMoCrSi+Cr₃C₂, CoMoCrSi+WC-CrC-Ni and CoMoCrSi+WC-12Co of HVOF, Flame sprayed coatings and Microwave fused coatings have been characterized. The characterization has been done using SEM/EDS studies, evaluation of porosity, microhardness, and adhesion strength.

4.1 MORPHOLOGY OF COATING POWDERS

The morphologies of as-received coating powders are investigated through SEM are shown in Figure 4.1. The CoMoCrSi feedstock is manufactured through gas atomization technique which is having spherically shaped particles with average dimensions of 53-150 μm before HEBM process, its morphology is shown in Figure 4.1 (a). The Cr₃C₂ powder is made by agglomerated and sintered process appeared in a spherical shape with a mean particles size of 15 to 45 μm , its morphology is shown in Figure 4.1 (b). The cermet coating powders such as WC-CrC-Ni and WC-12Co are produced by agglomeration and sintered method having a spherical structure with the average size of 15 to 45 μm as shown in Figure 4.1 (c and d). The flowing characteristics of feedstock powders are relatively good due to most particles of the nearly spherical shape.

The CoMoCrSi feedstock is subjected to a HEBM process to obtain a higher fraction of intermetallics and to reduce its particle size. The high impact energy and high milling temperature occurred during HEBM, results in an inter-diffusion of atoms in the layers of welded particles in 1 hr to 5 hr of milling time. Figure 4.2 (a-d) shows the typical morphology of particles which changes under milling operation. It is clearly observed that during HEBM, powder particle underwent flattening, cold welding, plastic deformation, and fracture in a sequence, which results in particles size reduction (Cinca et al., 2013 and Manne et al., 2017). Figure 4.3 (a-d) shows the particle morphology of HEBM CoMoCrSi powders from 2 hr to 5 hr. It is observed that powder particles changing its shape due to the impact of balls and decreasing its size with increasing milling time.

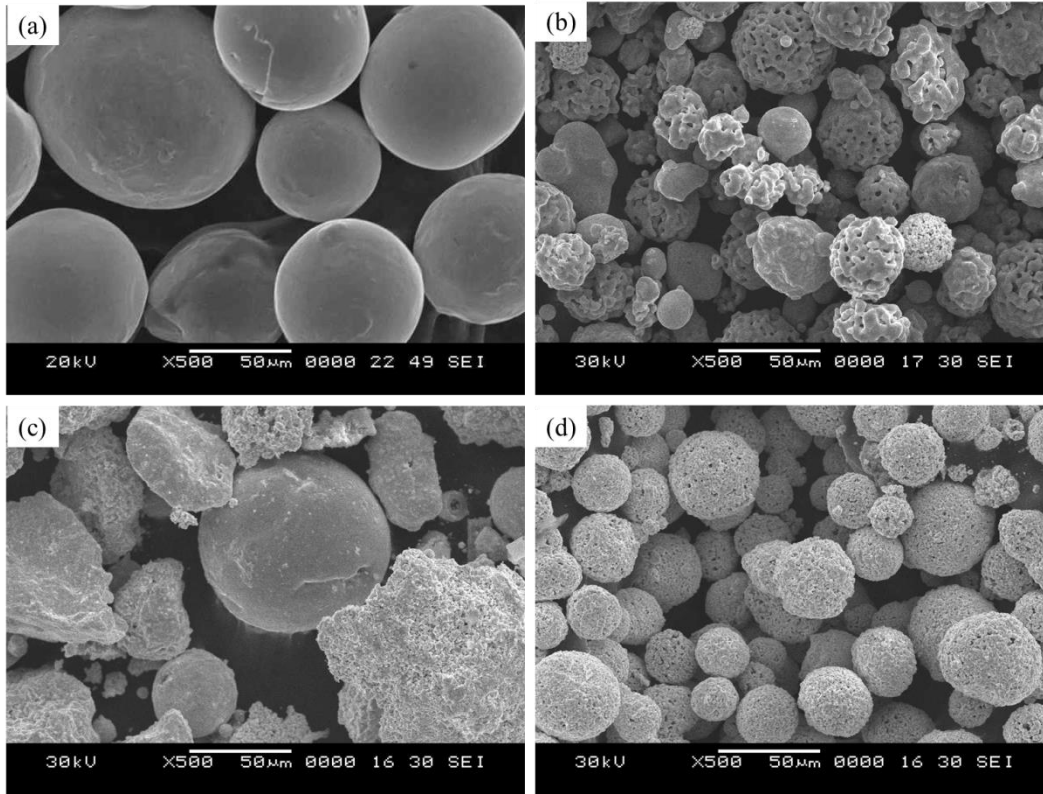


Figure 4.1 SEM morphology of coating powders before HEBM process (a) CoMoCrSi
 (b) Cr_3C_2 (c) WC-CrC-Ni (d) WC-12Co

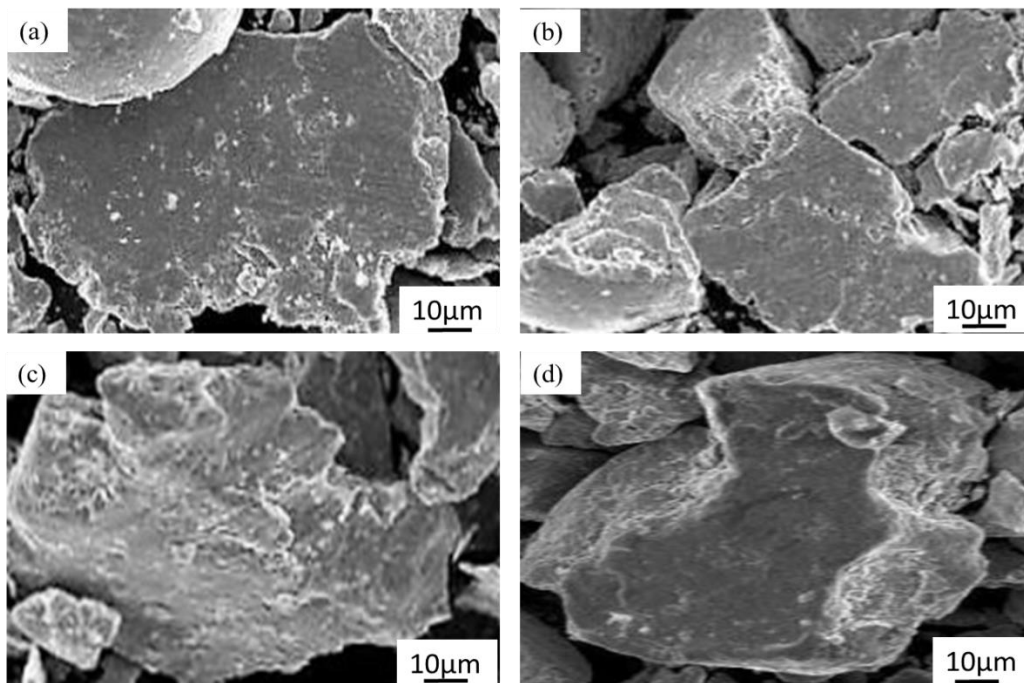


Figure 4.2 (a-d) typical morphology of CoMoCrSi powder subjected to HEBM operation

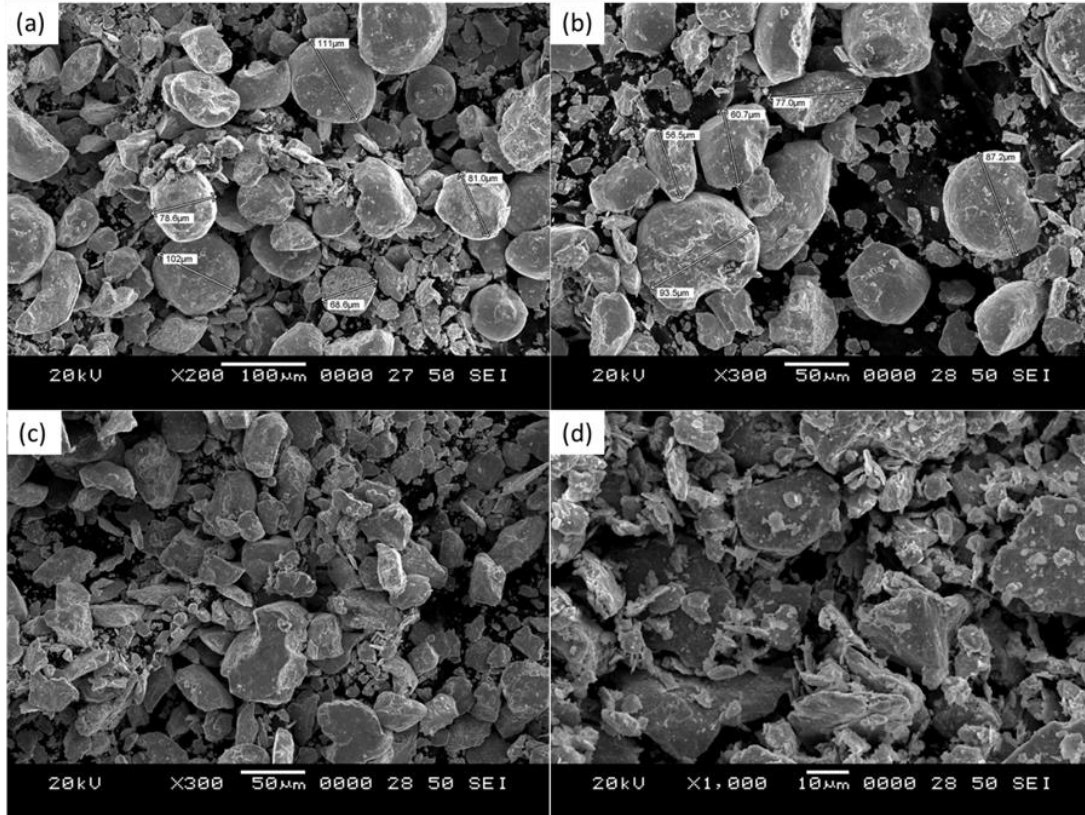


Figure 4.3 Morphology of CoMoCrSi powder milled for (a) 2 hr, (b) 3 hr (c) 4 hr and (d) 5 hr

4.2 COATING PARTICLE SIZE ANALYSIS

The particle size of CoMoCrSi milled feedstock is measured after every one hour of milling time. CoMoCrSi particle size distributions at different milling time and its density are reported in Table 4.1. Powders subjected to high impact energy for a long time leads to homogeneous composition due to the reaction between multiple particles distribution. The particle becomes finer with milling time and offered uniformity in particles size. After 5 hr of milling time, spherical particles turned into irregular shapes with a reduction in average particles size of 60.12 μm .

The presence of Mo and Cr decreases stacking fault energy, enhance the plastic deformation induced FCC to HCP crystal structure transformation in the cobalt base matrix (Kumar et al., 2006). This allotropic transformation increases the alloy's work hardening rate, which is the advantageous property of cobalt base elements for wear behavior of metals (Ozdemir et al., 2014, Zhao et al. 2014 and Tahari et al., 2014).

Table 4.1: CoMoCrSi particle size distribution and density at different milling time

Milling time, (hr)	Particle size, (μm)				Density, (g/cm^3) mean
	D (0.1)	D (0.5)	D (0.9)	Mean	
1	55.09	99.97	146.05	106.13	5.46
2	46.97	85.84	137.22	93.73	
3	34.73	75.56	122.23	79.59	
4	28.20	67.69	116.23	68.59	
5	19.96	53.93	109.23	60.12	

4.3 XRD STUDIES OF COATING POWDERS

4.3.1 Milled Coating Powder

The phase analysis of CoMoCrSi milled powder is carried out by XRD technique. Figure 4.4 shows the XRD spectrum of CoMoCrSi powder milled at different time durations. The sharp diffraction peaks characterize the crystalline nature of as received powder.

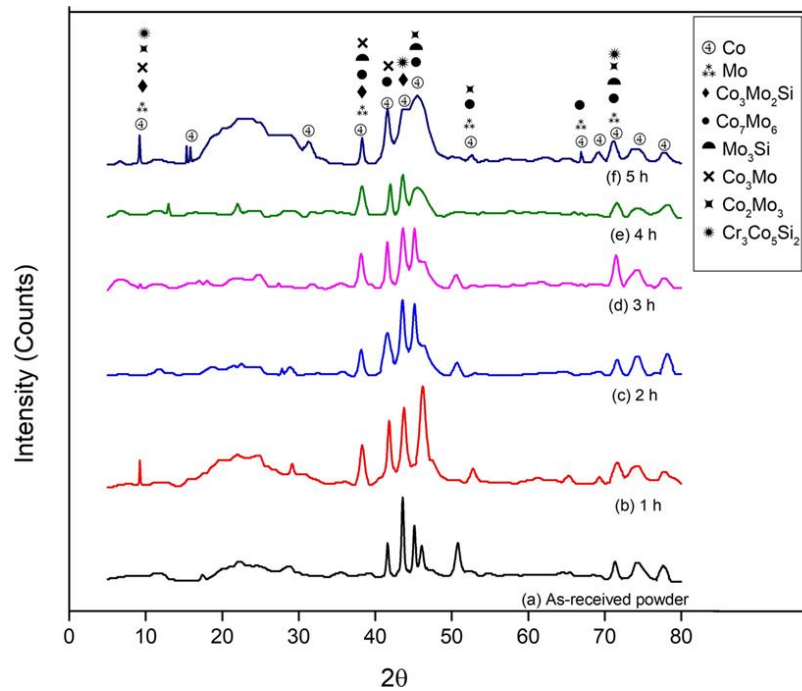


Figure 4.4 XRD pattern of milled CoMoCrSi powder at different milling time

The XRD patterns revealed the amorphous (bulk metallic glasses) structure of milled powders with respect to increasing in milling time. Broadening of peaks with a reduction in intensity is observed from 4 hours of milling shown in Figure 4.4 (e) and at 5 hours in Figure 4.4 (f). This is the indication of the formation of the amorphous phase in the milled feedstock. This can be attributed to the formation of hard intermetallic laves phases of $\text{Co}_3\text{Mo}_2\text{Si}$, Co_7Mo_6 , Mo_3Si , Co_3Mo , Co_2Mo_3 , and $\text{Cr}_3\text{Co}_5\text{Si}_2$, present in higher fraction due to atomic diffusion of active elements of the coating (Bolelli and Lusvarghi, 2006).

4.3.2 Composite Coating Powders

The milled CoMoCrSi feedstock is blended with different carbides such as Cr_3C_2 , WC-CrC-Ni, and WC-12Co as per mass ratio. The XRD pattern of CoMoCrSi+ Cr_3C_2 composite feedstock is represented in Figure 4.5. The pattern showed high intensities with reduction of broadening in peaks, after reinforcement of Cr_3C_2 powder the milled feedstock turned into crystalline nature with retaining original phases as exhibited by CoMoCrSi feedstock showed in Figure 4.4.

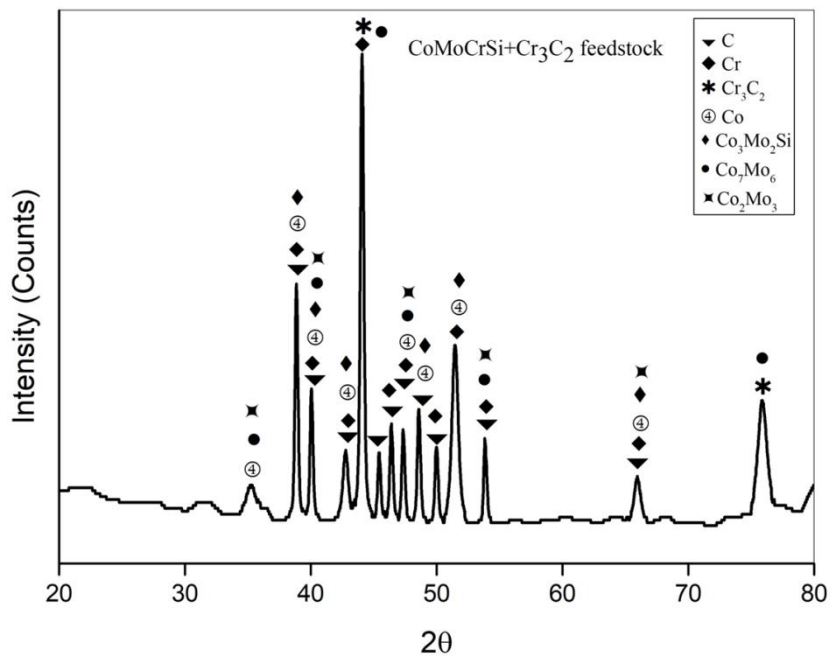


Figure 4.5 XRD pattern of CoMoCrSi+ Cr_3C_2 composite feedstock

The XRD spectrums of CoMoCrSi+WC-CrC-Ni and CoMoCrSi+WC-12Co composite feedstock powders are represented in Figure 4.6. After HEBM process, intermetallic laves

phases are identified. The phases are $\text{Co}_3\text{Mo}_2\text{Si}$, Co_7Mo_6 , and Co_2Mo_3 which are amorphous in nature (metallic glass structure) shown in Figure 4.4. Whereas due to the addition of WC powders to processed feedstock it converts into crystalline nature but retained the same phases as presented in CoMoCrSi processed feedstock. The coating powders CoMoCrSi+WC-CrC-Ni and CoMoCrSi+WC-12Co exhibit strong carbide phases of Cr_3C_2 , SiC, Co_3C , and WC. Ni_3C phase is identified in CoMoCrSi+WC-CrC-Ni feedstock which helps to improve coating hardness.

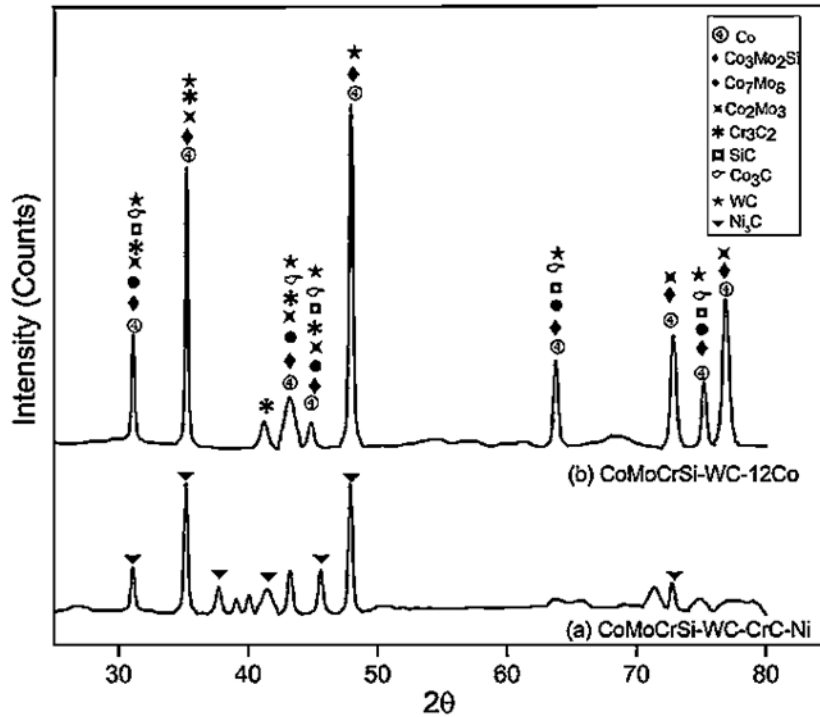


Figure 4.6 XRD patterns of (a) CoMoCrSi+WC-CrC-Ni (b) CoMoCrSi+WC-12Co composite feedstock

4.4 MEASUREMENT OF COATINGS THICKNESS

The thickness of as-deposited coatings by HVOF and flame spray process and fused coatings are assessed from BSE micrographs along the cross-section of coatings obtained from SEM. The average thickness of each coating is given in Table 4.2. The result indicates that after fusing of the thickness of as-sprayed coatings are significantly increased due to inter-diffusion of atoms at the substrate-interface region. The BSE micrographs of these as-sprayed and fused samples along the cross-section are presented in further sections.

Table 4.2: Average coatings thickness

Type of coating	Thickness, (μm)			
	HVOF sprayed coatings	Microwave fused HVOF coatings	Flame sprayed coatings	Microwave fused Flame sprayed coatings
CoMoCrSi	235	255	270	280
CoMoCrSi+Cr ₂ C ₃	250	264	210	225
CoMoCrSi+WC-CrC-Ni	160	185	210	224
CoMoCrSi+WC-12Co	240	260	176	192

4.5 HVOF SPRAYED AND MICROWAVE FUSED CoMoCrSi COATINGS

4.5.1 Surface SEM and EDS Analysis

The surface morphology of HVOF sprayed CoMoCrSi coatings and its EDS results are shown in Figure 4.7 (a and b). The morphology presents the lamellar structure of hard intermetallic laves phases present in a eutectic cobalt matrix. The presence of unmelted/semi-melted particles on the surface is observed and also no formation of oxide stringers in Figure 4.7 (a). This results in the formation of voids in between the two atoms lead to an increase in porosity of coatings. The surface roughness (Ra) is found to be 6.23 μm . The EDS analysis of as-sprayed CoMoCrSi coating shown in Figure 4.7 (b) reveals the presence of Co-rich phases and retains the phases of the milled powders. The surface morphology of the fused CoMoCrSi coating and corresponding EDS results are presented in Figure 4.8 (a and b). As observed from Figure 4.8 (a) fused coating surface exhibits uniform melting which eliminates all partial and unmelted particles presented at as-sprayed coating. Also due to remelting of as-sprayed coating surface exhibits homogeneous structure. The surface roughness of the fused coating is 3.15 μm . The presence of C and O on the surface as identified by EDS analysis in Figure 4.8 (b) indicates the formation of oxides and carbides during microwave remelting. Formation of metallurgical bonding by diffusion of titanium

element towards coating region is confirmed by EDS analysis. Graphite is used as a separator in order to introduce carbon on the surface, which acts as a self-lubricating agent as well as form harder carbides.

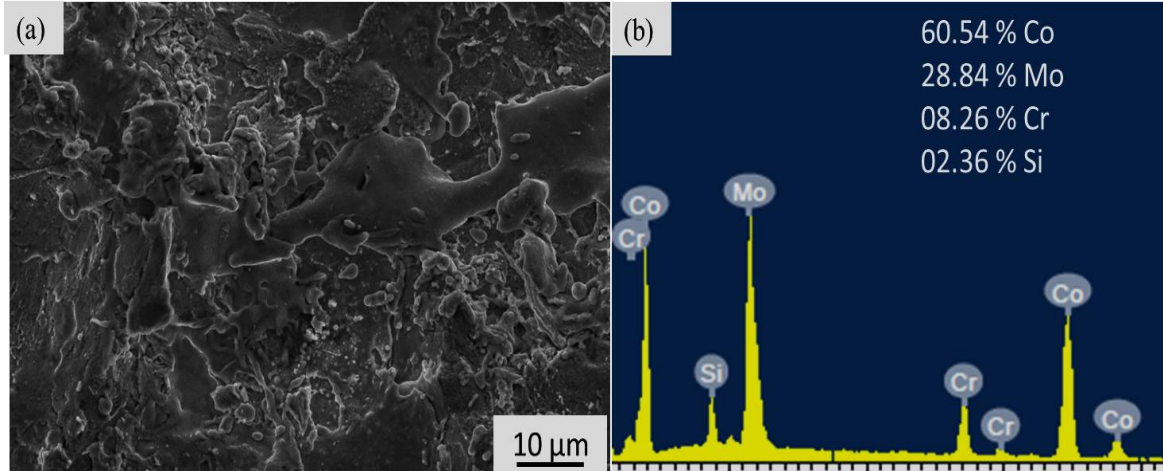


Figure 4.7 HVOF spray CoMoCrSi coating (a) SEM surface morphology and (b) EDS analysis

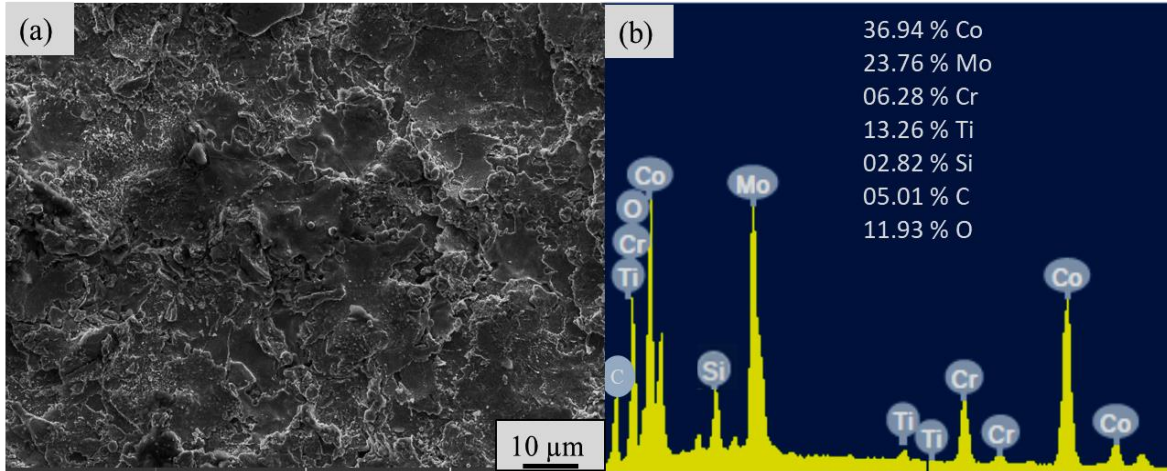


Figure 4.8 Fused CoMoCrSi coating (a) SEM surface morphology and (b) EDS analysis

4.5.2 Cross-Sectional Microstructure and Elemental Mapping

Figure 4.9 (a and b) shows the cross-sectional morphology of HVOF sprayed and fused coatings. Figure (4.9 a) shows the SEM micrograph of the as-sprayed coating along the cross-section shows the laminar and uniform structure, bonded well with the substrate. As-

sprayed coating produces major cracks and voids which is clearly visible from morphology. The white patches are observed in Figure 4.9 (a) represents the chromium and coexist with silicon are distributed around cobalt and molybdenum elements.

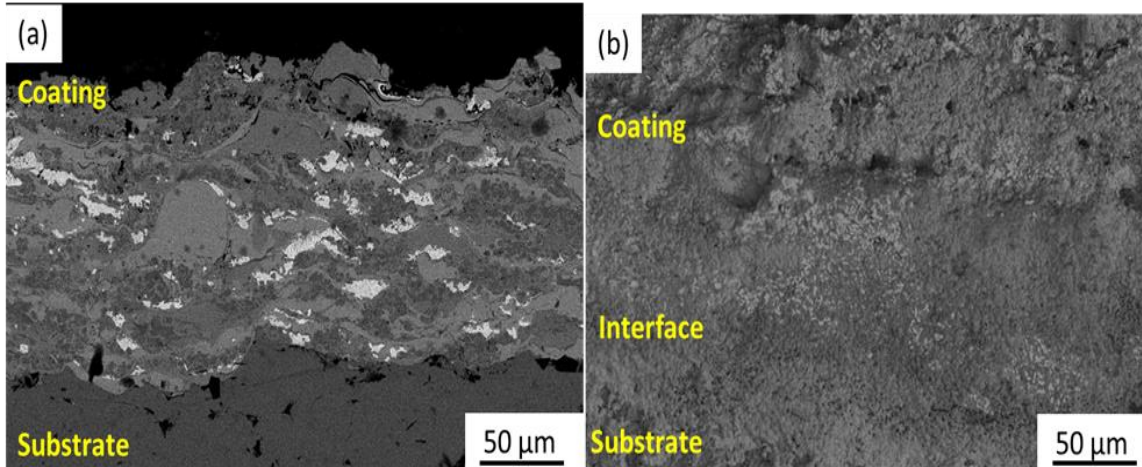


Figure 4.9 SEM micrographs along the cross-section of CoMoCrSi coatings (a) HVOF sprayed (b) microwave fused

SEM micrograph along the cross-section of microwave fused coating (Figure 4.9b) shows a homogeneous structure with fewer defects in the fused region. The remelted coatings display sound metallurgical bonding by inter-diffusion of elements across the interface of coating and substrate. The titanium substrate is easily penetrated into the coating region during diffusion process due to its lightweight compared to coating elements, so cobalt, molybdenum, chromium, and silicon are the less diffused elements at an interface area.

X-ray elemental mapping of the as-sprayed coating presents in Figure 4.10. It displays the existence of major constituent elements of cobalt, molybdenum, chromium, and silicon which is properly distributed throughout the coating. There is no presence of oxides in coating due to the high deposition rate of coating and solidified rapidly. The X-ray elemental mapping of the fused coating presents in (Figure 4.11) which confirms the existence of major constituent elements of cobalt, molybdenum, chromium, silicon along with titanium and carbon properly distributed throughout the fused coating. The diffusion of Ti into the coating is clearly observed and coexists with carbon, implies the formation of TiC. It leads to metallurgical bonding.

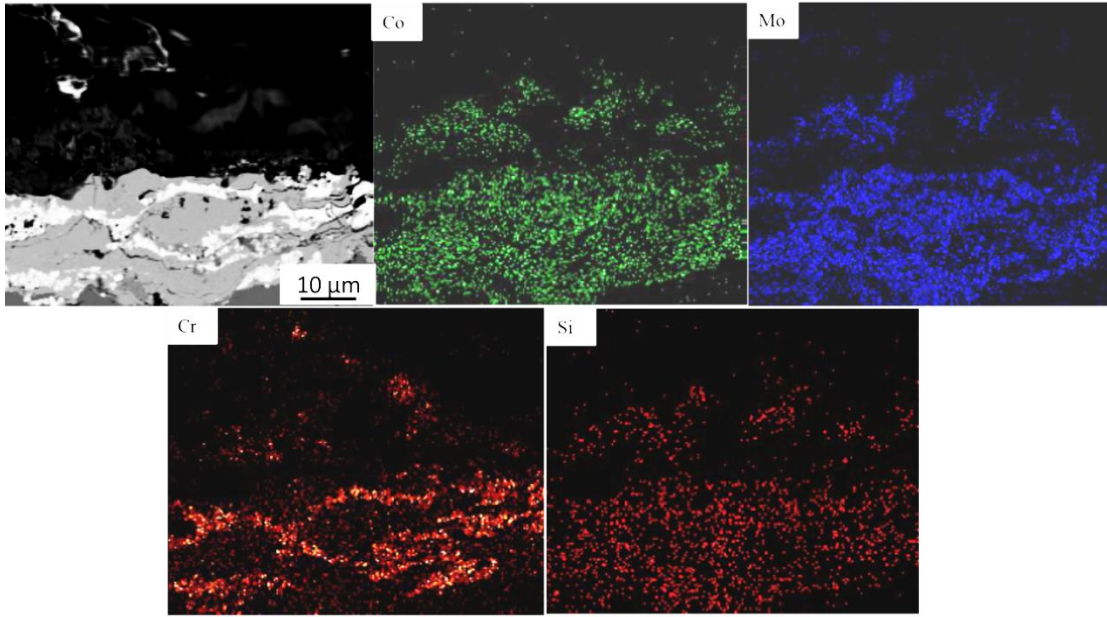


Figure 4.10 Elemental X-ray mapping of HVOF sprayed CoMoCrSi coating

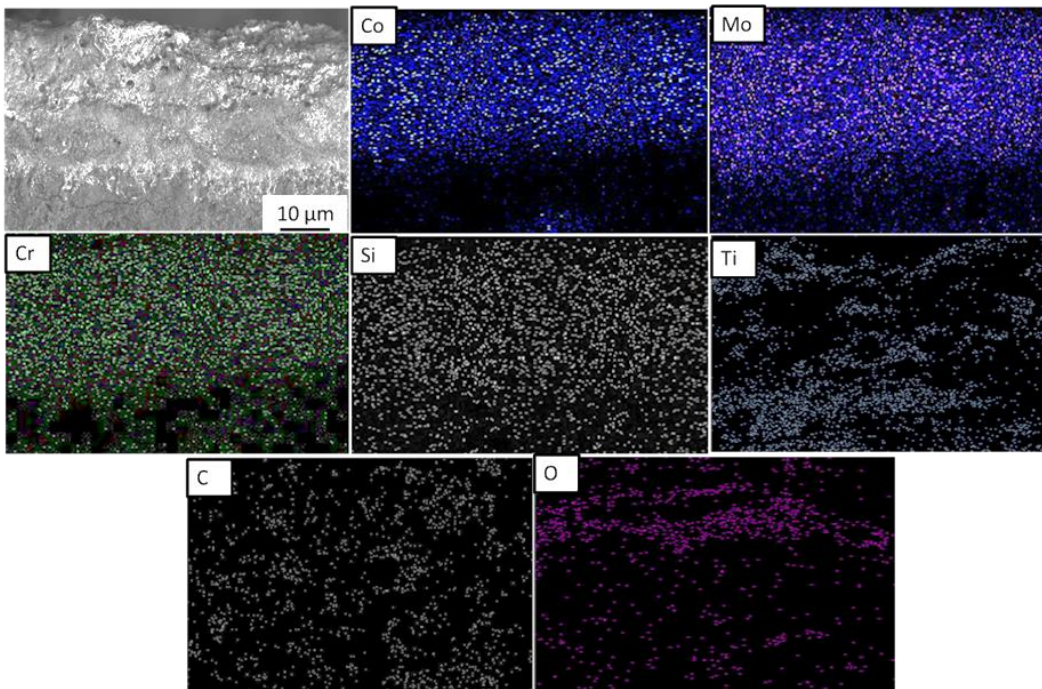


Figure 4.11 Elemental X-ray mapping of microwave fused CoMoCrSi coating

4.5.3 X-Ray Diffraction Studies

XRD pattern of HVOF sprayed CoMoCrSi coating shown in Figure 4.12 (a) confirms the presence of hard intermetallic laves phases in a eutectic cobalt matrix. The XRD pattern

indexed to $\text{Co}_3\text{Mo}_2\text{Si}$, Co_7Mo_6 , Mo_3Si , and Co_3C indicate no significant phase changes occurred during HVOF spraying. The XRD patterns of CoMoCrSi milled powder at 5 hr (Figure 4.4f) and HVOF sprayed CoMoCrSi coating (Figure 4.12a) are similar. The broadening of peaks of the as-sprayed coating at 2θ values of 38° to 49° indicates the formation of amorphous laves phases.

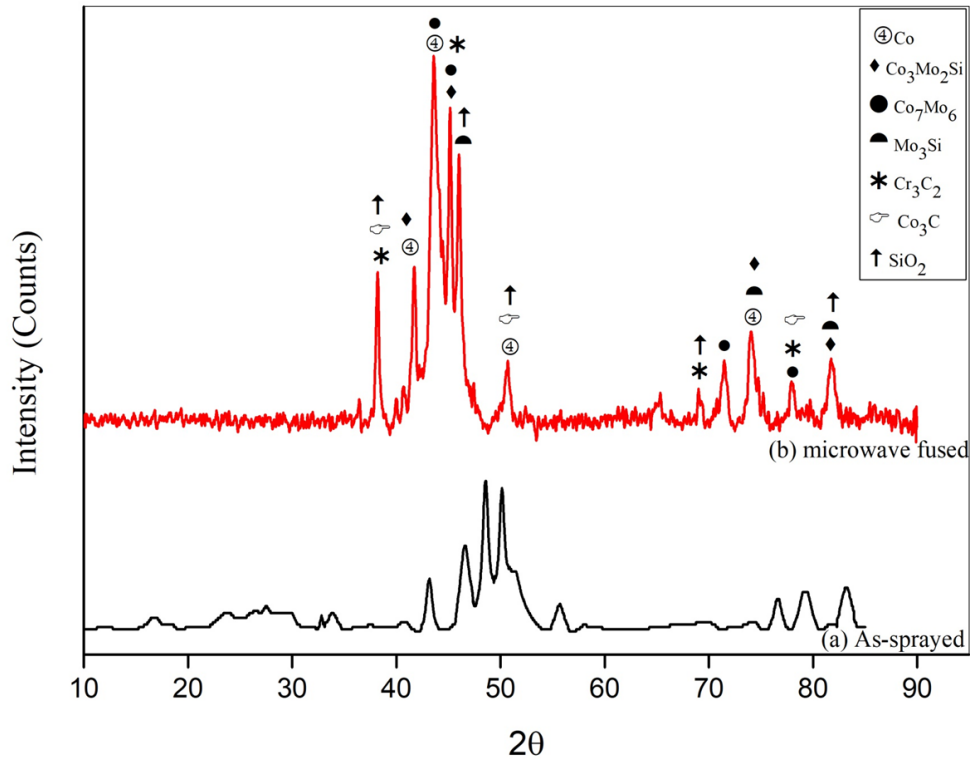


Figure 4.12 XRD patterns of CoMoCrSi coatings (a) HVOF sprayed (b) microwave fused

XRD pattern of the fused coating is shown in Figure 4.12 (b). During microwave remelting, titanium and carbon are diffused into the coating from the substrate and graphite separator respectively. Microwave fused coating shows the presence of peaks indexed to Cr_3C_2 , and Co_3C . As the microwave process is carried out in an open atmosphere, minor intensity peak of SiO_2 is identified. The oxides and carbide in the coating microstructure act as strengtheners. The intermetallic laves phases as identified in the coating powder and as-sprayed coatings shown in Figure 4.12 (a and b) are retained after microwave remelting. In the process of microwave remelting, graphite sheet is used as a separator, placed between as-sprayed coating and susceptor which helps to induce carbon into the as-sprayed coating.

The chromium present in the coating reacts with carbon to form carbides. According to the values of Gibbs free energy, the sequence of carbide formation is Cr_{23}C_6 , Cr_7C_3 , and Cr_3C_2 . However, Cr_{23}C_6 and Cr_7C_3 are not identified in the XRD analysis (Figure 4.12b) and high-intensity peaks are indexed to Cr_3C_2 . This may be attributed to the difference in phase constituent and complicated temperature distribution in the molten pool as investigated by (Kaiming et al., 2018).

4.6 HVOF SPRAYED AND MICROWAVE FUSED CoMoCrSi+Cr₂C₃ COMPOSITE COATINGS

4.6.1 Surface SEM and EDS Analysis

The surface micrograph of HVOF sprayed CoMoCrSi+Cr₂C₃ composite coating and its EDS results are shown in Figure 4.13 (a and b). The presence of microcracks and unmelted/partial melted particles on the coating surface are noticed. This represents the formation of a heterogeneous structure. The surface roughness of the as-sprayed coating is 8.23 μm . The result of the EDS of as-coated shows the presence of all the feedstock elements with a major percentage of Co and Cr elements as depicted in Figure 4.13(b).

CoMoCrSi+Cr₂C₃ fused coating surface morphology is shown in Figure 4.14. The rapid cooling of the microwave process which results in the microstructure of the fused CoMoCrSi+Cr₂C₃ composite coating is much finer than that of the conventional post-heat treatment processes. The carbides and intermetallic compounds are randomly distributed in a cobalt-rich solid solution, results in a homogeneous structure as shown in Figure 4.14. The surface roughness of microwave fused coating is 3.14 μm . The elemental composition of the fused coating is done on the same surface area showing in (Figure 4.14) it is evident that the carbon content is drastically increased compared to an as-sprayed coating which is mainly from graphite sheet during remelting. Also, titanium and oxide phases with minor percentages have been detected on the fused coating surface.

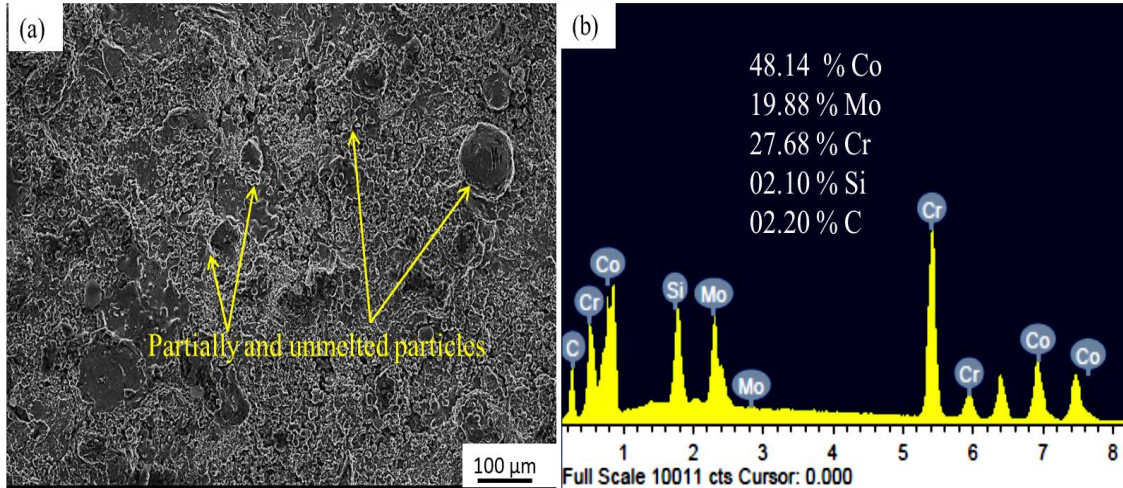


Figure 4.13 HVOF spray CoMoCrSi+Cr₂C₃ composite coating (a) SEM surface morphology and (b) EDS analysis

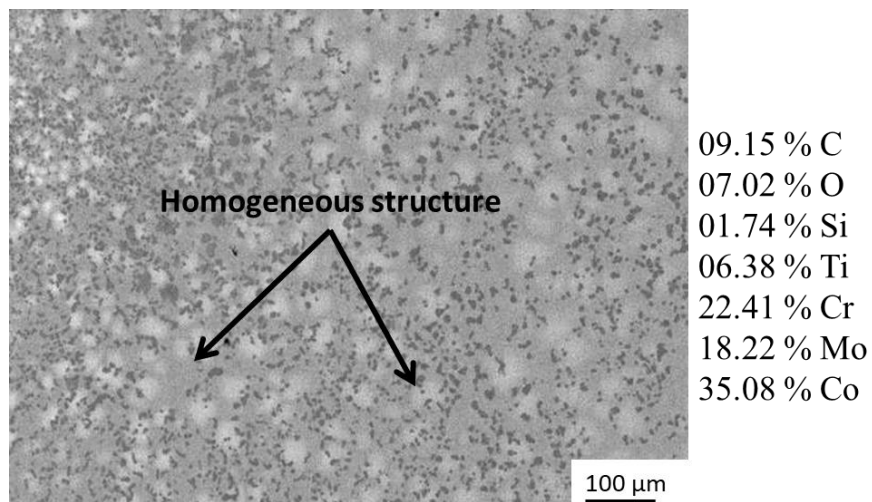


Figure 4.14 SEM surface micrograph of microwave fused CoMoCrSi+Cr₂C₃ composite coating

4.6.2 Cross Sectional Microstructure and Elemental Mapping

The SEM images of as-coated and microwave fused CoMoCrSi+Cr₃C₂ coatings along the cross-section, shown in Figure 4.15 (a and b) respectively. As observed in Figure 4.15 (a) the microstructure of the as-sprayed coating through cross-section presents various characteristics, such as unmelted and partially melted particles, mechanical discontinuities, interfacial cracks, and porosity. It also indicates that coating microstructural features of light

gray color reveals the Co-rich element with white patches of Cr present along the grain boundaries of the matrix constituent element. There are no cracks observed along the interface indicating strong bonding between coating and substrate.

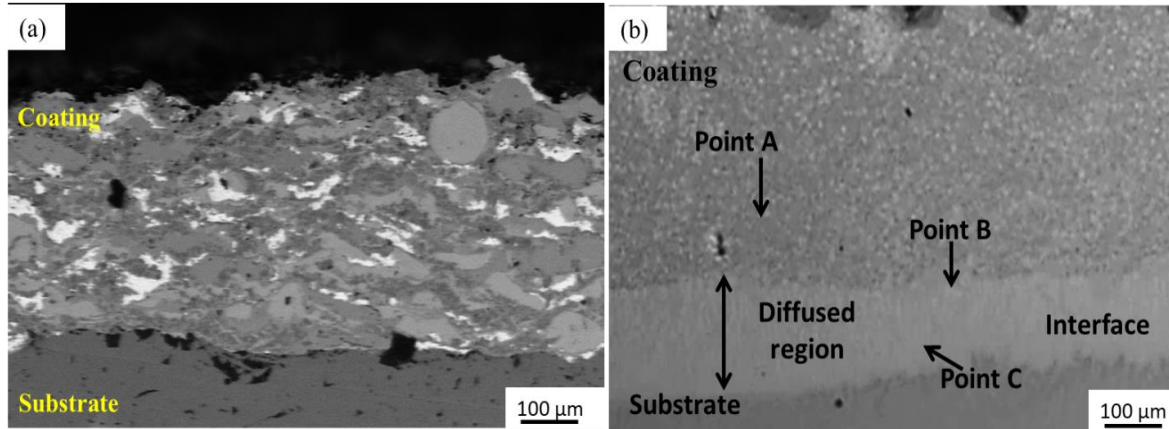


Figure 4.15 SEM micrographs along the cross-section of CoMoCrSi+Cr₃C₂ coatings (a) HVOF sprayed (b) Microwave fused

Table 4.3 EDS results of microwave fused CoMoCrSi+Cr₃C₂ composite coating for selected points representing in Figure 4.15 (b)

Element, wt %	Positions		
	A	B	C
O	01.12	01.87	02.59
Ti	-	12.72	35.46
C	04.88	05.32	05.19
Si	02.82	02.22	01.01
Cr	21.28	19.68	10.94
Mo	23.76	17.25	13.45
Co	46.14	40.94	31.36

The microwave heating process shows a positive effect on the characteristics of the HVOF-sprayed coating. It can be seen in Figure 4.15 (b) that fusing of the as-sprayed coating has dense and homogeneous microstructure. In the duration of 10 minutes, microwave re-melts the unmelted and partially melted particles in the as-sprayed coating. The micro-cracks, pores, voids, and lamellar structure are removed, and the inter-diffusion of elements of coating and substrate is observed along the interface region. Metallurgical bonding is formed between the substrate and coating which leads to the improvement of the adhesion to the

substrate. The amount of titanium is diffused into the coating region is quantified by EDS analysis. The EDS analysis of microwave fused coating points marked (Figure 4.15b) is taken at three different points at a distance of 50 μm each, and the readings are listed in Table 4.3. The EDS result confirms the chemical composition of enriched titanium substrate elements with some amount of oxide due to its diffusion in the fused coating.

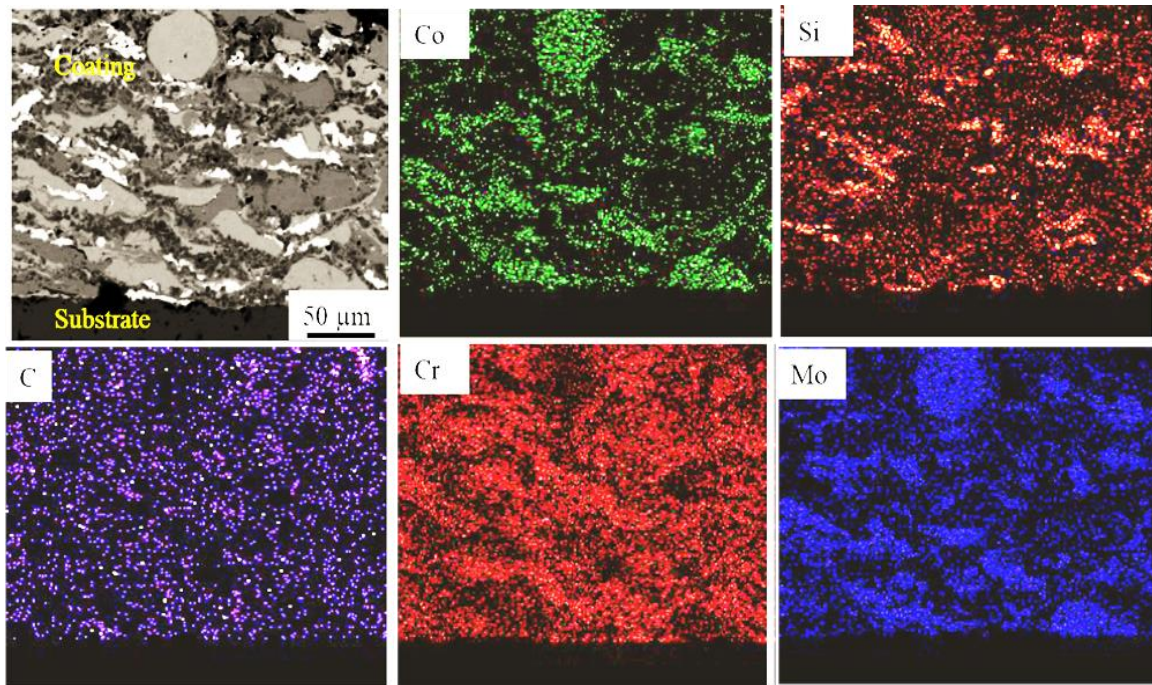


Figure 4.16 Elemental X-ray mapping of HVOF sprayed $\text{CoMoCrSi}+\text{Cr}_3\text{C}_2$ composite coating

The X-ray elemental mapping of HVOF sprayed and fused $\text{CoMoCrSi}+\text{Cr}_3\text{C}_2$ composite coatings along the cross-section are presented in Figure 4.16 and Figure 4.17 respectively. The as-sprayed coating result confirms the uniform distribution of major feedstock elements through the coating area as shown in Figure 4.15. It clearly shows distinct splats enriched with cobalt and molybdenum. Chromium carbide is distributed over the coating uniformly.

The fused coating reveals the uniform distribution of the coating and the diffusion of the substrate element to the coating region is shown in Figure 4.17. This indicates that titanium is enriched with cobalt, molybdenum, and chromium. The diffusion region or diffused band is clearly visible in mapping results. The number of valence electrons of titanium substrate is more than coating elements so diffusion of titanium is more rapid at interface location.

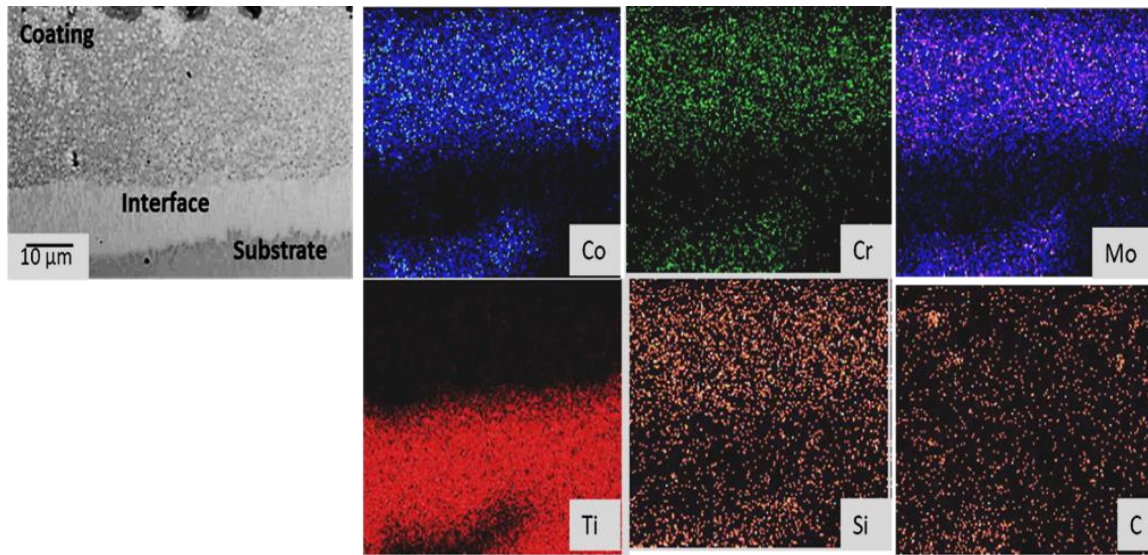


Figure 4.17 Elemental X-ray mapping of microwave fused CoMoCrSi+Cr₃C₂ composite coating

4.6.3 X-Ray Diffraction Studies

The XRD patterns of CoMoCrSi+Cr₃C₂ feedstock and as-sprayed coatings are similarly presented in Figure 4.18 (a and b). XRD of feedstock confirms the intermetallic laves phases and exhibits an amorphous structure (bulk metallic glass). After the HEBM process, the amorphous phases formed in CoMoCrSi feedstock are Co₃Mo₂Si, Co₇Mo₆, Co₃Mo, and Co₂Mo₃. No changes have been observed in the as-sprayed coating pattern. Some crystalline phases are identifiable; particularly, the CoMoCrSi+Cr₃C₂ as-sprayed coating containing Cr₃C₂, Co₃C, and a Co–Mo–Cr solid solution with an FCC lattice. It is also observed that no oxide phases are formed in as-sprayed coatings (Figure 4.18b). Figure 4.18 (c) demonstrates the XRD pattern of microwave fused CoMoCrSi+Cr₃C₂ coating. After microwave fusing, it is observed that the coating retained intermetallic laves phases as found in as-sprayed coating. Carbon is induced into the coating from the graphite sheet during the microwave process, by which a new rich Co₃C phase is formed. Although the microwave process is carried out at atmospheric conditions results in SiO₂ oxide phase is formed. Presence of carbides and oxides in the coating microstructure act as strengtheners.

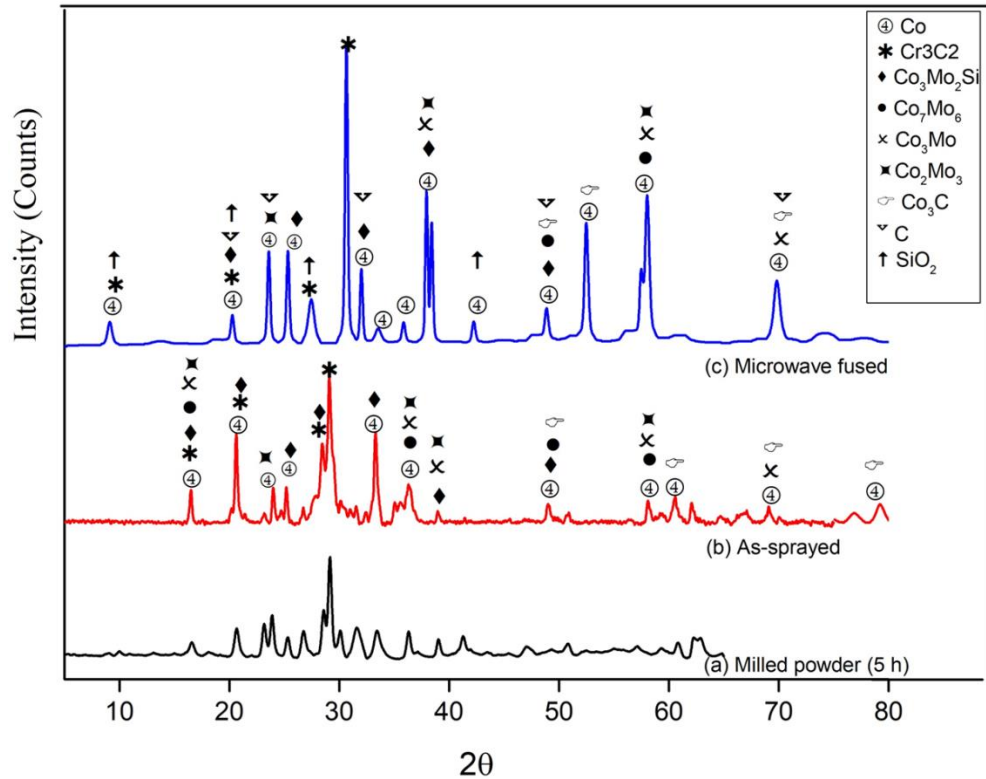


Figure 4.18 XRD patterns of CoMoCrSi+Cr₃C₂ (a) feedstock (b) HVOF sprayed
(c) Microwave fused

4.7 HVOF SPRAYED AND MICROWAVE FUSED CoMoCrSi+WC-CrC-Ni COMPOSITE COATINGS

4.7.1 Surface SEM and EDS Analysis

Figure 4.19 (a) shows the surface morphology of HVOF sprayed CoMoCrSi+WC-CrC-Ni composite coating. Presence of unmelted and partially melted particles at the surface leads to an increase in porosity percentage and surface is uneven. The measured coating roughness is 7 μm . Also noticed in (Figure 4.19a) morphology small cracks and tiny shaped pores are formed at the surface. The EDS results observed on the as-sprayed coating surface shown in Figure 4.19 (a) with the higher percentage of Co and W which represents the proper distribution of hard elements in the coating. After fusing, the surface exhibits a smooth and flat surface as observed in Figure 4.19 (b). The rapid cooling rate of the fused coating leads to eliminate cracks/pores results in a homogeneous structure. The surface roughness of the fused composite coating is 4.1 μm .

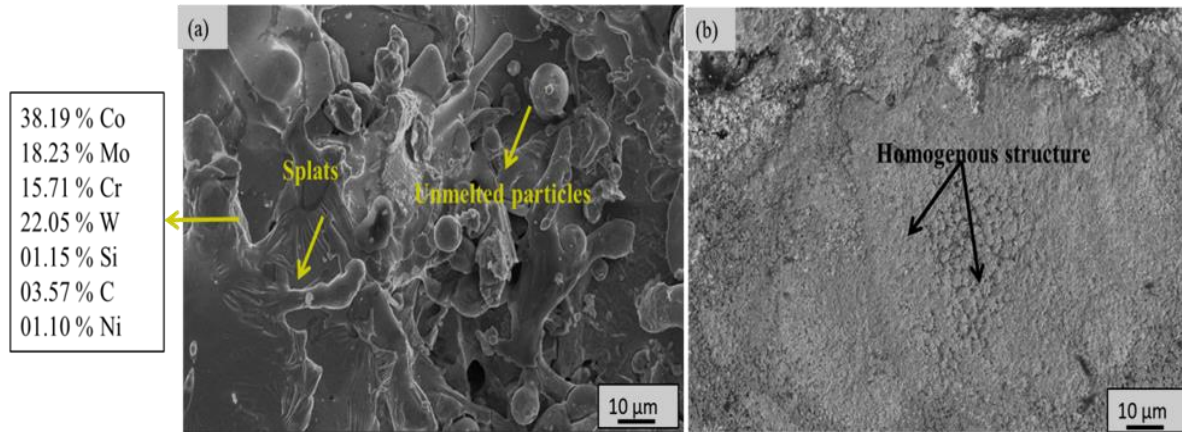


Figure 4.19 SEM micrograph taken on CoMoCrSi+WC-CrC-Ni composite coating surface

(a) HVOF sprayed (b) Microwave fused the coating

4.7.2 Cross-Sectional Microstructure and Elemental Mapping

Figure 4.20 (a and b) shows the SEM micrograph of HVOF sprayed and fused CoMoCrSi+WC-CrC-Ni composite coating along the cross-section. It has been observed in Figure 4.20 (a) that internal defects like porosity, cracks, unmelted or semi-melted particles in the as-deposited coatings structure.

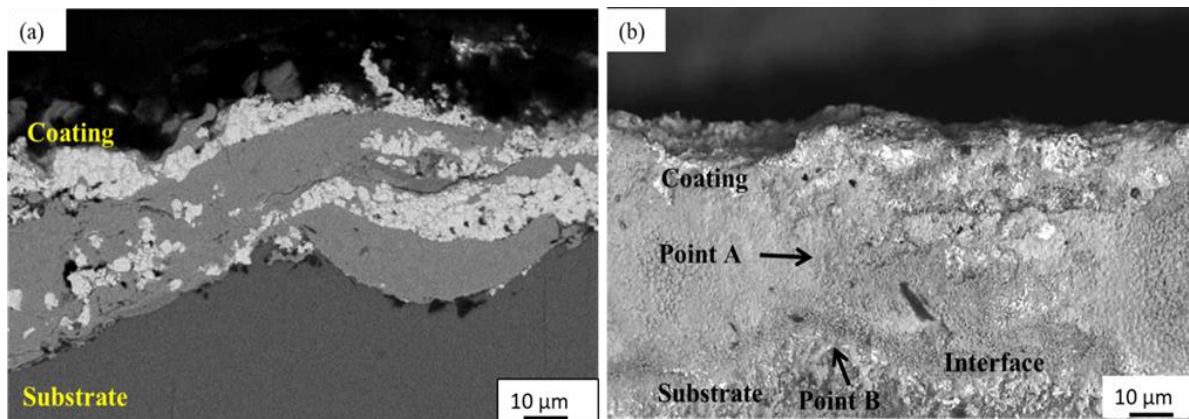


Figure 4.20 SEM micrograph of CoMoCrSi+WC-CrC-Ni composite coating along cross-section (a) HVOF sprayed (b) Microwave fused coating

The microwave heating process had a positive effect on the characteristics of the as-sprayed CoMoCrSi+WC-CrC-Ni composite coating. It can be seen from (Figure 4.20 b) fused cross-section; the remelted as-sprayed coating possesses a hard surface, homogeneous and uniform

structure. This also exhibits less porosity; no voids/cracks and achieved a titanium diffusion zone at the interface of the coating-substrate. This results in enhanced adhesion strength to the substrate. This shows the increase in coating thickness and improvement of surface roughness after microwave remelting. The EDS analyses of microwave fused composite coating at the interface and coating area are listed in Table 4.4. The EDS result confirms the chemical composition of enriched cobalt, molybdenum and tungsten elements at the cross-section. Presence of titanium and oxide elements in less percentage at the interface is confirmed.

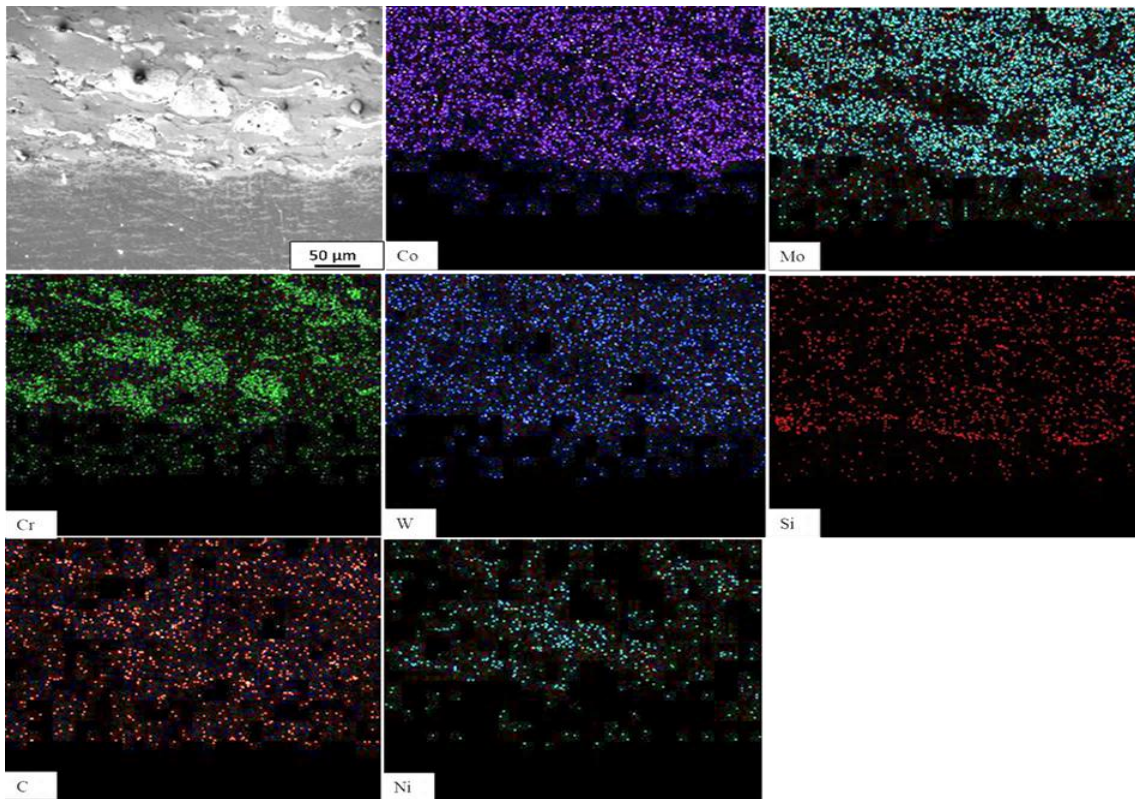


Figure 4.21 Elemental X-ray mapping of HVOF sprayed CoMoCrSi+WC-CrC-Ni composite coating

Figure 4.21 depicts the mapping results of the HVOF sprayed CoMoCrSi+WC-CrC-Ni composite coating. The major constituent elements such as cobalt, molybdenum, chromium, and tungsten are composed of carbon and silicon. The coating elements are uniformly dispersed along the thickness of the coating. Presence of nickel also confirms with less percentage which is dispersed along the coating thickness. Since the coating is deposited with

high acceleration and cooled quickly, results in no identification of oxides in coating structure.

The mapping results of fused CoMoCrSi+WC-CrC-Ni composite coating depicts in Figure 4.22. The additional inducement of carbon during microwave heating results in an increase in the percentage of carbon. The fused coating showed a homogenous structure which results in a proper distribution of coating constituents and composed of titanium made by sound metallurgical bonding. The presence of oxide element is less due to rapid solidification of remelted coatings.

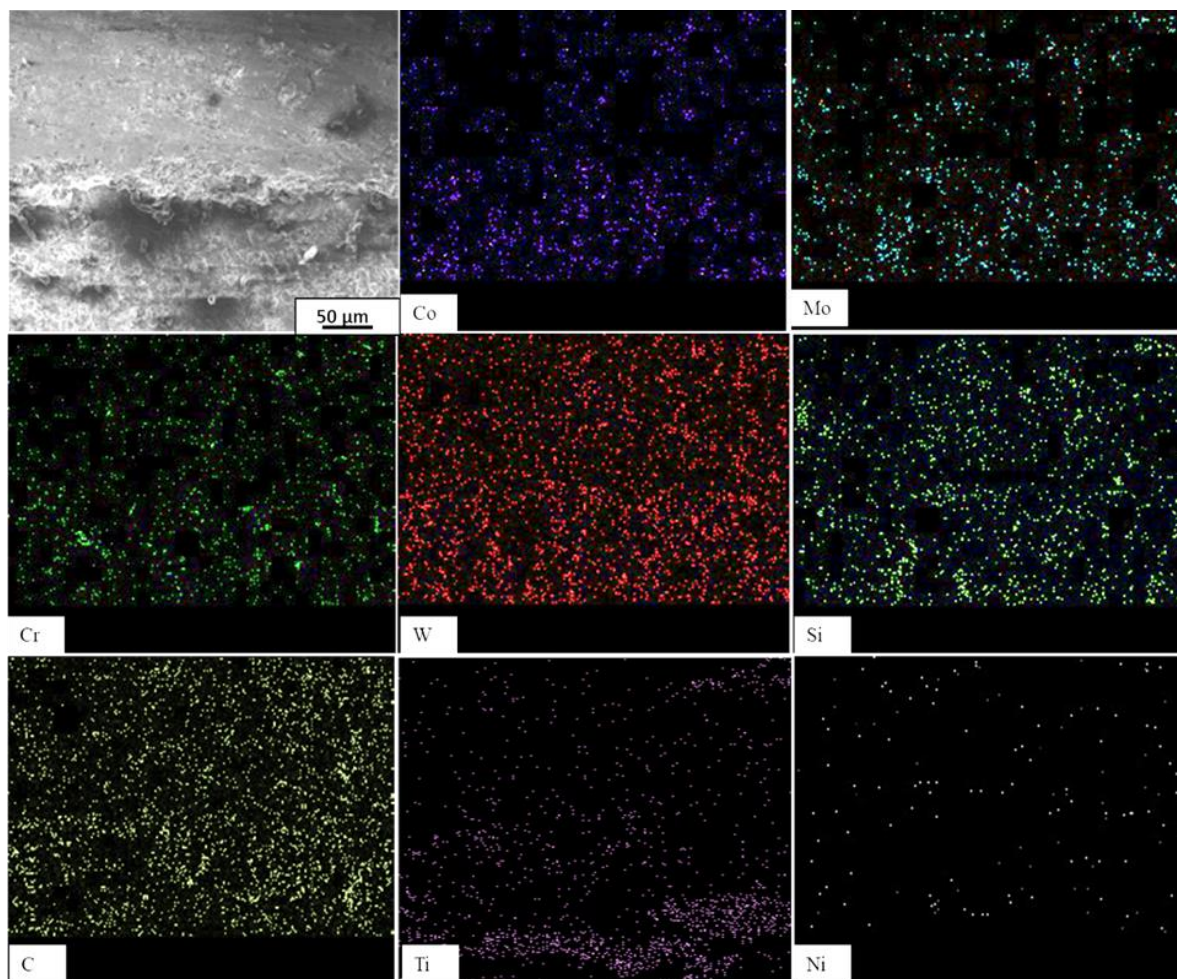


Figure 4.22 Elemental X-ray mapping of microwave fused CoMoCrSi+WC-CrC-Ni composite coating

Table 4.4 EDS results of microwave fused CoMoCrSi+WC-CrC-Ni composite coating with respect to points marked in Figure 4.20 (b)

Element, wt %	A	B (interface)
O	01.12	02.97
Ti	-	11.13
C	05.44	04.98
Si	02.60	01.12
Cr	13.55	11.45
Mo	20.87	15.23
W	19.29	18.05
Ni	01.41	01.10
Co	35.72	33.97

4.7.3 X-Ray Diffraction Studies

The XRD pattern of HVOF sprayed CoMoCrSi+WC-CrC-Ni composite coating shown in Figure 4.23 (a) exhibits similar peaks as compared to that of the CoMoCrSi+WC-CrC-Ni feedstock (Figure 4.6a) after coating on the substrate. This is achieved because of no decarburization of WC during HVOF spraying due to exposure time of powders to air is short. The XRD spectra of CoMoCrSi+WC-CrC-Ni composite coating showed Ni_3C peaks at 32, 44, 64, 66 and 72° with decreasing broad humps and strong Cr_3C_2 phases at 32, 38, 48, 74 and 78° is observed in Figure 4.23 (a). XRD pattern of fused CoMoCrSi+WC-CrC-Ni composite coating is depicted in Figure 4.23 (b). After fusing, retains the peaks obtained in case of as-sprayed coating with an increase in intensities. Inducing of carbon element into coating results in Co_3C and SiC phases are formed. The amorphous phases are Co-W-C recrystallization during heat treatment and form $\text{Co}_x\text{W}_y\text{C}_z$ crystalline phases which are detected by XRD (Dejuna and Tianyuan, 2014). The Cr_3C_2 phase intensity is remained the same after fusing and new phases such as $\text{Co}_6\text{W}_6\text{C}$, $\text{Co}_3\text{W}_9\text{C}$, and $\text{Co}_3\text{W}_3\text{C}$ are recorded denoted by the symbol “♥”. Oxide phases Co_3O_4 , and SiO_2 are to be formed due to remelting process conducted in an open atmosphere.

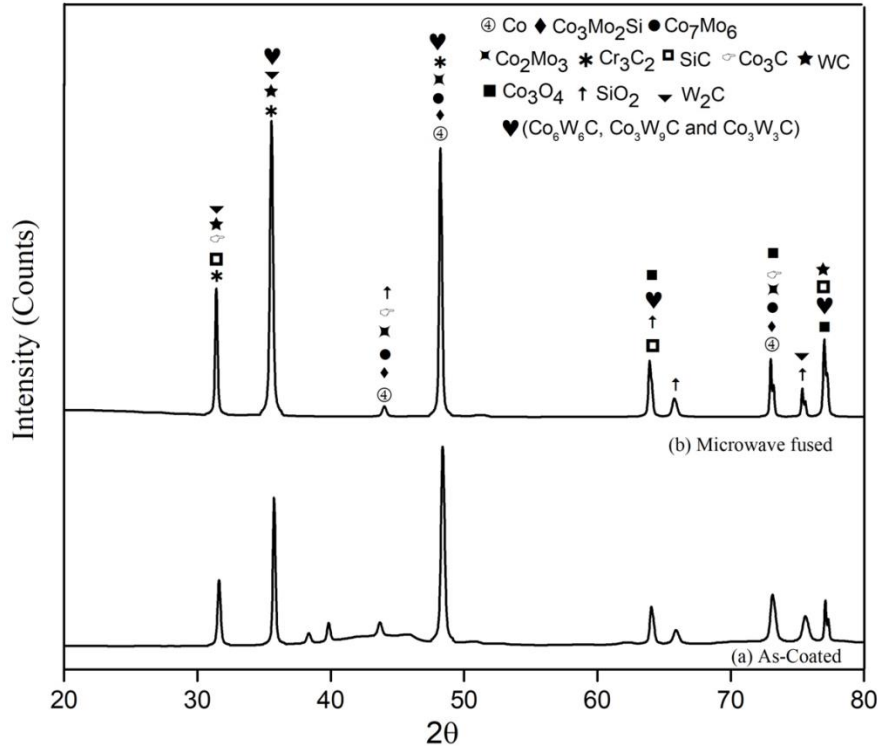


Figure 4.23 XRD pattern of CoMoCrSi+WC-CrC-Ni composite coatings (a) HVOF sprayed (b) Microwave fused

4.8 HVOF SPRAYED AND MICROWAVE FUSED CoMoCrSi+WC-12Co COMPOSITE COATINGS

4.8.1 Surface SEM and EDS Analysis

The surface morphology of HVOF sprayed and fused CoMoCrSi+WC-12Co composite coating are shown in Figure 4.24 (a and b). Unmelted particles are clearly visible at the coating surface shown in Figure 4.24 (a). The morphology displays many characteristics that presence of lamellar splats, internal porosity, discontinuities and interfacial defects like oxides. The measured coating roughness 5.5 μm . EDS analysis is conducted on the as-sprayed coating surface presents the chemical composition of the enriched Co and W element. Carbides distributed evenly in the coating which improves coating hardness. The fused coating exhibits unique features such as refinement of unmelted and semi-melted particles, obtained dense and compact coating microstructure shown in Figure 4.24 (b). The surface and subsurface defects like interfacial cracks, small pores and voids are decreased. The fused coating roughness is 2.7 μm .

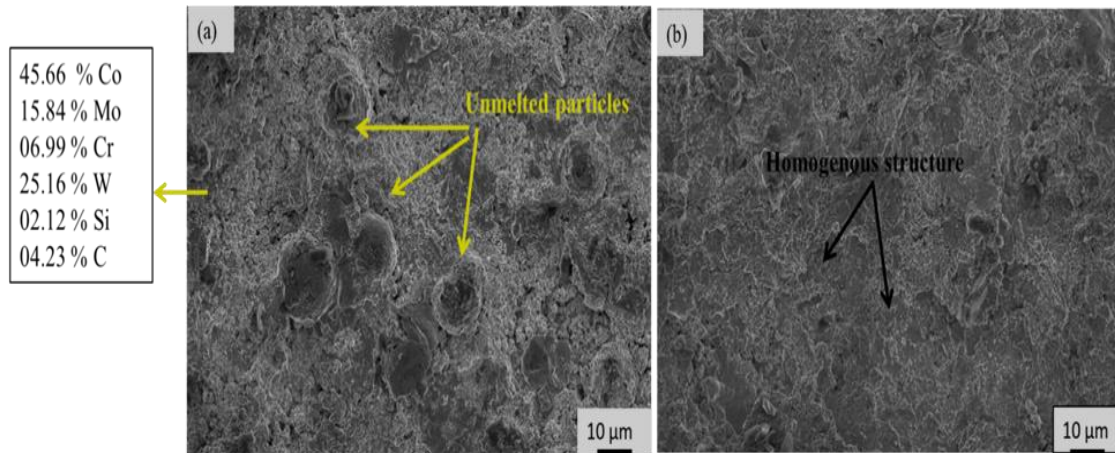


Figure 4.24 SEM micrograph of CoMoCrSi+WC-12Co composite coating surface
 (a) HVOF sprayed (b) Microwave fused coating

4.8.2 Cross-Sectional Microstructure and Elemental Mapping

Figure 4.25 (a and b) shows SEM micrograph of HVOF sprayed and fused CoMoCrSi+WC-12Co composite coating along the cross-section. The examined as-sprayed coating microstructure along cross-section presents porosity, uneven structure, and small voids can be seen in Figure 4.25 (a). The bonding between coating and substrate is good. The cross-section morphology of microwave fused CoMoCrSi+WC-12Co composite coating shown in Figure 4.25 (b). It is found that after remelting of as-sprayed composite coating exhibits uniform thickness, homogeneous structure, no presence of pores, and voids. It results in very fewer defects in coating structure. The fusing of a coating made diffusion of substrate element to coating region which provides good metallurgical bonding.

The EDS analysis of microwave fused coating is taken at interface and coating area and readings are listed in Table 4.5. The EDS result confirms the coating composition of enriched cobalt, molybdenum, and tungsten distributed evenly over the coating. A small percentage of oxides also found due to the process carried out under open atmospheric conditions.

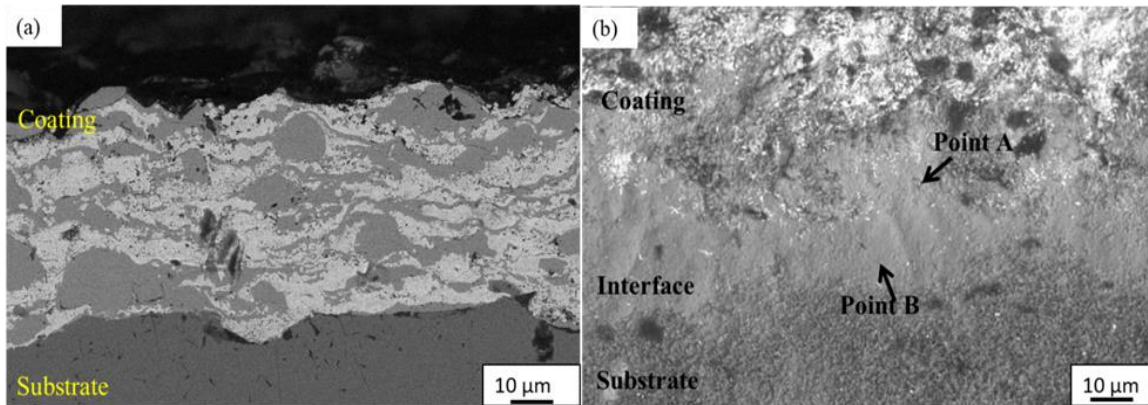


Figure 4.25 SEM micrograph of CoMoCrSi+WC-12Co composite coating along cross-section (a) HVOF sprayed (b) Microwave fused coating

Table 4.5 EDS results of microwave fused CoMoCrSi+WC-12Co composite coating with respect to points marked in (Figure 4.25b)

Element, wt %	A	B (interface)
O	02.07	04.80
Ti	-	13.25
C	03.10	04.61
Si	02.19	01.86
Cr	07.50	10.17
Mo	19.21	14.59
W	23.74	17.32
Co	42.19	33.40

The mapping results of the HVOF sprayed CoMoCrSi+WC-12Co composite coating shows in Figure 4.26. It confirms the presence of major coating constituent elements and uniformly distributed over the coating thickness. The reinforcement tungsten element is dispersed properly and coexists with the chromium element. The mapping results of the fused CoMoCrSi+WC-12Co composite coating present in Figure 4.27. It can be noticed that titanium is formed near the coating-substrate interface after microwave heat treatment, this results in metallurgical bonding.

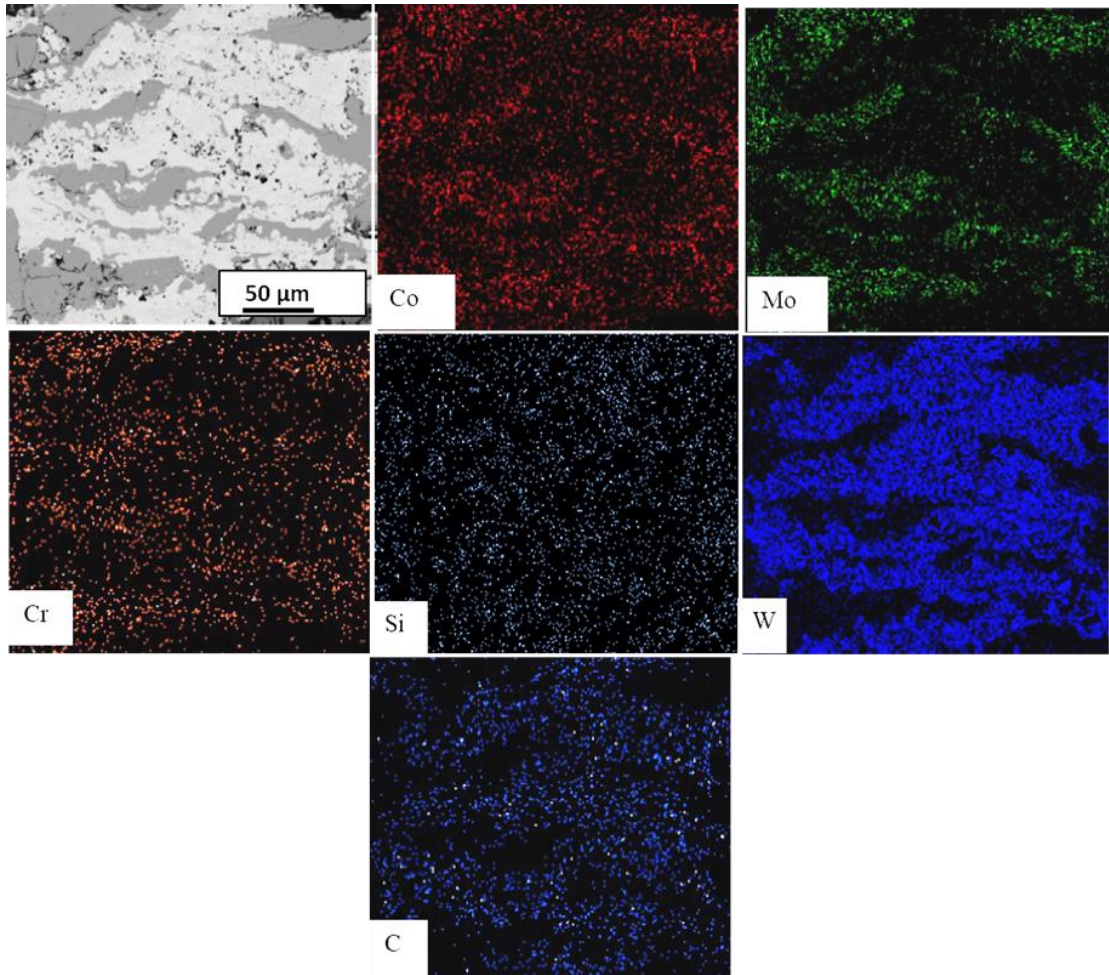


Figure 4.26 Elemental X-ray mapping of HVOF sprayed CoMoCrSi+WC-12Co composite coating

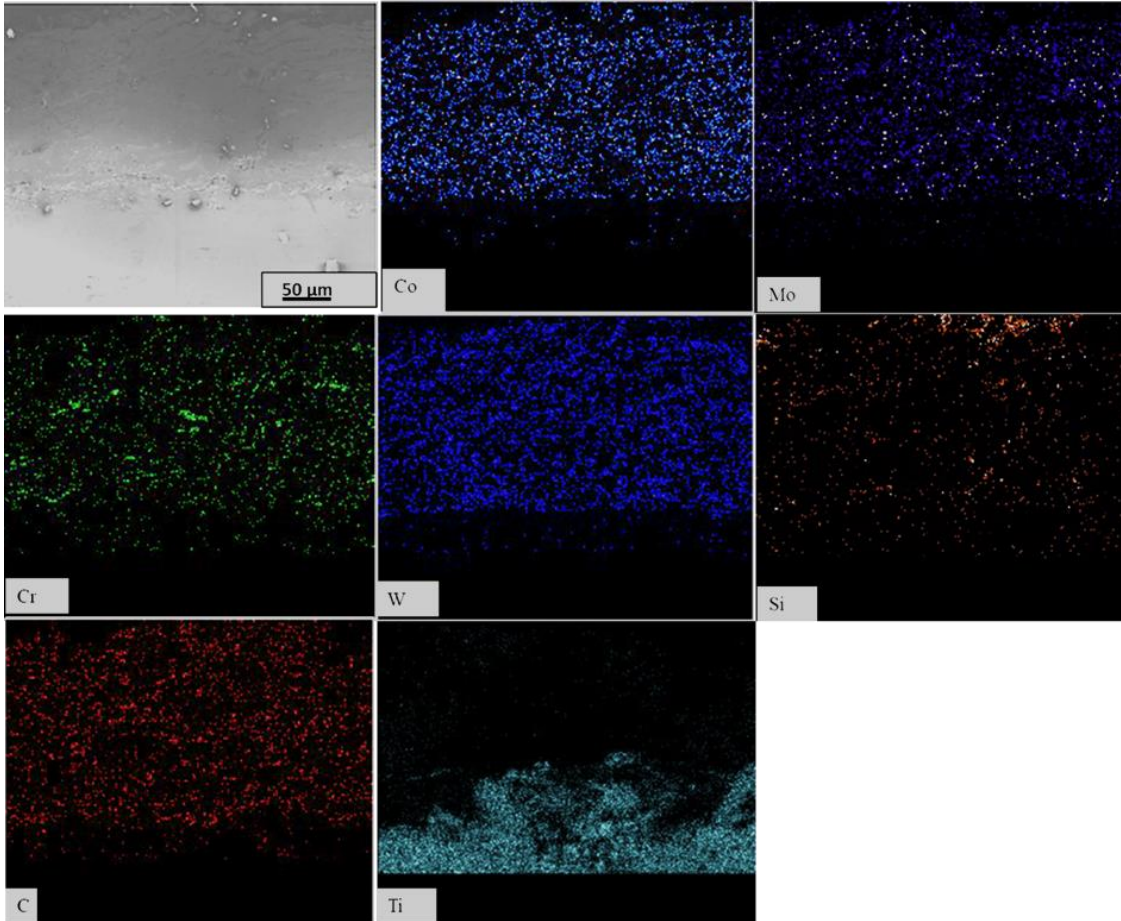


Figure 4.27 Elemental X-ray mapping of microwave fused CoMoCrSi+WC-12Co composite coating

4.8.3 X-Ray Diffraction Studies

The XRD spectrums of HVOF sprayed and fused CoMoCrSi+WC-12Co composite coating shown in Figure 4.28. The as-sprayed coating pattern displays the existence of peaks as present in powder phases. The diffraction peak of Co and WC is very strong, the coating is primarily composed of WC hard phase and hard laves of Co phase. The diffraction peaks of WC at 31° , 37° , and 42° are very strong, the other diffraction peaks are low. The as-sprayed coating also exhibits carbide phases like Cr_3C_2 with a strong intensity. In the case of fused XRD pattern of CoMoCrSi+WC-12Co composite coating (Figure 4.28b) reveals that very strong intensity with showing similar diffraction positions as identified in as-sprayed coating. Remelting of as-coated composite coating is carried out in atmospheric conditions, so oxygen entraps into fused composite coating results in minor oxide peaks like Co_3O_4 , and SiO_2 are

formed. New phases $\text{Co}_6\text{W}_6\text{C}$, $\text{Co}_3\text{W}_9\text{C}$, and $\text{Co}_3\text{W}_3\text{C}$ are identified denoted by the symbol “♥” during the remelting process due to recrystallize of Cobalt, tungsten and carbon elements (Dejuna and Tianyuan, 2014). Inducing of carbon element into coating results in Co_3C and SiC phases are to be formed.

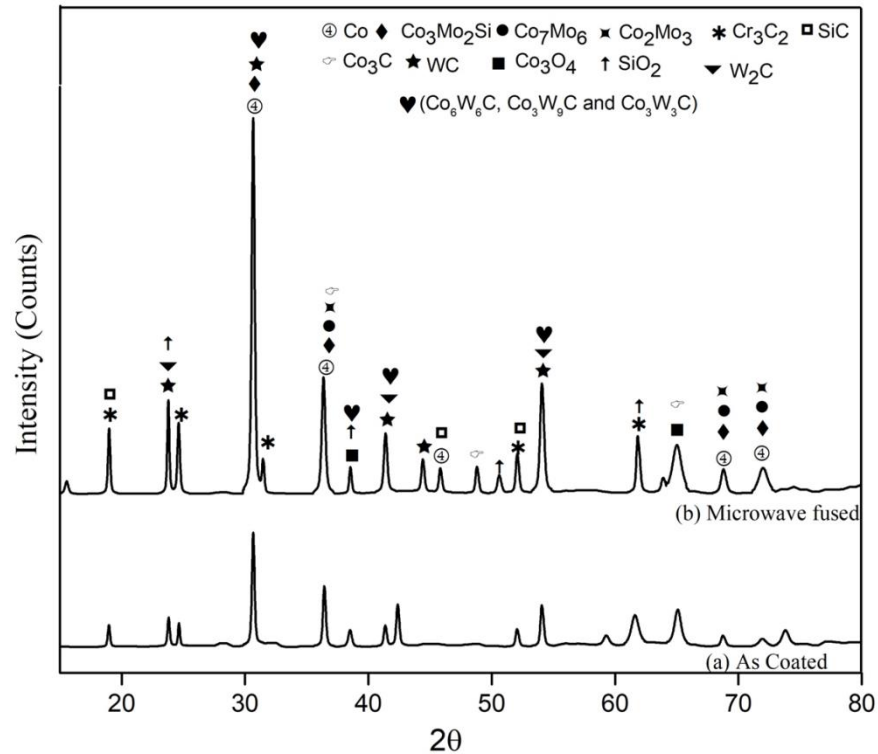


Figure 4.28 XRD pattern of CoMoCrSi+WC-12Co composite coatings (a) HVOF sprayed
(b) Microwave fused

4.9 FLAME SPRAYED AND MICROWAVE FUSED CoMoCrSi COATINGS

4.9.1 Surface SEM and EDS Analysis

Figure 4.29 (a and b) shows the SEM morphology of flame sprayed CoMoCrSi coating surface and its EDS report respectively. As-sprayed coating exhibits unmelted particles present at the surface shown in Figure 4.29 (a). The flame spray is a low-velocity process carried out in an open atmosphere causes gases entrapped into a coating which results in an increase in oxides percentage, these results are measured higher coating roughness of $16\ \mu\text{m}$ due to an uneven surface. In (Figure 4.29b) EDS results observed on the as-sprayed coating

surface shows a higher percentage of Co element which represents proper dispersion through the coating.

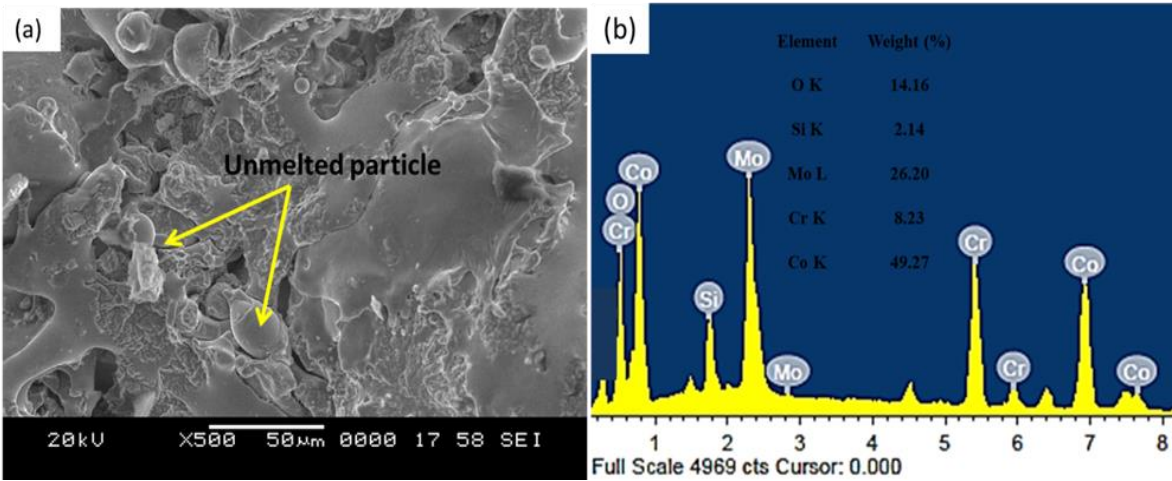


Figure 4.29 Flame sprayed CoMoCrSi coating (a) SEM surface morphology (b) EDS analysis

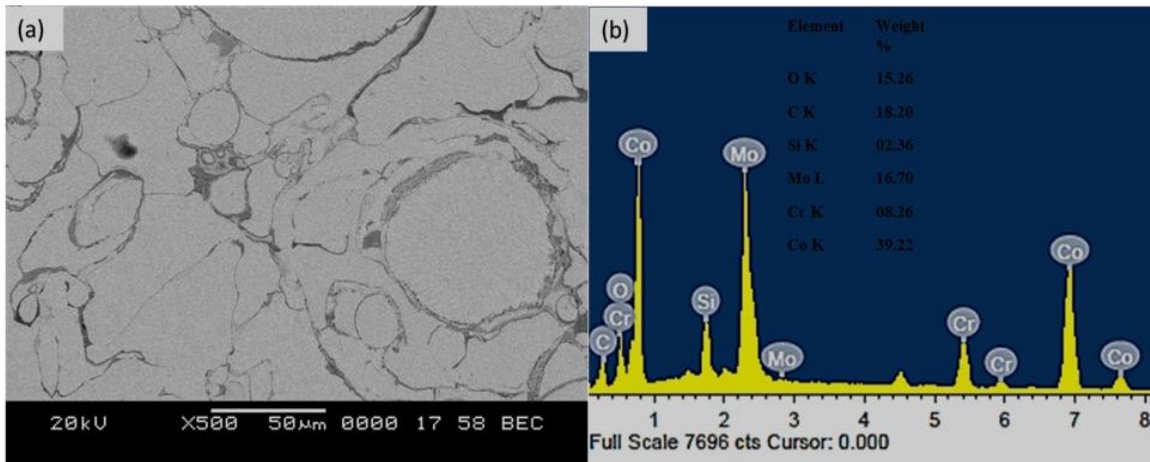


Figure 4.30 Microwave fused CoMoCrSi coating (Flame sprayed) (a) SEM surface morphology (b) EDS analysis

SEM image of microwave fused CoMoCrSi coating surface and its EDS report shown in Figure 4.30 (a and b). Fused coating reveals the uniform remelting of flame sprayed coating; there is no presence of partially melted particles in Figure 4.30 (a). After fusing surface roughness decreased drastically to 7.2 μm and became smooth surface. Additional carbon element from the graphite sheet is induced to the flame sprayed coating during microwave

heating, leads to becoming hard surface. It is confirmed from EDS results observed on the fused CoMoCrSi coating surface shown in Figure 4.30 (b). The percentage of oxide is more in fused coating because of the remelting performed in atmospheric conditions, so oxygen easily entraps in the coating during solidification.

4.9.2 Cross-Sectional Microstructure and Elemental Mapping

The SEM micrograph of flame sprayed CoMoCrSi and microwave fused coating along cross-section presents in 4.31 (a and b) respectively. It has been observed in (Figure 4.31a) surface features such as voids, the existence of unmelted and semi-melted droplets as well as oxide stringers; this leads to an increase in interfacial porosity. Whereas microwave fused flame sprayed coating shows a uniform and homogeneous structure in Figure 4.31(b). It is also observed that splat grains have been elongated due to heat supplied by microwave energy results in a decrease in porosity of coating. After the microwave treatment process, the thickness of the coating is slightly increased because of the partial diffusion of substrate elements. This results in the formation of metallurgical bonding between substrate and coating.

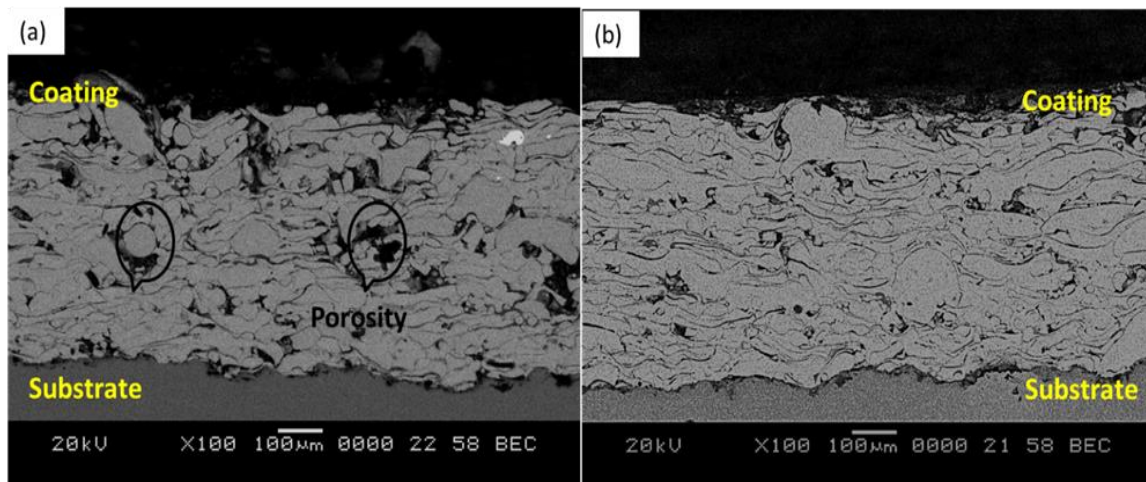


Figure 4.31 SEM micrograph of Flame sprayed CoMoCrSi coating along cross-section

(a) As-sprayed (b) Microwave fused coating

The mapping results of flame sprayed CoMoCrSi coating is depicted in Figure 4.32. The results reveal that coating materials are distributed uniformly with oxide content. However, due to low velocity, the oxide is induced into coating during spraying. The oxide element coexists with cobalt, chromium, molybdenum and silicon elements. The mapping results of

microwave fused CoMoCrSi coating is shown in Figure 4.33. This result demonstrates the diffusion phenomenon of the fused coating. The Ti element is diffused from the substrate to coating elements are partially diffused into the substrate, shown in Figure 4.33. The diffused elements coexist with carbon results in the formation of carbides with sound metallurgical bonding.

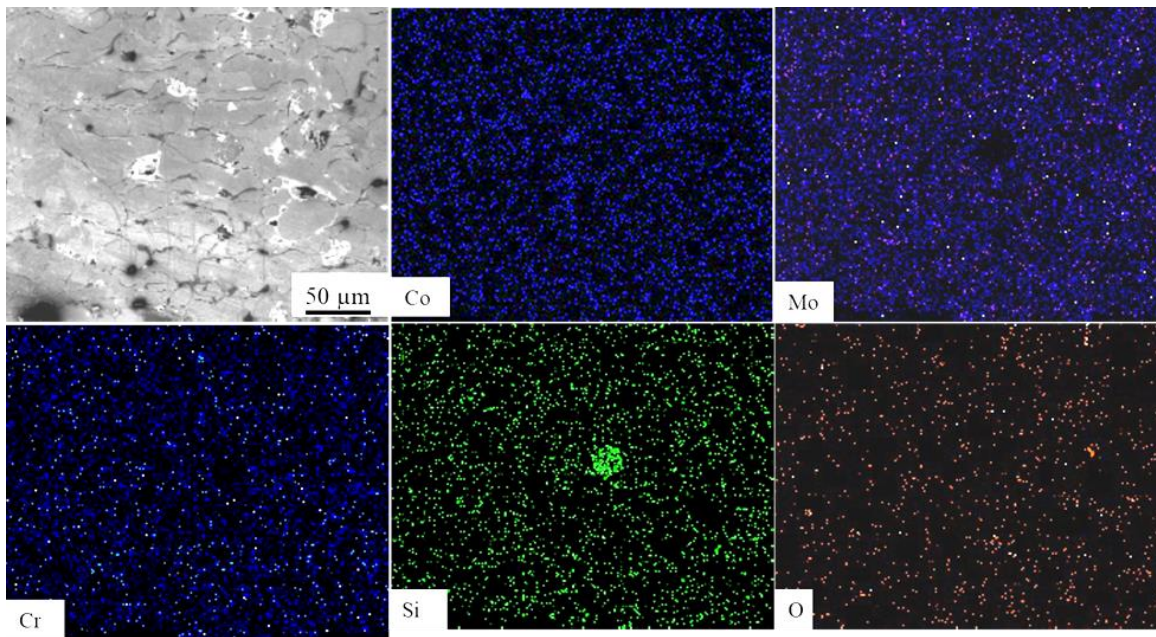


Figure 4.32 Elemental X-ray mapping of flame sprayed CoMoCrSi coating

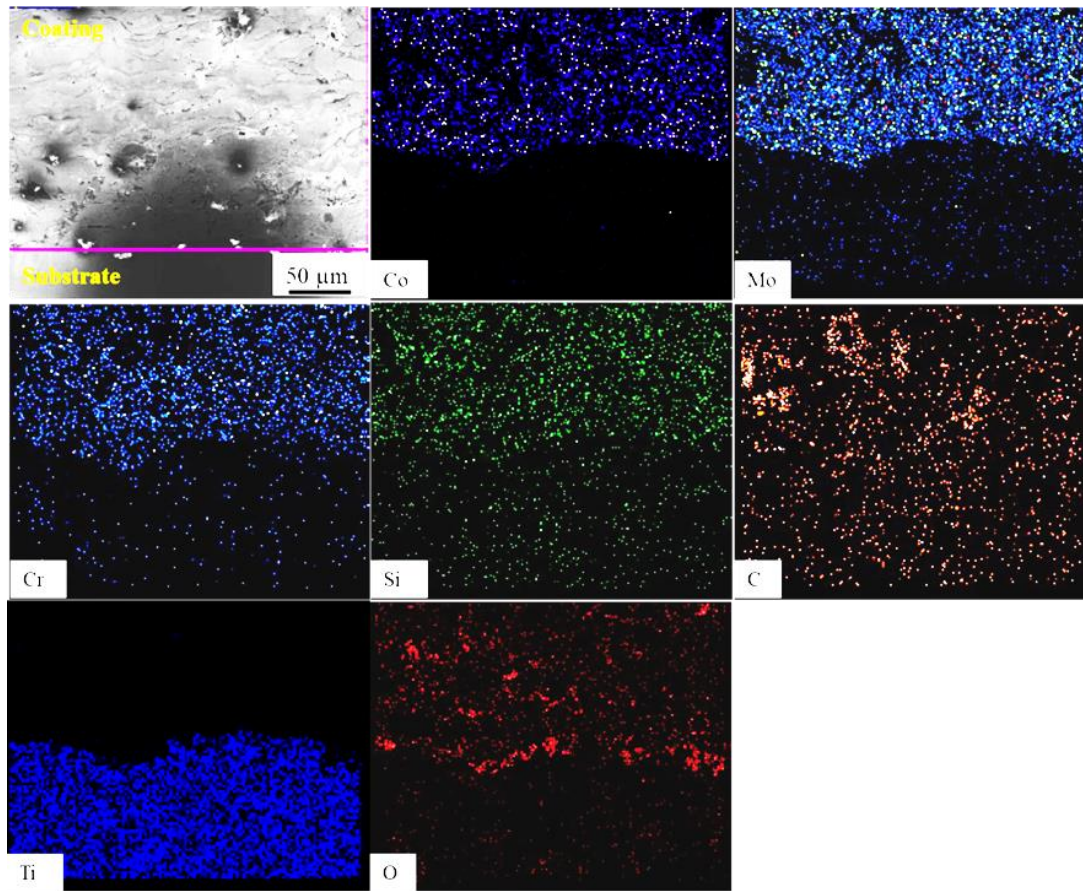


Figure 4.33 Elemental X-ray mapping of microwave fused CoMoCrSi coating

4.9.3 X-Ray Diffraction Studies

XRD spectrums of CoMoCrSi milled feedstock and flame sprayed coatings are presented in Figure 4.34 (a and b). It is observed that due to the influence of HEBM process the CoMoCrSi powder (Fig. 5 a) exhibits amorphous structure at 45° to 50° which mainly consist of Co, $\text{Co}_3\text{Mo}_2\text{Si}$, Co_7Mo_6 , and Co_2Mo_3 , along with minor phase of Mo_3Si . It is noticed that after flame sprayed coating retains the similar phases of intermetallics consists of Co, $\text{Co}_3\text{Mo}_2\text{Si}$, Co_7Mo_6 , Co_2Mo_3 , and Co_3O_4 as a major phase while, Mo_3Si , SiO_2 , and MoO_2 as a minor phase as presented in milled powder and obtained some oxide phases showed in Figure 4.34 (b). Similar phases are identified in the XRD pattern of microwave fused CoMoCrSi coating as seen in flame sprayed coating except for Co_3C , Cr_3C_2 and C phases in Figure 4.34 (c). After remelting of the flame sprayed coating and inducing of carbon element results in formation of carbide phases such as Co_3C and Cr_3C_2 . Also MoO_2 , SiO_2 and Co_3O_4 oxide phases have identified (Utu and Marginean, 2017).

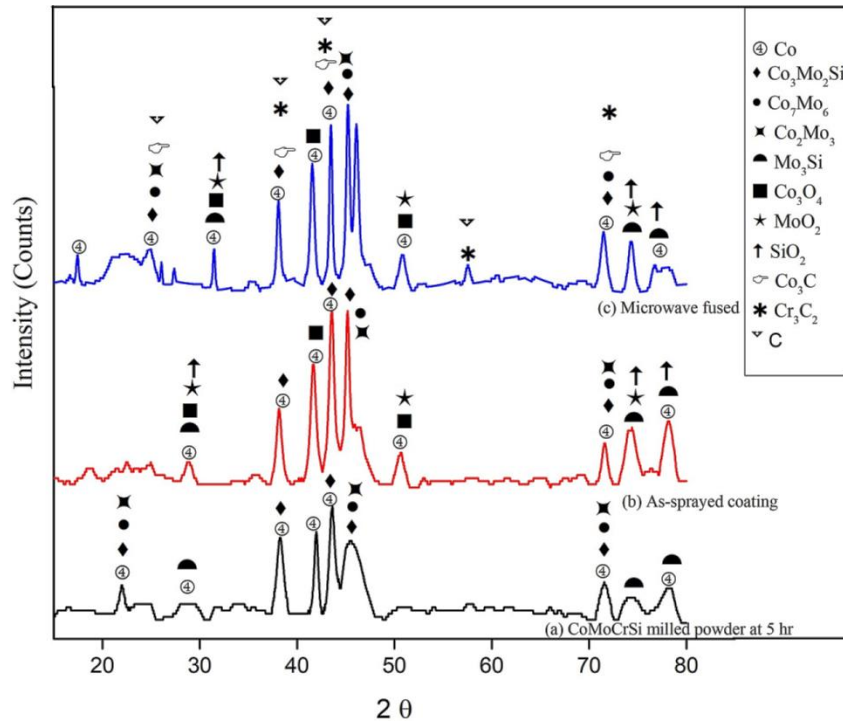


Figure 4.34 XRD patterns of (a) feedstock and flame sprayed CoMoCrSi coatings (b) As-sprayed (c) Microwave fused

4.10 FLAME SPRAYED AND MICROWAVE FUSED CoMoCrSi+Cr₃C₂ COMPOSITE COATINGS

4.10.1 Surface SEM and EDS Analysis

The SEM surface morphology of flame sprayed CoMoCrSi+Cr₃C₂ composite coating and its EDS report are shown in Figure 4.35 (a) and Figure 4.35 (b) respectively. Partial and unmelted particles are distinctly visible at the coating surface leads to an increase in coating roughness to 14.55 μm noticed from Figure 4.35(a). The EDS analysis illustrates (Figure 4.35b) the rich Cr element and amount of oxides is more during the spraying of coating powders. Figure 4.36 (a and b) describes the SEM surface morphology of microwave fused CoMoCrSi+Cr₃C₂ composite coating and its EDS report. Microwave energy provides proper remelting of flame sprayed coating which eliminates partial and unmelted particles. This is the reason for the reduction in porosity and filling up of cracks presented in as-sprayed coatings noticed in Figure 4.35 (a). EDS report in Figure 4.36 (b) shows that percentage increase in oxides not found but the percentage of carbon element is increased due to

inducing after post-treatment. It leads to becoming harder surface than flame sprayed coating and results in reduced coating surface roughness to 6.20 μm .

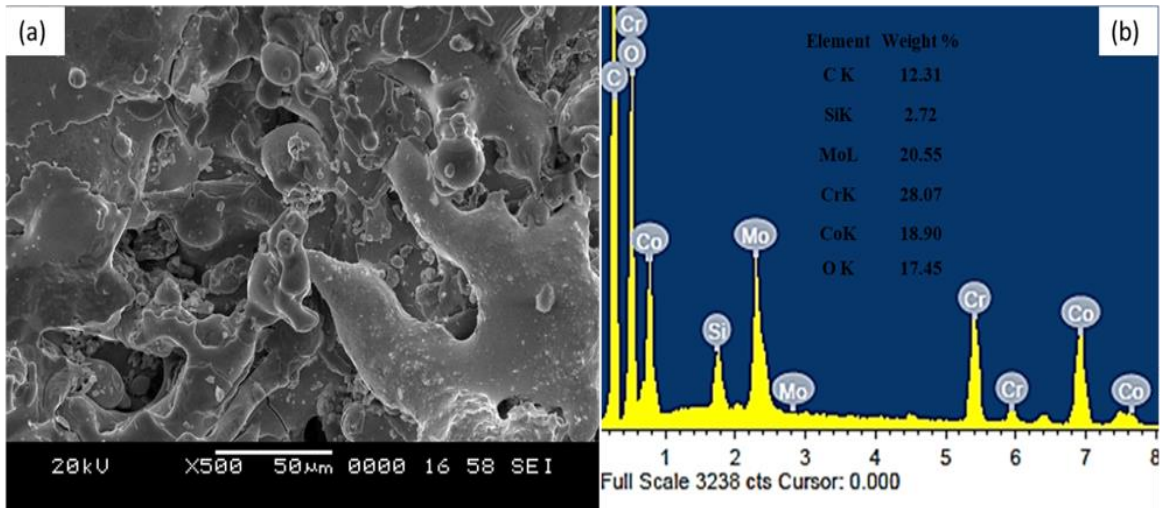


Figure 4.35 Flame sprayed CoMoCrSi+Cr₃C₂ composite coating (a) SEM surface morphology (b) EDS analysis

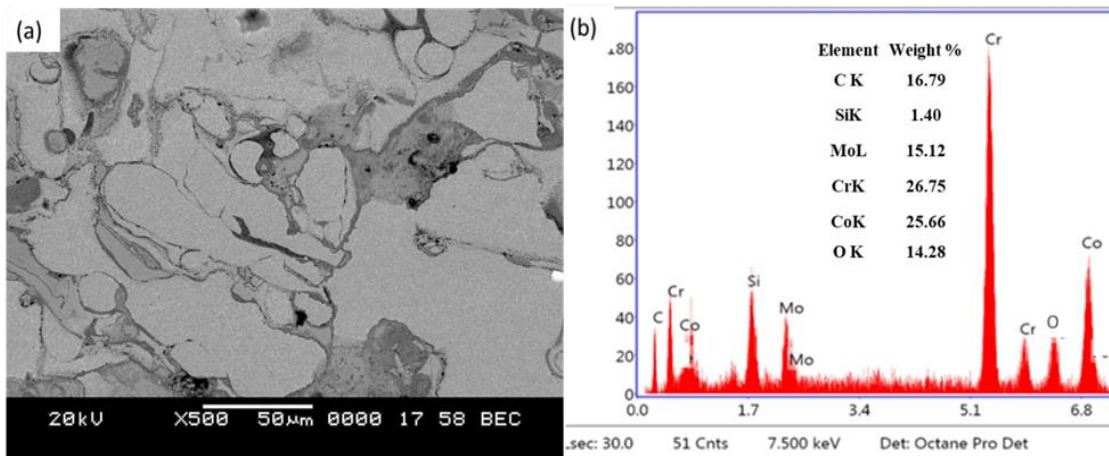


Figure 4.36 Microwave fused CoMoCrSi+Cr₃C₂ composite coating (a) SEM surface morphology (b) EDS analysis

4.10.2 Cross-Sectional Microstructure and Elemental Mapping

Figure 4.37 (a and b) shows the SEM micrograph along the cross-section of flame sprayed and microwave fused CoMoCrSi+Cr₃C₂ composite coating respectively. The examined microstructure (Figure 4.37a) of flame sprayed coating along thickness shows the existence

of an uneven structure and large voids. These defects are caused due to the low acceleration of flame spray during deposition of the coating. On the other hand, microwave fused flame sprayed CoMoCrSi+Cr₃C₂ composite coating shows a uniform and homogeneous structure in Figure 4.37(b). After fusing, process splats size is elongated and compacted rigidly. The white patches in Figure 4.37 (b) indicate Cr₃C₂ reinforcement distributed uniformly with matrix elements over the coating region. Increase in thickness ensures diffusion of substrate elements, results in metallurgical bonding.

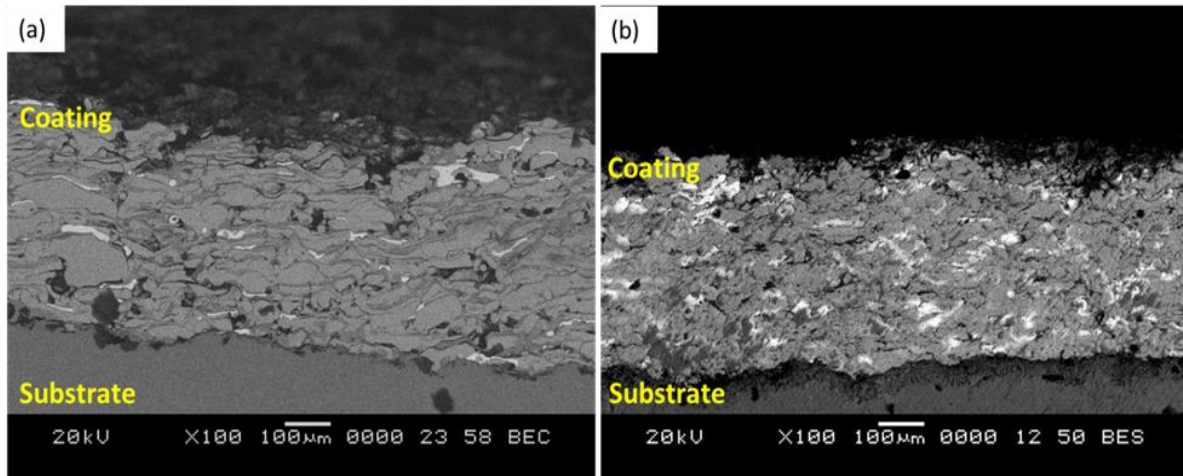


Figure 4.37 SEM micrograph of CoMoCrSi+Cr₃C₂ composite coating along cross-section
(a) Flame sprayed (b) Microwave fused coating

X-ray elemental mapping result of flame sprayed CoMoCrSi+Cr₃C₂ composite coating confirms the uniform distribution of major feedstock elements through the coating area as shown in Figure 4.38. It clearly shows the distinct splats enriched with cobalt and molybdenum. Carbon and oxides are distributed over the coating uniformly.

Elemental mapping of microwave fused CoMoCrSi+Cr₃C₂ composite coating reveals the proper distribution of coating and diffusion of coating-substrate elements at the interface is shown in Figure 4.39. It indicates that titanium co-exists with rich molybdenum, cobalt, and chromium. The volumetric heating effect of microwave results in heterogeneous structure and provides the equal distribution of properties over the coating thickness.

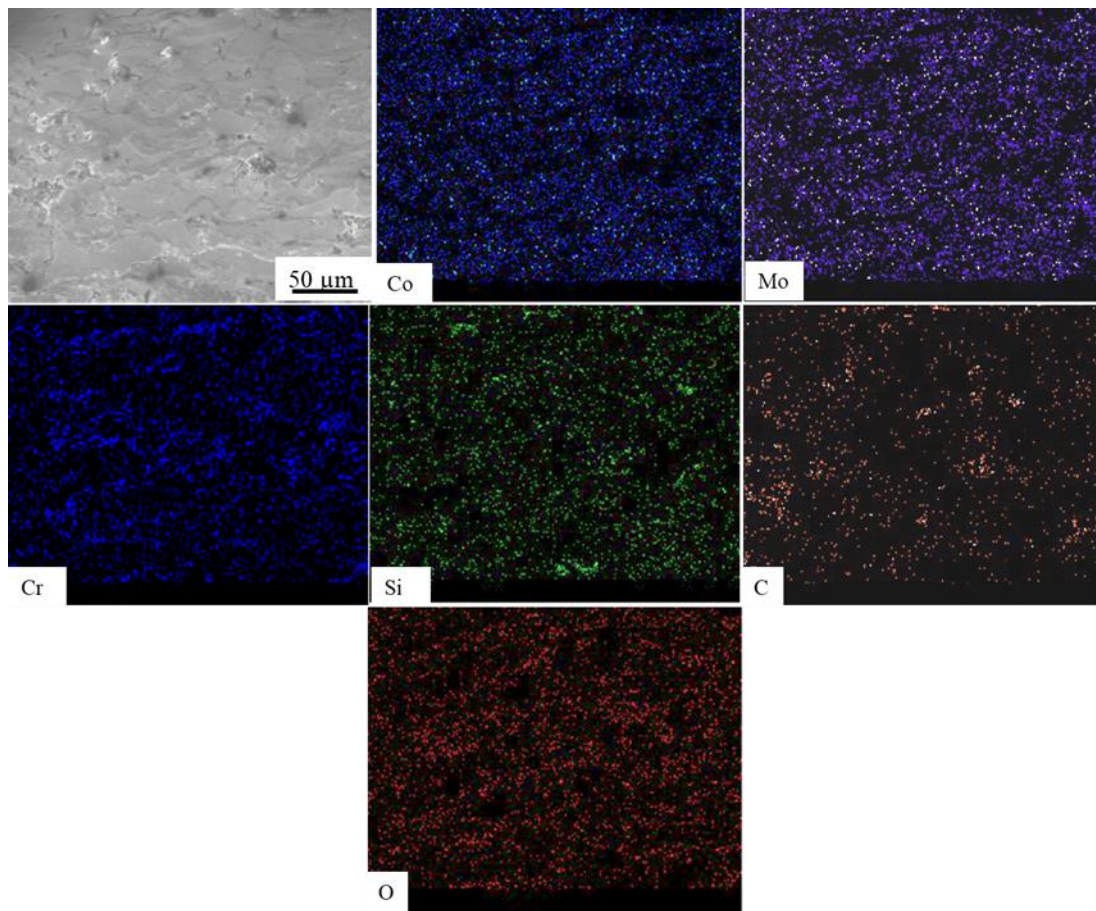


Figure 4.38 Elemental X-ray mapping of flame sprayed CoMoCrSi+Cr₃C₂ composite coating

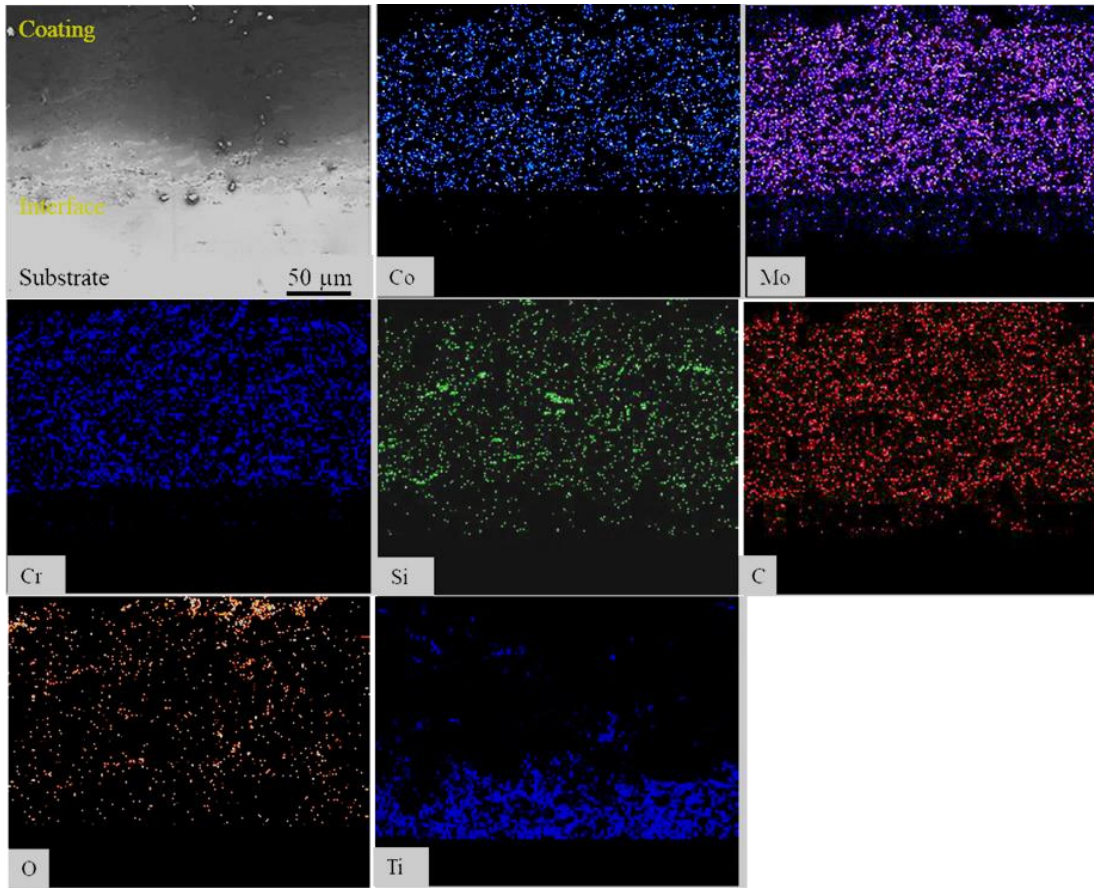


Figure 4.39 Elemental X-ray mapping of microwave fused CoMoCrSi+Cr₃C₂ composite coating

4.10.3 X-Ray Diffraction Studies

XRD spectrum of CoMoCrSi+Cr₃C₂ feedstock and flame sprayed composite coatings are presented in Figure 4.40 (a and b). There is significant changes in XRD pattern of CoMoCrSi+Cr₃C₂ powder comparing with XRD pattern of CoMoCrSi powder (Figure 4.4). The existence of intermetallic laves phases is confirmed with the addition phase of Cr₃C₂ showing as a sharp diffraction peak. XRD pattern of flame sprayed CoMoCrSi+Cr₃C₂ composite coating (Figure 4.40b) consists of Co, Cr₃C₂, and Co₃Mo₂Si as major phases at an angle range of 30 to 38°, along with Co₇Mo₆, Co₃Mo, Co₂Mo₃, Co₃O₄, Co₃C and MoO₂ as minor phases. Similar phases are detected in the XRD pattern of the CoMoCrSi+Cr₃C₂ microwave fused composite coating as noticed in flame sprayed coating (Figure 4.40 c). Presence of major phases such as Co, Cr₃C₂, Co₃Mo₂Si, Co₃O₄, Co₃C, and MoO₂ at angles of

32°, 40° and 60 °confirms the retaining of original phases identified in the as-sprayed coating.

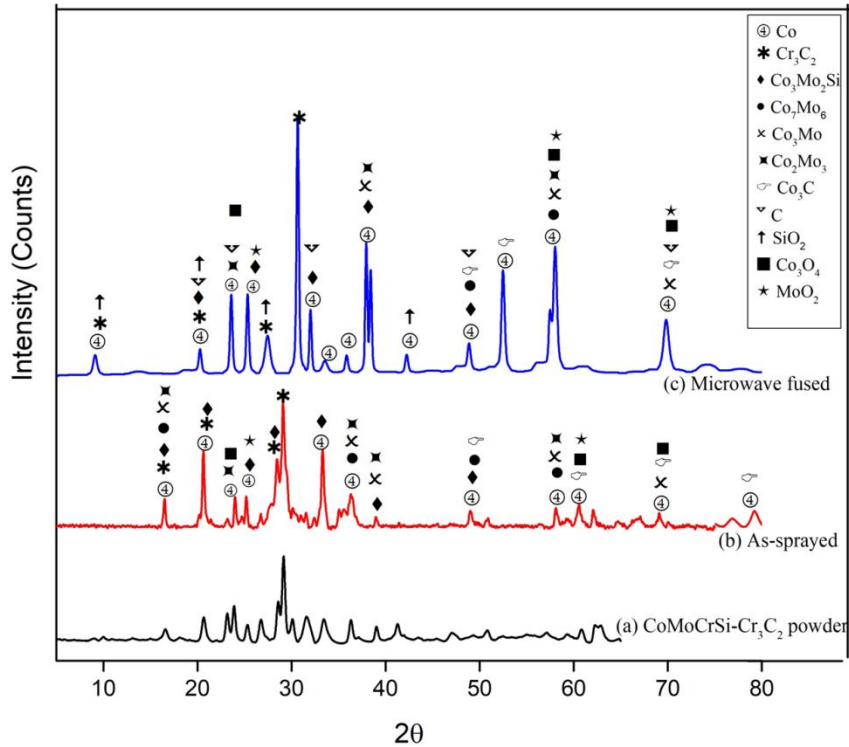


Figure 4.40 XRD patterns of CoMoCrSi+Cr₃C₂ composite coating (a) feedstock (b) flame sprayed (c) Microwave fused

4.11 FLAME SPRAYED AND MICROWAVE FUSED CoMoCrSi+WC-CrC-Ni COMPOSITE COATINGS

4.11.1 Surface SEM and EDS Analysis

The surface morphology of the flame sprayed CoMoCrSi+WC-CrC-Ni composite coating and its EDS analysis are presented in Figure 4.41 (a and b). The unmelted and semi-melted particles can be observed in the surface of as-sprayed coating (Figure 4.41a). The spray process employed in this work produces less velocity hence coating particles remains partial melted on the surface of the substrate. This leads to more roughness of the as-sprayed coating surface of 14.45 μm. The EDS analysis of the flame sprayed coating describes the presence of cobalt-rich element along with reinforced carbides and also confirms the presence of oxides on the coating surface in Figure 4.41(b). The surface morphology of the fused CoMoCrSi+WC-CrC-Ni composite coating and its EDS analysis are depicted in Figure 4.42

(a and b). The surface shows uniform remelting of flame sprayed coating with refining the unmelted and partially melted particles result in the smooth surface of $6.28 \mu\text{m}$ in Figure 4.42(a). The remelted coating surface has oxide stringers due to the process carried out under atmospheric conditions so the oxygen is entrapped into the fused coating. The substrate element titanium is identified by EDS analysis of fused coating due to the diffusion mechanism. Also, the percentage of oxide element is increased and observed no significant changes in the percentage of other major coating elements.

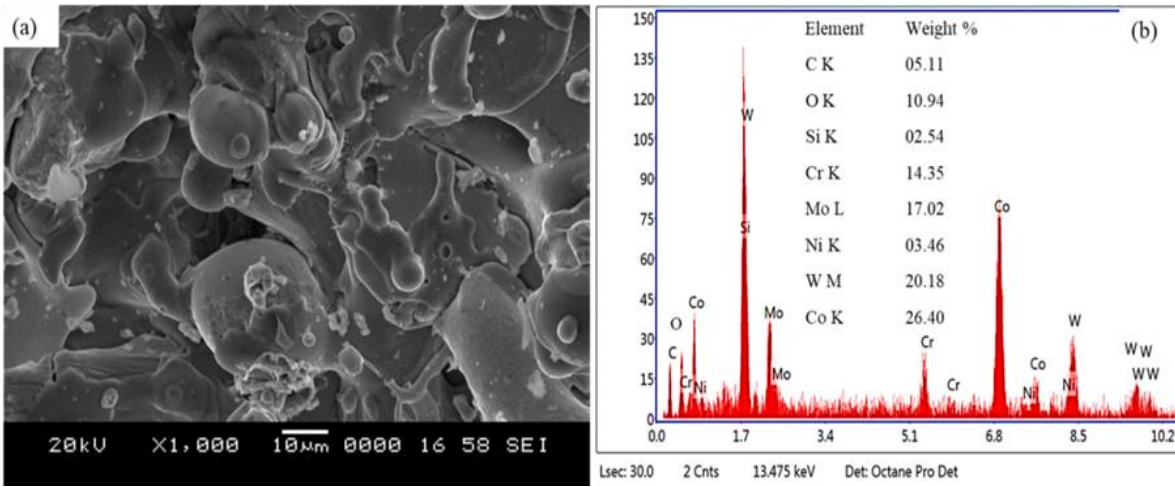


Figure 4.41 Flame sprayed CoMoCrSi+WC-CrC-Ni composite coating (a) SEM surface morphology (b) EDS analysis

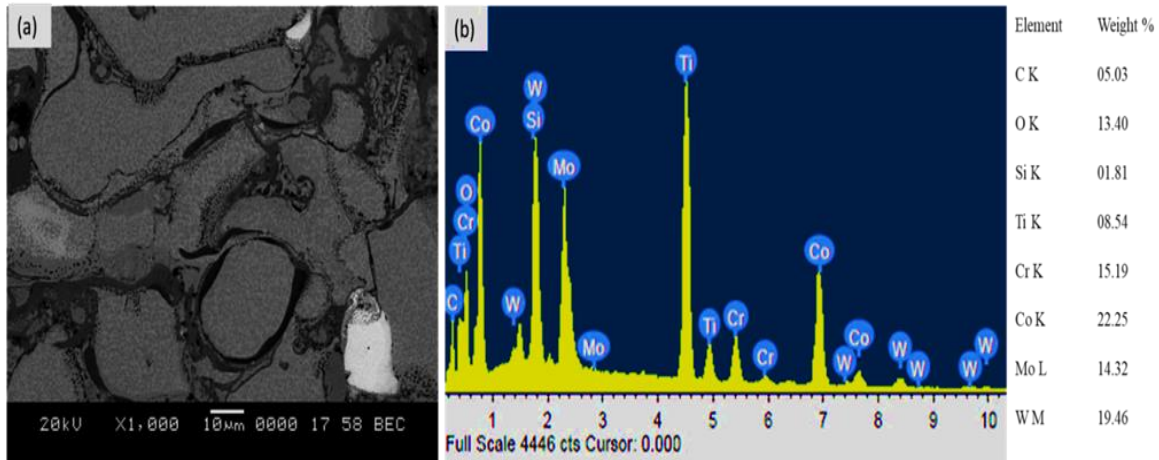


Figure 4.42 Microwave fused CoMoCrSi+WC-CrC-Ni composite coating (a) SEM surface morphology (b) EDS analysis

4.11.2 Cross-Sectional Microstructure and Elemental Mapping

The cross-section morphologies of flame sprayed and microwave fused CoMoCrSi+WC-CrC-Ni composite coatings are shown in Figure 4.43. The as-sprayed coating reveals the presence of cracks and pores throughout the thickness of the coating Figure 4.43(a). There is no such cracks have found near-interface region, results in a sound bonding between coating and substrate. The coating shows a uniform structure in terms of thickness. The post-treated coating exhibits significant changes in terms of microstructural features such as reduced cracks and pores results in a homogeneous structure in Figure 4.43(b). The influence of heat on as-sprayed coatings results in the formation of metallurgical bonding. This is caused due to inter-diffusion of coating elements near the interface region.

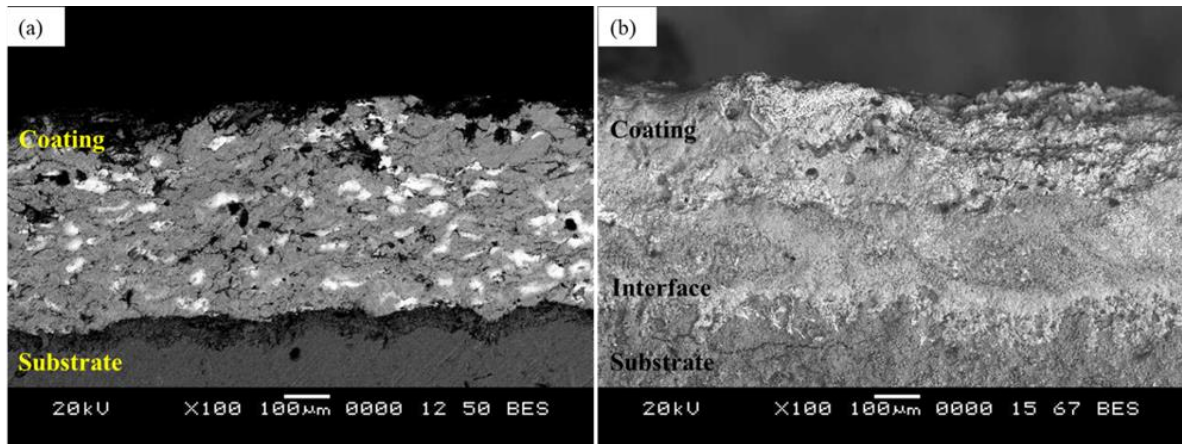


Figure 4.43 SEM micrograph of CoMoCrSi+WC-CrC-Ni composite coating along cross-section (a) Flame sprayed (b) Microwave fused the coating

The mapping of flame sprayed CoMoCrSi+WC-CrC-Ni composite coating along the cross-section is shown in Figure 4.44. The mapping results demonstrate the proper distribution of coating elements throughout the thickness during spraying. The carbides coexist with cobalt, molybdenum, chromium and silicon elements. The existence of oxide element in the coating is confirmed by mapping and also noticed Ni element which is less in percentage. The mapping result of fused CoMoCrSi+WC-CrC-Ni composite coating is presented in Figure 4.45. The inter-diffusion phenomenon caused by post-treatment is confirmed by mapping results. After heat treatment, the coating materials are dispersed uniformly. The percentage of oxide is more infused coating because of the remelting performed in atmospheric conditions, so oxygen easily entraps in the coating during solidification.

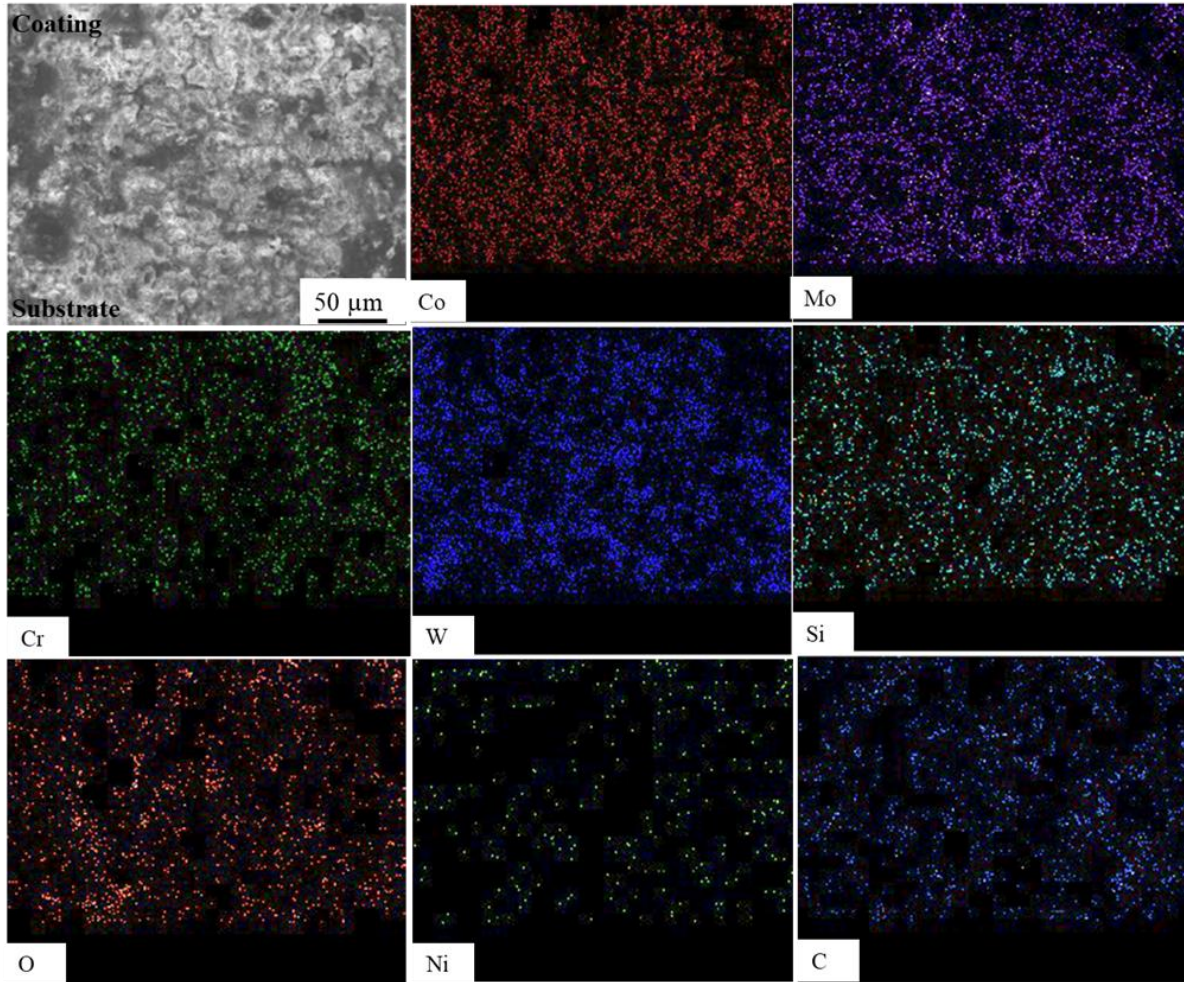


Figure 4.44 Elemental X-ray mapping of flame sprayed CoMoCrSi+WC-CrC-Ni composite coating

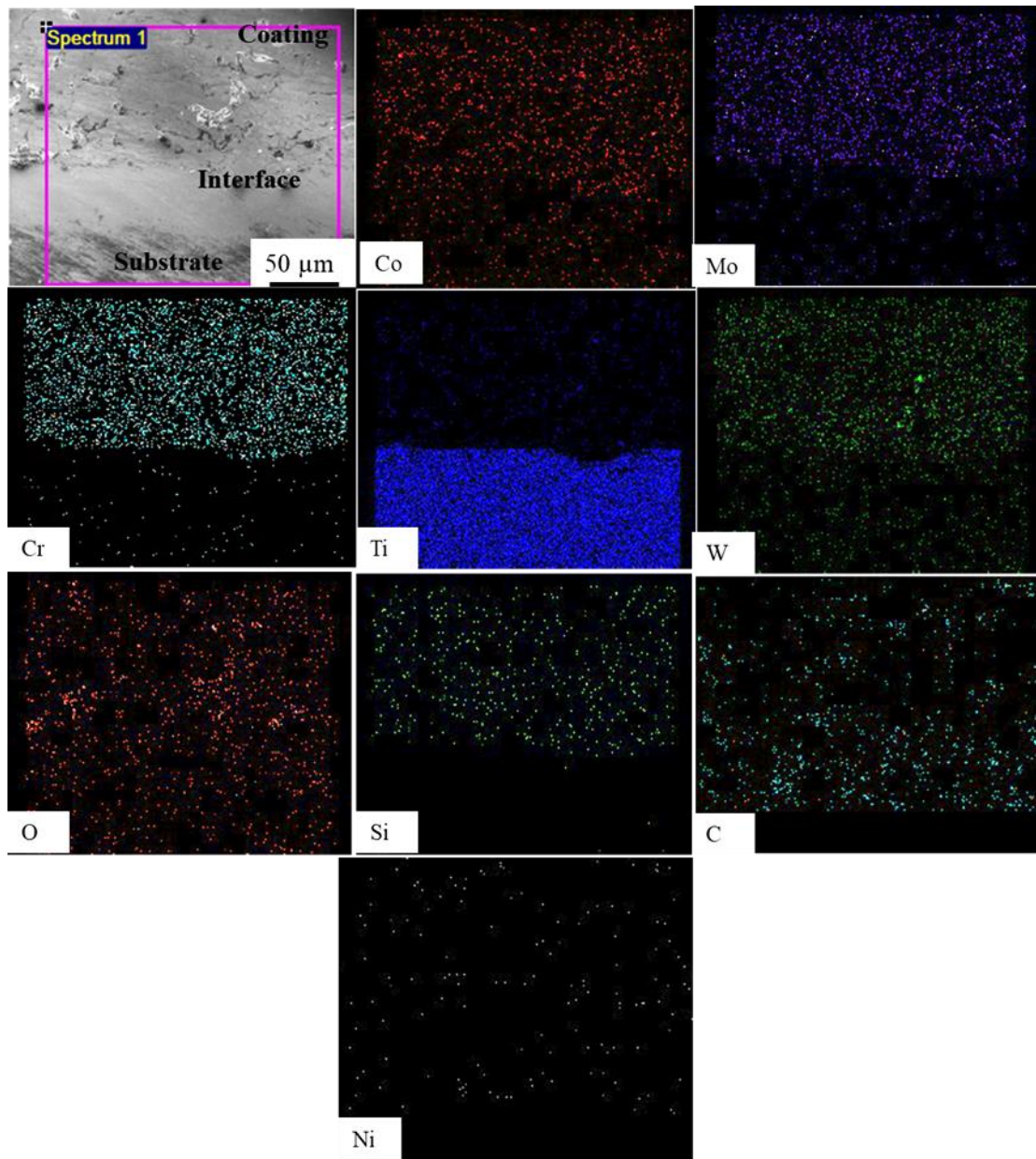


Figure 4.45 Elemental X-ray mapping of microwave fused CoMoCrSi+WC-CrC-Ni composite coating

4.11.3 X-Ray Diffraction Studies

The XRD patterns of flame sprayed and microwave fused CoMoCrSi+WC-CrC-Ni composite coatings depicts in Figure 4.46 (a and b). The flame sprayed coating spectrum has a sharp crystalline structure with lower intensity. The pattern exhibits intermetallic phases such as $\text{Co}_3\text{Mo}_2\text{Si}$, Co_7Mo_6 , and Co_2Mo_3 . At 38° , 48° and 72° showed WC peaks, whereas

Cr₃C₂ peaks are observed at 38°, 42°, 45°, and 47°. The new phases such as Co₆W₆C, Co₃W₉C, and Co₃W₃C are recorded which is represented by the symbol “♥” in Figure 4.46 (a and b). These phases strongly influence the coating properties reported by several researchers (Bolelli et al., 2014; Dejuna, and Tianyuan, 2017). The low velocity of the flame spray process results in the formation of oxide phases has been detected in its XRD pattern. The microwave fused CoMoCrSi+WC-CrC-Ni composite coating XRD spectrum is shown in Figure 4.46 (b). After post heat treatment significant changes in pattern and also a slight broadening of peaks has been noticed see in Figure 4.46 (b). The fused coating retains the similar phases as observed at flame sprayed coating. The inducing of carbon to the as-sprayed coating leads to formation of additional new carbide phases such as Co₃C and SiC. Also SiO₂ and Co₃O₄ oxide phases have found due to oxidation of fused coating.

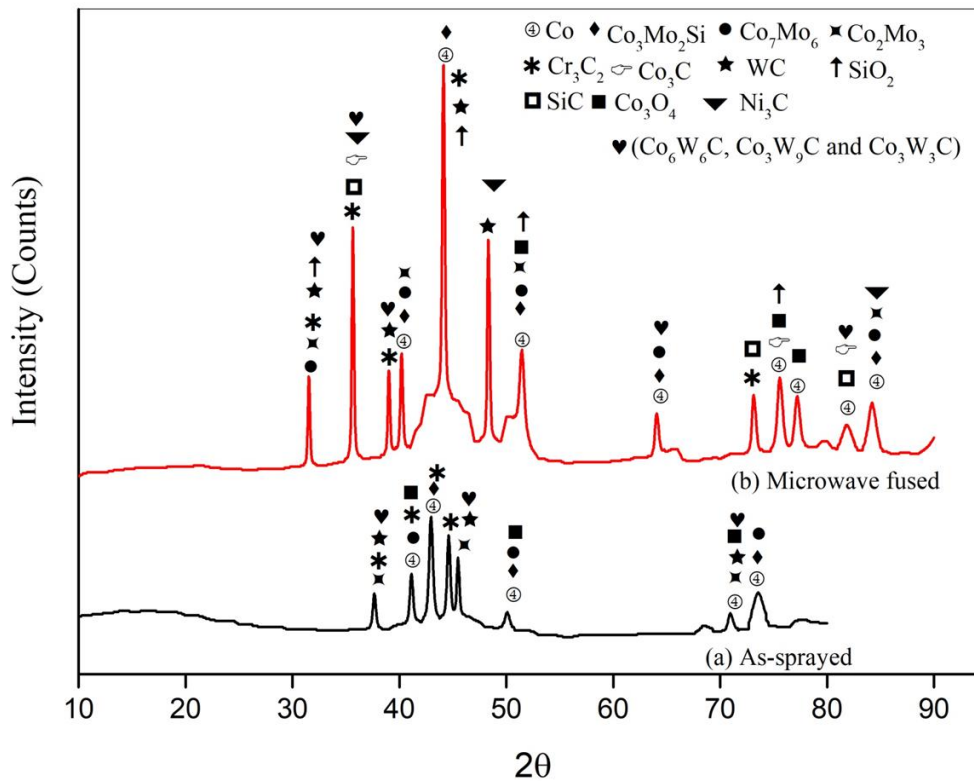


Figure 4.46 XRD patterns of CoMoCrSi+WC-CrC-Ni composite coatings (a) flame sprayed
(b) Microwave fused

4.12 FLAME SPRAYED AND MICROWAVE FUSED CoMoCrSi+WC-12Co COMPOSITE COATINGS

4.12.1 Surface SEM and EDS Analysis

The surface micrograph of flame sprayed CoMoCrSi+WC-12Co and the EDS report is shown in Figure 4.47 (a and b). The surface structure of the as-sprayed coating exhibits unmelted particles with large voids in Figure 4.47 (a). The presence of lamellar splats on the surface increases coating roughness to 11.32 μm , results in the variation of surface properties. The cobalt and tungsten are the dominant elements present in the as-sprayed coating revealed by the EDS report in Figure 4.47(b). The presence of oxide and carbides acts as a strengthener in the coating.

The effect of microwave volumetric heating leads to complete remelting of flame sprayed coating and its surface reveals least defects with no existence of unmelted/semi-melted particles. The surface roughness of the coating reduced to 5.50 μm Figure 4.48(a). The EDS of fused coating presents an increase in the percentage of oxide and carbon elements due to oxidation and graphite sheet effect respectively. The presence of the titanium element is confirmed along with major coating elements in the EDS report Figure 4.48 (b).

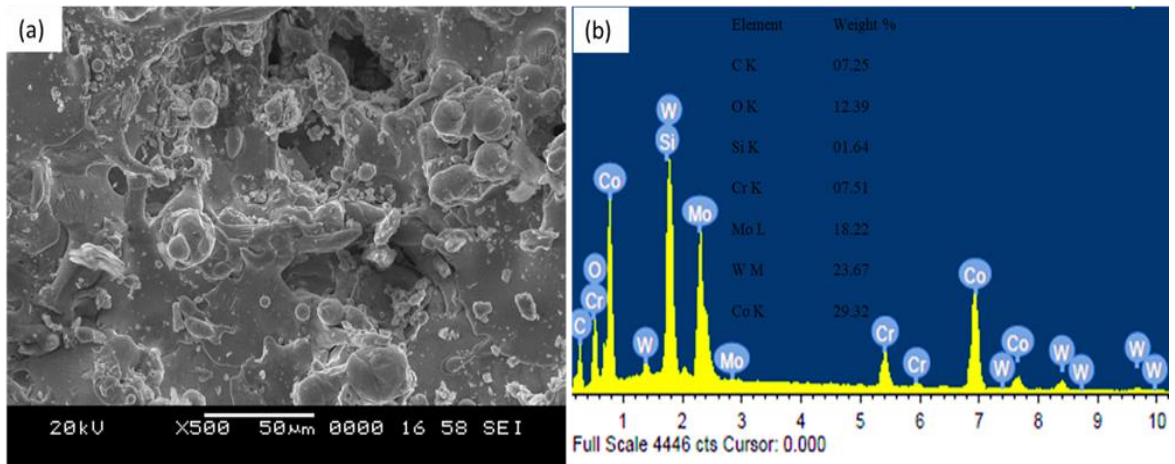


Figure 4.47 Flame sprayed CoMoCrSi+WC-12Co composite coating (a) SEM surface morphology (b) EDS analysis

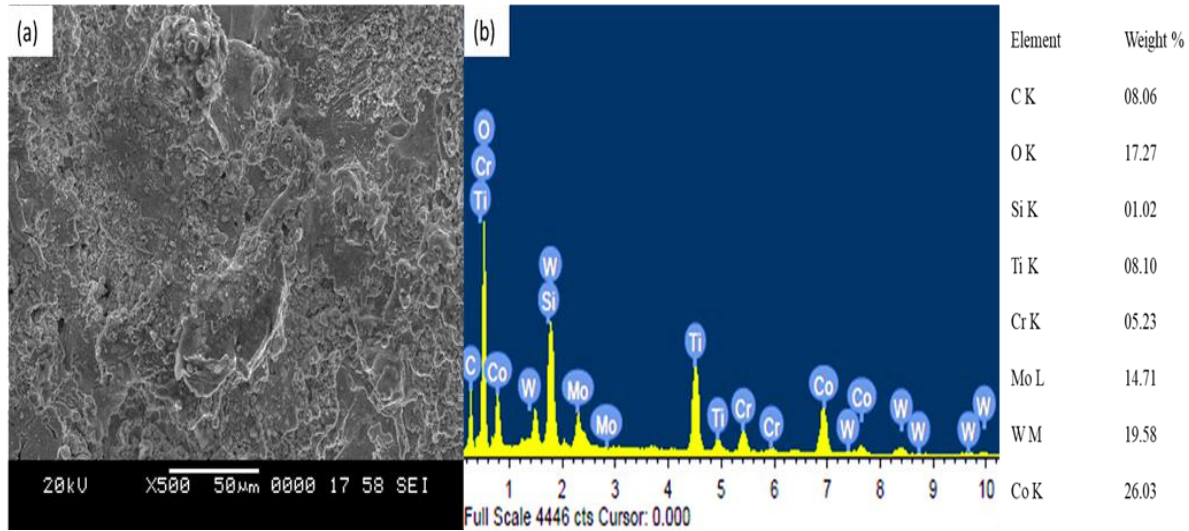


Figure 4.48 Microwave fused CoMoCrSi+WC-12Co composite coating (a) SEM surface morphology (b) EDS analysis

4.12.2 Cross-Sectional Microstructure and Elemental Mapping

The SEM cross-section morphology of flame sprayed and microwave fused CoMoCrSi+WC-12Co composite coatings are shown in Figure 4.49 (a and b). The as-sprayed coating cross-section has many defects such as large voids in between splats, semi-melted particles, and large cracks inhomogeneous coating structure in Figure 4.49 (a). The white patches in the as-sprayed coating (Figure 4.49a) represents the chromium element is surrounded by other major coating constituent elements.

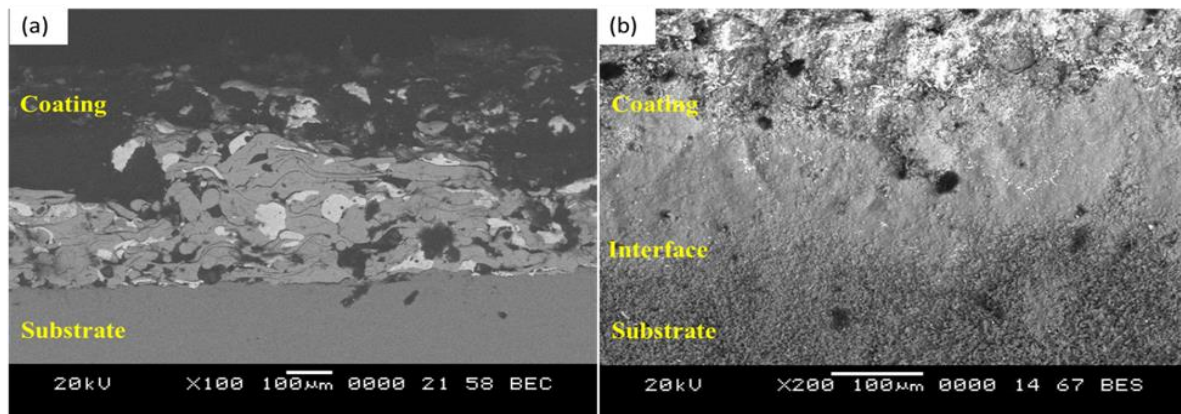


Figure 4.49 SEM micrograph of CoMoCrSi+WC-12Co composite coating along cross-section (a) Flame sprayed (b) Microwave fused coating

However, the cross-section of microwave fused CoMoCrSi/WC-12Co composite coatings shows the homogeneous structure. After remelting, the discontinuities and voids caused during spraying are filled results in a reduction of porosity. The atomic diffusion near the interface zone (Figure 4.49b) is observed due to remelting effect made by the microwave heating process.

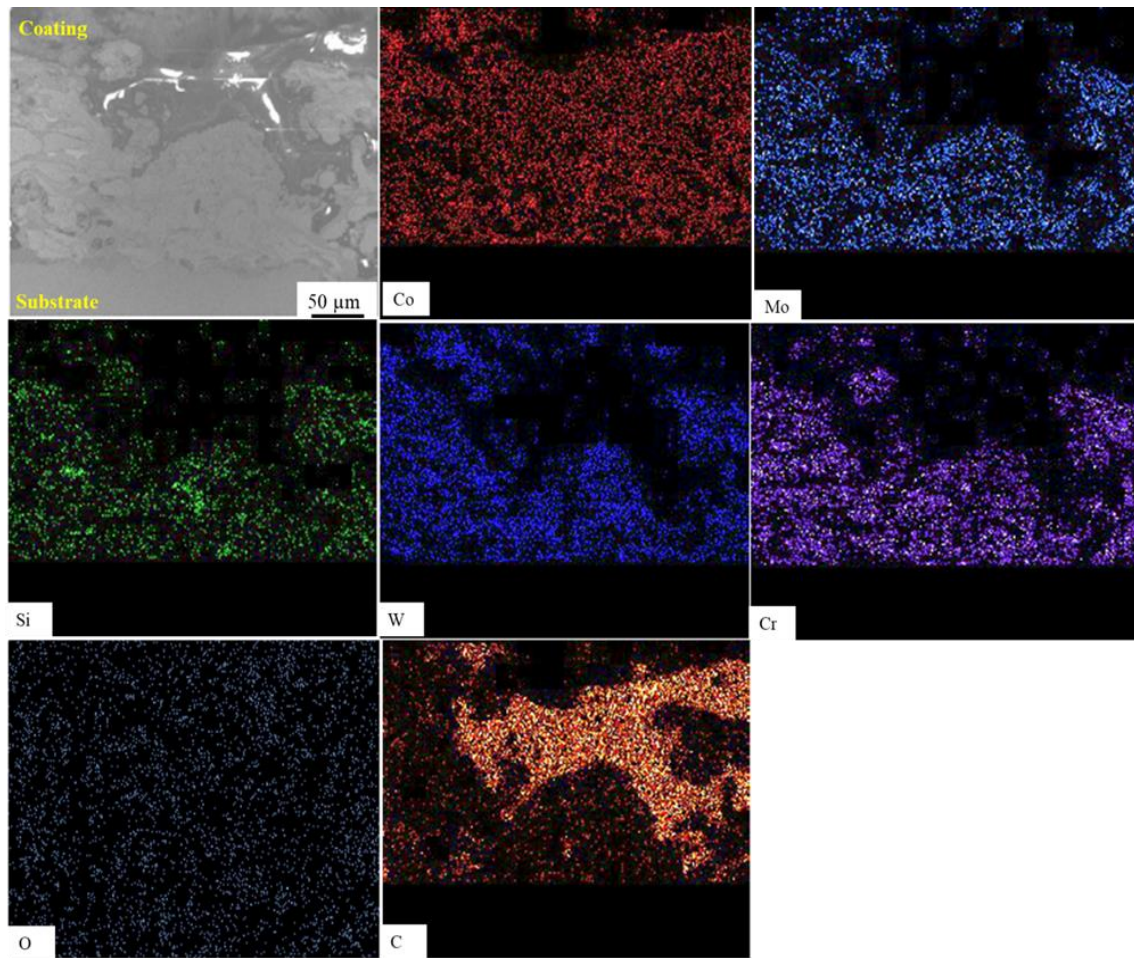


Figure 4.50 Elemental X-ray mapping of flame sprayed CoMoCrSi+WC-12Co composite coating

The mapping results of flame sprayed and microwave fused CoMoCrSi+WC-12Co composite coatings are shown in Figure 4.50 and Figure 4.51 respectively. The as-sprayed coating shows carbon and tungsten is co-existed with cobalt, molybdenum, chromium and silicon elements (Figure 4.50). The sprayed coating has an oxide phase which is distributed over the coating thickness leads to an increase in porosity percentage. The mapping results of

the fused coating describe the inter-diffusion mechanism at the interface zone. The diffusion of tungsten element is more than cobalt and molybdenum; this is due to the valence of elements. The tungsten has more electrons than other coating elements results in a high diffusion rate. The mapping results of the fused coating are evident for even distribution of coating materials after remelting.

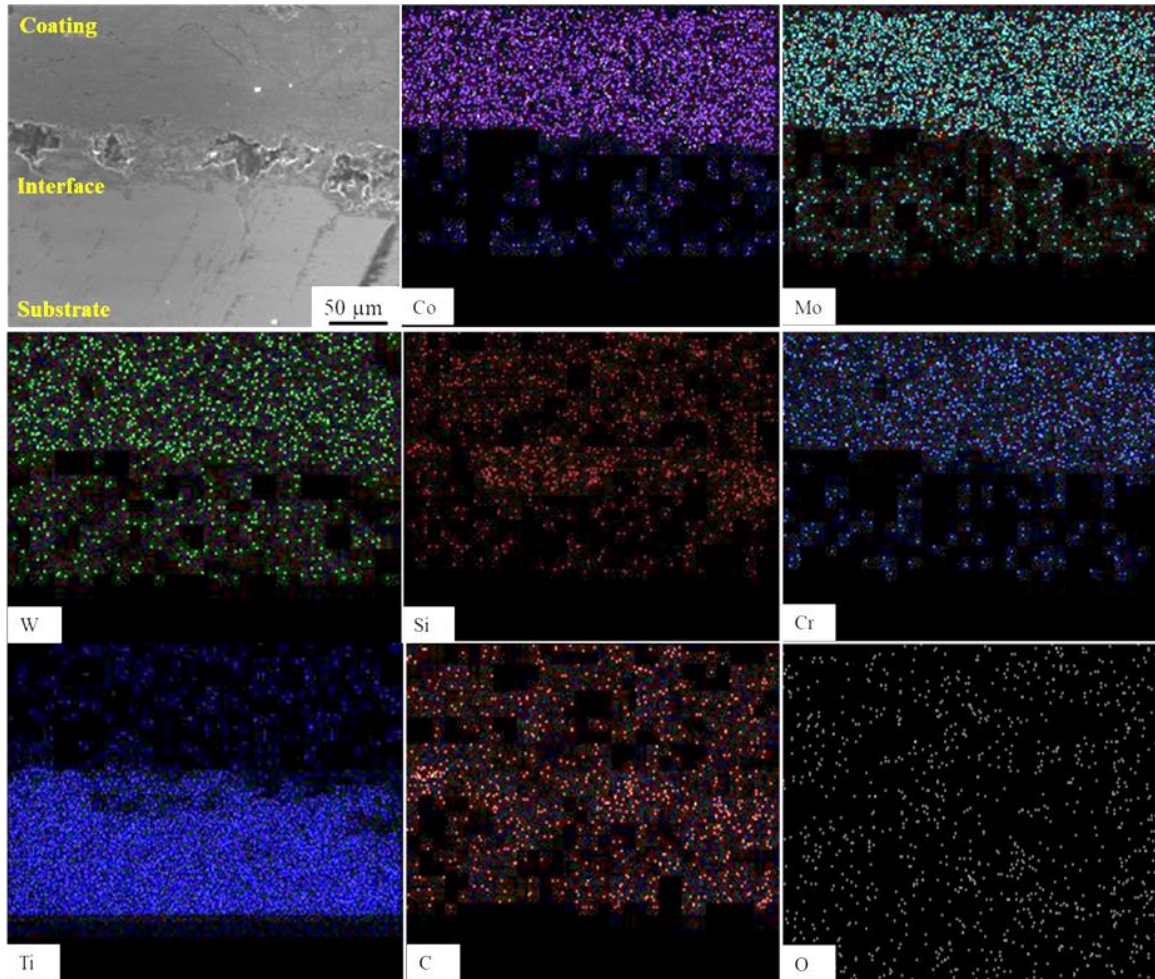


Figure 4.51 Elemental X-ray mapping of microwave fused CoMoCrSi+WC-12Co composite coating

4.12.3 X-Ray Diffraction Studies

The XRD patterns of flame sprayed and microwave fused CoMoCrSi+WC-12Co composite coatings are presented in Figure 4.52 (a and b). The XRD spectrum of the as-sprayed coating has broadening peaks due to the amorphous structure of cobalt solid solution. This confirms

the presence of intermetallic laves phase. The WC phase is identified at 38°, 42°, 54°, the Cr₃C₂ peak is observed at 28°, 34°, 38°, 45°, and 54°. The other carbides such as Co₃C and SiC are existed and also oxide phases Co₃O₄ and SiO₂ are found. The addition of cermets produces new phases which are denoted by the symbol “♥” in Figure 4.52 (a and b). The existence of these phases strengthens the coating properties. The fused coating has changed in its pattern structure due to volumetric heating effect by microwave process. The fused coating retains all the phases identified at as-sprayed coating and spectrum having higher intensities.

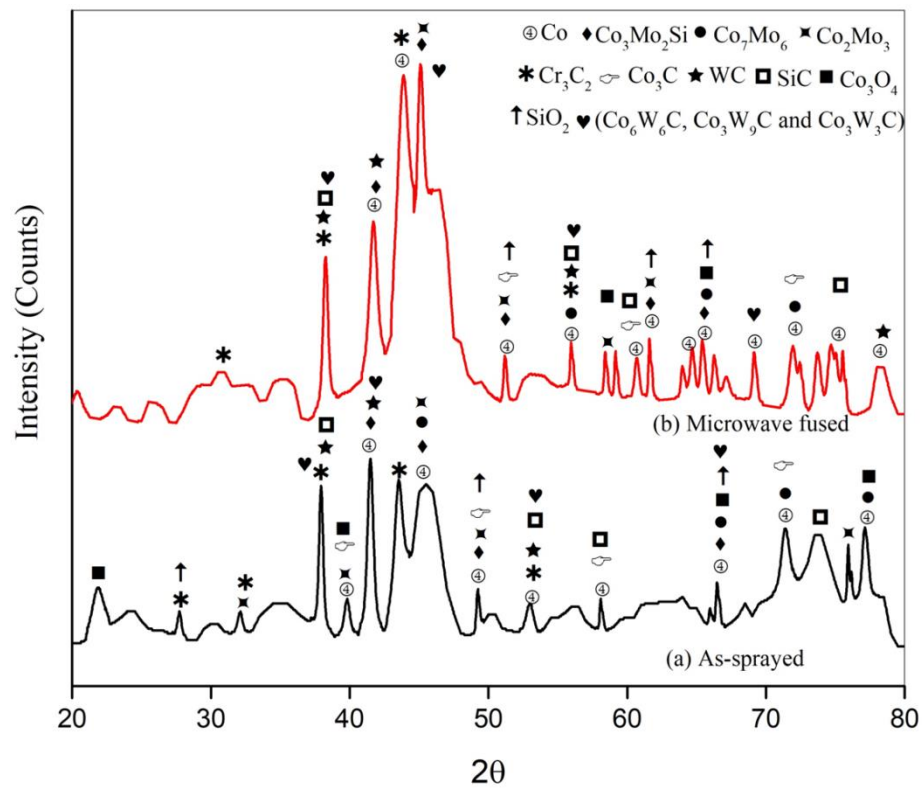


Figure 4.52 XRD patterns of CoMoCrSi+WC-12Co composite coatings (a) flame sprayed
(b) Microwave fused

4.13 POROSITY OF AS-SPRAYED AND FUSED COATINGS

4.13.1 HVOF Sprayed and Microwave Fused Coatings

Porosity is a chief physical characteristic that mainly affects the properties of coatings. The porous coatings deposited by various thermal spray processes provide less resistance to wear and corrosion. This can be improved by post-treatment of as-sprayed coatings to obtain dense

and homogeneous coatings. The porosity of HVOF sprayed and microwave fused coatings are measured and average values are reported in Table 4.6. The porosity of HVOF sprayed CoMoCrSi showed the highest porosity compared with CoMoCrSi+ Cr₃C₂, CoMoCrSi+WC-CrC-Ni, CoMoCrSi+WC-12Co composite coatings. The higher the porosity and pore size increases with a higher particle size of sprayed coatings. The presence of higher particle size on coatings creates space in between splats results in the formation of pores. The milled CoMoCrSi feedstock particles are having higher size than hard phase carbides feedstock particles. The porosity and pore size influence on the feedstock particle size. The HVOF sprayed CoMoCrSi+WC-12Co composite coating exhibits lower porosity due to much finer in feedstock particles. Once after homogenizing the HVOF sprayed coatings through microwave hybrid heating, the porosity of all four types of coatings reduced to less than 1 % is given in Table 4.6. This is mainly due to resolving the surface defects of inclusions or voids and unmelted/partial melted particles present in as-sprayed coatings.

Table 4.6: Average porosity of the coatings

Type of coating	Porosity, (% age)			
	HVOF sprayed coatings	Microwave fused HVOF coatings	Flame sprayed coatings	Microwave fused Flame sprayed coatings
CoMoCrSi	1.52 ± 0.15	0.78 ± 0.15	13.60 ± 1.51	4.87 ± 0.75
CoMoCrSi+Cr ₃ C ₂	1.44 ± 0.10	0.95 ± 0.12	11.35 ± 1.15	5.10 ± 1.15
CoMoCrSi+WC-CrC-Ni	1.31 ± 0.30	0.64 ± 0.10	11.10 ± 1.12	3.42 ± 0.92
CoMoCrSi+WC-12Co	1.12 ± 0.20	0.25 ± 0.10	10.05 ± 1.05	3.10 ± 0.75

4.13.2 Flame Sprayed and Microwave Fused Coatings

The porosity results of flame sprayed and microwave fused coatings are listed in Table 4.6. Compared to HVOF spray coatings, flame spray process has a low velocity of spraying of feedstock particles, these results in the formation of porosity during in-flight particle duration and same as deposited on the substrate surface. The CoMoCrSi+Cr₃C₂, CoMoCrSi+WC-CrC-Ni, CoMoCrSi+WC-12Co composite coatings reveal lower porosity than flame sprayed

CoMoCrSi coatings. Post heat treatment of flame sprayed coatings; the porosity has been decreased drastically due to homogeneous effect by microwave heating. CoMoCrSi+WC-12Co composite coatings deposited by flame spray and microwave fused showed lower porosity compared with the other three types of coatings.

4.14 MICROHARDNESS OF COATINGS

4.14.1 HVOF Sprayed and Microwave Fused Coatings

The microhardness of HVOF sprayed and microwave fused four types of coatings is measured along the cross-section of coatings. The measured microhardness of each coating is showed by bar chart along with an error bar in order to represent the standard deviation in Figure 4.53. The measured average microhardness values of HVOF sprayed and microwave fused coatings are tabulated in Table 4.7. The average microhardness of substrate is 185 ± 15 H_V. The HVOF sprayed CoMoCrSi+WC-12Co composite coating showed the highest hardness of 1290 ± 35 H_V than other sprayed coating, whereas CoMoCrSi coating exhibits a lower hardness of 705 ± 35 H_V. The HVOF sprayed coatings possess heterogeneous structure results in variation of hardness. In the case of as-sprayed coating interface substrate, hardness is increased due to the work hardening effect from sandblasting of the substrate prior to the coating process. The hardness is significantly increased from the interface coating region due to high compressive stress achieved by higher particle velocity of coating with a decrease in powder feed rate (Murugan et al., 2014). The as-sprayed coating has a certain characteristic features such as voids, cracks and unmelted/semi-melted particles which affects the coating hardness near surface region. Microhardness of the four types of fused coatings increased drastically because of the homogeneous structure as well as metallurgical bonding caused due to inter-diffusion of elements. Also the addition of carbon into as-sprayed coatings during microwave heating results in the formation of the hard surface layer. The percentage increase in microhardness of as-sprayed coatings after fusing is given in Table 4.7. The hardness of the fused CoMoCrSi+Cr₃C₂ composite coating is increased by 26.40 % than as-sprayed coating which is the highest percentage increase of hardness compared to other coatings. Another reason for improving microhardness is due to the rapid solidification of fused coatings which strengthens the grains. Also, the presence of hard

carbides such as Cr_3C_2 , Co_3C WC, and intermetallic laves phases leads to increase the hardness of the fused coating (Kaiming et al., 2018), (Bolelli and Lusvarghi, 2006).

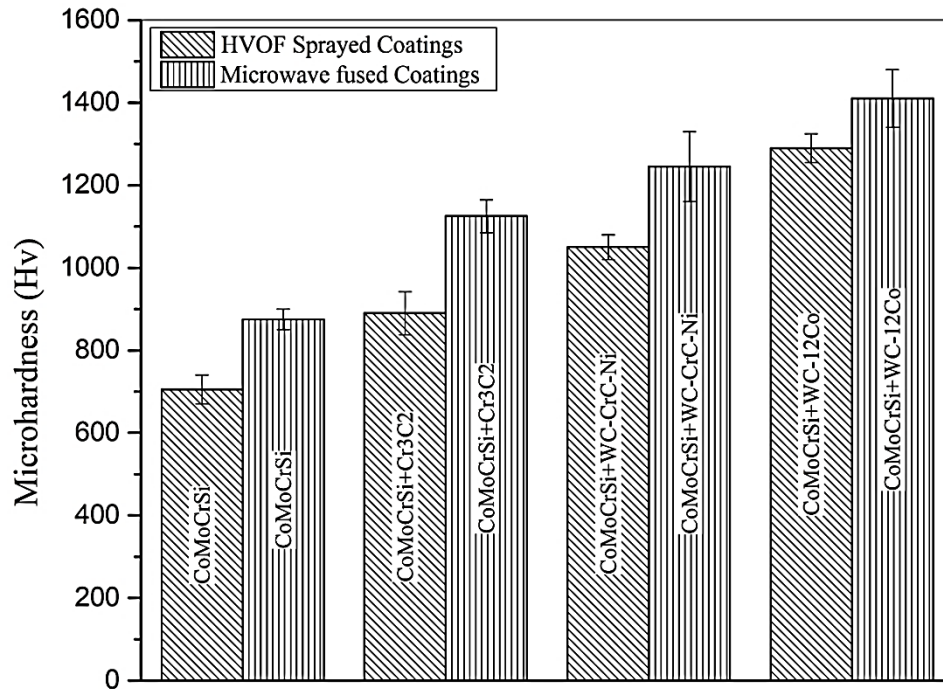


Figure 4.53 Bar chart showing average microhardness of HVOF sprayed and Microwave fused coatings

Table 4.7: Average Microhardness of HVOF sprayed and Microwave fused coatings

Type of coating	Microhardness (Hv)		
	HVOF sprayed coatings	Microwave fused HVOF coatings	Percentage of increase in microhardness after fusing
CoMoCrSi	705 ± 35	875 ± 25	24.11 %
CoMoCrSi+Cr ₃ C ₂	890 ± 52	1125 ± 40	26.40 %
CoMoCrSi+WC-CrC-Ni	1050 ± 30	1245 ± 85	18.57 %
CoMoCrSi+WC-12Co	1290 ± 35	1410 ± 70	09.30 %

4.14.2 Flame Sprayed and Microwave Fused Coatings

The microhardness of flame sprayed and microwave fused four types of coatings is measured along the cross-section of coatings. The computed microhardness of all four types of coatings is represented by bar chart along with an error bar in order to denote the standard deviation in Figure 4.54. As discussed in section 4.13.2 porosity of flame spray coatings is strongly influence on the microhardness property. The measured average microhardness values of flame sprayed and microwave fused coatings are listed in Table 4.8. In case of flame sprayed the all four types of coatings, near interface zone hardness is slightly increased due to treatment with abrasive particles prior to coating. The hardness is varying with corresponding to thickness and hardness is started decreasing near-surface region of coatings. This is because of compressive stresses acting in between splats at the interface zone enhances hardness at interface zone whereas hardness is decreasing in between coating layers due to tensile stresses. CoMoCrSi+WC-12Co flame sprayed coating produced the highest hardness than other coatings. Similarly in the case of fused coatings experienced fluctuations in hardness values due to compressive and tensile stresses phenomenon. However, the hardness of fused coatings at the interface is high due to metallurgical bonding. Since the coating comprises of cobalt-rich solid solution intermetallics embedded into hard face carbides, CoMoCrSi+WC-12Co fused coating exhibits 1387 ± 25 Hv by increasing 32.09 % of hardness than other three coatings.

Table 4.8: Average Microhardness of Flame sprayed and Microwave fused coatings

Type of coating	Microhardness (Hv)		
	Flame sprayed coatings	Microwave fused flame sprayed coatings	Percentage of increase in microhardness after fusing
CoMoCrSi	610 ± 30	745 ± 15	22.13 %
CoMoCrSi+Cr ₃ C ₂	650 ± 10	836 ± 15	28.61 %
CoMoCrSi+WC-CrC-Ni	915 ± 30	1156 ± 15	26.33 %
CoMoCrSi+WC-12Co	1050 ± 10	1387 ± 25	32.09 %

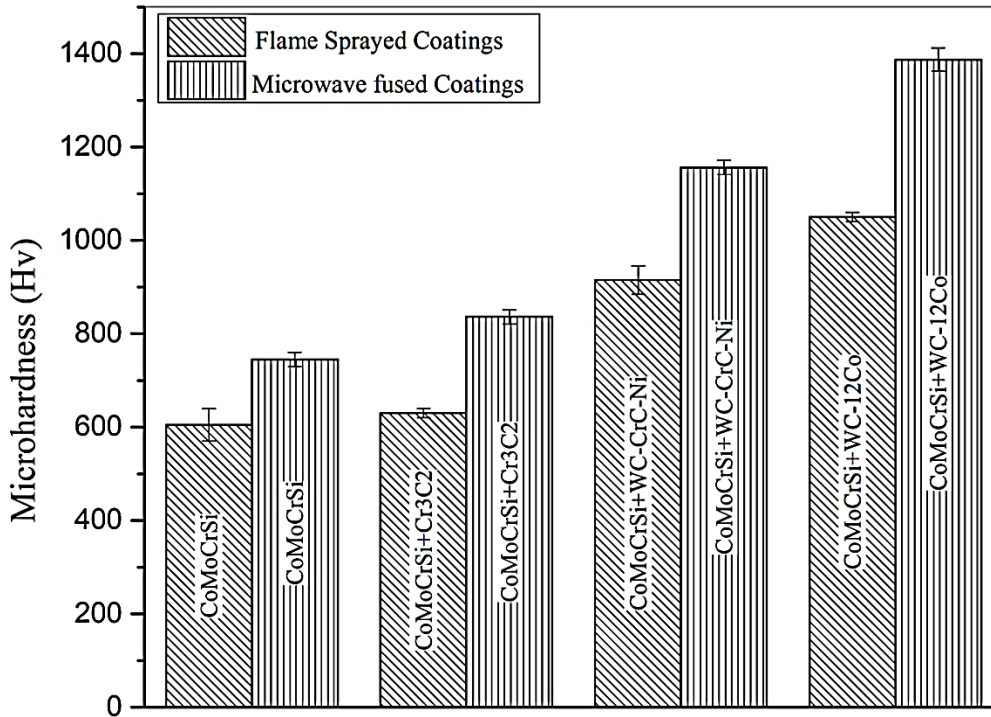


Figure 4.54 Bar chart showing average microhardness of flame sprayed and Microwave fused coatings

4.15 ADHESION STRENGTH OF COATINGS

4.15.1 HVOF Sprayed Coatings

It is important to assess the adhesion strength of the coatings which correlates the bonding between coating and substrate. The estimated adhesion strength values of HVOF sprayed coatings are listed in Table 4.9. CoMoCrSi+WC-12Co as-sprayed coating exhibits the highest adhesion strength of 64.22 MPa compared to other three coatings, this is because of least porosity and higher hardness obtained. Figure 4.55 represents the macrograph of the fracture surface of HVOF sprayed coating subjected to bond strength test. It is observed that adhesive failure occurred between the coating and substrate interface. Such failure indicates that the coating cohesive strength is superior to the coating adhesive strength. The bond strength between individual structure parts (splats and phases) is higher than the bond strength of the coating to the substrate. Cho et al., (2009) reported similar test values of HVOF-sprayed cobalt-based coatings.

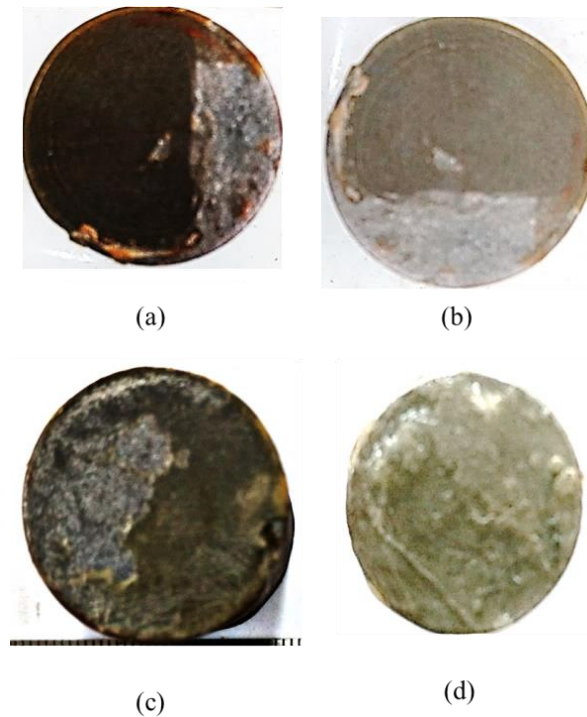


Figure 4.55 Macrograph of fractured surface of HVOF sprayed coatings during adhesion test samples (a) CoMoCrSi (b) CoMoCrSi+Cr₃C₂ (c) CoMoCrSi+WC-CrC-Ni (d) CoMoCrSi+WC-12Co

4.15.2 Microwave Fused HVOF Coatings

Figure 4.56 depicts the macrographs of the fractured surface of microwave fused HVOF coatings. The average value of adhesion strength of microwave fused HVOF coatings is given in Table 4.9. It is clearly noticed after post heat treatment due to eliminating of surface defects like voids, pores, unmelted or semi-melted particles, the surface results in a homogeneous structure. This enhanced the adhesion strength of fused coatings. CoMoCrSi+WC-12Co fused HVOF coating exhibits the highest adhesion strength of 79.45 MPa. But CoMoCrSi+Cr₃C₂ composite fused coating showed the highest increase in adhesion strength from 58.31 MPa to 75.46 MPa with increased 29.41 % due to sound metallurgical bonding. The fractured surface of the fused coating clearly reveals that the failure is caused due to the adhesive between the substrate and fused coatings shown in Figure 4.56.

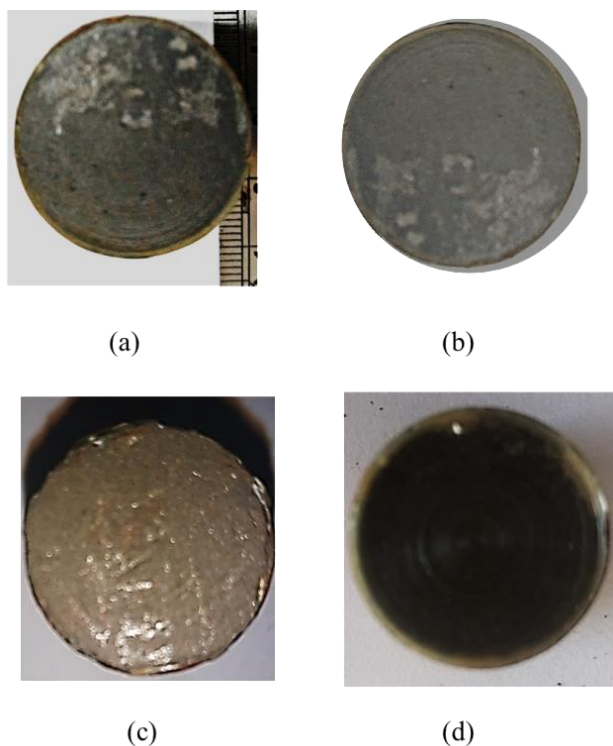


Figure 4.56 Macrograph of fractured surface of microwave fused HVOF sprayed coatings subjected to adhesion test (a) CoMoCrSi (b) CoMoCrSi+Cr₃C₂ (c) CoMoCrSi+WC-CrC-Ni (d) CoMoCrSi+WC-12Co

Table 4.9: Adhesion strength of HVOF sprayed and Microwave fused coatings

Type of coating	Adhesion strength, (MPa)		
	HVOF sprayed coatings	Microwave fused HVOF coatings	% age of increase of adhesion strength after fusing of HVOF coatings
CoMoCrSi	61.31	72.65	18.34 %
CoMoCrSi+Cr ₃ C ₂	58.31	75.46	29.41 %
CoMoCrSi+WC-CrC-Ni	60.81	77.60	27.60 %
CoMoCrSi+WC-12Co	64.22	79.45	23.71 %

4.15.3 Flame Sprayed Coatings

The average adhesion strength of flame sprayed coatings are tabulated in Table 4.10 and fractured macrographs of all four types of coatings are demonstrated in Figure 4.57. It is clear evidence that flame sprayed coatings exhibit lower adhesion strength compared with HVOF coatings. It is because of higher porosity and lower hardness attributed in to flame sprayed coatings due to the low velocity of spraying feedstock particles. The defects such as voids, cracks generated during solidification between splats lead to the formation of stress concentration. The CoMoCrSi+WC-12Co flame sprayed coating reveals higher adhesion strength of 35.49 MPa compared to the other three types of coatings. The failure of coatings caused due to adhesive between coating and substrate can be observed in Figure 4.57.

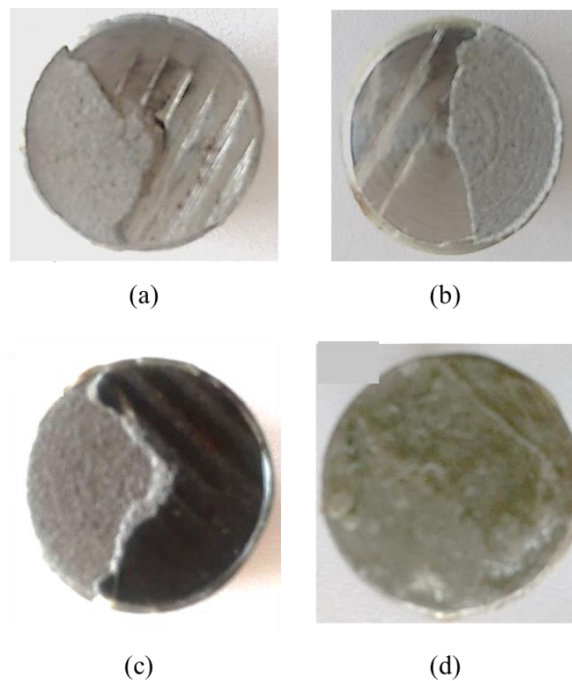


Figure 4.57 Macrograph of fractured surface of flame sprayed coatings subjected to adhesion test (a) CoMoCrSi (b) CoMoCrSi+Cr₃C₂ (c) CoMoCrSi+WC-CrC-Ni (d) CoMoCrSi+WC-12Co

Table 4.10: Adhesion strength of Flame sprayed and Microwave fused coatings

Type of coating	Adhesion strength, (MPa)		
	Flame sprayed coatings	Microwave fused Flame sprayed coatings	% age of increase of adhesion strength after fusing of Flame sprayed coatings
CoMoCrSi	28.12	46.53	65.46 %
CoMoCrSi+Cr ₃ C ₂	31.02	51.74	66.79 %
CoMoCrSi+WC-CrC-Ni	32.18	49.74	54.56 %
CoMoCrSi+WC-12Co	35.49	54.04	52.26 %

4.15.4 Microwave Fused Flame Sprayed Coatings

Figure 4.58 presents the fractured macrographs of microwave fused flame sprayed coatings. After fusing, the adhesion strength of all coatings is drastically increased. The fused coatings exhibit greater than 50 % increase in its adhesion compared to flame sprayed coatings.

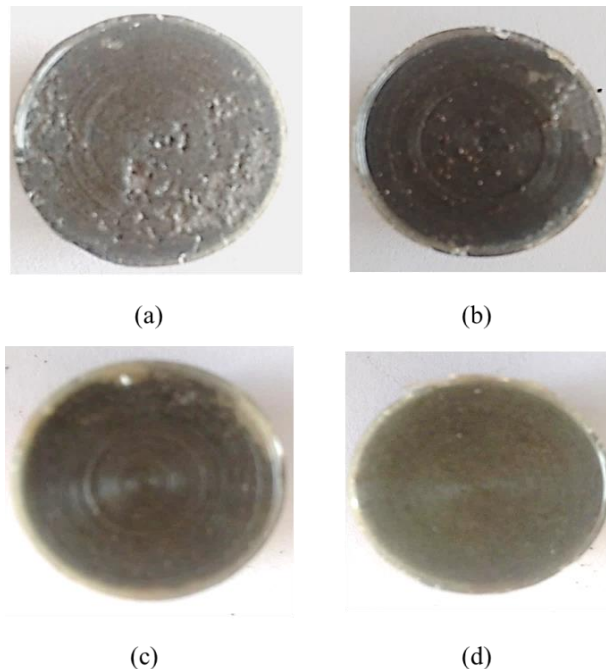


Figure 4.58 Macrograph of fractured surface of microwave fused flame sprayed coatings subjected to adhesion test (a) CoMoCrSi (b) CoMoCrSi+Cr₃C₂ (c) CoMoCrSi+WC-CrC-Ni (d) CoMoCrSi+WC-12Co

The average value and its percentage of increase in adhesion strength are listed in Table 4.10. CoMoCrSi+WC-12Co fused coating produced the highest bond strength of 54.04 MPa. The CoMoCrSi and CoMoCrSi+Cr₃C₂ fused coatings showed the highest percentage of increase in its adhesion strength 65.46 % and 66.79 % respectively. This is mainly due to elongation of grains during remelting results in penetration of material which eliminates the voids and cracks present in between splats. Also, inter-diffusion of elements improves the bond strength of coating and substrate. The fractured surface of the fused coating clearly reveals that the failure is caused due to the adhesive between the substrate and fused coatings shown in Figure 4.58

4.16 SUMMARY

The HEBM process is successfully used to obtain a higher fraction of intermetallic laves phases as well as to decrease in particle size of CoMoCrSi feedstock. The CoMoCrSi feedstock during milling changed its particle morphology due to high impact energy, and the process ends with the plastic deformation of CoMoCrSi particles shown in Figure 4.2 and Figure 4.3. The milled feedstock at 5 hr confirms the reduction in its particle size to 60.12 μm given in Table 4.1. The formation of intermetallic laves phases amorphous structure (bulk metallic glass structure) is confirmed with respect to milling time at 5 hr shown by XRD analysis (Figure 4.4). Also, hard carbides such as Cr₃C₂, WC-CrC-Ni, and WC-12Co are successfully reinforced into milled CoMoCrSi feedstock with a mass fraction of 70:30 using HEBM process. In the present work, four types of coatings such as CoMoCrSi, CoMoCrSi+Cr₃C₂, CoMoCrSi+WC-CrC-Ni, and CoMoCrSi+WC-12Co are successfully deposited on pure titanium grade-15 substrate by using HVOF and Flame spray process. To refine the metallurgical and mechanical properties of coatings deposited by HVOF and Flame spray process are successfully fused by microwave hybrid heating technique. The HVOF spray system with hydrogen fuel is used to deposit the coatings. The hydrogen fuel helps in the formation of quality coatings with a high acceleration rate. The powder with a lower feed rate of 17 g/min is used to develop coatings, this parameter strongly influenced coatings microhardness and porosity.

The coatings deposited by HVOF system shows a typical splat surface with dense microstructure also exhibits lower porosity. All four types of HVOF coatings having a highly

lamellar structure with distinct splat regions and splats with long axis are oriented parallel to the surface of the substrate. The cross-section of all as-sprayed coatings exhibits some defects such as unmelted/semi-melted particles, oxide stringers along the grain boundaries and small pores have been observed. The HVOF CoMoCrSi+WC-CrC-Ni composite coating (Figure 4.20) exhibits less thickness than the other three types of coatings is given in Table 4.2. The surface roughness of HVOF sprayed coatings is slightly higher due to the existence of unmelted or partially particles. Higher the surface roughness of the coating part would lead to higher wear rate (Kamal, 2010). The CoMoCrSi+WC-12Co HVOF coating produces less surface roughness of 5.5 μm as discussed in section 4.8.1. Microwave fusing of HVOF sprayed coatings reveals that the presence of unmelted particles with defects like voids, pores have been eliminated by forming a homogeneous structure. The effect of post heat treatment leads to the inter-diffusion of elements at the substrate interface region, results in a sound metallurgical bonding between coating and substrate. This also reduces the surface roughness of HVOF sprayed coatings. After fusing CoMoCrSi+WC-12Co composite coating reveals better surface roughness of 2.7 μm compared to other coatings. The EDS analysis of HVOF sprayed CoMoCrSi coating shown rich in Co and Mo elements which is near to coating composition without presence of carbon and oxide elements (Figure 4.7b), after fusing due to inducing of carbon from graphite sheet CoMoCrSi fused coating exhibits carbon and oxide element is found due to process carried out under atmospheric conditions (Figure 4.8b). Its elemental mapping confirms the uniform distribution of coating elements before and after fusing. Also, the diffusion phenomenon can be clearly observed through X-ray mapping results (Figure 4.10 and Figure 4.11). The other three types of coatings such as CoMoCrSi+Cr₃C₂, CoMoCrSi+WC-CrC-Ni, and CoMoCrSi+WC-12Co before and after fusing show rich in Co element along with reinforced elements which confirm the required coating composition from its EDS analysis. The titanium element is found in the EDS analysis of all fused coatings due to diffusion. The elemental mapping of fused coatings confirms the presence of substrate traces in the fused coatings.

As observed from XRD patterns of feedstock powders and HVOF coatings, slight changes with higher intensities in the structure of XRD patterns have been noticed for HVOF sprayed coatings. The HVOF sprayed and fused coatings retain the phases as obtained at feedstock, whereas fused coatings showed TiC, TiO₂ phases due to diffusion of the substrate towards

coatings. The formation of oxides in fused coatings due to the process conducted under atmospheric conditions. The XRD pattern of CoMoCrSi+WC-CrC-Ni and CoMoCrSi+WC-12Co as-sprayed and fused coatings exhibit new phases such as $\text{Co}_6\text{W}_6\text{C}$, $\text{Co}_3\text{W}_9\text{C}$, and $\text{Co}_3\text{W}_3\text{C}$ (Figure 4.23 and Figure 4.28) during the remelting process due to recrystallization of cobalt, tungsten and carbon elements (Dejuna and Tianyuan, 2014). The presence of carbides and oxides acts as strengtheners to enhance microhardness and wear resistance.

The porosity results of HVOF sprayed and microwave fused coatings shown that CoMoCrSi+WC-12Co coating before and after fusing exhibits least porosity compared to other types of coatings. The HVOF sprayed coatings reveals the porosity of less than 2 %, whereas after the treatment of coatings by microwave the porosity of all coatings reduced to less than 1 % is given in Table 4.6. The reason is remelting of coatings which eliminates the unmelted particles and decreases the size of pores results in a reduction of porosity.

The measured substrate hardness is $185 \pm 15 \text{ H}_v$ which is too lower hardness to resist high vibrations at elevated temperature working conditions. The CoMoCrSi+WC-12Co HVOF sprayed and microwave fused coating reveals the highest microhardness among other types of coatings. The HVOF sprayed coatings produced heterogeneous structure due to this reason variation in microhardness is noticed (Prasad et al., 2018). The homogeneous structure of fused coatings significantly improves its microhardness. The estimated microhardness values of HVOF sprayed and fused coatings are listed in Table 4.7. The adhesion strength of coatings confirms that CoMoCrSi+WC-12Co coatings before and after microwave fusing have highest bond strength. The CoMoCrSi+ Cr_3C_2 composite coating after fusing increased its bond strength percentage by 29.41 % due to better metallurgical bonding compared to other coatings. The HVOF sprayed and fused coatings clearly disclose that the failure of adhesive results in fracturing of coatings. The measured values of adhesion strength of coatings are given in Table 4.9.

In this study, the flame sprayed coatings are having significant variations in terms of the quality of coatings produced comparing with the HVOF process. The flame spray process is a low-velocity technique in which the deposited coatings exhibit high surface roughness and porosity, moderate hardness and adhesion strength. The cross-section microstructure of flame sprayed coatings reveals the lamellar structure; larger splats are formed surrounded by oxide

stringers and bonded well with the substrate. The presence of unmelted or semi-melted particles is higher than coatings deposited by HVOF process. The CoMoCrSi flame sprayed coating has a higher thickness of 270 μm than other three types of coatings. The CoMoCrSi+Cr₂C₃ and CoMoCrSi+WC-CrC-Ni as-sprayed coatings are having similar thickness whereas CoMoCrSi+WC-12Co as-sprayed coating exhibit a lower thickness of 176 μm is given in Table 4.2. The coatings deposited by flame spray are having more surface roughness, CoMoCrSi coating reveals the higher value of 16 μm (Figure 4.29), whereas CoMoCrSi+WC-12Co coating is the lower value of 11.32 μm (Figure 4.47). In CoMoCrSi coating presence of unmelted or partially melted particles are more than the CoMoCrSi+WC-12Co coating results in higher surface roughness. From CoMoCrSi+Cr₂C₃ and CoMoCrSi+WC-CrC-Ni as-sprayed coatings observed marginal difference in its surface roughness values. After microwave fusing of flame sprayed coatings, the coating surface roughness has been decreased drastically due to homogeneous structure results in smooth layer formation at the surface. The CoMoCrSi+WC-12Co fused coating shown better roughness value of 5.50 μm (Figure 4.48). The EDS results of flame sprayed CoMoCrSi coating shown rich in Co and Mo elements and also oxide phase has been identified (Figure 4.34). The post heat treatment provides a carbon element from the graphite sheet into CoMoCrSi coating leads to the formation of carbides, the presence of carbon is confirmed by EDS analysis of fused CoMoCrSi coatings (Figure 4.30). The EDS and elemental mapping results of flame sprayed coatings shown the presence of major coating constituent elements such as Co, Mo, Cr, Si, and reinforced elements like WC, Ni. The elemental mapping results had shown the proper distribution of coating elements over the thickness. After fusing, titanium is diffused towards coating region results in the formation of metallurgical bonding. The elemental mapping results of flame sprayed fused coatings shown the diffused layer of the substrate near the coating interface and it is extended further (Figure 4.33, Figure 4.39, Figure 4.45 and Figure 4.51).

The XRD results of flame sprayed coatings present significant changes in its pattern structure compared to feedstock due to the formation of oxides during spraying. The coatings before and after fusing retain the original phases as found at feedstock, but fused coatings showed the TiC and TiO₂ phases due to substrate diffusion. The XRD pattern of CoMoCrSi+WC-

CrC-Ni and CoMoCrSi+WC-12Co flame sprayed and fused coatings exhibits new phases such as $\text{Co}_6\text{W}_6\text{C}$, $\text{Co}_3\text{W}_9\text{C}$, and $\text{Co}_3\text{W}_3\text{C}$ (Figure 4.46 and Figure 4.52) during the remelting process due to recrystallize of cobalt, tungsten and carbon elements (Dejuna and Tianyuan, 2014).

The porosity results of flame sprayed and microwave fused coatings shown that CoMoCrSi+WC-12Co coating before and after fusing exhibits least porosity compared to other types of coatings. The flame sprayed coatings reveals that the porosity is more than 10 %, whereas after the treatment of coatings by microwave the porosity of all coatings reduced to less than 6 % is given in Table 4.6. The reason is remelting of coatings which eliminates the unmelted particles and decreases the size of voids or pores results in a reduction of porosity.

The CoMoCrSi+WC-12Co flame sprayed and microwave fused coating reveals the highest microhardness among other types of coatings. The flame sprayed coatings produced heterogeneous structure due to this reason significant variations in hardness has been noticed (Prasad et al. 2018B) The homogeneous structure of fused coatings significantly improves its microhardness. The computed microhardness values of flame sprayed and fused coatings are listed in Table 4.8. The flame sprayed and fused CoMoCrSi+WC-12Co composite coating exhibits the highest bond strength compared to other coatings. On the other hand, the bond strength of fused coatings increased more than 50 % in its value compared to flame sprayed coatings. However the CoMoCrSi+ Cr_3C_2 composite coating after fusing increased its bond strength percentage by 66.79 % due to better metallurgical bonding compared to other coatings. The all flame sprayed and fused coatings fractured due to the failure of adhesive. The measured values of adhesion strength of flame sprayed and fused coatings are given in Table 4.10.

CHAPTER 5

WEAR STUDIES

This chapter deals with the sliding wear behavior of substrate, HVOF sprayed coatings, flame sprayed coatings, and microwave fused coatings at different temperatures i.e. 200 °C, 400 °C and 600 °C under dry conditions for 10 N and 20 N normal loads. The coefficient of friction is determined and the wear rate calculated by the volume loss method. The wear out samples is analyzed using XRD and SEM/EDS techniques. The computed results have been compiled to provide the comparative performance of the coatings.

5.1 WEAR STUDIES ON HVOF SPRAYED AND MICROWAVE FUSED CoMoCrSi COATINGS

5.1.1 Volume loss and Wear rate of Coatings

Figure 5.1 (a and b) and Figure 5.2 (a and b) depicts the wear volume loss and wear rate plots of HVOF sprayed and microwave fused CoMoCrSi coatings. These plots represent the volume loss and wear rate of coatings corresponding to varying temperature. It is noted that volume loss and wear rate of as-sprayed coatings increases with a rise in temperature at both 10 N and 20 N normal load. Whereas microwave fused coating shows less volume loss and wear rate for both test loads Figure 5.1 (a and b) and Figure 5.2 (a and b). The wear rate of fused coating at 200°C, 400°C, and 600°C is reduced by 6, 8 and 10 times respectively than that of as-sprayed coatings. The dry sliding wear behavior of fused CoMoCrSi coating reveals lower volume loss and lower wear rate than HVOF sprayed coatings. This is mainly attributed to laves phases mostly amorphous (bulk metallic glass) present in hyper-eutectic cobalt matrix of fused CoMoCrSi coating which provides high-temperature strength, hardness and wear stability (Prasad et al., 2018).

Finally, the Archard Model ($W/LC = k$, W = wear in mm^3 , L = sliding length in m, C = normal load in N) used to calculate the wear rate coefficient k in $\text{mm}^3/\text{N m}$ (Fernandez et al., 2005). The graph in Figure 5.3 relates the average wear rate of HVOF sprayed and fused coating. The linear regression's slope gives the average value of the wear rate coefficient k . The value

of k for the HVOF sprayed coating is $2 \times 10^{-6} \text{ mm}^3/\text{N m}$ and the fused coating is $1 \times 10^{-6} \text{ mm}^3/\text{N m}$. Hence the fused coating has better wear resistance than an as-sprayed coating.

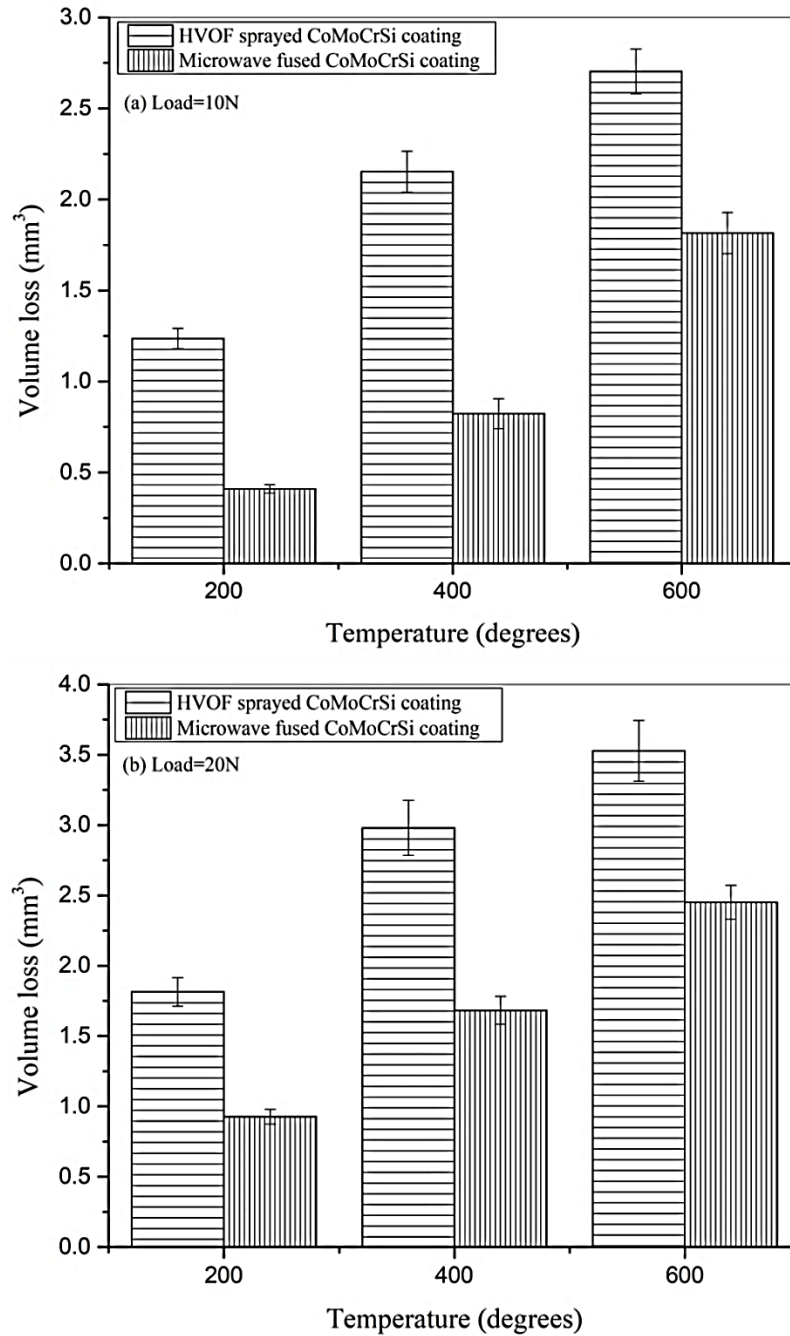


Figure 5.1 Wear volume loss of HVOF sprayed and microwave fused CoMoCrSi coatings with respect to temperature (a) 10 N, (b) 20 N

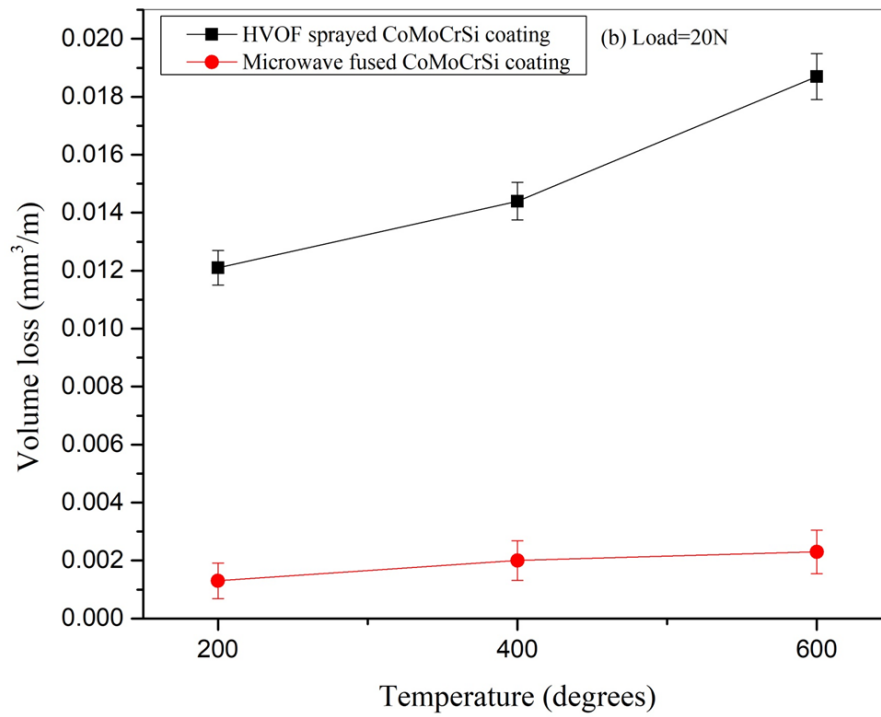
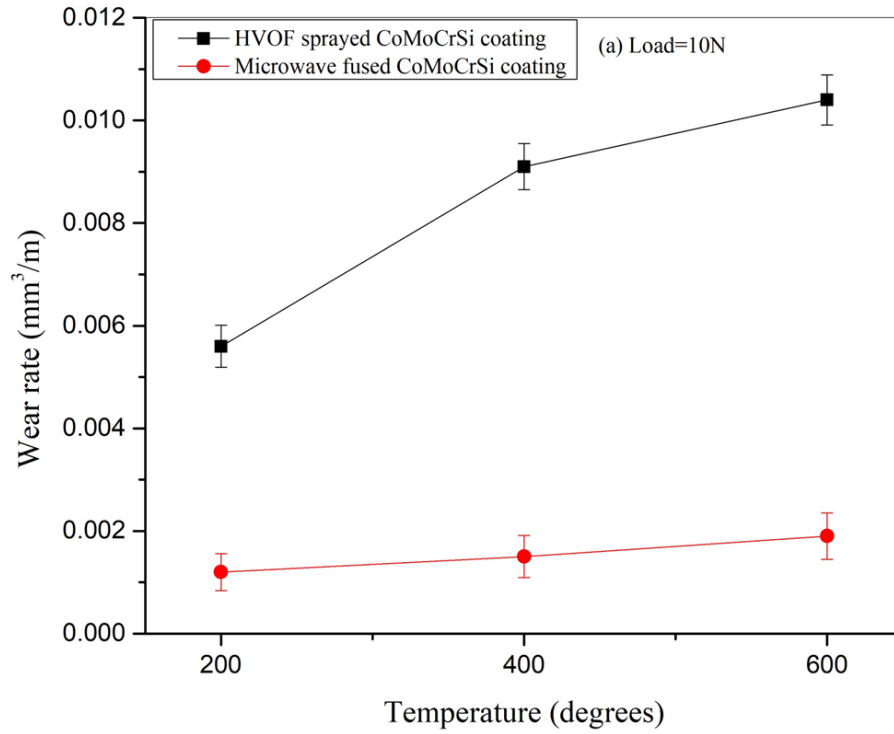


Figure 5.2 Wear rate plots of HVOF sprayed and microwave fused CoMoCrSi coatings

(a) 10 N, (b) 20 N

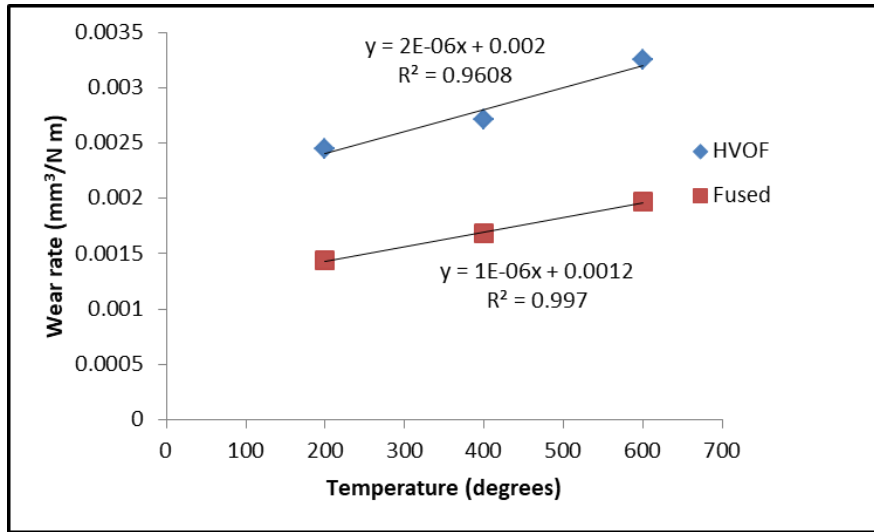


Figure 5.3 Wear rate coefficient k plot of HVOF sprayed and fused CoMoCrSi coating

5.1.2 Coefficient of Friction

Figure 5.4 (a and b) shows the coefficient of friction (COF) plots of HVOF sprayed and microwave fused CoMoCrSi coatings corresponding to the sliding distance. The results revealed that the COF of microwave fused coating at 200°C, 400°C and 600°C is reduced by 25 %, 38.14 %, and 41.76 % respectively compared to as-sprayed coatings. The friction coefficient is measured for each test and the average value of the as-sprayed coating is 0.76, which are significantly higher than the average values of fused coatings (0.48-0.54) measured at high temperature. In the case of as-sprayed coatings rapid loss of material by the adhesive phenomenon and increase in a flash-temperature is the reasons to increase friction coefficient (Figure 5.4 (a and b)). Whereas in fused coatings due to the fast oxidation process, it is observed that increasing trend up to 300 m, after that friction trend remains constant (Figure 5.4 (a and b)). This indicates that oxidized regions on the coating wear scar are finer and more numerous when compared to the coarser ones produced by as-sprayed coatings. However there is no sign of adhesive wear, it eliminates the increase in repeated periodic friction due to the rapid formation of oxides reported by Bolelli and Lusvarghi (2006). This is due to the effect of microwave heating the fused coatings experienced lower values than the CoMoCrSi heat treated coatings as reported by Prasad et al. (2018). Hence it is clearly noticed that fused coatings exhibit less friction as compared with as-sprayed coatings.

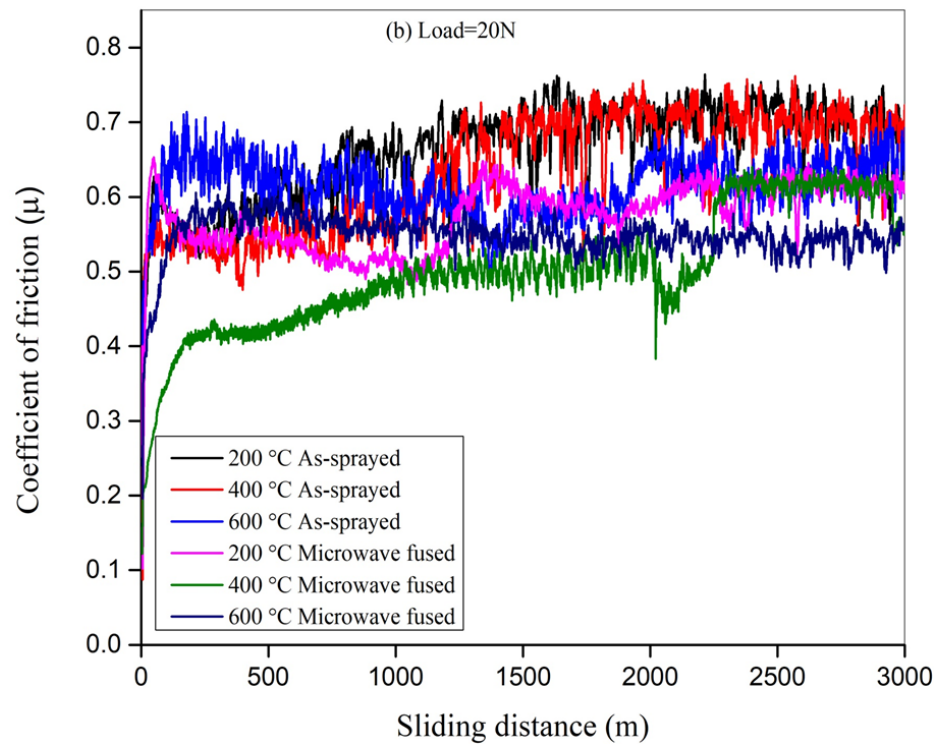
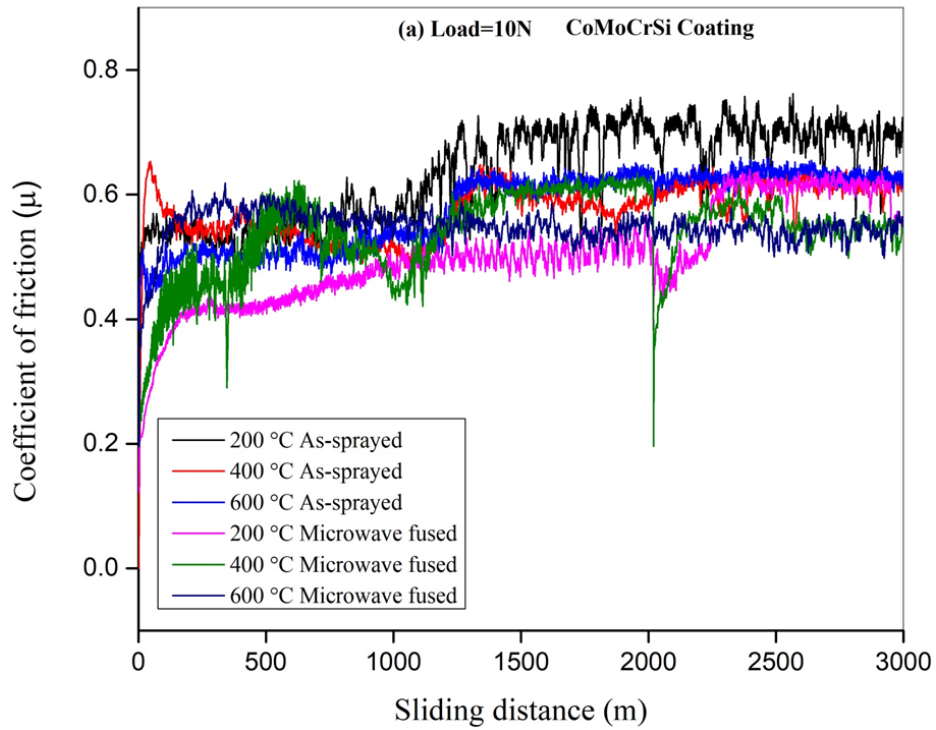


Figure 5.4 Friction coefficient of HVOF sprayed and microwave fused CoMoCrSi coatings with respect to sliding distance (a) 10 N, (b) 20 N

5.1.3 X-Ray Diffraction analysis of Fused Coatings

X-ray diffraction pattern of worn surfaces of microwave fused CoMoCrSi coating are shown in Figure 5.5. At the high temperature of sliding test, oxides are actively formed on the sliding surface heavily at the asperities by oxidation of reactive metallic Co-alloy have reported by some researchers Gao et al., (2010), Cho et al., (2009), and Lin and Chen, (2006). Co_3O_4 is observed to be formed at 200°C , whereas the CoO phase is formed at 400°C . Also, MoO_2 is formed at 400°C and MoO_3 is formed at 600°C . During the sliding test, oxides are formed due to rise in temperature at the interface. Active elements of the coatings are oxidized with the rise in temperature, but the oxides of cobalt and molybdenum are stable on the surface. The experiments are conducted under atmospheric conditions where oxygen entraps into sliding surfaces and generally, these oxides are brittle in nature stated by some authors Matikainen et al., (2017), Zhou et al., (2017), Hong et al., (2017). Wear rate and friction coefficient is less in case of the fused coating due to the rapid formation of oxides at the surface which eliminates the adhesive phenomenon results in less material loss.

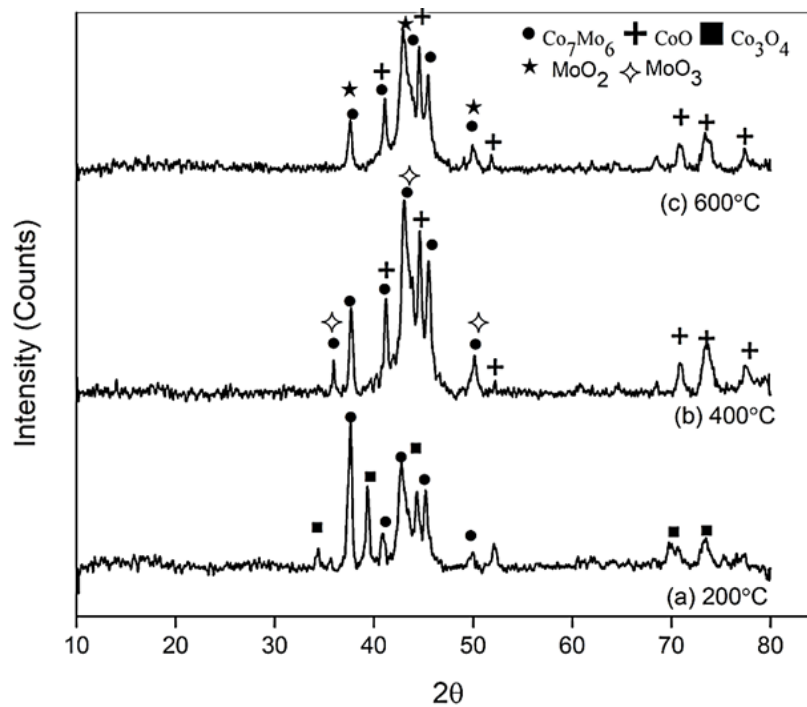


Figure 5.5 XRD pattern of CoMoCrSi fused coating worn surfaces at all test temperatures

5.1.4 Worn Surface SEM and EDS analysis

The damaged surfaces of HVOF sprayed CoMoCrSi coating during sliding wear test at high temperature are presented in Figure 5.6 (a-f). A smooth oxide tribo-layer at 200°C is formed on the wear track of the as-sprayed coatings. The layer probably forms at the start of the test as a result of breaking and dispersal of the oxide scale developed on the coating surface can be seen in Figure 5.6 (a). Wear scars at 400°C observed in Figure 5.6 (b) typical ploughing marks is observed with local plastic deformation. The smooth tribo-layer breaks out into small flakes exposing new coating surface to the oxidation environment. However, at 600°C (Figure 5.6 c) the plastic flow is observed to a great extent, some areas show material removed in bulk from the surface as wear scars.

As applied load increased to 20 N, larger plastic deformation with the partial breakup of the tribo-layer at 200°C can be seen in (Figure 5.6 d), where minor cracks have formed on the coating surface. As observed in Figure 5.6 (e) at 400°C, more loss of material occurs by splat detachment indicates abrasion (ploughing and cutting) stated by Cho et al., (2009). On the coating wear scar, individual splats (surrounded by thin oxide inclusions) are recognizable. At 600°C, it seems that some poorly bonded splats are detached and voids are filled by oxides formed during the sliding contact (Figure 5.6 f). In as-sprayed coatings, the wear scar is roughened by material removal due to adhesive wear. The wear rate of as-sprayed coatings is more in case of 20 N load due to severe adhesive wear caused cracks to be formed in the coating which results in the removal of material. With the progress of sliding action at elevated temperatures, cracks are developed and result in brittle fracture of coating, leading to high wear rate as observed in the micrograph Figure 5.6 (a-f).

An EDS result with respect to points selected on worn coating surface showing in (Figure 5.6 a-f) is reported in Table. 5.1. In fact, besides adhesive wear, a significant degree of oxidation exists, as above mentioned, on as-sprayed coatings. The coating mostly contributes to oxidation. For 10 N load, the percentage of O at point A is started increasing, as a rise in temperature the percentage of O also increased at point B and point C respectively. Similarly, for 20 N load at same test temperatures, the oxide scale at points D, E, and F is drastically increased compared to points A, B and C. This indicates an oxide inclusion is more at higher loads and rise in temperature.

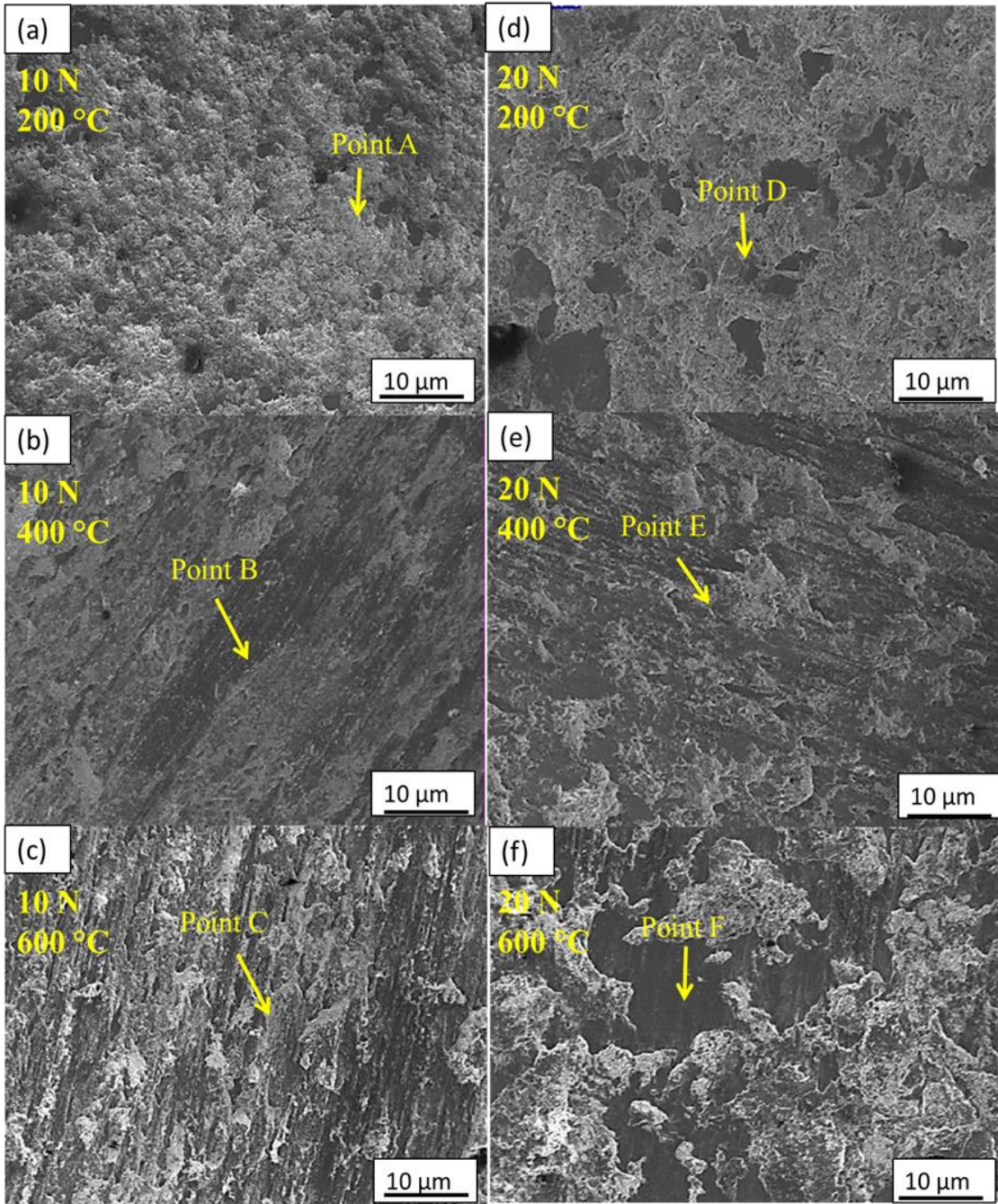


Figure 5.6 Morphology of HVOF sprayed CoMoCrSi coating worn surface (a-c) under 10 N and (d-f) under 20 N at temperatures of 200 °C, 400°C, 600°C

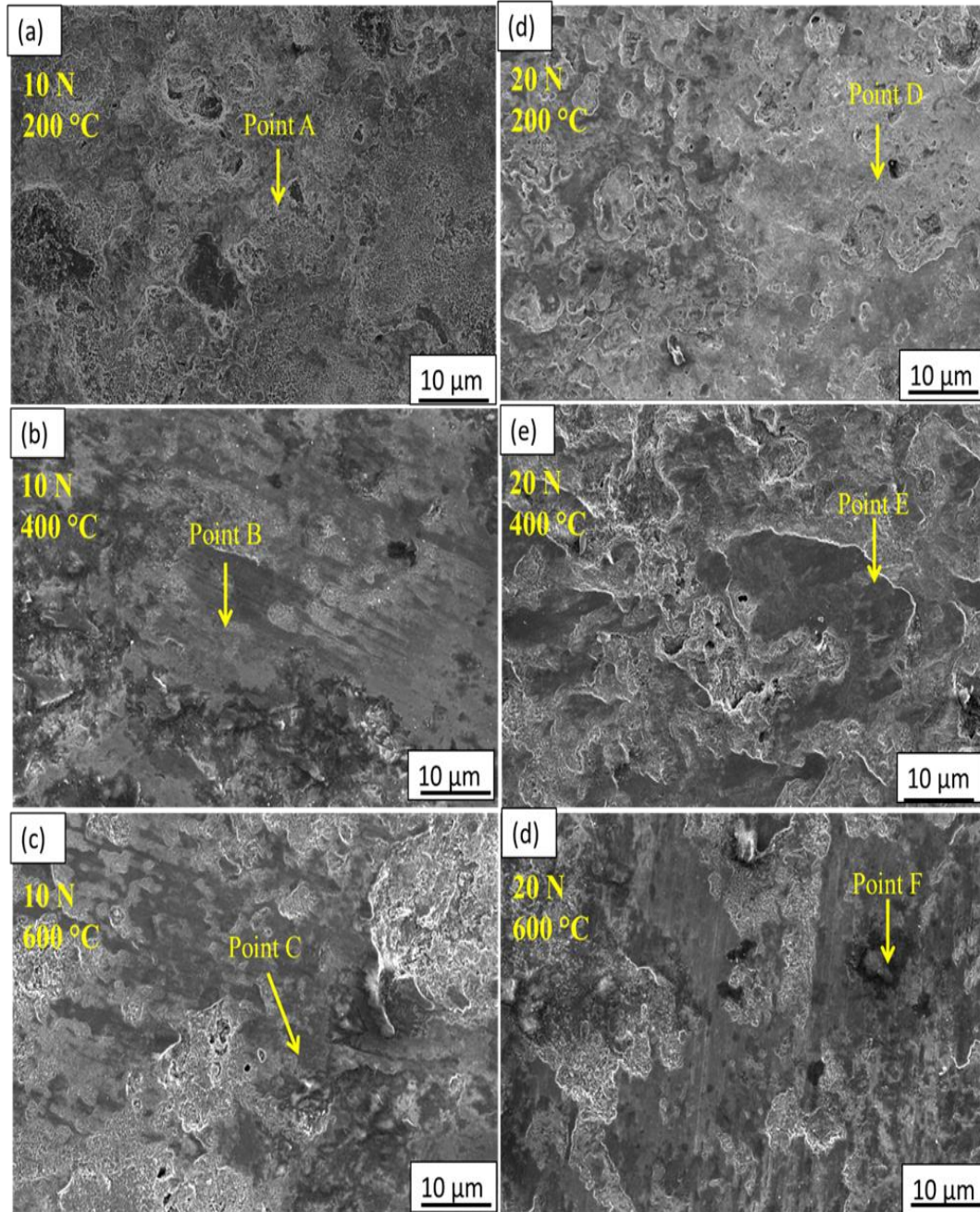


Figure 5.7 Morphology of microwave fused CoMoCrSi coating worn surface (a-c) under 10 N and (d-f) under 20 N at temperatures of 200 °C, 400°C, 600°C

In case of microwave fused CoMoCrSi coating, at 200°C, the tribo-layer is eventually reformed by the combination of rubbing of the debris and oxidation of the exposed surface seen in Figure 5.7 (a). As observed in (Figure 5.7 b) at 400°C the wear traces of fused coatings are much smaller than as-sprayed coatings due to the lubricant effect of attired oxide debris. SEM micrographs see in (Figure 5.7 c) at 600°C reveal that wear scar phenomenon is restricted by showing a much smoother and increased in width traces. This indicates the formation of tribo-layer oxides which covers the hard particles of coating results in no effect of adhesive material removal. However in (Figure 5.7 b and c) seen that the fused coating exhibits small cracks at the weak positions, where most of the cracks existed only on the coating surface, which had little effect on the coating performance (Fernandez et al., 2005).

As the increase in load to 20 N, no sign of material detachment by adhesion processes is observed in Figure 5.7 (d-f). At 200°C, cracks have found on the surface due to the oxide layer disintegrate leading to three body abrasion mechanism observed in Figure 5.7 (d). As the increase in temperatures to 400°C and 600°C see in (Figure 5.7 e and f) under dry conditions hard particles of coating experienced a fatigue spalling due to high friction compared to the morphology of fused coatings under 10 N load (Dejun and Tianyuan, 2017). This indicates that under 20 N loads there is a slight increase in wear rate of fused coatings than 10 N load.

EDS results with respect to points selected on worn fused coating surface shown in Figure 5.7 (a-f) is reported in Table. 5.2. Compared to HVOF sprayed CoMoCrSi coating, EDS of fused coating indicates that the percentage of O is less at points A, B, and C for 10 N load and in case of 20 N load oxide percentage is increased slightly at points D, F, and E respectively. As the rise in load and temperature wear phenomenon is limited by oxidation of the active elements of the fused coating.

Table 5.1: EDS results of HVOF sprayed CoMoCrSi coating worn surfaces at selected points shown in Figure 5.6

Element (wt %)	EDS analysis at designated regions in the microstructure					
	10 N load			20 N load		
	A	B	C	D	E	F
O	11.93	17.77	25.85	34.03	40.02	42.41
Al	03.01	06.28	07.33	04.55	08.21	12.40
Si	02.82	02.73	02.82	01.42	00.76	01.11
Cr	06.28	05.68	05.94	05.20	04.51	06.23
Mo	23.76	19.25	18.45	16.52	18.95	13.97
Co	52.19	48.28	39.61	38.28	27.55	23.88

Table 5.2: EDS results of fused CoMoCrSi coating worn surfaces at selected points shown in Figure 5.7

Element (wt %)	EDS analysis at designated regions in the microstructure					
	10 N load			20 N load		
	A	B	C	D	E	F
O	06.71	13.40	22.31	08.20	16.14	26.59
Al	04.23	08.62	12.45	05.45	11.10	15.68
Si	01.12	01.20	01.80	01.04	01.48	01.33
Cr	07.42	06.02	05.44	08.07	06.14	04.10
Mo	18.34	15.20	14.27	16.35	14.11	11.23
Ti	09.88	07.05	10.25	07.31	10.22	09.20
Co	52.30	48.51	33.48	53.58	40.81	31.87

5.2 WEAR STUDIES ON HVOF SPRAYED AND MICROWAVE FUSED CoMoCrSi+Cr₃C₂ COMPOSITE COATINGS

5.2.1 Volume loss and Wear rate of Coatings

The wear volume loss and wear rate of HVOF sprayed and microwave fused CoMoCrSi+Cr₃C₂ composite coatings shown in Figure 5.8 (a and b) and Figure 5.9 (a and b). The volume loss and wear rate increase with an increase in the test temperature and applied load. The HVOF sprayed coating shows an increase in the volume loss and wear rate with increase in load and temperature as compared to fused coating. The effect of temperature indicates that the wear resistance of the as-sprayed coating is decreased dramatically at the high temperatures of 400°C and 600°C Figure 5.8 (a and b) and Figure 5.9 (a and b)). Generally, at elevated temperatures, most of the metallic materials decrease their bulk strength. This results in an increased wear rate at higher temperatures due to their reduced hardness as stated by Bolelli and Lusvarghi, (2007).

Though the applied load is increased, there is a continuous disruption of the protective tribo-oxidation layer; this allows more metallic interaction and adhesion results in higher wear rate (Yao et al., 2006). The higher volume loss Figure 5.8 (a and b) and higher wear rate Figure 5.9 (a and b) of the as-sprayed coating are observed at 400°C and 600°C.

The microwave fused coating shows less volume loss and wear rate as compared to the as-sprayed coating. This is due to higher coating hardness with sound metallurgical bonding and also homogeneous microstructure leads to decrease in loss of material during sliding operation.

Wear rate coefficient k plot of HVOF sprayed and fused CoMoCrSi+Cr₃C₂ composite coatings in Figure 5.10. The linear regression's slope gives the average value of the wear rate coefficient k , of the HVOF, sprayed and fused CoMoCrSi+Cr₃C₂ composite coatings are $3 \times 10^{-6} \text{ mm}^3/\text{N m}$, and $9 \times 10^{-7} \text{ mm}^3/\text{N m}$, respectively. This result clearly confirms the effect of post heat treatment significantly improved the wear resistance of CoMoCrSi+Cr₃C₂ composite coatings.

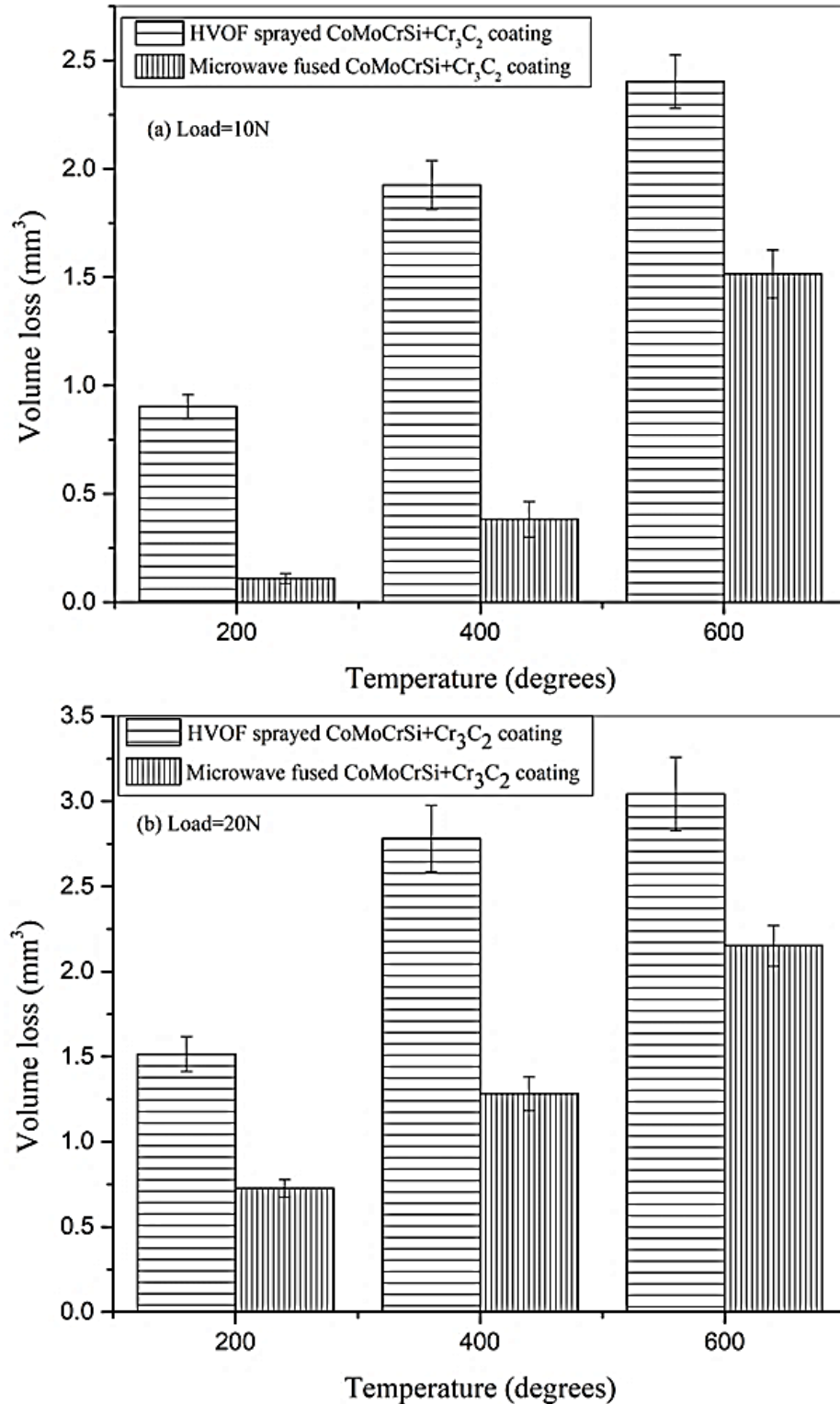


Figure 5.8 Wear volume loss of HVOF sprayed and microwave fused CoMoCrSi+Cr₃C₂ composite coatings with respect to temperature (a) 10 N, (b) 20 N

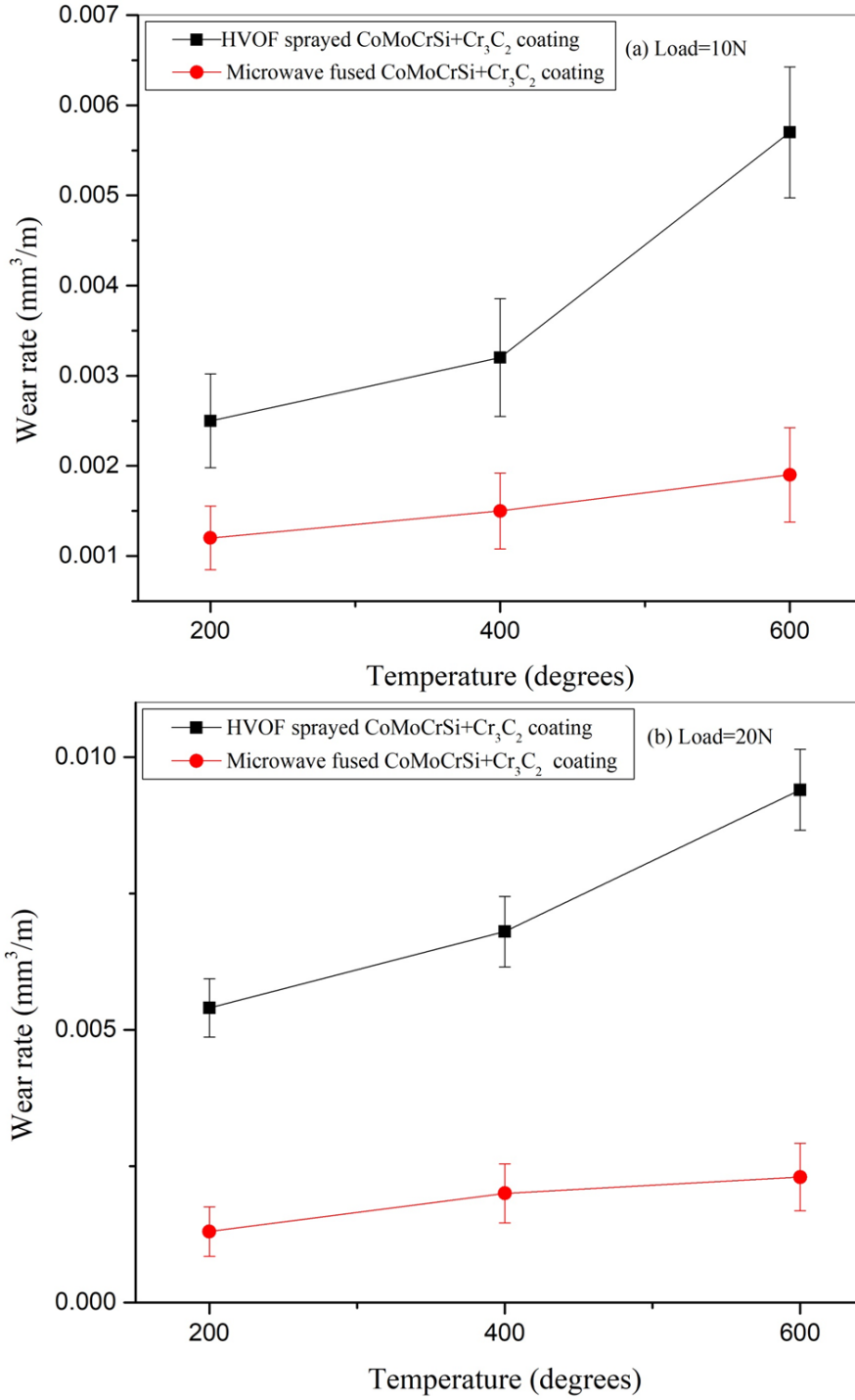


Figure 5.9 Wear rate plots of HVOF sprayed and microwave fused CoMoCrSi+Cr₃C₂ composite coatings (a) 10 N, (b) 20 N

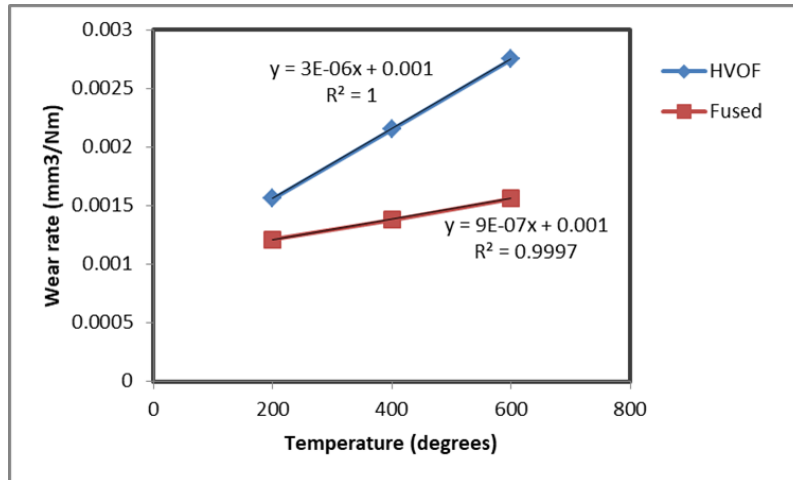


Figure 5.10 Wear rate coefficient k plot of HVOF sprayed and fused CoMoCrSi+Cr₃C₂ composite coating

5.2.2 Coefficient of Friction

The COF curves of coatings before and after fusing are shown in Figure 5.11 (a and b). The COF is not constant for as-sprayed and fused coatings but instead decreases as the load and temperature are increased (Prasad et al., 2018). The average value of the friction coefficient of the as-sprayed coating is 0.71. This value is very high as compared to the fused coating values (0.38–0.46).

The friction coefficient of the fused coating at an elevated temperature of 400°C and 600°C is lower compared to 200°C temperature (Figure 5.11 a and b). However, the results clearly reveal that microwave fused coating causes very less friction as compared to as-sprayed coatings. This indicates that CoMoCrSi+Cr₃C₂ microwave fused coating is highly suggested for high-speed spindle machine components which are weak to frictional heat and require coating (Cho et al., 2009).

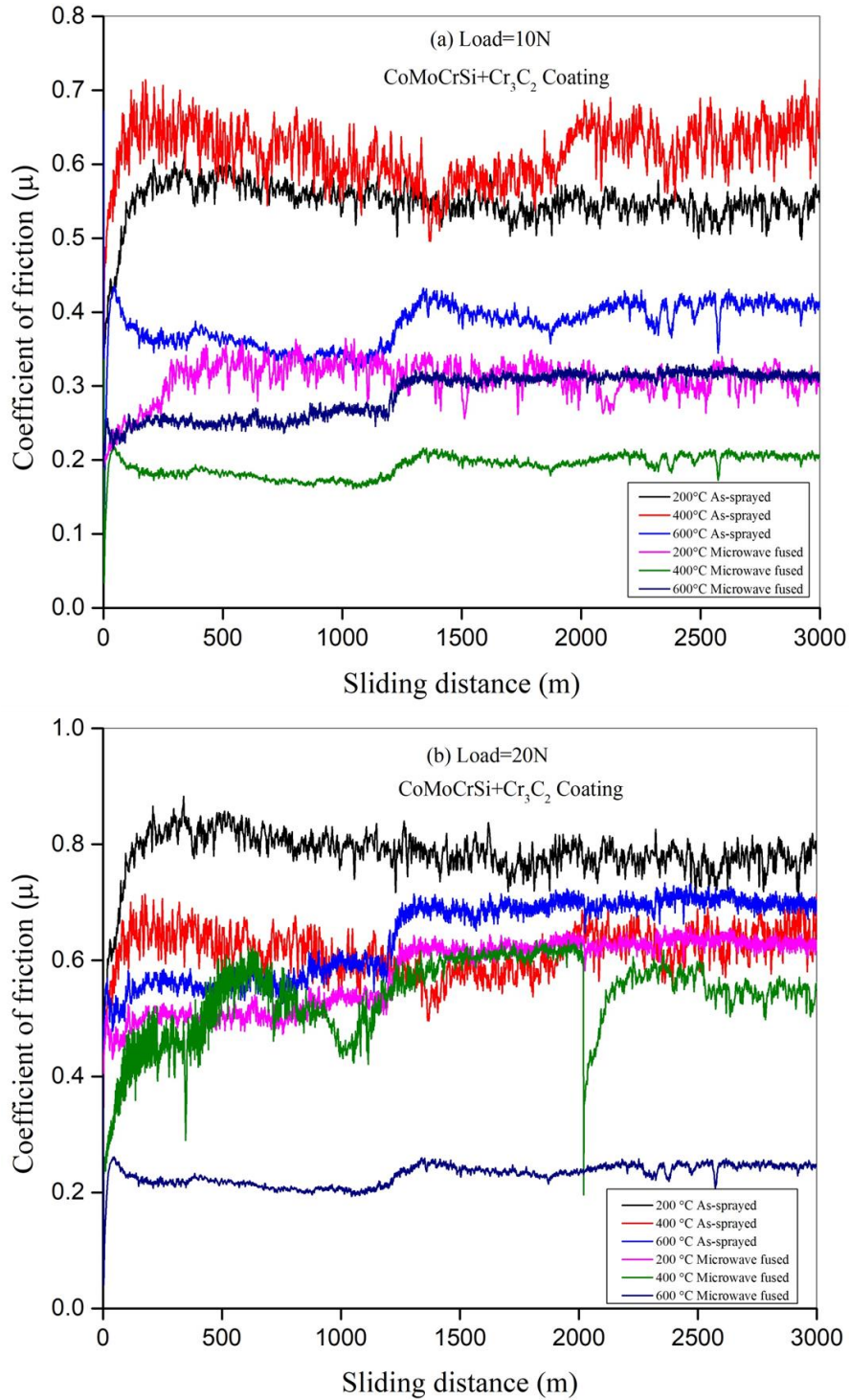


Figure 5.11 Friction coefficient of HVOF sprayed and microwave fused CoMoCrSi+Cr₃C₂ composite coatings with respect to sliding distance (a) 10 N, (b) 20 N

5.2.3 X-Ray Diffraction analysis of Fused Coatings

The XRD spectrum of the fused coating has worn surfaces at all test temperatures shown in Figure 5.12. During the sliding action, oxides are actively formed by oxidation of reactive metallic Co, Mo, and Cr elements on the sliding surface at elevated temperatures (Cho et al., 2009). At 200°C test temperature, the Co_3O_4 phase is formed, whereas at 400°C and 600°C, MoO_3 and MoO_2 phases are formed, respectively. The CoO phase is formed at elevated temperatures of 400°C and 600°C. Co_7Mo_6 and Cr_2O_3 phases are to be formed at all test temperatures (Khameneh et al., 2006). Cobalt, molybdenum, and chromium elements are rich in coating; hence, the increment in temperatures forms oxide layers. During the sliding test, rises in temperature oxides phases are easily formed. The test is carried out under atmospheric conditions, so the oxygen is being easily entrapped into sample surfaces during testing (Wood et al., 2010). At elevated temperatures, the sliding action wear debris continuously contacting the counter disc and sample creates heat because of the friction. It leads to the melting of small particles which results in the formation of lubricants at the coating surface.

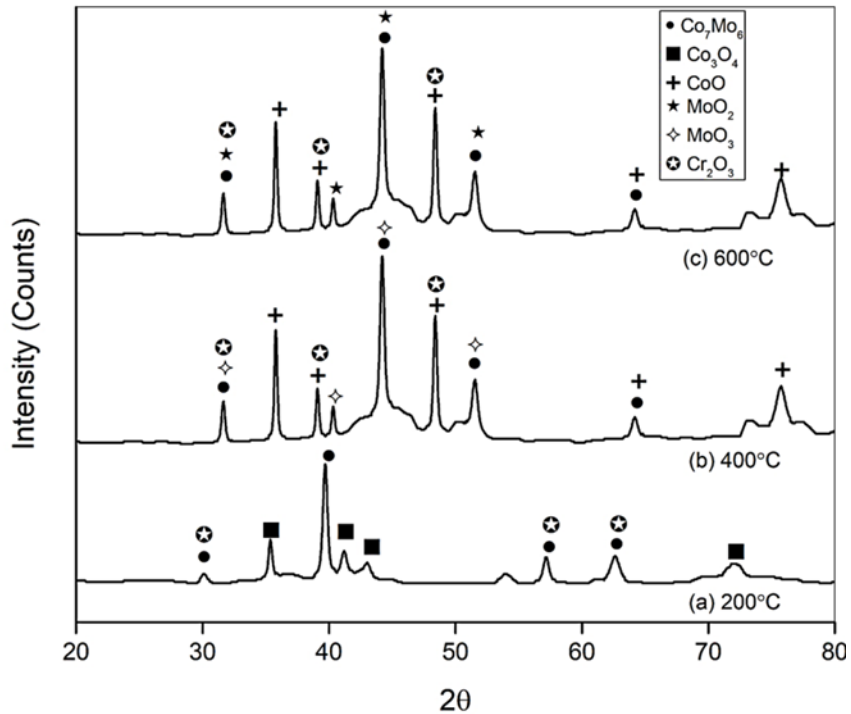


Figure 5.12 XRD pattern of fused $\text{CoMoCrSi}+\text{Cr}_3\text{C}_2$ composite coating worn surfaces at all test temperatures

5.2.4 Worn Surface SEM and EDS analysis

The worn surface morphology of HVOF sprayed CoMoCrSi+Cr₃C₂ composite coating is shown in Figure 5.13 (a-f). At 200°C, the wear traces are small since the applied load is 10 N (Figure 5.13 a) and due to friction, heat oxidation of the alloy surface is identified because of the dark spots that are observed. In Figure 5.13 (b) shows that as temperature increases to 400°C, typical groove marks with splat detachment results in brittle fracture of the coating. The oxide layer prevents the coating surface from further oxidation. Though the oxide layers are brittle in nature, it is certainly broken down under constant sliding action during the wear operation and spalled off from the coating surface which results in a material loss. The rise in test temperature to 600°C Figure 5.13 (c) causes severe ploughing marks with large cracks and some regions show material removal in bulk from the coating surface as wear grooves travel deep. When there is an increase in the temperature, promoted oxidation of the coating surface produces an oxide layer. This oxide layer is disrupted, and the fresh surface of the coating is exposed to the oxidation conditions leading to the cyclic process. However, at a high temperature of 600°C, the material removal is increased.

At 20 N normal load (see in Figure 5.13 d) there is a more severe deformation of the coating layer by disruption of oxide layers at 200°C. Subsurface cracking of as-sprayed coatings during the sliding test is one of the reasons for the increase in material loss in the 400°C test. The cracking of the top layer and splat detachment of coating is shown in Figure 5.13 (e). The cracks formed in coating structure might be due to brittle fractures caused due to the increase in the applied load during the wear process. This cracking in subsurface leads to removal of oxide layer and subjects the underlying coating material to oxidation and wear. As observed in (Figure 5.13 f), rough and more wear scars with lesser width are observed; this indicates large deformation of materials at 600°C. The regenerated oxide film is broken and more amount of material from the coating surface is removed which results in severe adhesive wear (Matikainen et al., 2017).

The EDS results of as-sprayed coatings are tabulated in Table. 5.3. The results are analyzed based on the points selected on worn surfaces which are marked in Figure 5.13 (a-f). During the test, an increase in test temperatures leads to increase in oxide percentage which is observed at points A, B, and C. This reveals that as-sprayed coating is subjected to severe

oxidation and adhesive phenomenon at elevated temperatures. The presence of a higher amount of oxygen and aluminium under 20 N normal load; confirms that as an increase in test load, the coating will be subjected to severe adhesive wear mechanism with increasing oxide percentage.

The worn surfaces of microwave fused CoMoCrSi+Cr₃C₂ composite coating during sliding wear test at elevated temperatures is shown in Figure 5.14 (a–f). The mechanism of wear is changed from adhesive wear to tribo-oxidative wear. As seen in (Figure 5.14 a), the morphology is quite typical and loose oxide particles are present on the coating surface. Lower scars with no presence of cracks are observed to result in less wear loss. This type of typically worn surface with a tribo-oxidative wear mechanism is reported by Fernandez et al., (2005) and Kato and Adachi, (2001).

During an increment in temperature to 400°C (Figure 5.14 b), wear traces are observed and the increased width and tribo-oxide layer are reformed which reduces the adhesion between the contacting surfaces. This results in a decrease in the chemical affinity between mating surfaces and Co and Mo elements which are known to possess self-lubricating properties (Bolelli and Lusvardi, 2006). Figure 5.14 (c) shows results at 600°C, there are very large oxide inclusions which mainly consist of oxidized particles stuck together. The white patches observed in the morphology indicate that the chromium carbides strengthen the alloy surface from ploughing action (Gao et al., 2010). Small cracks are formed at weak positions since it exists only on the surface which causes a higher amount of material loss.

The fused coating under 20 N normal load also exhibits similar phenomenon as observed under 10 N. The worn morphology presents smooth and large wear scars at all test temperatures shown in Figure 5.14 (d–f). At test temperatures 200°C, 400°C, and 600°C, (Figure 5.14 d–f) it is observed that the fused coating surface is very hard and results in fatigue spalling and exhibits less damage on the surface. On the other hand, tribo-oxide layer phenomenon is more under 20 N normal load. This layer protects the hard particles and results in a decrease in loss of coating material. At 400°C and 600°C Figure 5.14 (e–f), some areas show little damages caused due to the effect of an increase in normal load to 20 N.

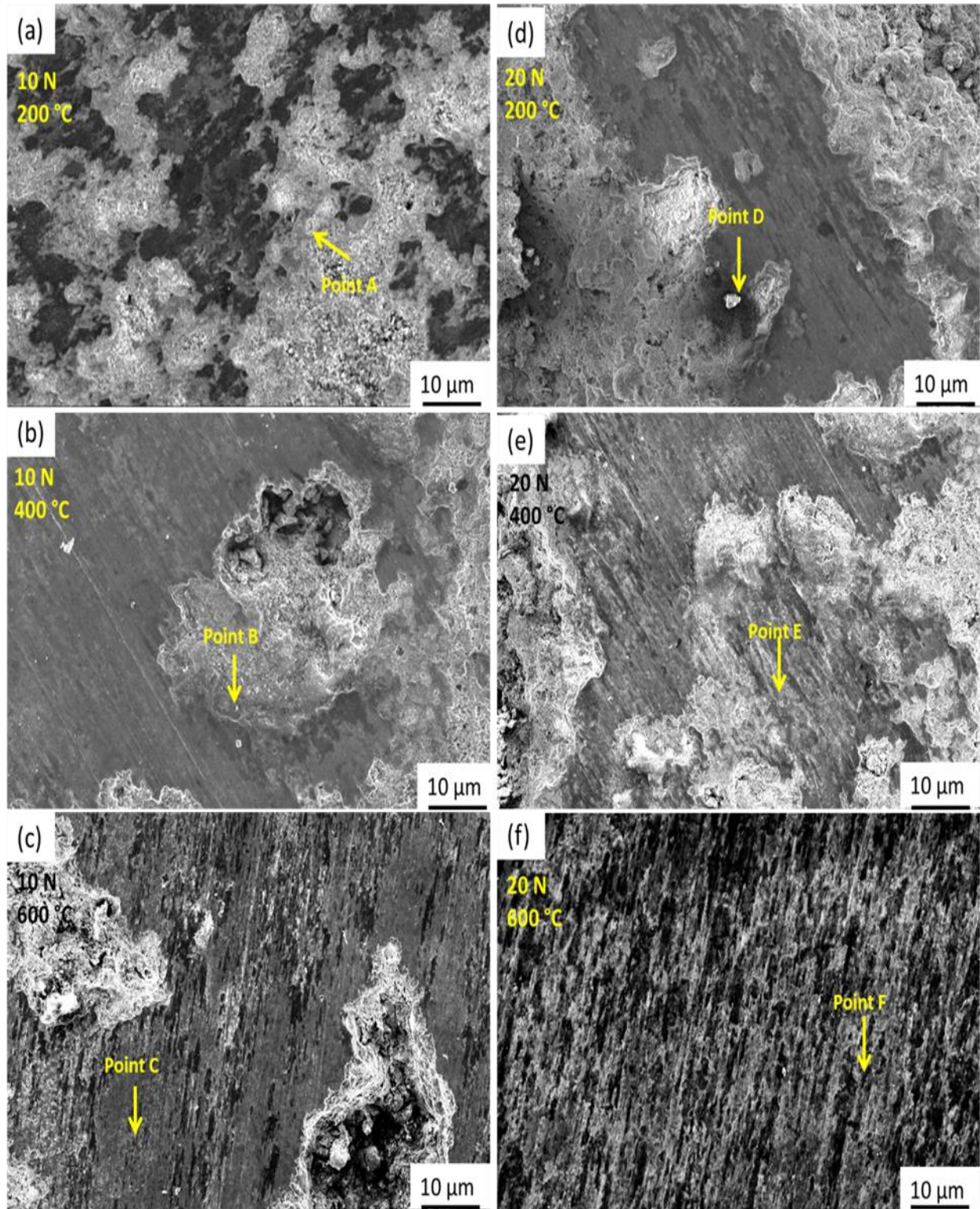


Figure 5.13 Morphology of HVOF sprayed CoMoCrSi+Cr₃C₂ composite coating worn surfaces (a-c) under 10 N and (d-f) under 20 N at temperatures of 200 °C, 400°C, 600°C

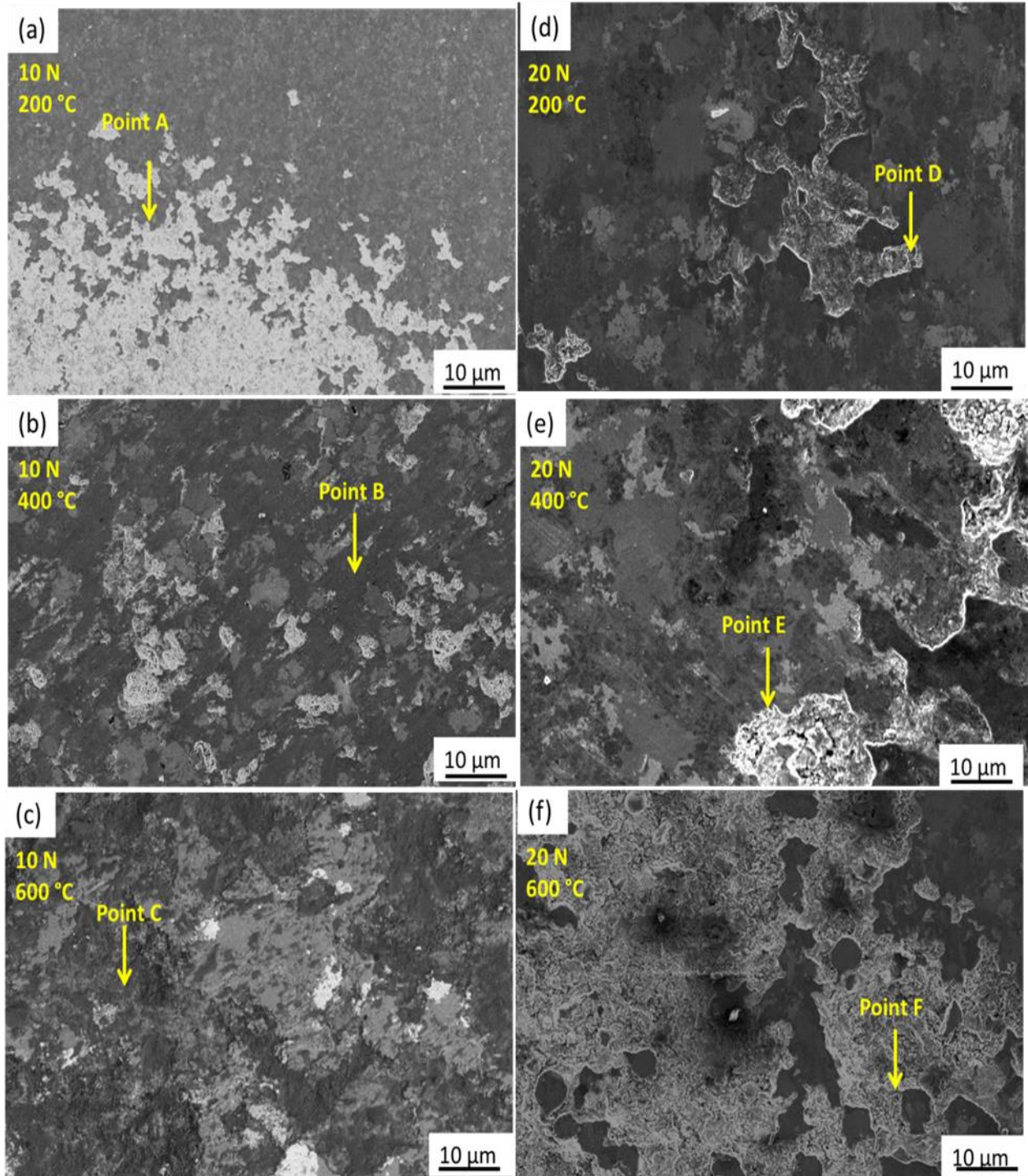


Figure 5.14 Morphology of microwave fused CoMoCrSi+Cr₃C₂ composite coating worn surface (a-c) under 10 N and (d-f) under 20 N at temperatures of 200 °C, 400°C, 600°C

Table 5.3 EDS results of HVOF sprayed CoMoCrSi+Cr₃C₂ composite coating worn surfaces at selected points shown in Figure 5.13

Element (wt %)	EDS results at selected points in the microstructure					
	10 N load			20 N load		
	A	B	C	D	E	F
O	07.93	12.77	25.85	19.23	32.05	42.20
Al	03.01	06.28	07.33	09.01	12.01	14.25
Si	02.82	02.73	02.82	01.60	01.10	01.02
C	04.11	03.45	03.04	02.28	03.89	02.14
Cr	21.28	19.68	16.72	22.43	18.36	15.48
Mo	17.76	13.12	10.03	14.10	09.22	07.89
Co	43.09	41.97	34.21	31.35	23.37	17.02

Table 5.4 EDS results of fused CoMoCrSi+Cr₃C₂ composite coating worn surfaces at selected points shown in Figure 5.14

Element (wt %)	EDS results at selected points in the microstructure					
	10 N load			20 N load		
	A	B	C	D	E	F
O	04.59	11.44	22.20	10.17	16.13	28.48
Al	04.66	10.32	16.48	07.40	15.27	17.10
Si	02.14	02.17	02.55	01.65	01.04	01.20
Ti	08.28	12.79	13.52	05.84	10.90	10.11
C	05.41	05.09	04.99	03.33	05.98	07.18
Cr	20.12	16.13	15.43	24.59	17.51	13.50
Mo	16.88	10.40	09.22	15.22	11.04	07.43
Co	37.92	31.66	15.61	31.80	22.13	15.00

5.3. WEAR STUDIES ON HVOF SPRAYED AND MICROWAVE FUSED CoMoCrSi+WC-CrC-Ni COMPOSITE COATINGS

5.3.1. Volume loss and Wear rate of Coatings

The wear volume loss and wear rate of HVOF sprayed and microwave fused CoMoCrSi+WC-CrC-Ni is shown in Figure 5.15 (a and b) and Figure 5.16 (a and b). The lowest wear volume is obtained with the fused composite coating compared to HVOF as-sprayed coatings at 10 N and 20 N normal loads with respect to test temperatures. This is mainly due to low friction, high hardness and least surface defects compared to as-sprayed CoMoCrSi+WC-CrC-Ni composite coating. The CoMoCrSi+WC-CrC-Ni as-sprayed coating increases volume loss as a rise in temperature and showed the highest material loss at 600°C for both normal loads compared to fused CoMoCrSi+WC-CrC-Ni composite coating. The main reasons are decreased in surface roughness, increased hardness, and refining of the as-sprayed coating microstructure leads to less rupture of the coating surface (Bolelli et al., 2014). Moreover, low friction leads to easy sliding which avoids the failure of the material.

The wear rate of as-sprayed and fused coatings gradually increases with respect to test temperatures. The wear rate of CoMoCrSi+WC-CrC-Ni as-sprayed coating is 2.5-3.5 times higher than fused CoMoCrSi+WC-CrC-Ni composite coating present in Figure 5.16 (a and b). This is because of surface defects such as cracks, voids and also lower microhardness. This indicates that CoMoCrSi+WC-CrC-Ni fused coating is having higher wear resistance than CoMoCrSi+WC-CrC-Ni as-sprayed composite coating.

The microwave treated coating exhibits very less wear rate with respect to test temperature. The reason is improved hardness by metallurgical bonding and phases such as TiC, Co₆W₆C, Co₃W₉C, and Co₃W₃C and Cr₃C₂ are formed shown in Figure 4.23. The wear rate coefficient k in mm³/N m is estimated by employing Archard model. The mean wear rate of coatings before and after microwave fusing is shown in Figure 5.17. The wear rate of coatings before and after fusing of CoMoCrSi+WC-CrC-Ni composite coating is 3×10^{-6} mm³/N m and 9×10^{-7} mm³/N m respectively. Based on the comparison of tested composite coatings it is observed that the microwave fused CoMoCrSi+WC-CrC-Ni composite coating is having better wear resistance and lower friction at high temperatures.

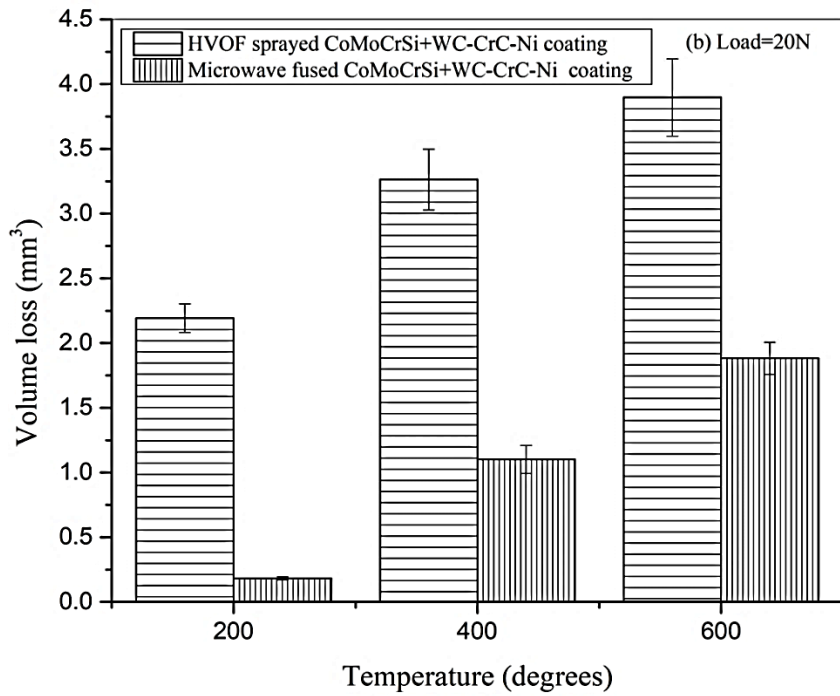
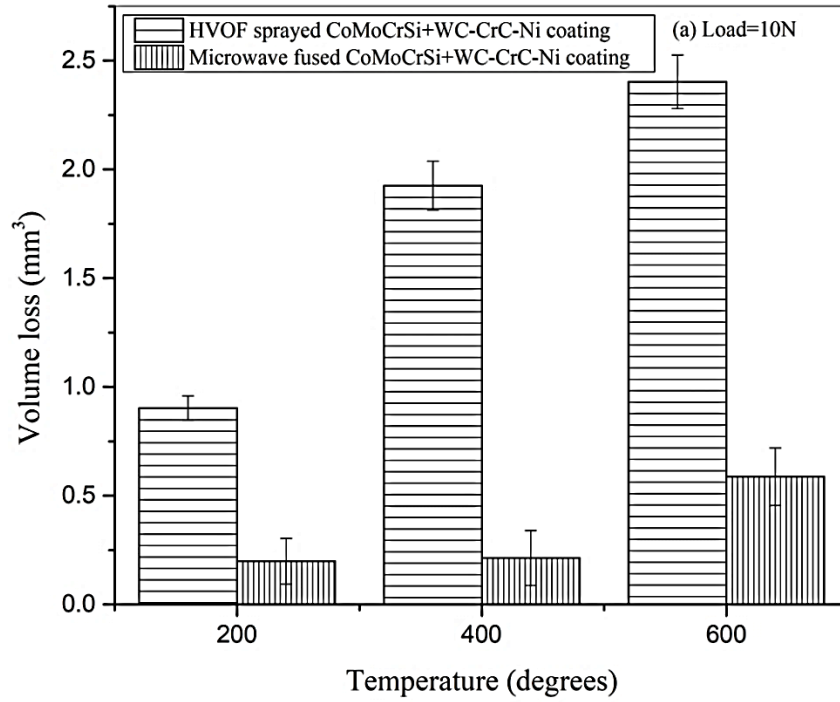


Figure 5.15 Wear volume loss of HVOF sprayed and microwave fused CoMoCrSi+WC-CrC-Ni composite coatings with respect to temperature at loads of (a) 10 N, (b) 20 N

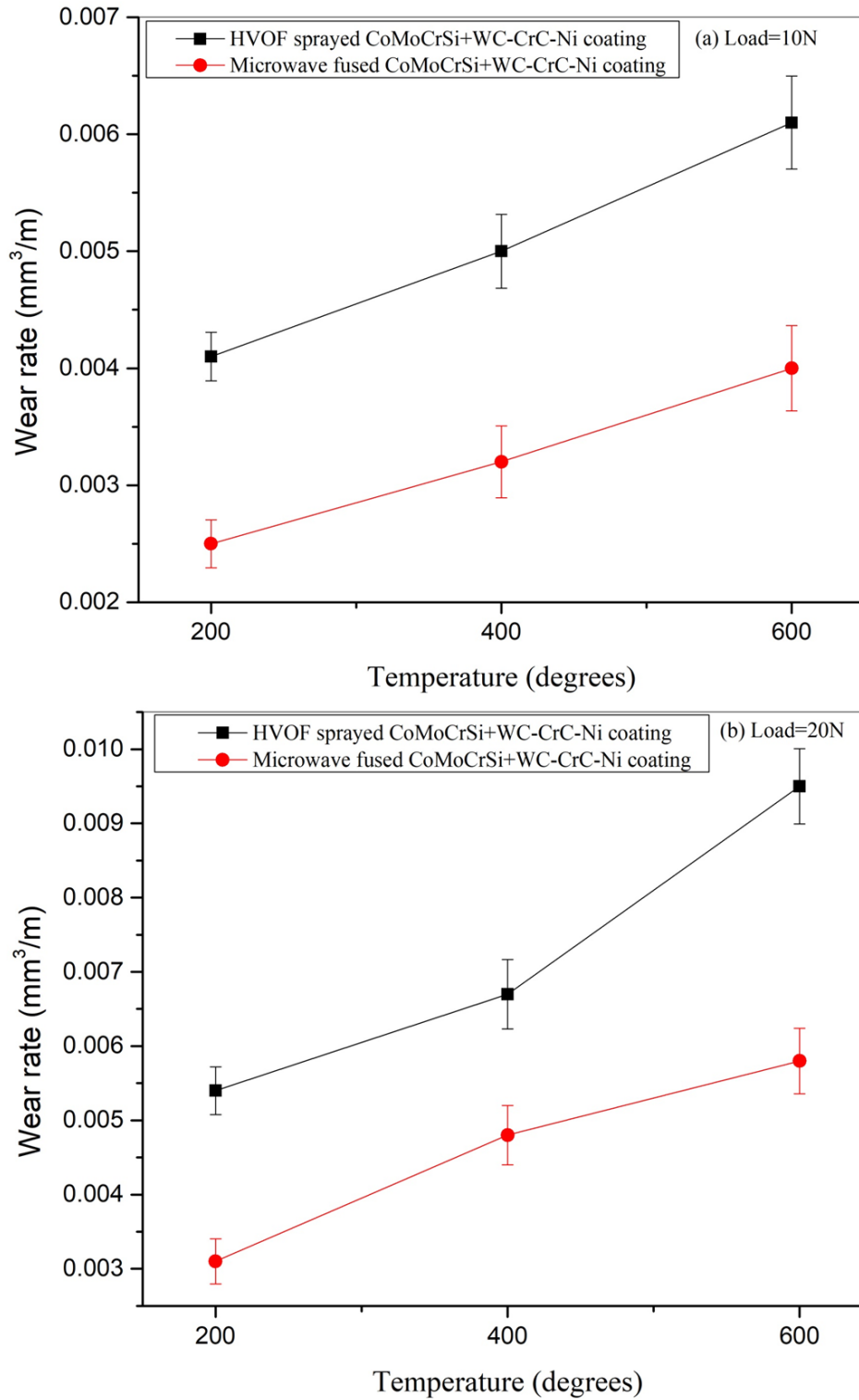


Figure 5.16 Wear rate plots of HVOF sprayed and microwave fused CoMoCrSi+WC-CrC-Ni composite coatings (a) 10 N, (b) 20 N

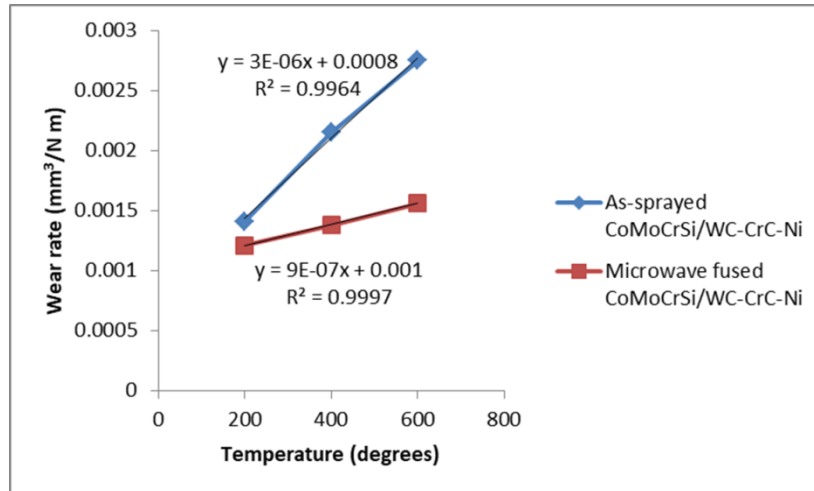


Figure 5.17 Wear rate coefficient k plot of HVOF sprayed and fused CoMoCrSi+WC-CrC-Ni composite coating

5.3.2. Coefficient of Friction

The COF curves of HVOF sprayed and fused CoMoCrSi+WC-CrC-Ni composite coatings are shown in Figure 5.18 (a and b). The friction coefficient of as-sprayed and fused coatings shows a decreasing trend as a rise in temperature. The as-sprayed coating under both normal loads at all test temperatures revealed an average friction coefficient of 0.74, which is significantly high value than fused coating value (0.38-0.56). The coefficient of friction of as-sprayed and fused coating fluctuates greatly during sliding action. The friction of the as-sprayed coating is slowly raised from 0.4 to 0.79 increased by 86% in the running cycle (0-10 min) this is due to improper contact between the counter disc and test sample. However, during a stable cycle (10–35 min), the coefficient of friction of the as-sprayed coating becomes smooth, floating around a fixed value (Wood et al., 2010).

In the case of the fused coating coefficient of friction increased from 0.2 to 0.55 nearly increased by 65% in the running cycle (0–10 min) which is better than an as-sprayed coating. The coefficient of friction of fused coating in the stable cycle (10–30 min) becomes steady and floating around a fixed value. Compared to the as-sprayed coating, the fixed value is small, this result in the effect of microwave-treated coating hardness influenced to reduce the coefficient of friction.

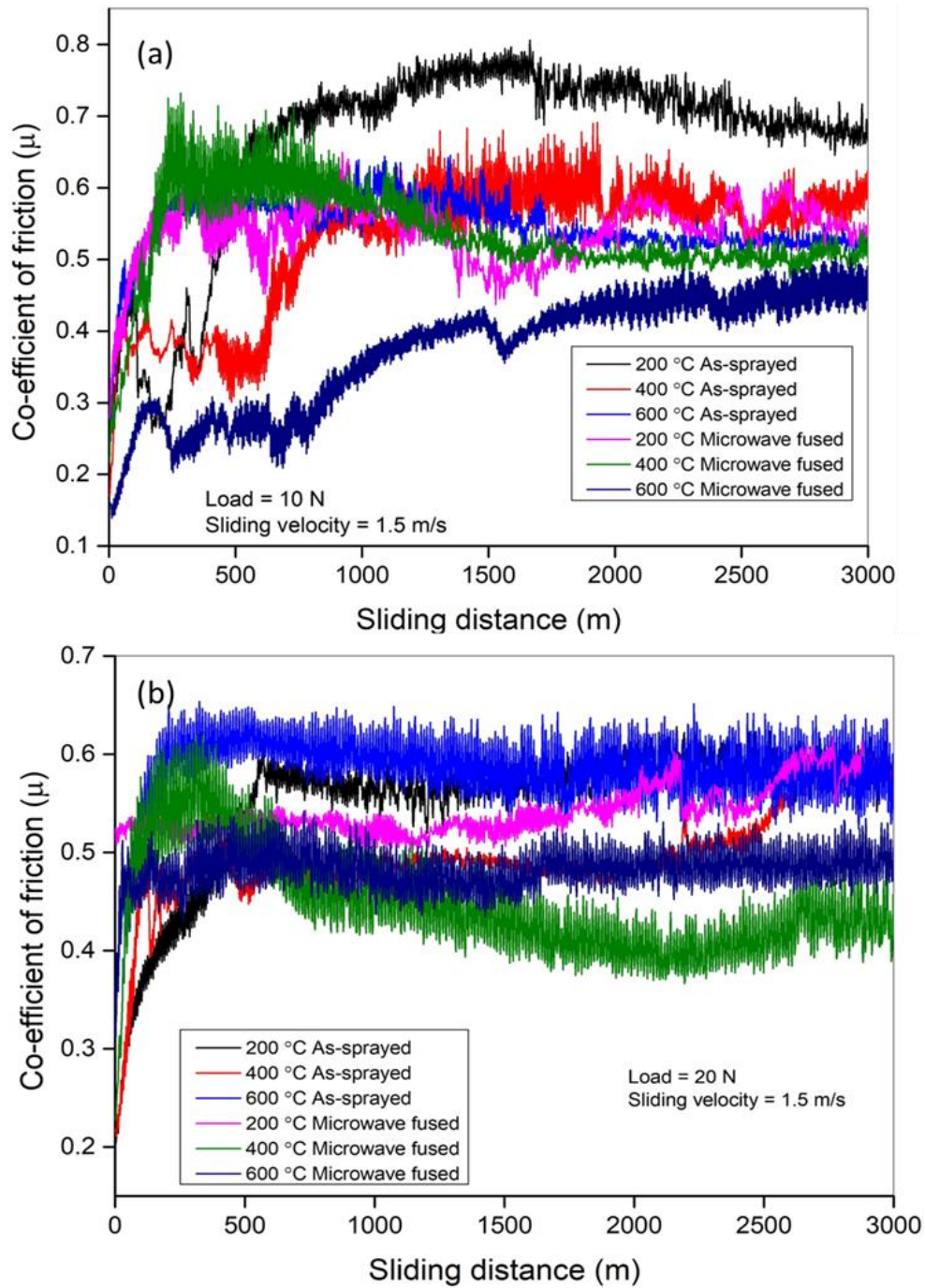


Figure 5.18 Friction coefficient of HVOF sprayed and microwave fused CoMoCrSi+WC-CrC-Ni composite coatings with respect to sliding distance (a) 10 N, (b) 20 N

5.3.3. X-Ray Diffraction analysis of Fused Coatings

The X-ray spectrum of microwave fused CoMoCrSi+WC-CrC-Ni worn coating is shown in Figure 5.19. Since the test is carried out at elevated temperatures obviously, Co alloy is subjected to oxidation at elevated temperatures and easily oxides are formed at coating surfaces (Bemporad et al., 2008); (Yao et al., 2006). As observed in (Figure 5.19) Co_7Mo_6 phase is to be formed at all test temperatures. At 200°C Co_3O_4 phase is identified and CoO , Cr_2O_3 phases are formed at 400°C and 600°C on the other hand MoO_2 and CoWO_4 , is formed at 600°C . The NiCr_2O_4 phase is identified at 600°C in Figure 5.19. The fused coating exhibits less wear rate and friction coefficient because oxides are actively formed which leads to cover the exposed coating surface from adhesive wear mechanism.

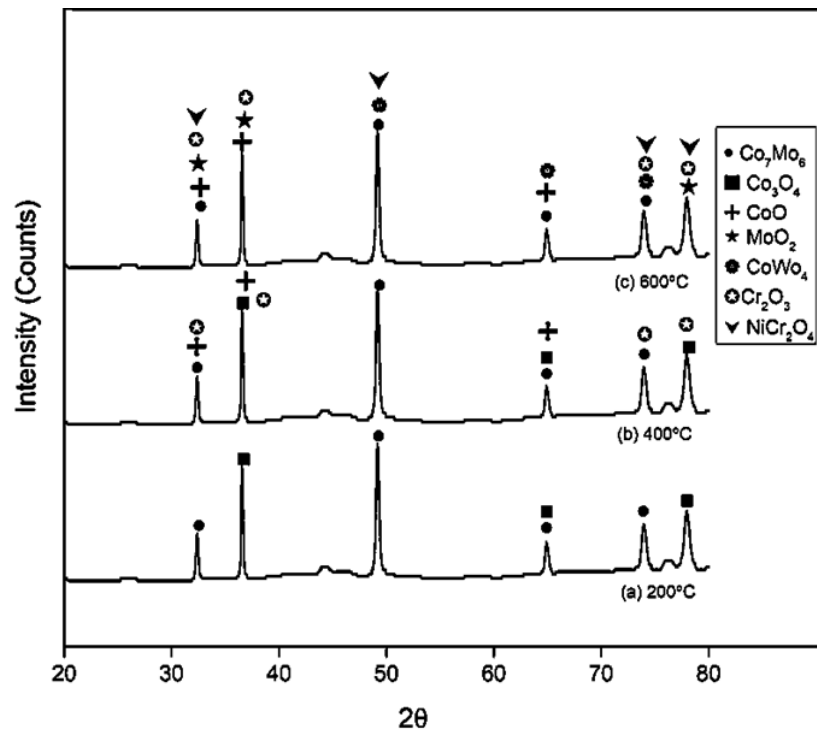


Figure 5.19 XRD pattern of fused CoMoCrSi+WC-CrC-Ni composite coating worn surfaces at all test temperatures

5.3.4. Worn Surface SEM and EDS analysis

Worn morphology of as-sprayed CoMoCrSi+WC-CrC-Ni composite coating is shown in Figure 5.20 (a-f). It is observed that, the Co matrix is very soft and ductile between the WC particles are found to deform and extrude out of the coatings (Gisario et al., 2015). In Figure 5.20 (a) at 200°C coating produces microcracking which is existed in weaker splats resulting in detachment of coating is observed. However, at 400°C and 600°C, (Figure 5.20 b and c) coating experienced shallower grooves and brittle fracture are produced on the surface which affects the coating performance. The formation of protective oxide layers on the surface is observed leads to decrease in a material loss at elevated temperatures. In Figure 5.20 (d-f) wear scar reveals cracking of WC particle and fragmentation is observed as test load increased at 20 N. However, under 20 N normal load test, noticed severe cobalt matrix deformation (Honga et al., 2017). In addition, brittle fracture and small pits are formed results in rapid detachment of coatings splats. As the rise in temperatures, the amount of oxide films is increased on coating sliding face. As the increase in temperatures and test load, hard particles in coating subjected to more brittle fracture due to high friction observed in Figure 5.20 (e-f). Based on the worn morphologies of coatings, it is clear evident that the wear rate is more under 20 N normal load due to rapid rupture of splats.

The EDS results (wt%) corresponding to chosen points on the surface of a worn as-sprayed coating presented in (Figure 5.20 a-f) the values are listed in Table. 5.5. The result reveals that the regions A, B, and C in dark regions have O, W and surrounded by Co, showing oxide formation. The coatings also exhibit roughened surface due to clusters of oxides, when rising in test load to 20 N. The elements Al, W, and Co are composed of oxides and drastically percentage of oxide content is raised under 20 N normal as observed at points D, F, and E respectively.

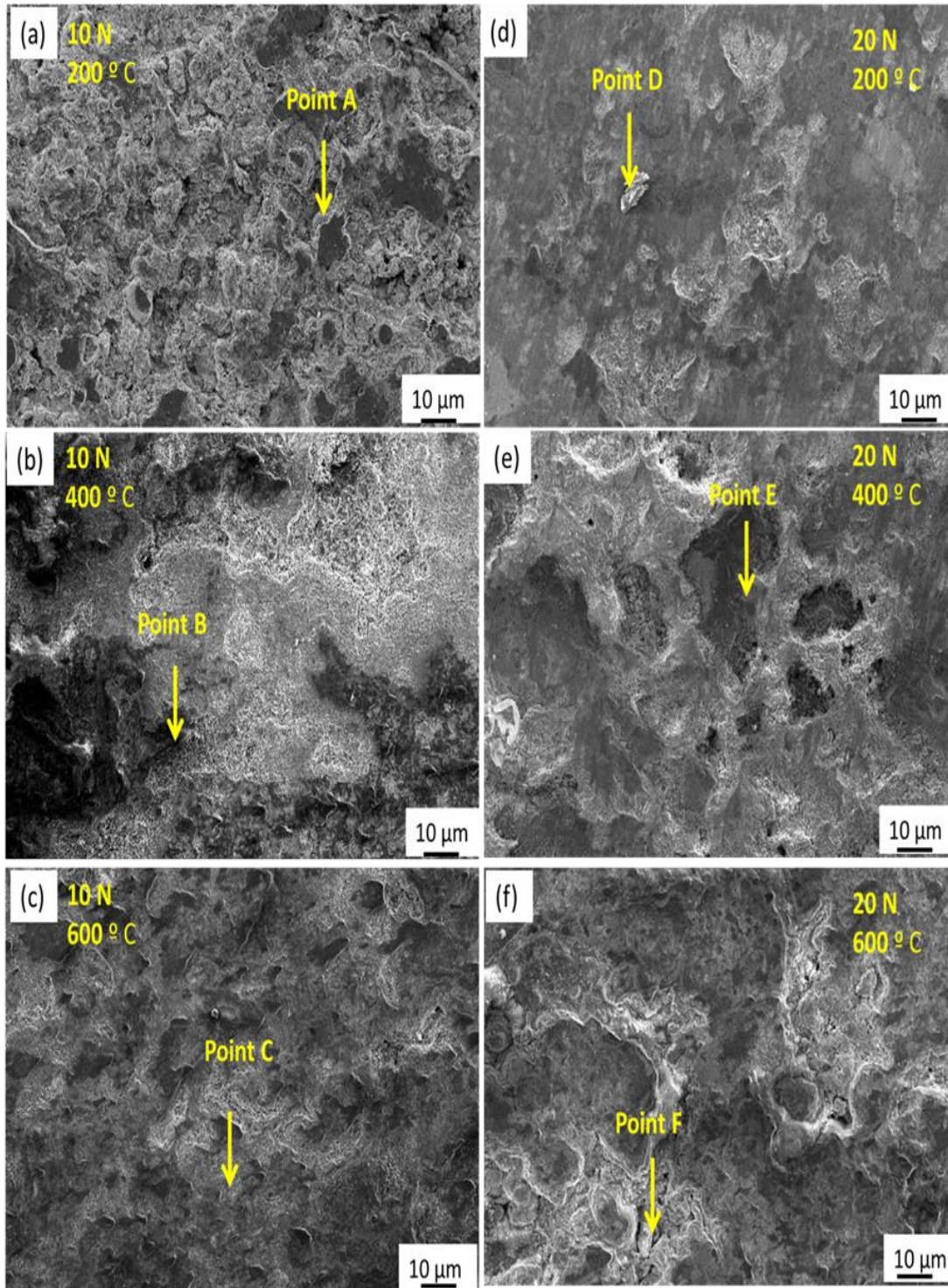


Figure 5.20 Morphology of HVOF sprayed CoMoCrSi+WC-CrC-Ni composite coating worn surfaces (a-c) under 10 N and (d-f) under 20 N at temperatures of 200 °C, 400°C, 600°C

Table 5.5: EDS analysis of HVOF sprayed CoMoCrSi+WC-CrC-Ni composite coating worn surfaces on points marked in Figure 5.20

Element (wt %)	EDS results at selected points					
	10 N load			20 N load		
	A	B	C	D	E	F
O	06.12	12.31	17.88	16.22	25.10	33.15
C	04.30	03.81	03.02	04.10	04.56	03.44
Al	02.38	05.22	07.33	04.55	08.21	09.40
Si	01.62	01.23	02.82	01.42	00.76	01.11
Cr	14.59	12.03	13.26	11.20	12.51	11.23
Ni	01.14	01.10	01.19	01.66	00.89	00.73
W	19.20	18.56	17.73	15.11	14.60	15.49
Mo	16.71	14.32	13.05	12.98	10.07	08.17
Co	33.94	31.42	23.27	32.76	23.30	17.28

Figure 5.21 (a-f) shows the typical morphologies of wear tracks produced on fused CoMoCrSi+WC-CrC-Ni composite coatings. From Figure 5.21 (a) it is observed that the worn surface of the fused coating is relatively smooth under 10 N after sliding at 200°C temperature for 34 min. It is also observed that pits and small grooves like the breaking of a layer on the fused coating surface. At elevated temperatures (Figure 5.21 b and c) it is evident that the formations of a tribo-oxide layer on coating surface results in increasing of wear trace width. This oxide layer acts as a protective shield leads to a decrease in material loss, some of the researchers have reported the similar wear mechanisms by Prasad et al., (2018), Bolelli et al., (2014) and Dejuna and Tianyuan, (2017). At 20 N normal load, it is observed that similar morphologies as obtained under 10 N load. Figure 5.21 (d-f) the wear scars under 20 N normal load at 200°C 400°C and 600°C presents no transfer of materials (adhesive) but noticed fatigue spalling due to the presence of new hard carbide phases seen in Figure 5.21 (d). During sliding action at high temperatures severe oxidation is caused results in less removal of materials as described by Asgari et al., (2017), Xu et al., (2007) and Zhang et al., (2009).

The EDS analysis corresponding to chosen points on the surface of worn fused coatings presenting in Figure 5.21 (a-f), the values are listed in Table. 5.6. The fused coatings show an increase in oxide percentages for both test loads. The oxide content under 10 N normal load is showing increasing trend at points A, B, and C, whereas similar tendency, is observed under 20 N normal load at points D, E, and F.

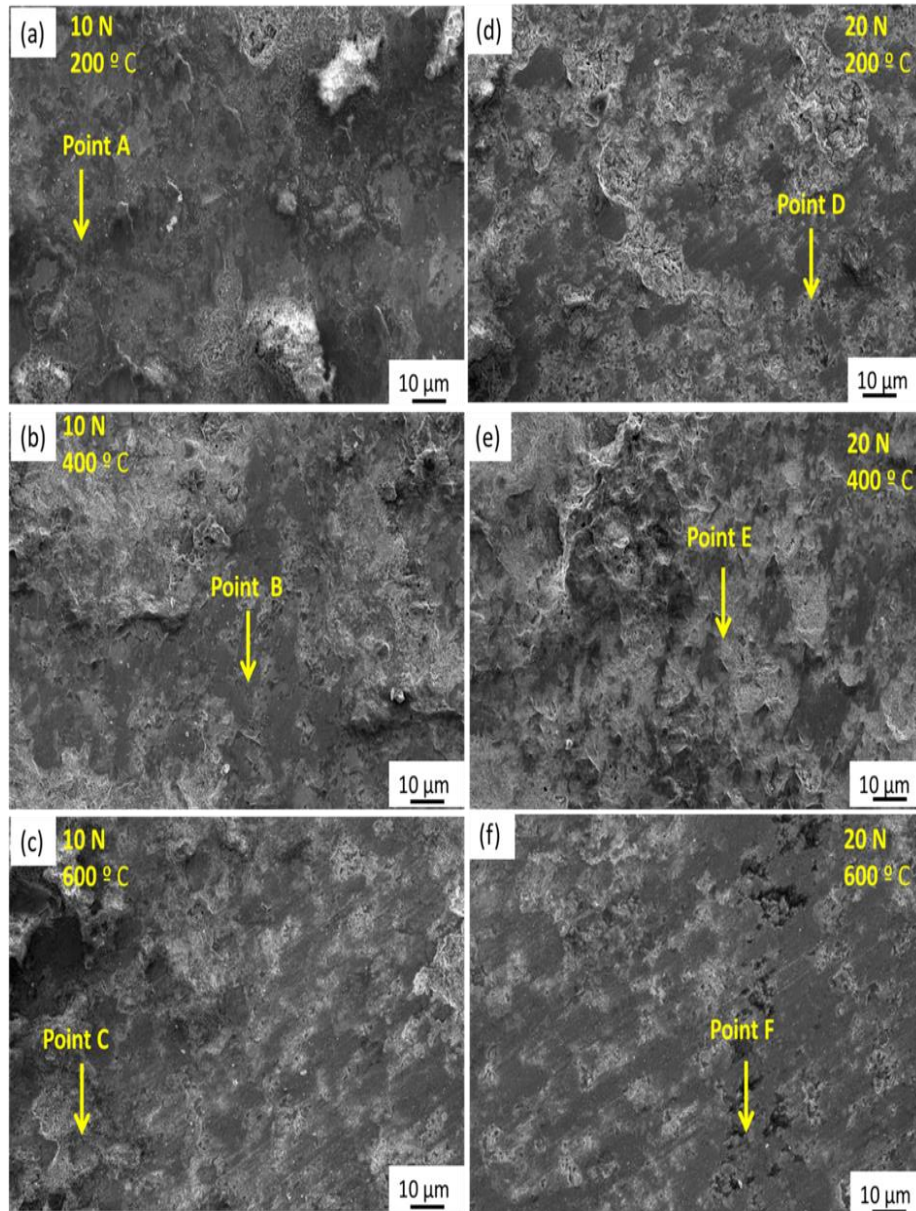


Figure 5.21 Morphology of microwave fused CoMoCrSi+WC-CrC-Ni composite coating worn surfaces (a-c) under 10 N and (d-f) under 20 N at temperatures of 200 °C, 400°C, 600°C

Table 5.6: EDS analysis of fused CoMoCrSi+WC-CrC-Ni composite coating worn surfaces on points marked in Figure 5.21

Element (wt %)	EDS results at selected points					
	10 N load			20 N load		
	A	B	C	D	E	F
O	08.71	15.40	22.31	20.28	29.11	37.27
C	02.15	03.46	03.88	03.31	04.02	03.11
Al	01.53	02.14	03.45	02.45	03.10	05.68
Si	01.12	01.20	01.80	01.04	01.48	01.33
Cr	15.19	14.05	12.10	12.28	09.66	07.41
Ni	01.18	01.23	01.72	00.69	00.81	00.72
W	17.01	16.52	14.82	14.89	11.30	10.75
Mo	15.51	13.39	11.90	12.31	07.26	06.02
Ti	09.88	07.05	06.12	07.31	10.22	09.20
Co	27.72	25.56	21.90	25.44	23.04	18.51

5.4. WEAR STUDIES ON HVOF SPRAYED AND MICROWAVE FUSED CoMoCrSi+WC-12Co COMPOSITE COATINGS

5.4.1. Volume loss and Wear rate of Coatings

The wear volume loss and wear rate of HVOF sprayed and microwave fused CoMoCrSi+WC-12Co composite coatings are shown in Figure 5.22 (a and b) and Figure 5.23 (a and b). The CoMoCrSi+WC-12Co composite coatings exhibit a marginal difference in its volume loss and wear rate compared to CoMoCrSi+WC-CrC-Ni composite coatings since both coatings produced similar microhardness. The CoMoCrSi+WC-12Co as-sprayed coating shown higher volume loss and wear rate for test loads at all test temperatures. Fused coating shown marginal variations in its volume loss and wear rate at 200°C and 400°C temperatures as shown in Figure 5.22 (a and b) and Figure 5.23 (a and b). At 600°C fused coating exhibits a slight increase in its volume loss and wear rate. The effect of microwave heating provides a significant decrease in the wear volume loss of coating. The main reasons are decreased in surface roughness, increased hardness, and refining of the as-sprayed

coating microstructure leads to less rupture of the coating surface. The volume loss of CoMoCrSi/WC-12Co as-sprayed coating is 2.5-3 times higher than CoMoCrSi+WC-12Co fused coating Figure 5.22 (a and b).

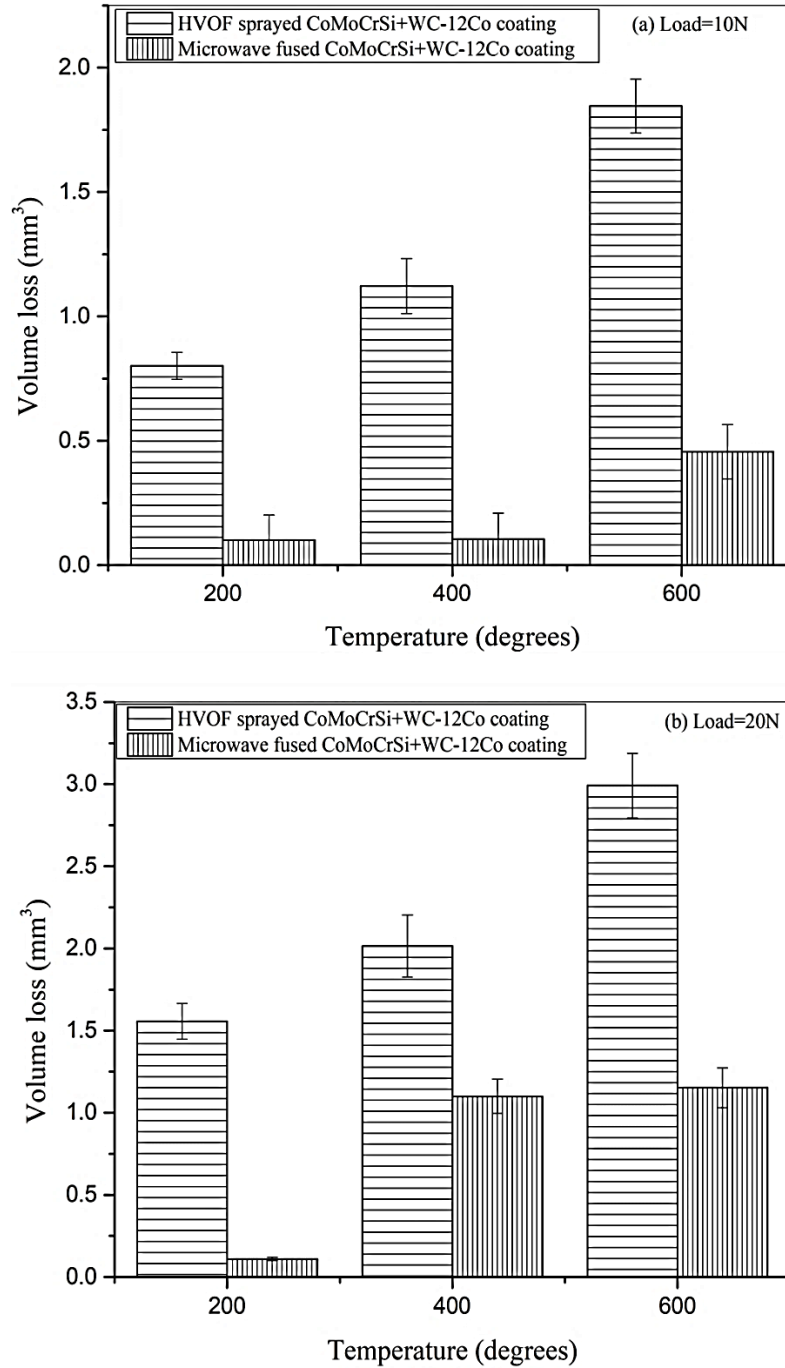


Figure 5.22 Wear volume loss of HVOF sprayed and microwave fused CoMoCrSi+WC-12Co composite coatings with respect to temperature (a) 10 N, (b) 20 N

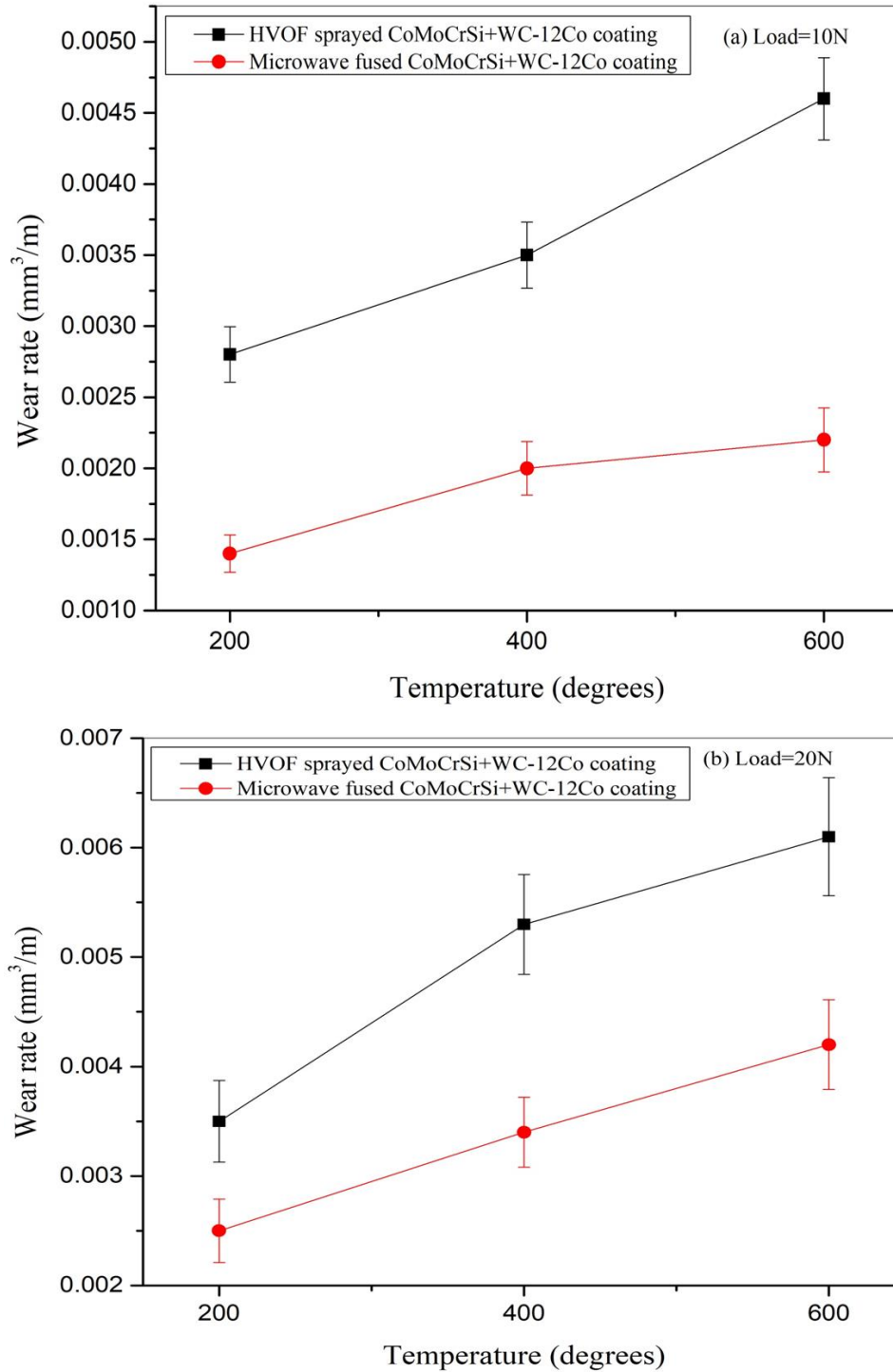


Figure 5.23 Wear rate plots of HVOF sprayed and microwave fused CoMoCrSi+WC-12Co composite coatings (a) 10 N, (b) 20 N

The wear rate of CoMoCrSi+WC-12Co as-sprayed coating is 3.5-4.5 times higher than CoMoCrSi+WC-12Co fused coating is observed in Figure 5.23 (a and b). This indicates that CoMoCrSi+WC-12Co fused coating is having superior wear resistance than CoMoCrSi+WC-12Co as-sprayed coating. The post heat treatment of as-sprayed coatings results in an increase in microhardness and formation of metallurgical bonding, eliminating surface defects such as pores, cracks, and unmelted particles. These are the reasons for the improvement of wear resistance of fused coatings in comparing with as-sprayed coatings. Also, hard phases have been formed such as TiC, $\text{Co}_6\text{W}_6\text{C}$, $\text{Co}_3\text{W}_9\text{C}$ and $\text{Co}_3\text{W}_3\text{C}$ Cr_3C_2 which provides substantial strength to the surface to resist material loss during sliding action.

The wear rate coefficient plot of the CoMoCrSi+WC-12Co before and after the fused composite coating is shown in Figure 5.24. The average wear rate coefficient values of as-sprayed and fused coatings are $1 \times 10^{-6} \text{ mm}^3/\text{N m}$ and $4 \times 10^{-7} \text{ mm}^3/\text{N m}$ respectively. Based on the comparison of tested composite coatings it is observed that the best wear resistance coating is microwave fused CoMoCrSi+WC-12Co.

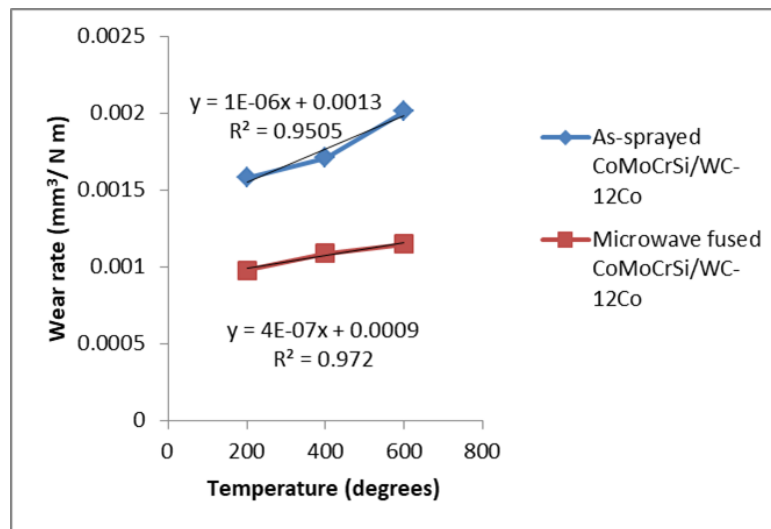


Figure 5.24 Wear rate coefficient k plot of HVOF sprayed and fused CoMoCrSi+WC-12Co composite coating

5.4.2. Coefficient of Friction

The COF plots of CoMoCrSi+WC-12Co as-sprayed and fused composite coating are shown in Figure 5.25 (a and b). At 200 °C temperature as-sprayed and fused coating exhibit slight higher friction. The rise in flash temperatures to 400 °C and 600 °C the COF of as-sprayed and fused coatings is shown a decreasing trend.

The COF of the as-sprayed coating reported an average value under both normal loads is 0.68. Whereas the average values of fused coatings are (0.2-0.4) measured at high temperature. The as-sprayed coating produced more variation in friction coefficient due to the presence of uneven coating surface which leads to poor contact during the sliding test (Liang Hou et al., 2011).

The COF of fused coating exhibits decreasing trend due to the smooth contact between two mating surfaces. This is achieved because of homogeneous structure of the coating. Friction of as-sprayed coating is increased from 0.38 to 0.72 in the running cycle (0-10 min) which is increased by 80% and once it reaches stable cycle (10–35 min), friction becomes linear and floating around a fixed value. Fused coating reveals steady and smooth sliding action, it increased from 0.15 to 0.4 in the running cycle (0–10 min) which is better than an as-sprayed coating. The COF of the fused coating in the stable cycle (10–30 min) becomes steady and floating around a fixed value. The quick formation of oxides leads to decrease in repeated periodic friction (Peat et al., 2016), (Karaoglanli et al., 2017). Fused coating obtains low COF comparing to as-sprayed coating, the fixed value is very small, and this result in microwave fused coating exhibits better wear resistance.

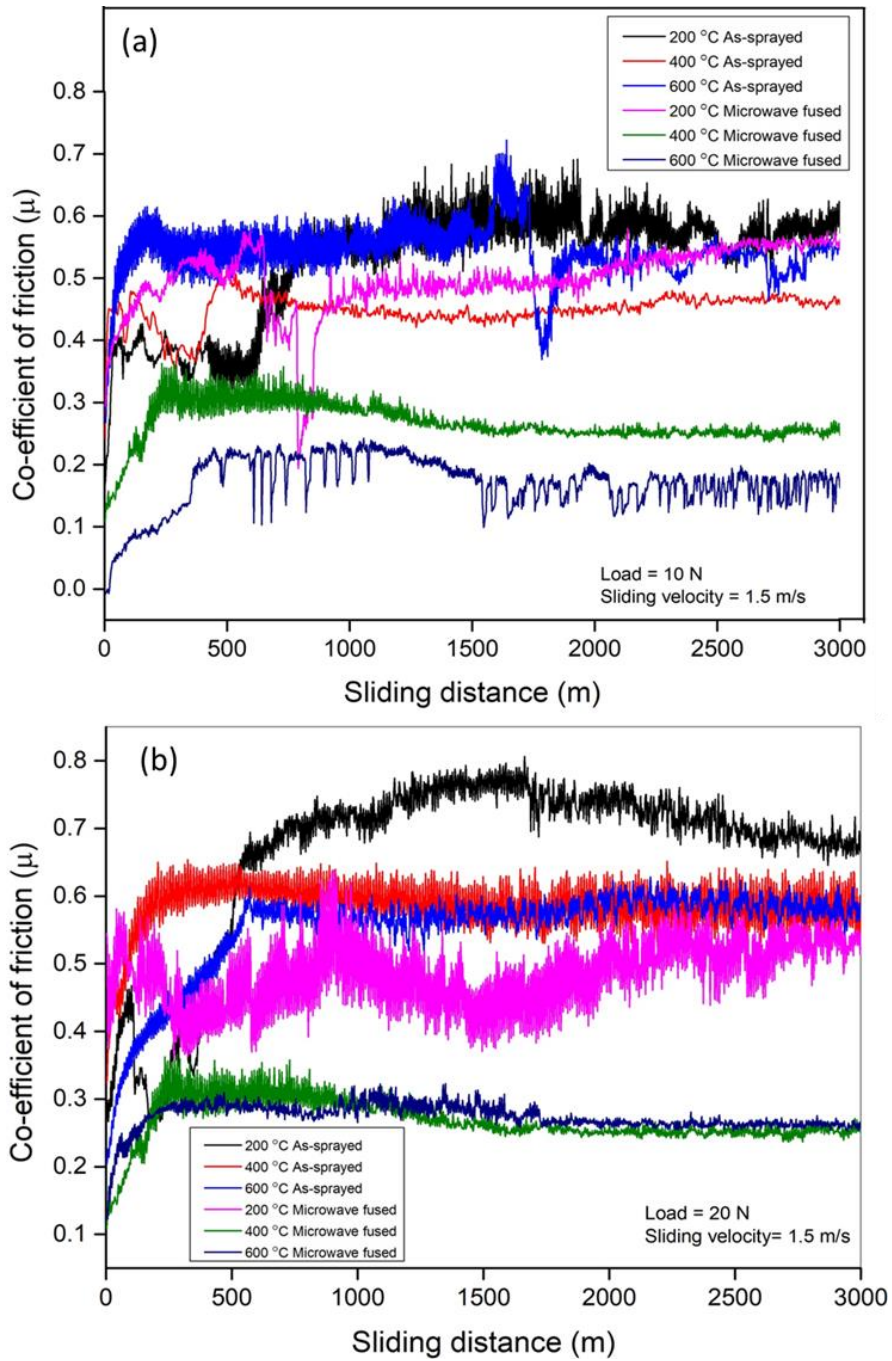


Figure 5.25 Friction coefficient of HVOF sprayed and microwave fused CoMoCrSi+WC-12Co composite coatings with respect to sliding distance (a) 10 N, (b) 20 N

5.4.3. X-Ray Diffraction analysis of Fused Coatings

The XRD pattern of microwave fused CoMoCrSi+WC-12Co worn coating is present in Figure 5.26. As observed in (Figure 5.26) Co_7Mo_6 phase is to be formed at all test temperatures. At 200°C Co_3O_4 phase is found, whereas CoO , Cr_2O_3 phases are formed at 400°C and 600°C . The MoO_2 and CoWo_4 is detected at 600°C . During sliding action, the coating elements subjected to oxidation due to frictional heat generated between two contact surfaces under atmospheric conditions. These results in Co element subjected to severe oxidation at all test temperatures, whereas Mo element oxidized at elevated temperature due to its higher melting point compared to other coatings elements. This tribo-film protects the fused coating surface during sliding action.

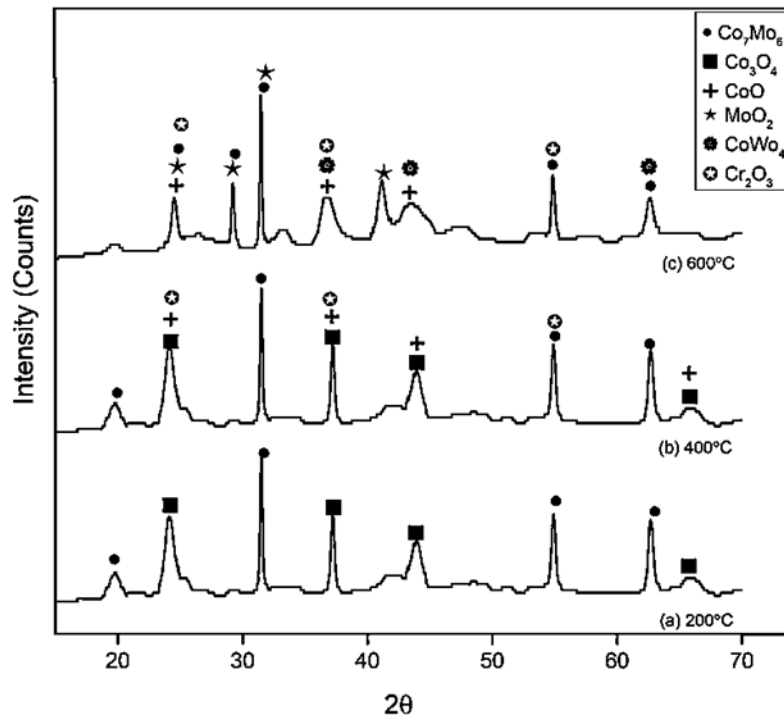


Figure 5.26 XRD pattern of fused CoMoCrSi+WC-12Co composite coating worn surfaces at all test temperatures

5.4.4. Worn Surface SEM and EDS analysis

The typical morphologies of wear tracks produced on as-sprayed CoMoCrSi+WC-12Co composite coating are shown in Figure 5.27. At 200°C it is observed from Figure 5.27 (a) wear scar is rough and width of the trace is decreased, results in adhesive wear of coating

material. As the rise in test temperature at 400 °C and 600 °C (Figure 5.27 b and c), brittle fracture observed with minor cracks are present on the sliding coating surface. Also, dark grey spots show oxidation of coating which prevents further loss of coating. With the increase in test load to 20 N, the width of wear trace is further decreased. This indicates the removal of material by splat detachment process is more and there are many severe brittle fractures of CoMoCrSi+WC-12Co as-sprayed coating at all test temperatures seen in Figure 5.27 (d-f). Coating experienced more amount of oxide layers are formed under 20 N than 10 N normal, these confirm that slightly higher friction as well as wear rate at higher temperatures.

The corresponding points chosen on the worn surface of the CoMoCrSi+WC-12Co as-sprayed coating shown in Figure 5.27 (a-f) are used for EDS analysis and values are tabulated in Table. 5.7. From the EDS analysis, it reveals that the formation of oxides at high temperatures is an important phenomenon to restrict material loss during sliding action. The damaged as-sprayed coatings exhibits rise in oxide percentage with respect to rise in load and temperatures. At points A, B and C under 10 N normal load showed growth of oxides, similar characteristic results are obtained for 20 N normal load at points D, E, and F.

Figure 5.28 (a-f) shows the wear out surface morphologies produced on CoMoCrSi+WC-12Co fused composite coatings. As observed in Figure 5.28 (a-c) exhibits smooth wear traces with small pits is present on the surface. A tribo-oxide layer is initiated at beginning of the test and continues to form as test proceeds which act as a protective layer for fused coating. The presence of WC hard phase leads to brittle coating and also due to tangential stresses coating yields only less depth (Fang et al., 2009). Presence of addition carbides due to microwave effect produces a very hard surface which results in fatigue spalling at 400°C and 600°C test temperatures. Similar kind of morphologies is obtained for 20 N normal load test, (Figure 5.28 d-f) some microcracking and fatigue spalling wear mechanism are observed for CoMoCrSi+WC-12Co fused coating for both test loads. Another interesting fact is noticed that fused coating experienced less adhesive wear. This is confirmed by EDS results by showing less percentage of alumina inclusions compared to as-sprayed coating results.

EDS analysis corresponding to chosen points on the surface of a worn fused coating presented in Figure 5.28 (a-f) the values are listed in Table. 5.8. Rapid oxidation layer is

formed as for an increase in test temperatures and more in 20 N normal load tests. Comparing with points A, B, and C, oxides scale is higher at points D, E and F also aluminium element is slightly increased for 20 N load. Due to an increase in carbon content allowed forming new carbide phases which strengthen the fused coating during sliding action.

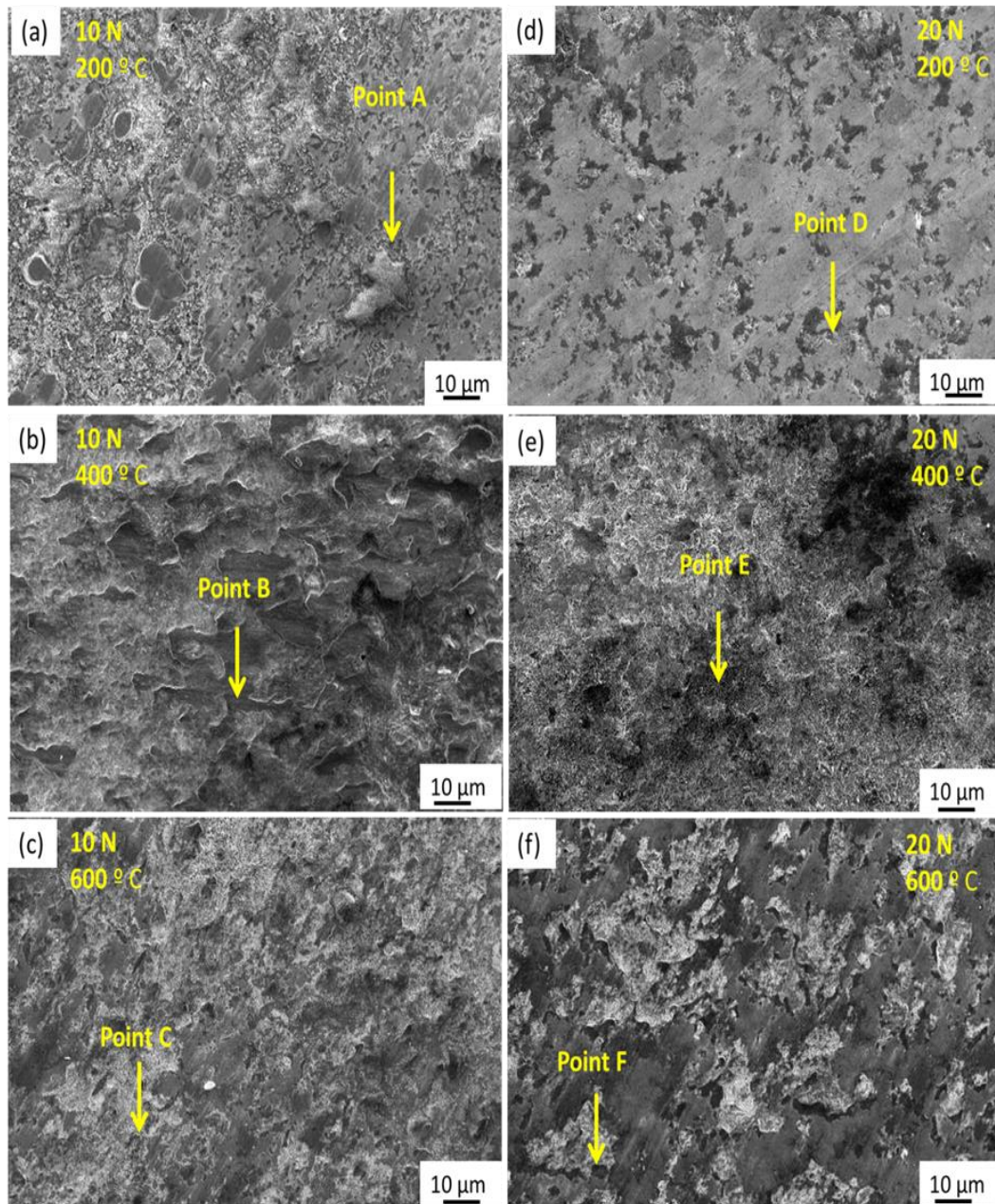


Figure 5.27 Morphology of HVOF sprayed CoMoCrSi+WC-12Co composite coating worn surfaces (a-c) under 10 N and (d-f) under 20 N at temperatures of 200 °C, 400°C, 600°C

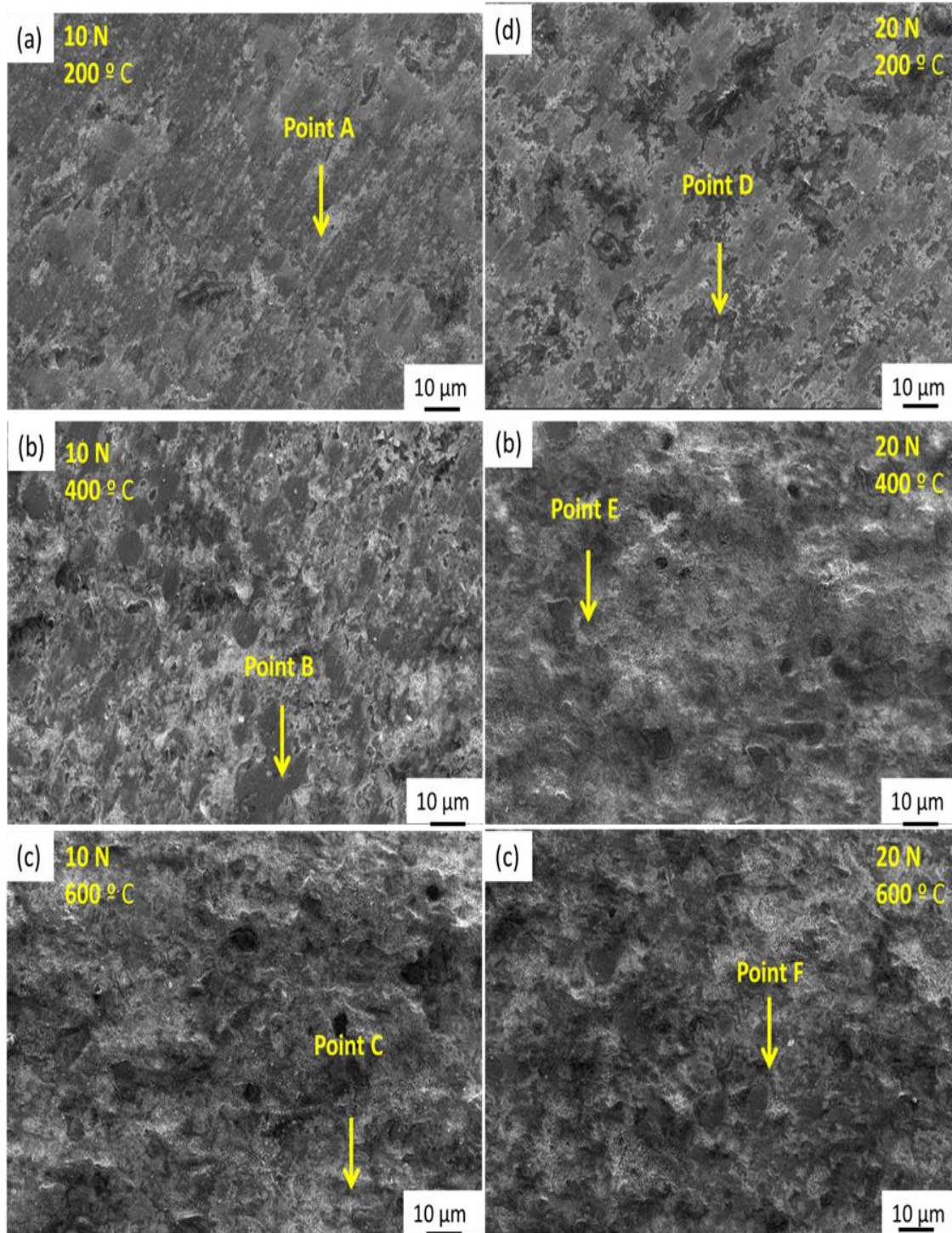


Figure 5.28 Morphology of microwave fused CoMoCrSi+WC-12Co composite coating worn surfaces (a-c) under 10 N and (d-f) under 20 N at temperatures of 200 °C, 400°C, 600°C

Table 5.7: EDS analysis of HVOF sprayed CoMoCrSi+WC-12Co composite coating worn surfaces on points marked in Figure 5.27

Element (wt %)	EDS results at selected points					
	10 N load			20 N load		
	A	B	C	D	E	F
O	09.15	12.20	19.10	17.05	26.44	39.59
C	02.19	03.39	02.54	02.20	02.86	03.61
Al	04.61	04.11	06.65	05.35	08.14	12.47
Si	00.95	01.42	01.70	01.13	01.01	00.63
Cr	07.55	06.02	07.21	08.52	06.38	06.94
W	25.33	22.81	23.17	19.09	17.74	11.82
Mo	14.75	15.20	12.42	13.87	12.03	10.31
Co	35.47	34.85	27.21	32.79	25.40	14.63

Table 5.8: EDS analysis of fused CoMoCrSi+WC-12Co composite coating worn surfaces on points marked in Figure 5.28

Element (wt %)	EDS results at selected points					
	10 N load			20 N load		
	A	B	C	D	E	F
O	11.13	16.45	24.59	19.33	31.58	40.08
C	04.25	05.42	05.10	05.76	06.02	05.69
Al	01.08	02.74	03.17	02.45	03.10	04.68
Si	01.28	01.32	01.51	00.83	00.49	01.16
Cr	08.56	07.20	06.09	07.45	06.19	05.56
W	24.12	20.51	19.34	20.39	15.22	13.38
Mo	16.20	11.10	08.47	12.04	09.87	07.30
Ti	07.02	09.95	09.55	08.14	07.36	06.77
Co	26.36	25.31	22.18	23.61	20.17	15.38

5.5. COMPARATIVE DISCUSSION OF HVOF SPRAYED AND FUSED COATINGS SUBJECTED TO WEAR

The loss of volume and wear rate of HVOF sprayed and microwave fused of four different coatings are shown in Figure 5.29 (a and b) and Figure 5.30 (a and b). Based on the experimental results, it is observed that HVOF sprayed coatings in terms of volume loss, wear rate and wear rate coefficient in the ascending sequence are CoMoCrSi+WC-12Co, CoMoCrSi+WC-CrC-Ni, CoMoCrSi+Cr₃C₂, and CoMoCrSi.

The HVOF sprayed CoMoCrSi and CoMoCrSi+Cr₃C₂ coatings under both normal loads exhibit higher volume loss and wear rate compared to CoMoCrSi+WC-12Co, CoMoCrSi+WC-CrC-Ni HVOF sprayed coatings. The loss of volume of CoMoCrSi and CoMoCrSi+Cr₃C₂ coatings are increased with respect to rising in temperature. This is mainly due to lower hardness produced by CoMoCrSi and CoMoCrSi+Cr₃C₂ as-sprayed coatings (Prasad et al., 2018). These coatings also showed the higher value of COF during the test and worn surface morphologies of CoMoCrSi and CoMoCrSi+Cr₃C₂ as-sprayed coatings demonstrates short wear tracks with rough layer results in detachment of splats, brittle fracture, and adhesive wear phenomenon as stated by Bolelli and Lusvarghi, (2007).

The CoMoCrSi+WC-12Co and CoMoCrSi+WC-CrC-Ni as-sprayed coatings produced lower volume loss and wear rate since the microhardness of these coatings are significantly higher and COF values also decreased at elevated temperature. The presence of intermetallic laves phases with additional hard carbides possess higher hardness and protects the coating surface from counter sliding disc at high speed and temperatures (Prasad et al., 2018). The worn surface morphologies of these coatings confirm that very few regions of coating surfaces cause damage and rapid formation of oxide films protects the further loss of material by acts as lubricants (Matikainen et al., 2017).

In the case of 20 N normal load, the as-sprayed coatings produced a similar trend in loss of volume (Figure 5.29 b). The effect of the rise in normal load from 10 N to 20 N produced higher loss of volume and wear rate (Figure 5.29 b) and (Figure 5.30 b). This effect also made to produce higher COF profiles and coating surfaces results in the formation of large pits with localized plastic deformation is observed at 400°C and 600°C temperatures. After

microwave fusing of as-sprayed coatings, the loss of volume and wear has been reduced drastically. As noticed in (Figure 5.29) and (Figure 5.30), the ascending order of volume loss of fused coatings are CoMoCrSi+WC-12Co, CoMoCrSi+WC-CrC-Ni, CoMoCrSi+Cr₃C₂ and CoMoCrSi. The homogeneous structure of fused coatings is the main reason for reducing the loss of volume and wear rate compared to as-sprayed coatings. The penetration of substrate element into coatings and minimizing of surface defects results in lower wear rate of fused coatings. Also, additional inducing of carbon to the as-sprayed coating during remelting results in the formation of hard surface. After fusing, noticed that all coatings exhibit a marginal difference in its volume loss and wear, this confirms the positive effect of microwave hybrid heating. The fused coatings reveal lower COF profiles and due to the formation of tribo-oxide films restrict the loss of materials by allowing the coating surface to slide smoothly with exhibiting large wear scars (Fernandez et al., 2005). The hard surface of fused coatings produced a fatigue spalling effect by forming irregular cavities and grooves (Dejun and Tianyuan, 2017). As the increase in normal load to 20 N, all fused coatings produced a very marginal increase in its volume loss and wear rate. EDS analysis confirms the higher percentage of oxides at elevated temperatures also these stable oxides near the coating surface, serves as lubricants as described by Asgari et al., (2017), Xu et al., (2007) and Zhang et al., (2009). The percentage of alumina transformation is less compared to the as-sprayed coating.

Based on the comparison results of HVOF sprayed coating results, the CoMoCrSi + WC-12Co composite coating exhibits superior wear and friction resistance than other three as-sprayed coatings. The as-sprayed CoMoCrSi+WC-CrC-Ni composite coating reveals better wear resistance than CoMoCrSi+Cr₃C₂ and CoMoCrSi coatings. In the present study after fusing improves the wear resistance of four HVOF sprayed coatings among in that, CoMoCrSi + WC-12Co composite coating presents the superior wear resistance, it reveals least volume loss and wear rate as well as lower COF profile compared to other HVOF sprayed and fused coatings. The fused CoMoCrSi+WC-CrC-Ni composite coating had shown the good wear resistance than HVOF sprayed and fused CoMoCrSi+Cr₃C₂ and CoMoCrSi coatings.

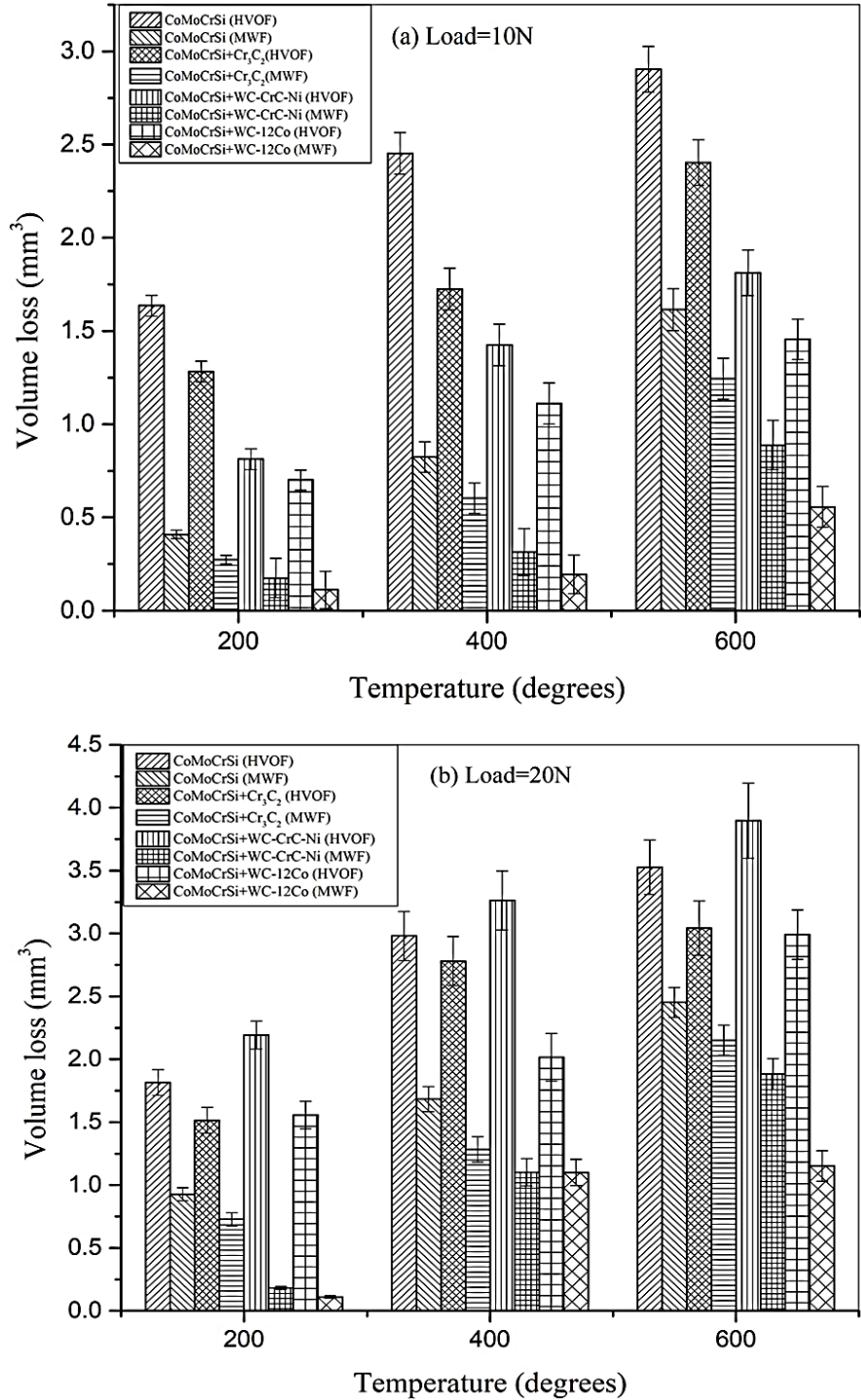


Figure 5.29 Wear volume loss of HVOF sprayed and microwave fused of four different coatings with respect to temperature (a) 10 N, (b) 20 N

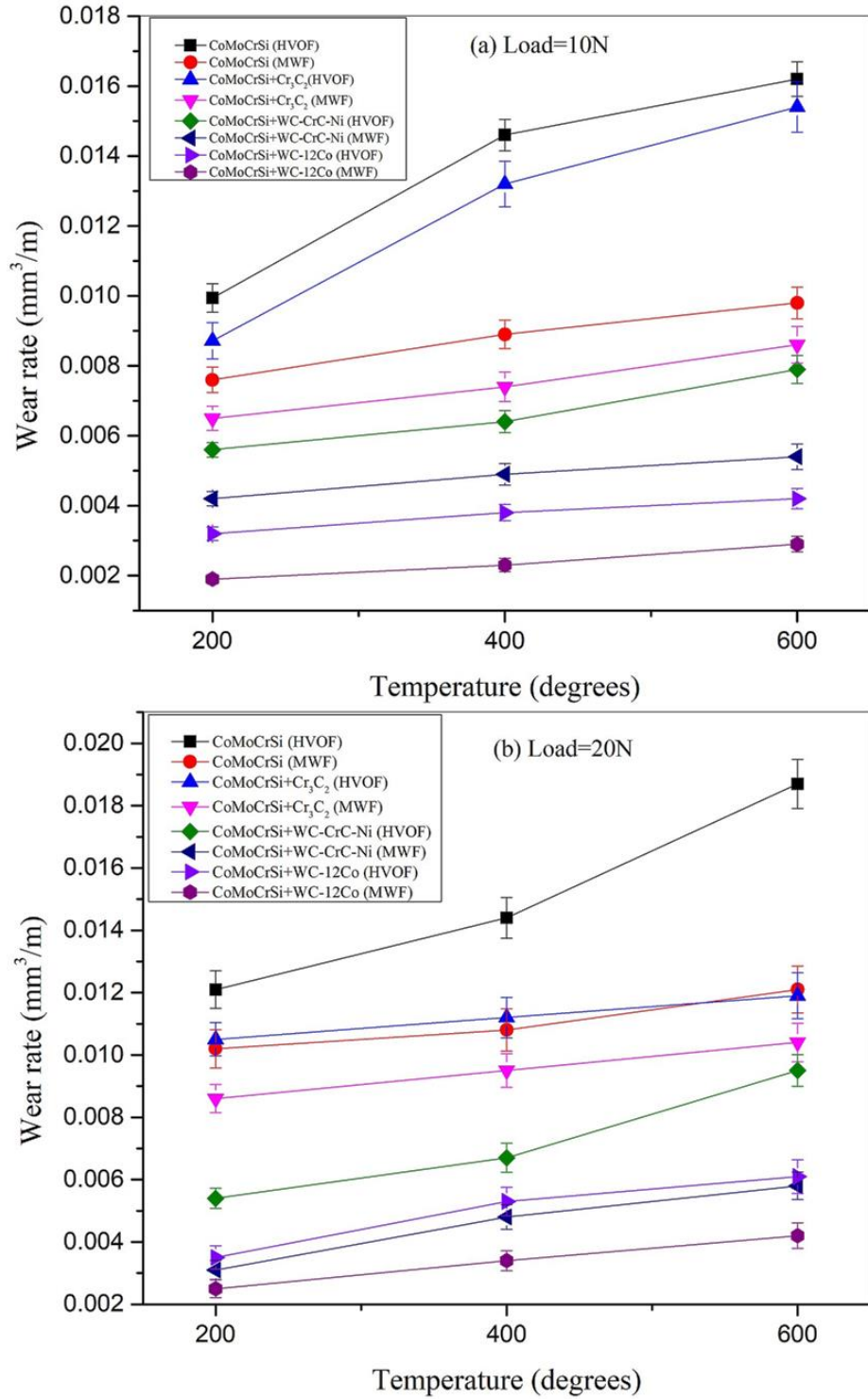


Figure 5.30 Wear rate plots of HVOF sprayed and microwave fused of four different coatings with respect to temperature (a) 10 N, (b) 20 N

5.6. WEAR STUDIES ON FLAME SPRAYED AND MICROWAVE FUSED CoMoCrSi COATINGS

5.6.1. Volume loss and Wear rate of Coatings

The wear volume loss and wear rate plots of flame sprayed and microwave fused CoMoCrSi coatings are shown in Figure 5.31 (a and b) and Figure 5.32 (a and b). As the increase in normal load and test temperatures, increases the amount of wear volume loss of as-sprayed coating Figure 5.31 (a and b). The volume loss of CoMoCrSi as-sprayed coating increases as a rise in temperature and showed the highest material loss at 600°C for both normal loads compared to fused coating Figure 5.31 (a and b). It is due to lower microhardness, presence pores, voids, unmelted particles; rough surface results in higher volume loss during in contact with a sliding disc.

The effect of microwave heating provides a significant decrease in the wear volume loss of both coatings. The main reasons are decreased in surface roughness, increased hardness, and refining of the as-sprayed coating microstructure leads to less rupture of the coating surface obtained from metallurgical bonding by diffusion of elements from the substrate to coating (Utua and Marginean, 2017). Another reason is the presence of a higher fraction of intermetallic laves phases in CoMoCrSi microwave fused coating. The CoMoCrSi as-sprayed exhibits wear rate of 4-4.5 times higher than CoMoCrSi fused coating under both test loads shown in Figure 5.32 (a and b). This is caused due to brittle fracture of unmelted particles which is loosely bonded in the form of splats. This issue has been resolved by fused coatings producing homogeneous structure results in lower volume loss and wear rate.

The calculated wear rate coefficient K in $\text{mm}^3/\text{N m}$ of flame sprayed and fused CoMoCrSi coatings is shown in Figure 5.33. The K value of flame sprayed and fused CoMoCrSi coating is $3 \times 10^{-6} \text{ mm}^3/\text{N m}$ and $1 \times 10^{-6} \text{ mm}^3/\text{N m}$ respectively. Based on the comparison results of tested coatings it is observed that the flame sprayed fused CoMoCrSi coating improved its wear resistance.

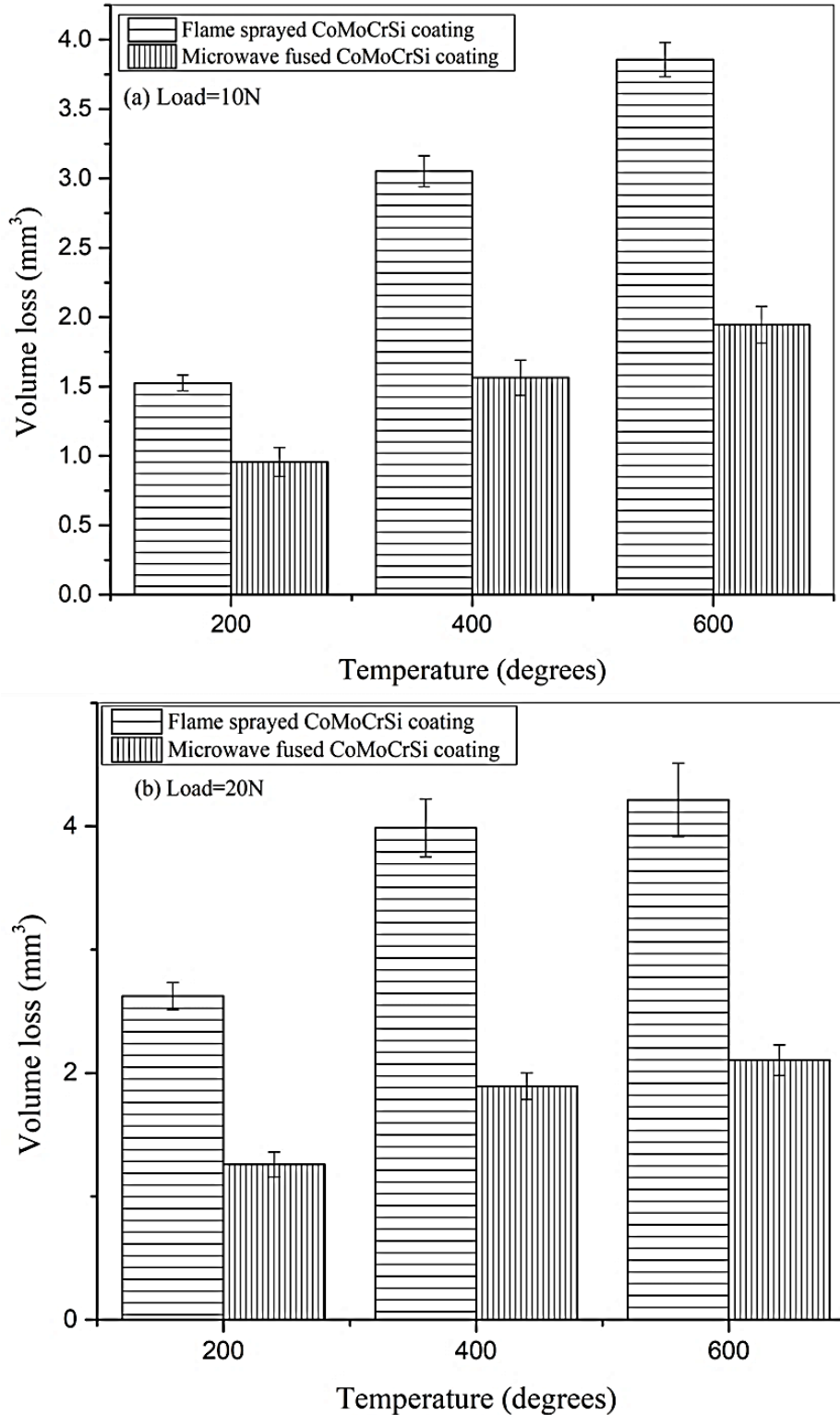


Figure 5.31 Wear volume loss of flame sprayed and microwave fused CoMoCrSi coatings with respect to temperature (a) 10 N, (b) 20 N

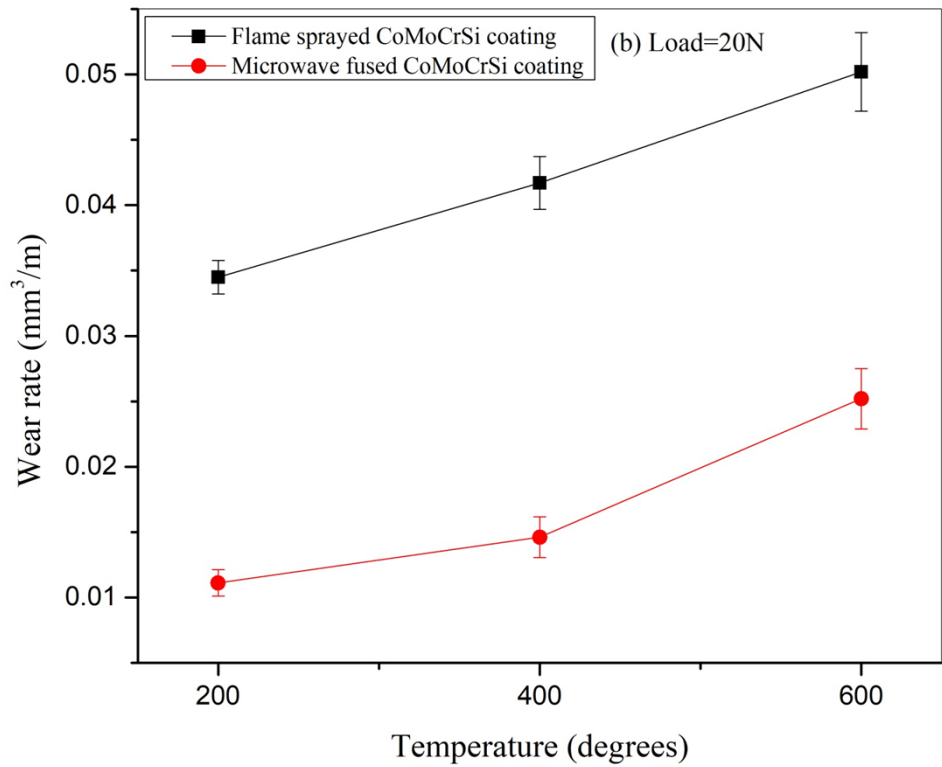
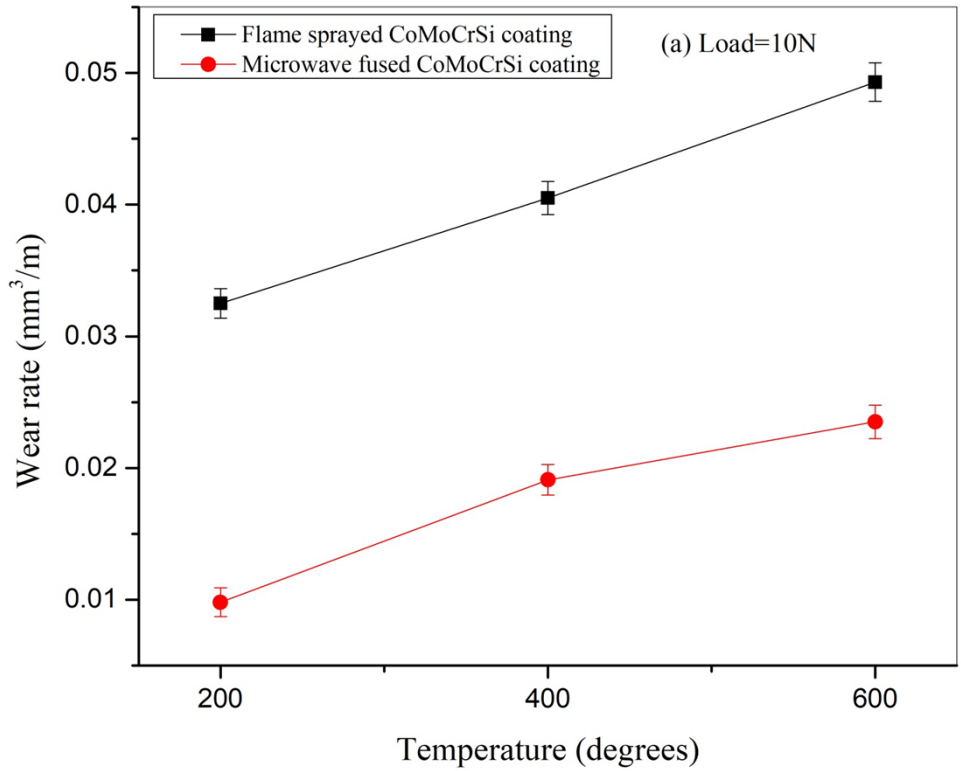


Figure 5.32 Wear rate plots of flame sprayed and microwave fused CoMoCrSi coatings

(a) 10 N, (b) 20 N

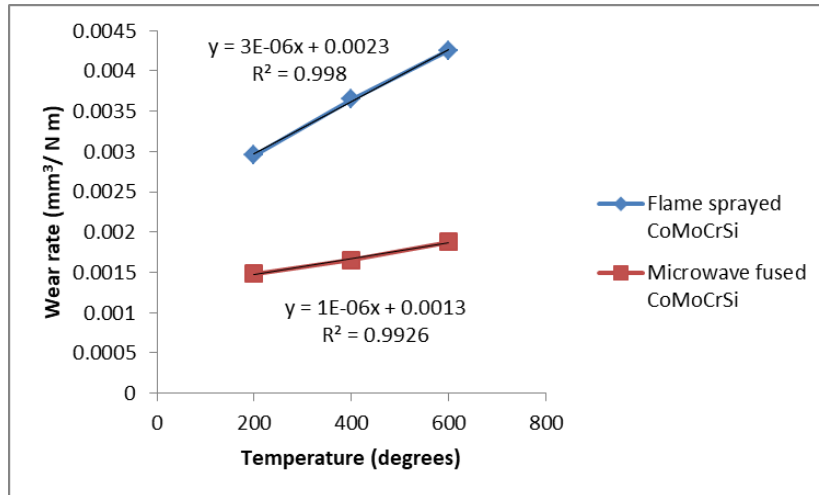


Figure 5.33 Wear rate coefficient k plot of flame sprayed and fused CoMoCrSi coating

5.6.2. Coefficient of Friction

The COF plots of flame sprayed and fused CoMoCrSi coatings are shown in Figure 5.34 (a and b). The COF of as-sprayed and fused coatings tends to show a decreasing trend as a rise in temperature. The COF of the as-sprayed coating under both normal loads experienced average values of 0.67; this is more than the mean values of fused coatings (0.22-0.36) computed at elevated temperatures. The COF of as-sprayed and fused coatings fluctuates greatly during sliding action. The friction of the as-sprayed coating is increased slowly from 0.36 to 0.79 increased by 86% in the running cycle (0-10 min) because of weak contact between the counter disc and coating sample. However, during the stable cycle (10–35 min), the COF of the as-sprayed coating becomes smooth, floating around a fixed value. This is because of the existence of laves phases in coating restricts occurring of friction during sliding action (Khameneh et al., 2006), (Wood et al., 2010). In the case of fused coating, COF increased from 0.2 to 0.38 nearly increased by 63% in the running cycle (0–10 min) which is better than an as-sprayed coating. The COF of the fused coating in the stable cycle (10–30 min) becomes steady and floating around a fixed value. Compared to as-sprayed coating, the fixed value is small, this result in effect of fused coating hardness on the COF is low, and hence microwave treated coating played a significant role in reducing COF.

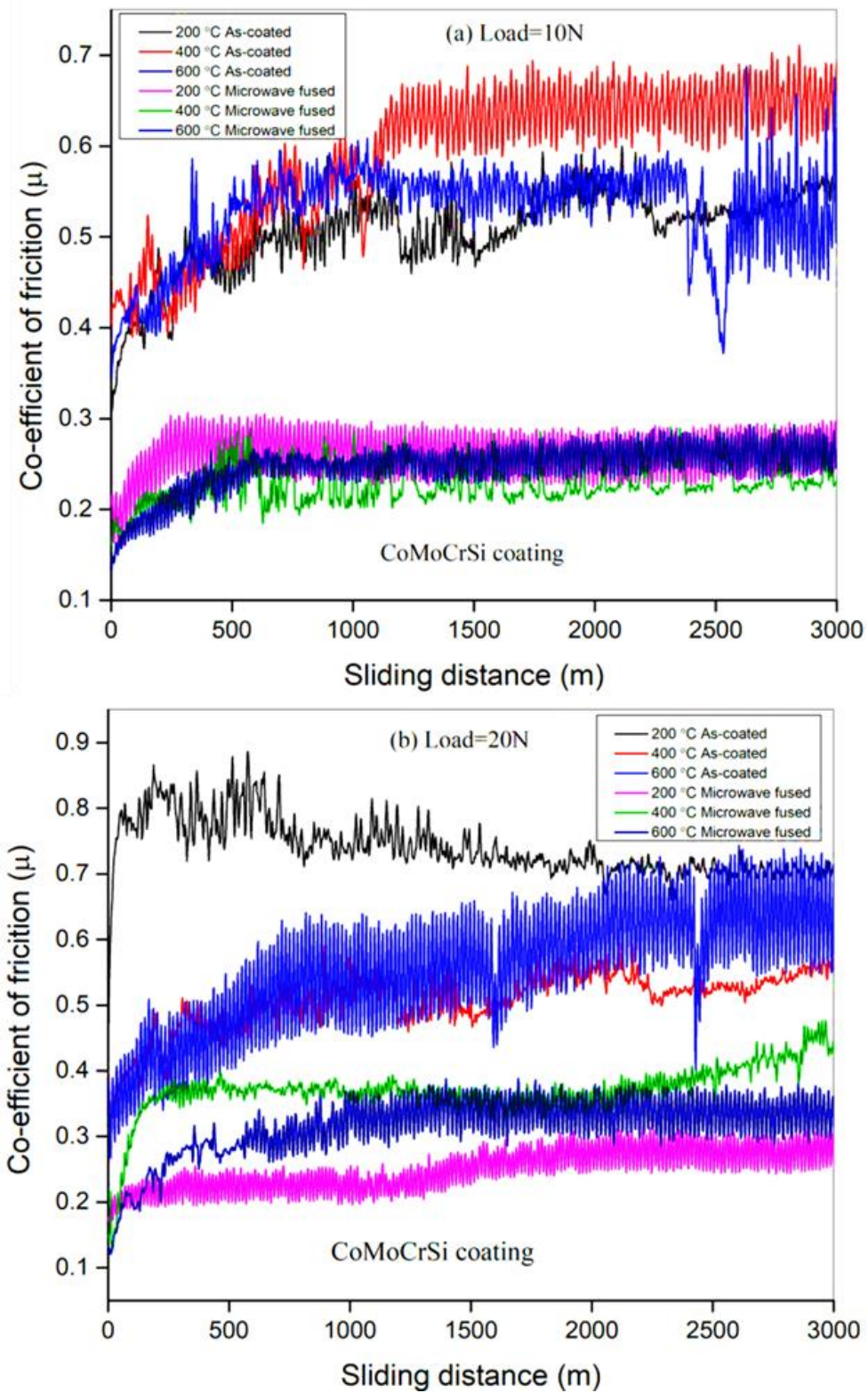


Figure 5.34 Friction coefficient of flame sprayed and microwave fused CoMoCrSi coatings with respect to sliding distance (a) 10 N, (b) 20 N

5.6.3. X-Ray Diffraction analysis of Fused Coatings

The XRD spectrum of microwave fused flame sprayed CoMoCrSi worn surface coating is shown in Figure 5.35. Since the test is carried out at elevated temperatures obviously, the cobalt is prone to oxidation severely during the sliding action (Cho et al., 2009), (Sharma, 2014). As observed in (Figure 5.35) CoMoCrSi fused coating exhibits Co_7Mo_6 and Cr_3C_2 phases are to be formed at all test temperatures. At test temperatures of 200°C , the Co_3O_4 phase is identified. Whereas MoO_3 phase is identified at 400°C and also CoO and Cr_2O_3 phases are formed at 400°C and 600°C on the other hand MoO_2 is formed at 600°C . These oxides are formed on the fused coating surface acts as a protective film during sliding action. This results in smooth sliding of fused coatings and no sign of adhesive wear mechanism is observed.

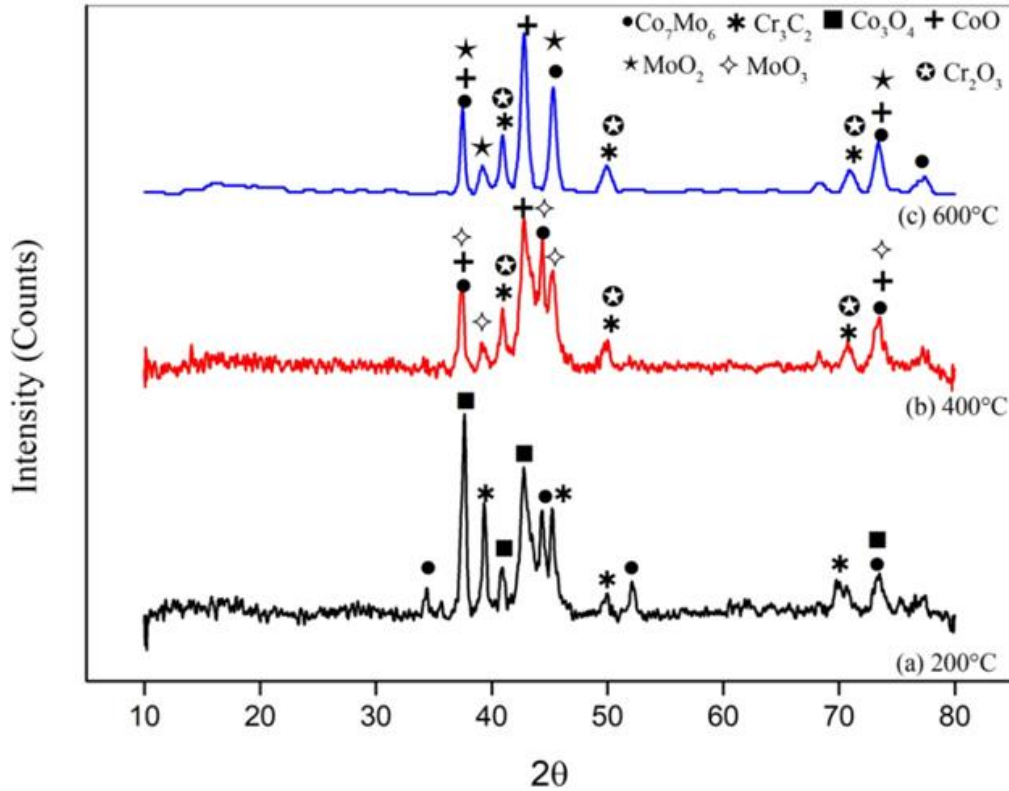


Figure 5.35 XRD pattern of microwave fused flame sprayed CoMoCrSi coating worn surfaces at all test temperatures

5.6.4. Worn Surface SEM and EDS analysis

The worn surface morphologies and EDS analysis of flame sprayed CoMoCrSi coating is presented in Figure 5.36 (a-f). It can be seen that (Figure 5.36 a-c) the worn surfaces of the as-sprayed coating under 10 N normal load is characterized by a groove, brittle fracture, and detachment of splats. Though at all the test temperatures observed rough wear scars showing large width traces and flaking pits. As the increase in normal load to 20 N the wear of flame as-sprayed coating is influenced by intersplat cohesion seen in Figure 26 (d-f). Also observed during sliding action, results in massive loss of coating material is caused by the pulling out of maximum splats infers severe wear. This may be due to the presence of unmelted/semi-melted cobalt, molybdenum elements (Yu et al., 2016). As the rise in flash temperature the oxide layer of coating active elements to be formed between coating and counterpart surface. These prevent further loss of coating material at higher loads, leading to lower wear loss subsequently. EDS results (wt %) on CoMoCrSi as-sprayed coating worn surfaces shown in Figure 5.36 (a-f). The result reveals that the dark grey regions contain primarily Co, Mo, and O, indicating that oxides are formed. It is noticed that the worn surface is roughened with oxidized clusters as the test load increased to 20 N, the dark clusters are confirmed the presence of mixed oxides of Co, Mo, Cr, and Al. The oxidation of coating is influenced on wear phenomenon and also coating exhibits severe adhesive wear mechanism which is confirmed by an increase in aluminum percentage from EDS results (Bergant et al., 2014).

The damaged surfaces of flame sprayed CoMoCrSi fused coating under 10 and 20 N normal at 200°C, 400°C and 600°C temperatures are shown in Figure 5.37 (a-f). In the case of microwave fused coating, the remelting increases the intersplat cohesion strength results in less material loss. As observed in (Figure 5.37 a-c) under 10 N normal load, the worn surface is smooth on several areas, very small parts of coating material are pulled out and also noticed some small flaking pits on worn surfaces. A tribo-oxide layer is initiated at beginning of the test and continues to form as test proceeds which act as a protective layer for fused coating (Kim et al., 2003). Presence of addition carbide like Co_3C due to microwave effect produces a very hard surface which results in fatigue spalling at 400°C and 600°C test temperatures. Similar kind of morphologies is obtained for 20 N normal load test, observed in Figure 5.37 (d-f) Another interesting fact is noticed that fused coating experienced less adhesive wear. This is confirmed by EDS results (Figure 5.37 a-f) by showing less

percentage of alumina inclusions compared to as-sprayed coating, results in less friction and high wear resistance due to improved hardness by microwave effect. Rapid oxidation layer is formed as for an increase in test temperatures and more in 20 N normal load tests. Higher percentages of oxides are responsible for less wear rate and low friction (Prasad et al., 2018).

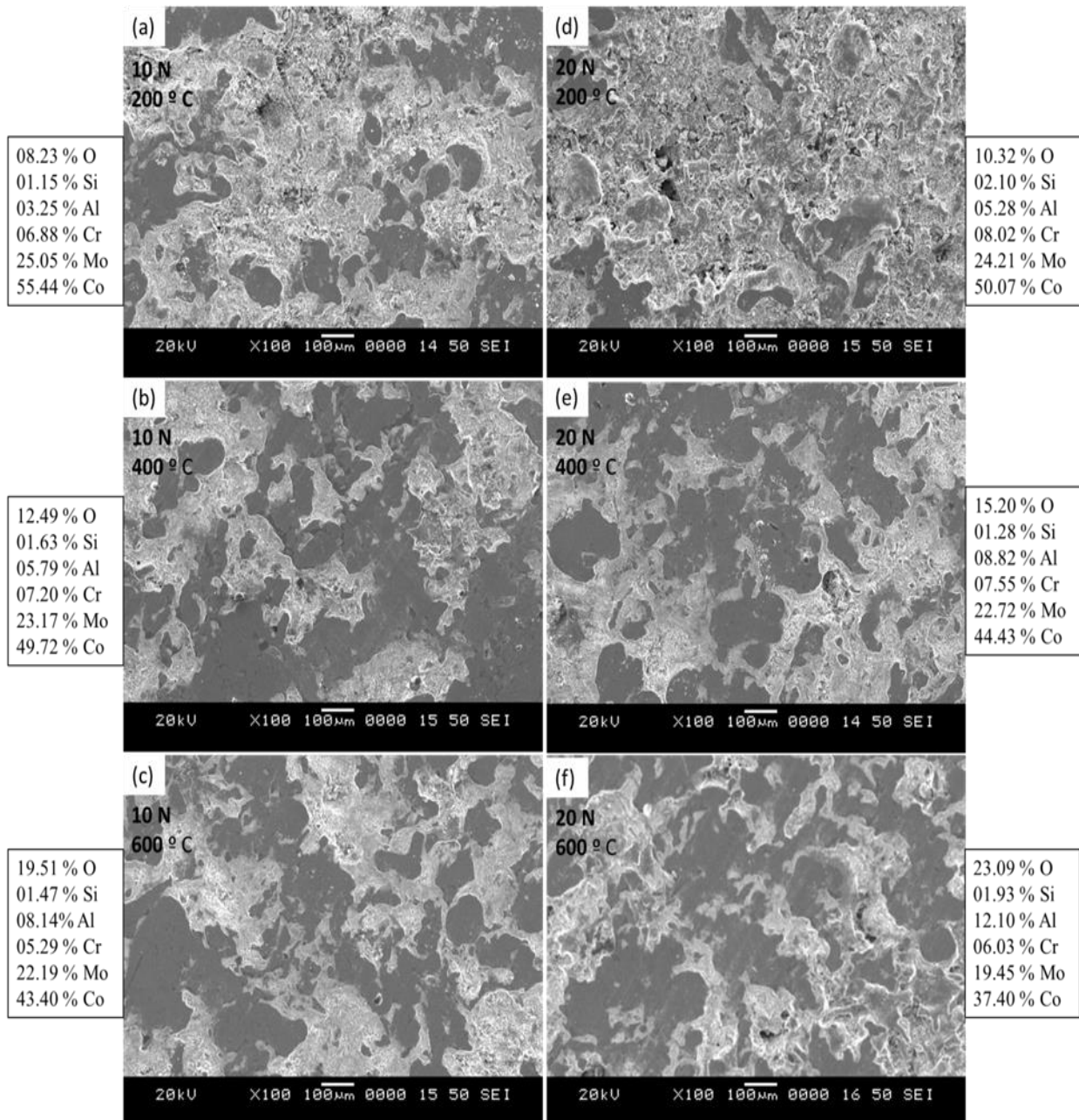


Figure 5.36 Morphology of flame sprayed CoMoCrSi coating worn surfaces (a-c) under 10 N and (d-f) under 20 N at temperatures of 200 °C, 400°C, 600°C

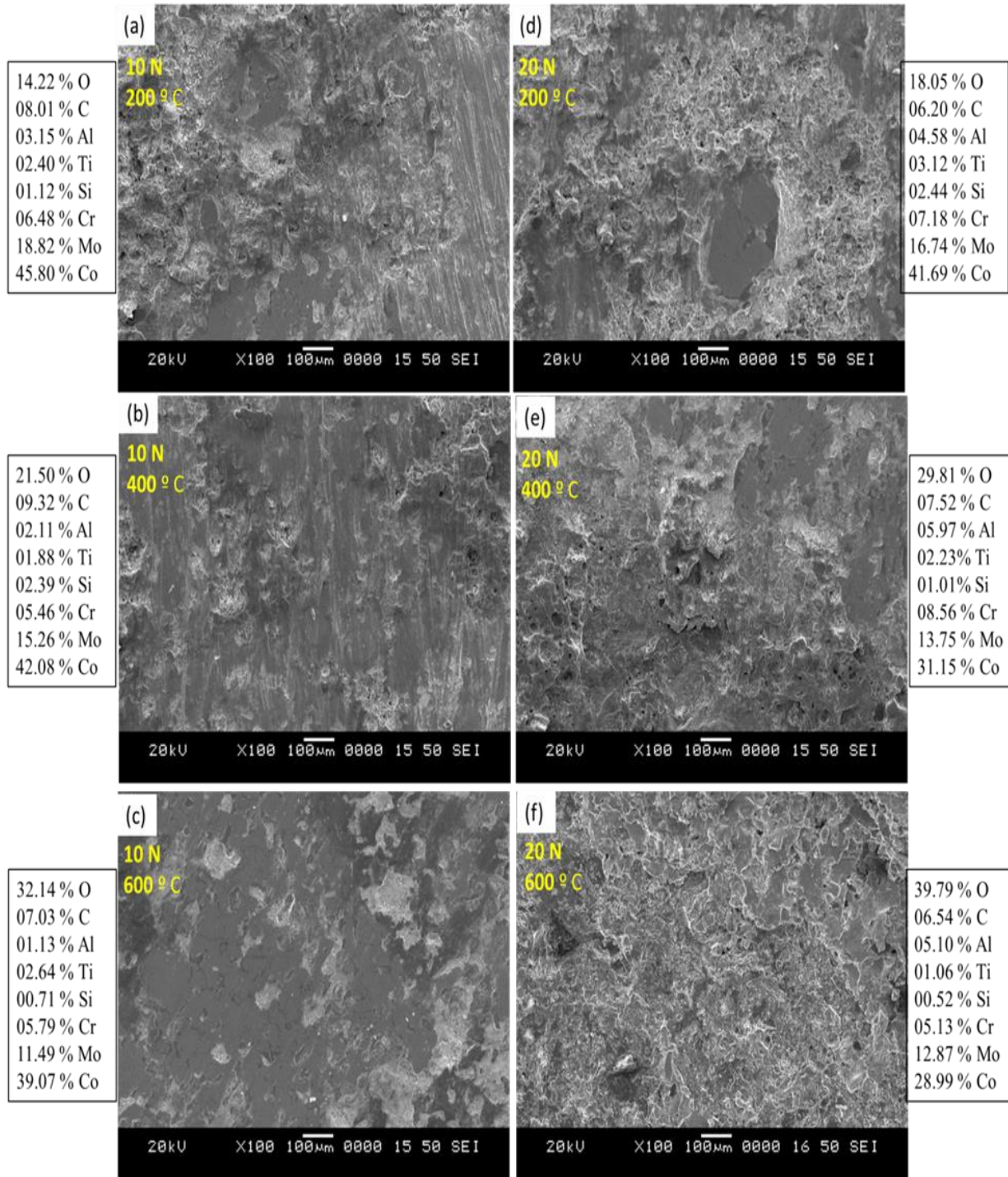


Figure 5.37 Morphology of microwave fused flame sprayed CoMoCrSi coating worn surfaces (a-c) under 10 N and (d-f) under 20 N at temperatures of 200 °C, 400°C, 600°C

5.7. WEAR STUDIES ON FLAME SPRAYED AND MICROWAVE FUSED CoMoCrSi+Cr₃C₂ COMPOSITE COATINGS

5.7.1. Volume loss and Wear rate of Coatings

The wear volume loss and wear rate of flame sprayed and microwave fused CoMoCrSi+Cr₃C₂ composite coatings shown in Figure 5.38 (a and b) and Figure 5.39 (a and b). The wear volume loss of as-sprayed coating had shown increasing corresponding to temperatures and load. At 20 N normal load as-sprayed coating exhibits higher volume loss compared to 10 N normal load Figure 5.38 (a and b). This reveals that as a rise in a normal load, leads to an increase in the deformation of the as-sprayed coating. It is mainly due to the breaking of splats during the sliding test.

After fusing due to homogeneous and enhanced microhardness of fused coating exhibits lower volume loss in comparison with as-sprayed coating Figure 5.38 (a and b). Whereas CoMoCrSi+Cr₃C₂ composite coatings exhibit higher hardness due to the presence of Co₃C and Cr₃C₂ phases result in improved wear resistance compared to CoMoCrSi coatings. The CoMoCrSi+Cr₃C₂ as-sprayed exhibits wear rate of 3-3.5 times higher than CoMoCrSi+Cr₃C₂ fused coating Figure 5.39 (a and b).

The (Figure 5.40) depicts the average wear rate of flame sprayed and fused composite coatings. The *K* value as-sprayed and fused CoMoCrSi+Cr₃C₂ composite coatings are $3 \times 10^{-6} \text{ mm}^3/\text{N m}$ and $9 \times 10^{-7} \text{ mm}^3/\text{N m}$ respectively. From these results, it is clearly evidence that fused CoMoCrSi+Cr₃C₂ composite coating has better wear resistance than an CoMoCrSi+Cr₃C₂ as-sprayed coating.

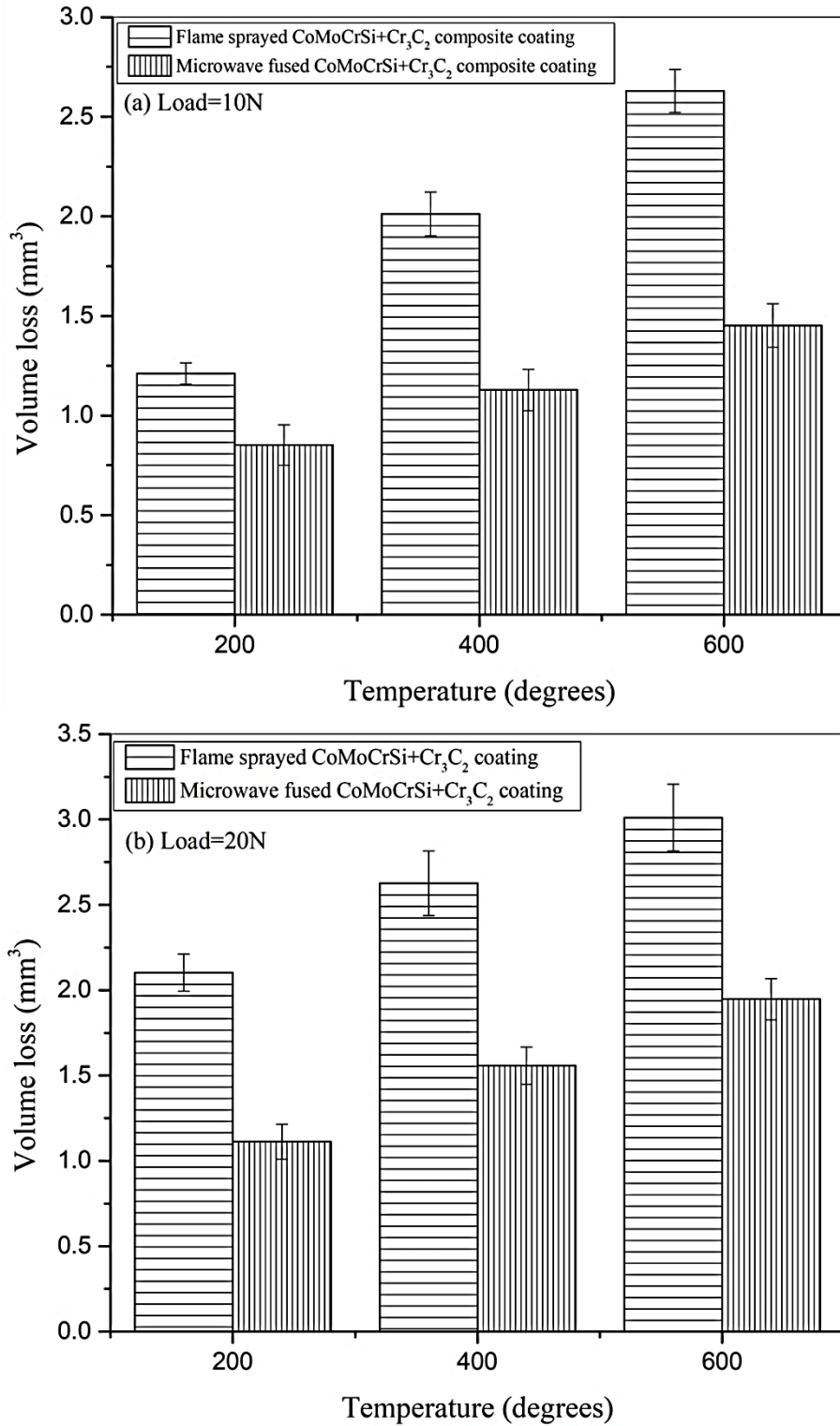


Figure 5.38 Wear volume loss of flame sprayed and microwave fused CoMoCrSi+Cr₃C₂ composite coatings with respect to temperature (a) 10 N, (b) 20 N

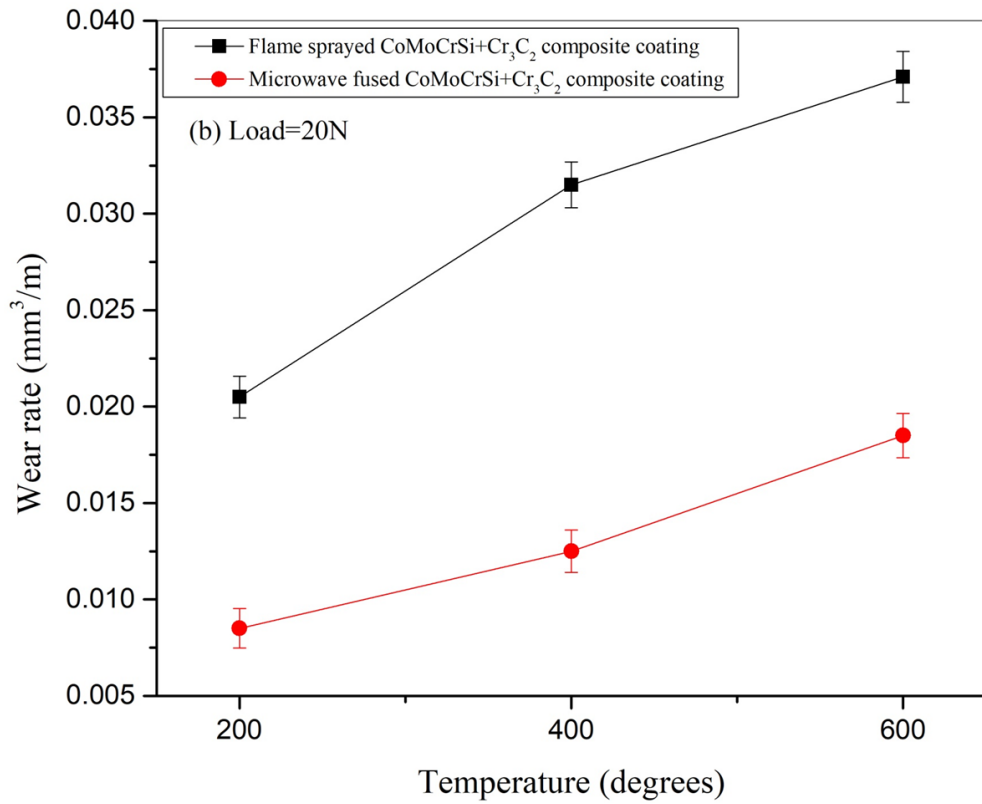
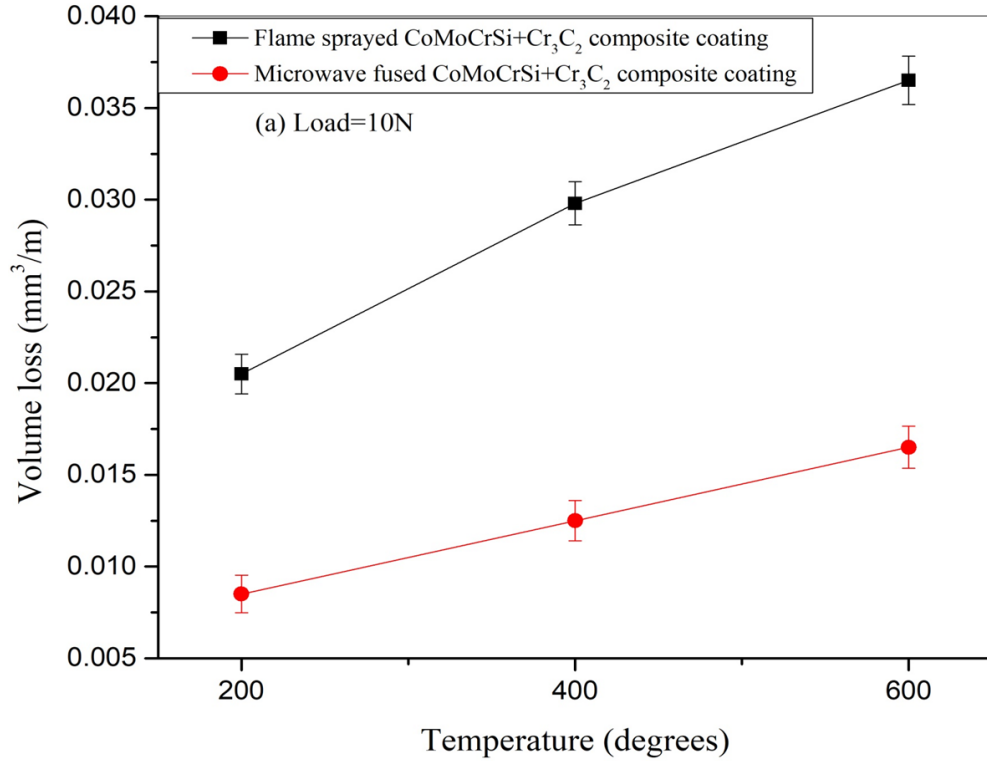


Figure 5.39 Wear rate plots of flame sprayed and microwave fused CoMoCrSi+Cr₃C₂ composite coatings with respect to temperature (a) 10 N, (b) 20 N

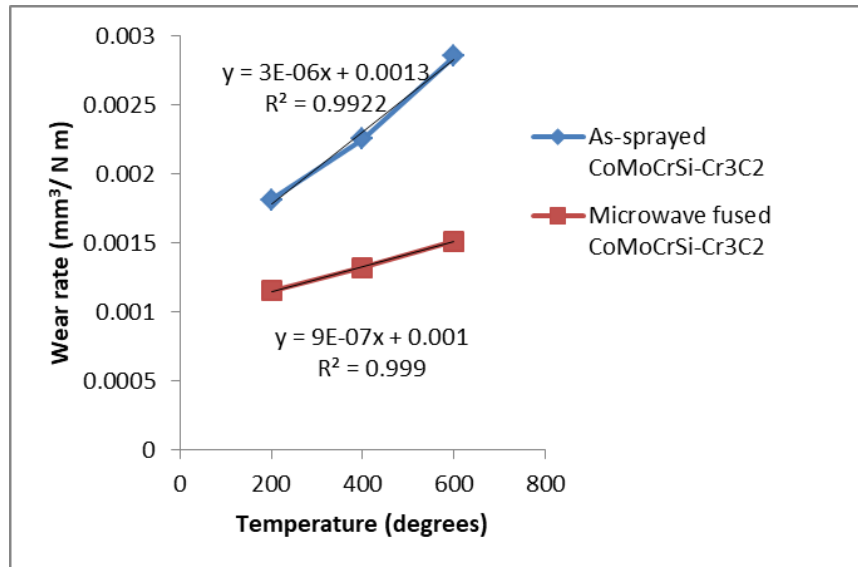


Figure 5.40 Wear rate coefficient k plot of flame sprayed and fused $\text{CoMoCrSi}+\text{Cr}_3\text{C}_2$ composite coatings

5.7.2. Coefficient of Friction

The COF plots of flame sprayed and fused $\text{CoMoCrSi}+\text{Cr}_3\text{C}_2$ composite coatings are shown in Figure 5.41 (a and b). At 200°C temperature coatings before and after fusing shows higher friction. When the temperatures at 400 °C and 600 °C the COF of as-sprayed and microwave fused coatings is showed a decreasing trend. The COF of the as-sprayed coating reported an average value under both normal loads is 0.59. Whereas the average values of fused coatings measured at high temperature are (0.25-0.48). The as-sprayed coating produced more variation in COF due to the presence of uneven coating surface which leads to poor contact during the sliding test (Li et al., 2002). In case of fused coating, observed variation in COF due to poor contact of the coating. During wear test observed friction of as-sprayed coating is increased from 0.35 to 0.68 in the running cycle (0-10 min) which is increased by 74% and once it reaches stable cycle (10–35 min), friction becomes linear and floating around a fixed value. Fused coating reveals steady and smooth sliding action, it increased from 0.25 to 0.49 in the running cycle (0–10 min) which is better than an as-sprayed coating. The COF fused coating in the stable cycle (10–30 min) becomes steady and floating around a fixed value. This decreases friction periodically due to the rapid formation of oxides (Gonzalez et al., 007). Fused coating obtains low COF comparing to as-sprayed coating, the fixed value is

very small, and this result in microwave fused coating exhibits better wear resistance by showing less friction and wear rate.

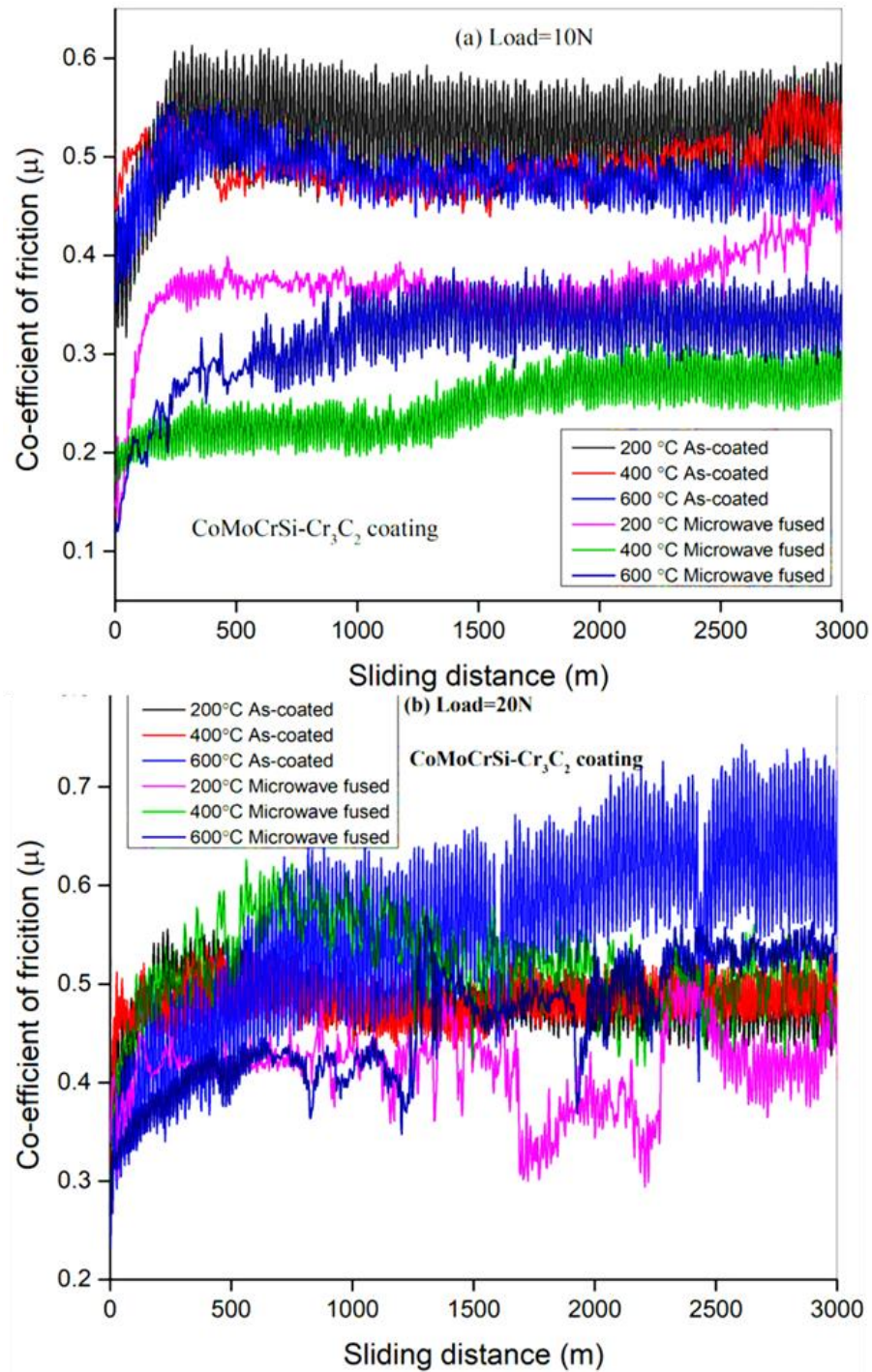


Figure 5.41 Friction coefficient of flame sprayed and microwave fused CoMoCrSi+Cr₃C₂ composite coatings with respect to sliding distance (a) 10 N, (b) 20 N

5.7.3. X-Ray Diffraction analysis of Fused Coatings

Figure 5.42 demonstrates the X-ray diffraction pattern of microwave fused CoMoCrSi+Cr₃C₂ composite coating. It reveals the similar phases as identified in CoMoCrSi fused coating as shown in Figure 5.35. At all test temperatures, Co₇Mo₆ and Cr₃C₂ phases are formed, whereas, the Co₃O₄ phase is found at 200°C. At 400°C MoO₃ phase is detected and CoO and Cr₂O₃ phases are produced at 400°C and 600°C on the other hand MoO₂ is formed at 600°C. During the sliding test, these oxides are formed due to the rise in temperature at the interface. Since the test is performed under atmospheric conditions, where oxygen is formed at the surface of the test sample and forming a protective layer, it leads to a decrease in material loss under high speeds with high temperatures. The fewer alumina inclusions are also identified on the worn surface by EDS analysis this is due to the effect of fatigue spalling observed during the sliding test.

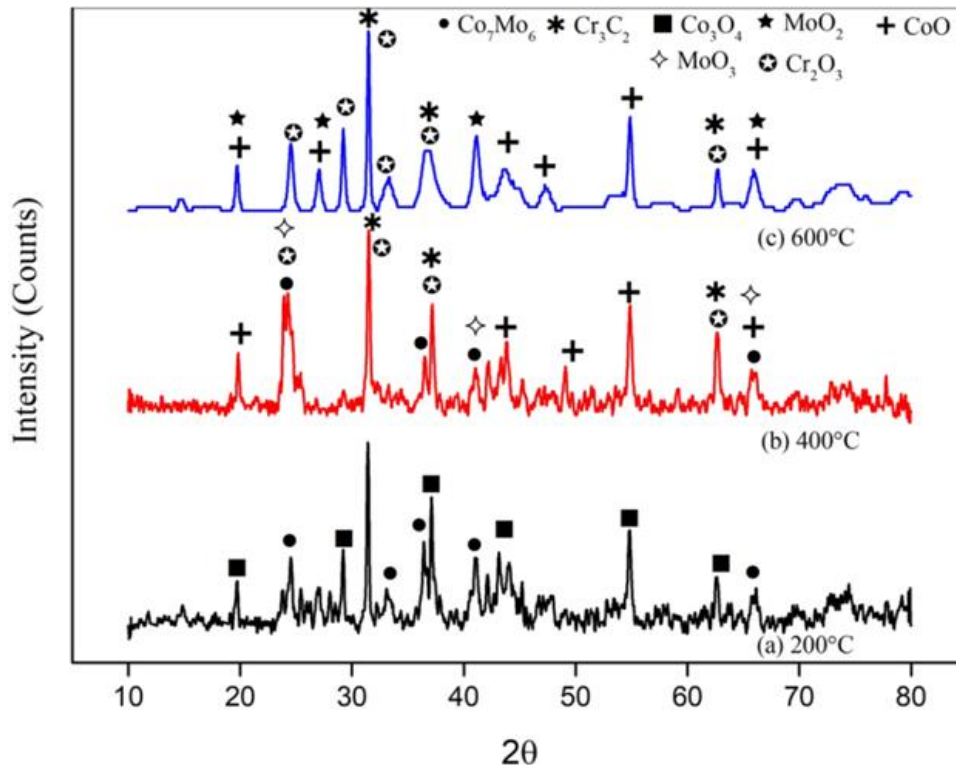


Figure 5.42 XRD pattern of microwave fused flame sprayed CoMoCrSi+Cr₃C₂ composite coatings worn surfaces at all test temperatures

5.7.4. Worn Surface SEM and EDS analysis

The wear out surface morphologies of flame sprayed CoMoCrSi+Cr₃C₂ composite coating is shown in Figure 5.43 (a-f). The wear out surfaces of CoMoCrSi+Cr₃C₂ flame sprayed composite coating reveals similar morphologies as observed on worn samples of flame sprayed CoMoCrSi coating shown in Figure 5.36 (a-f). The presence of Co₃C and Cr₃C₂ phases in the as-sprayed CoMoCrSi+Cr₃C₂ coating which possesses much higher hardness than CoMoCrSi flame sprayed coating, results in reduced plastic deformation during wear test. The wear scars with shorter width have been observed at 400°C and 600°C under both test loads. It encounters the loose splats on the coating surface which is in the form of unmelted or semi-melted particles are detached as shown in Figure 5.43 (a-f). The uneven surface and large humps have been observed, this is formed due to deformation of material through rough wear tracks. When the normal load raised to 20 N observed massive loss of coating material is caused by the pulling out of maximum splats infers severe wear shown in Figure 5.43 (e-f). The EDS results are obtained for worn surfaces of flame sprayed CoMoCrSi+Cr₃C₂ composite coatings shown in Figure 5.43 (a-f). Presence of carbon is confirmed on the worn coating surface. Both as-sprayed coating worn surface EDS results reveals that increases in oxide percentage as a rise in load and temperature. The oxidation of coatings is influenced by wear phenomenon and also coating exhibits adhesive wear mechanism due to an increase in aluminum percentage (Prasad et al., 2018).

The worn surfaces of the fused CoMoCrSi+Cr₃C₂ composite coating are shown in Figure 5.44 (a-f) The fused coating worn surface produced smooth wear scars, no observation of brittle fracture of splats since the surface has been homogenized. At higher temperatures 400°C and 600°C under both test loads, observed fatigue spalling effect caused due to the hard surface of the fused coating. Some regions of fused coating surface have slightly damaged under 20 N normal load is noticed in Figure 5.44 (e-f). When the fused coating surface had a contact with a sliding disc, the coating elements are subjected to severe oxidation, results in a tribo-oxide layer have been formed which decreases the further loss of coating material. The significant increase in oxide percentage compared to the as-sprayed coating is confirmed by EDS analysis. Also, the percentage of aluminium has been reduced which shown no sign of adhesive wear mechanism during sliding action. EDS results of

fused CoMoCrSi+Cr₃C₂ coating on worn surfaces are shown in Figure 5.44 (e-f). Rapid oxidation layer is formed as for an increase in test temperatures and more in 20 N normal load tests. The higher the percentage of oxides has formed which decreases the material deformation and friction during sliding against the hard counter disc.

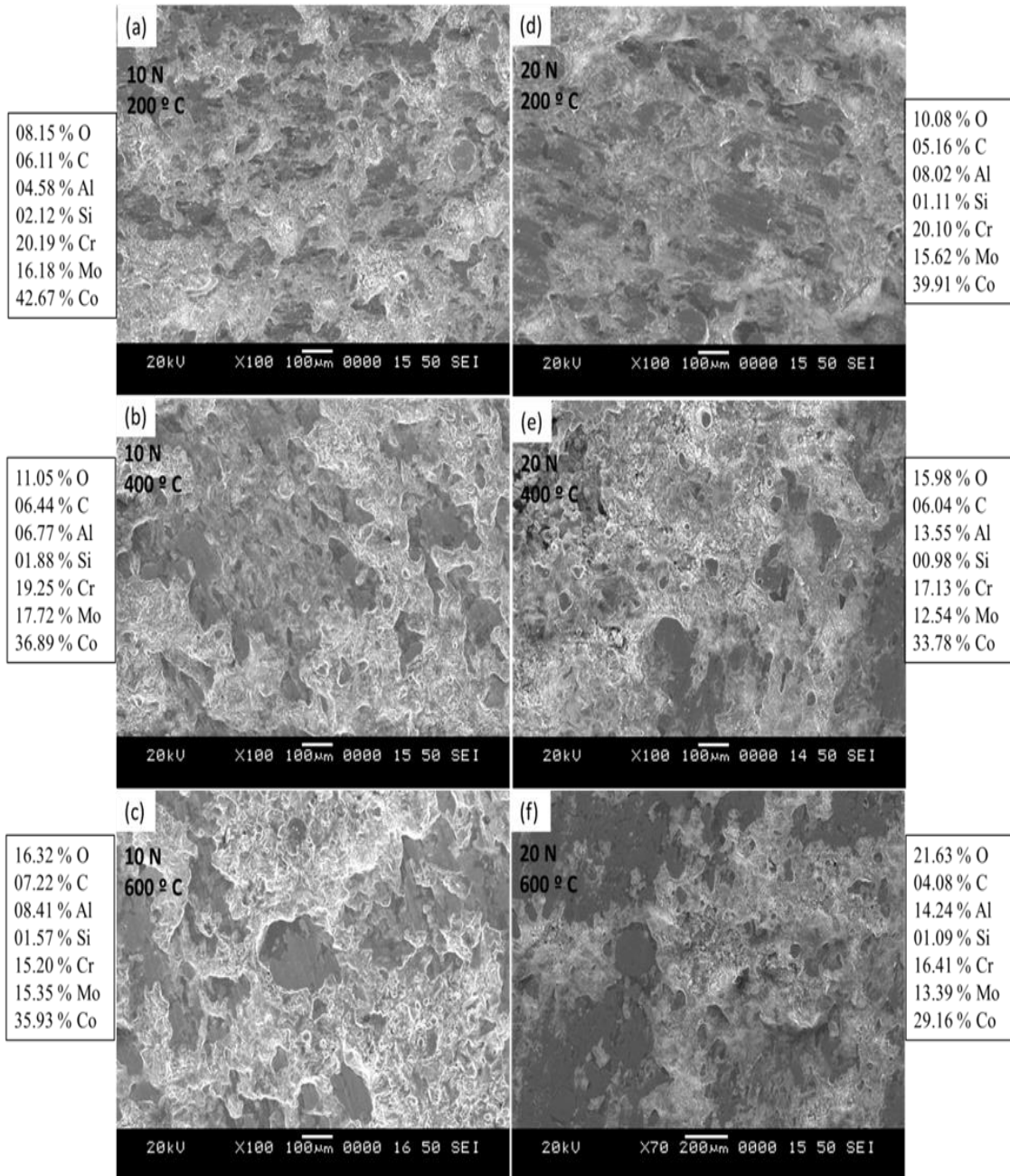


Figure 5.43 Morphology of flame sprayed CoMoCrSi+Cr₃C₂ composite coating worn surfaces (a-c) under 10 N and (d-f) under 20 N at temperatures of 200°C, 400°C, 600°C

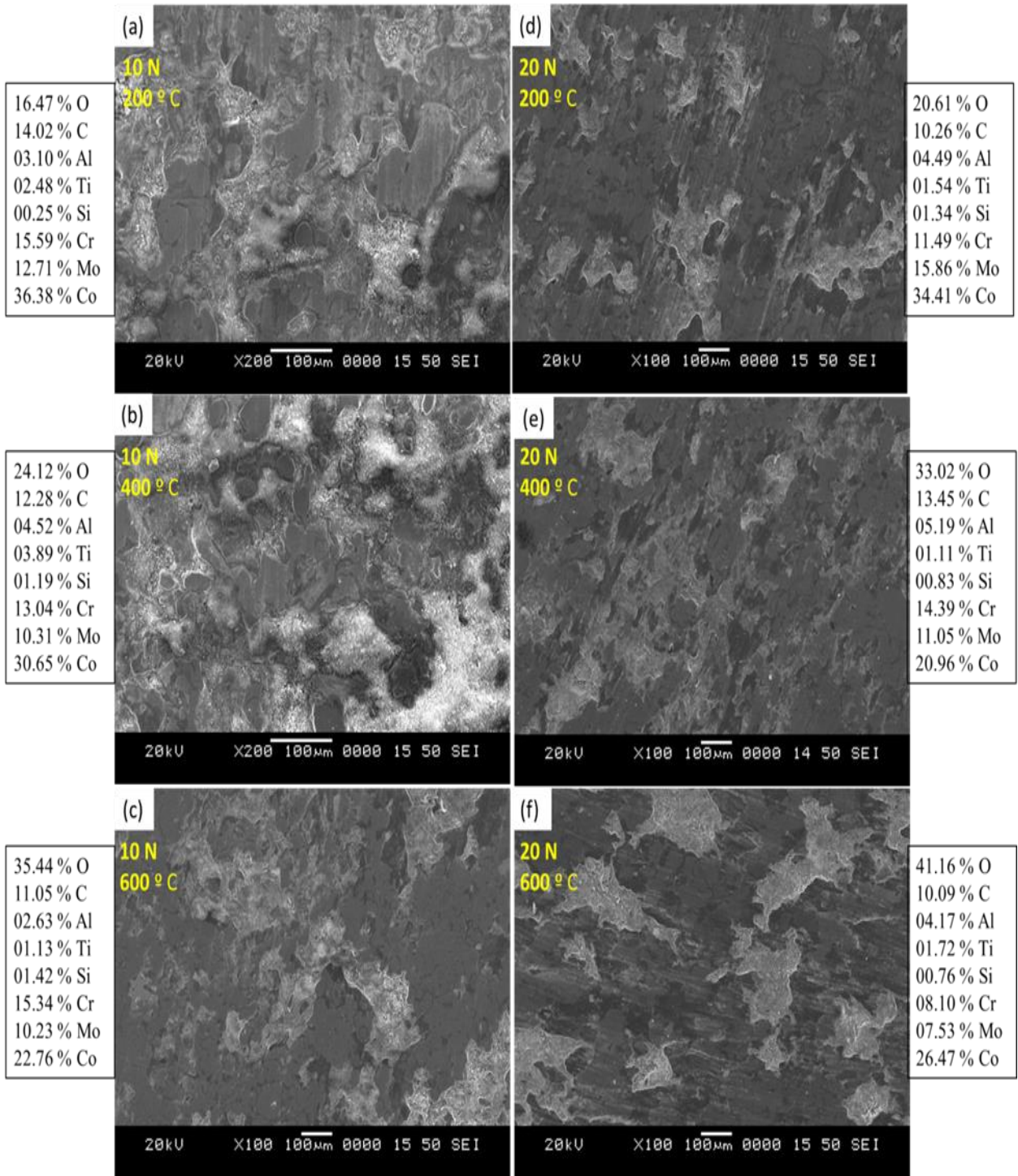


Figure 5.44 Morphology of microwave fused flame sprayed CoMoCrSi+Cr₃C₂ composite coating worn surfaces (a-c) under 10 N and (d-f) under 20 N at temperatures of 200°C, 400°C, 600°C

5.8. WEAR STUDIES ON FLAME SPRAYED AND MICROWAVE FUSED CoMoCrSi+WC-CrC-Ni COMPOSITE COATINGS

5.8.1. Volume loss and Wear rate of Coatings

The wear volume loss and wear rate graphs of flame sprayed and microwave fused CoMoCrSi+WC-CrC-Ni composite coatings are presented in Figure 5.45 (a and b) and Figure 5.46 (a and b). The as-sprayed coating exhibits an increasing trend in loss of volume due to rough surface and presence of unmelted or semi-melted particles leads to easy deformation during sliding action under both test loads Figure 5.45 (a and b). However, the presence of intermetallics and formation of metallurgical bonding infused coating results in less volume loss for both test loads compared to as-sprayed coating.

The wear rate of coatings is calculated using volume loss and sliding distance. As observed in (Figure 5.46 a and b) the CoMoCrSi+WC-CrC-Ni as-sprayed coating exhibits wear rate of 2-2.5 times higher than CoMoCrSi+WC-CrC-Ni fused coating under both test loads. This is due to the heterogeneous structure of the as-sprayed coating which has more pores and cracks. The post-treated coating has a lower wear rate due to enhanced hardness by diffusion mechanism and obtained phases such as TiC, TiO₂, Co₆W₆C, Co₃W₉C, and Co₃W₃C Cr₃C₂ are formed. Also, the presences of intermetallic amorphous phases like (bulk metallic glass structure) and oxide phases formed during the sliding test play a role in reducing the wear rate of the treated coating.

The estimated wear rate coefficient K in mm³/N-m of flame sprayed and fused CoMoCrSi+WC-CrC-Ni composite coatings is shown in Figure 5.47. The assessed K values of CoMoCrSi+WC-CrC-Ni as-sprayed and fused composite coatings are 4×10^{-6} mm³/N-m and 1×10^{-6} mm³/N-m respectively.

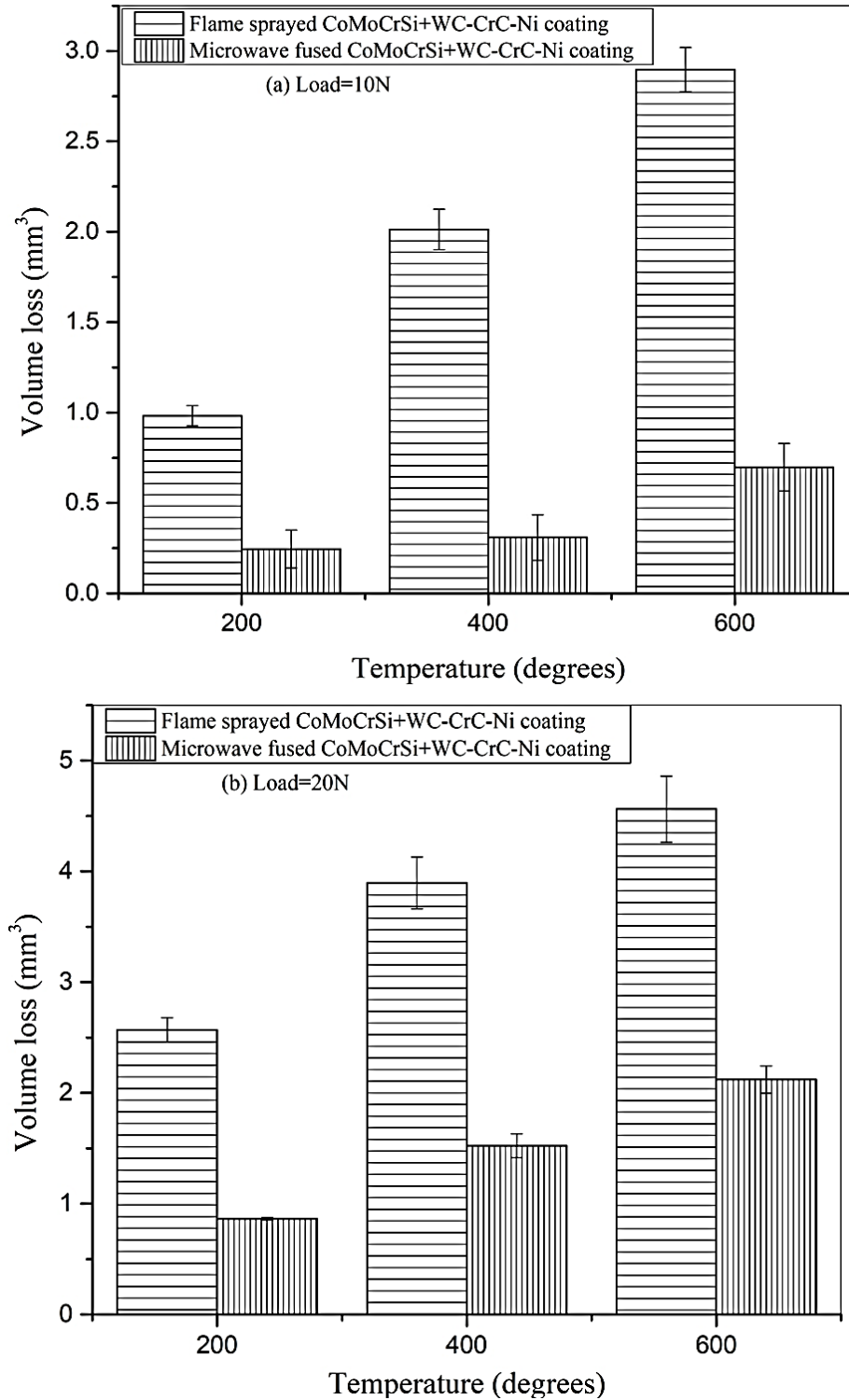


Figure 5.45 Wear volume loss of flame sprayed and microwave fused CoMoCrSi+WC-CrC-Ni composite coatings with respect to temperature (a) 10 N, (b) 20 N

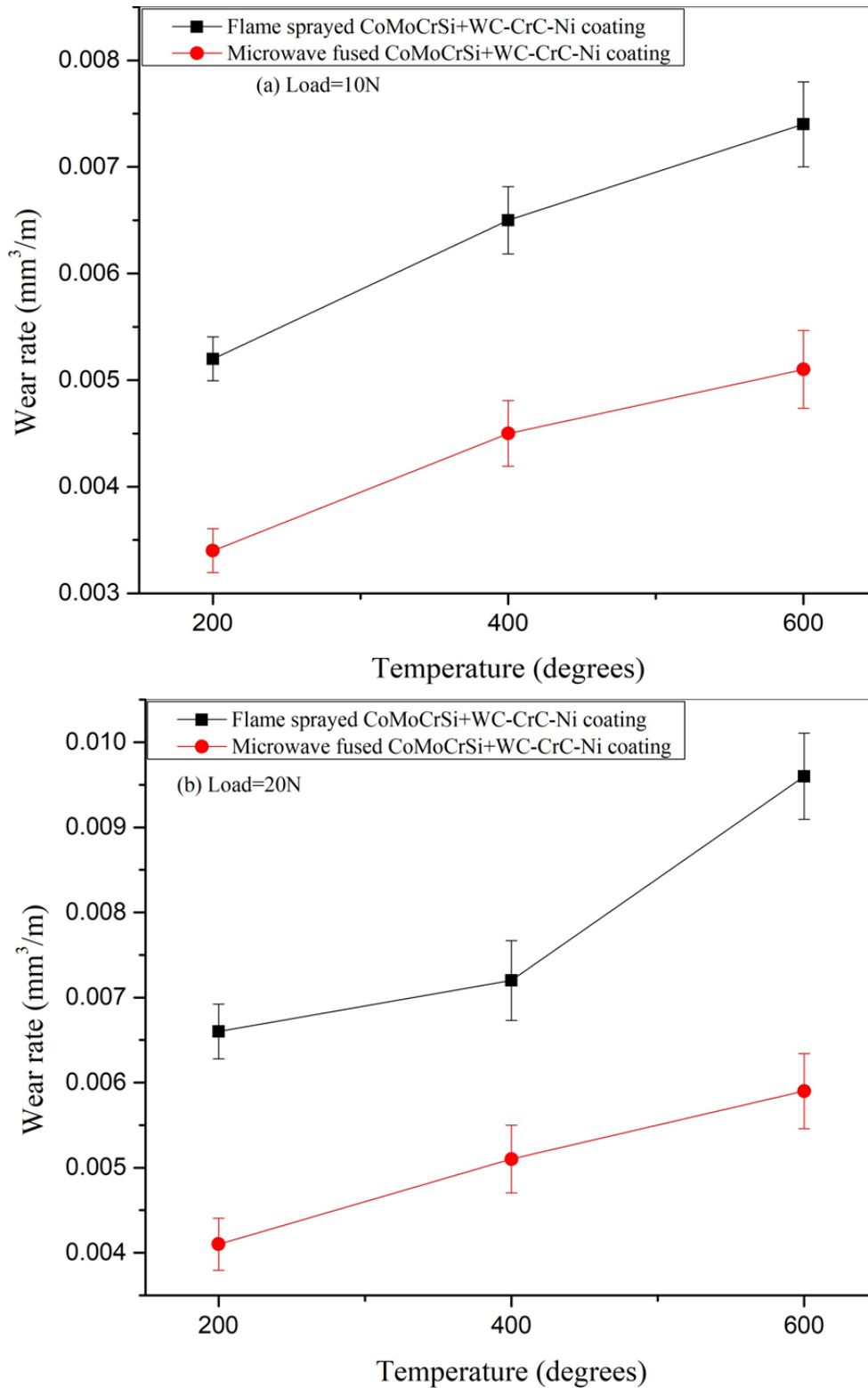


Figure 5.46 Wear rate plots of flame sprayed and microwave fused CoMoCrSi+WC-CrC-Ni composite coatings with respect to temperature (a) 10 N, (b) 20 N

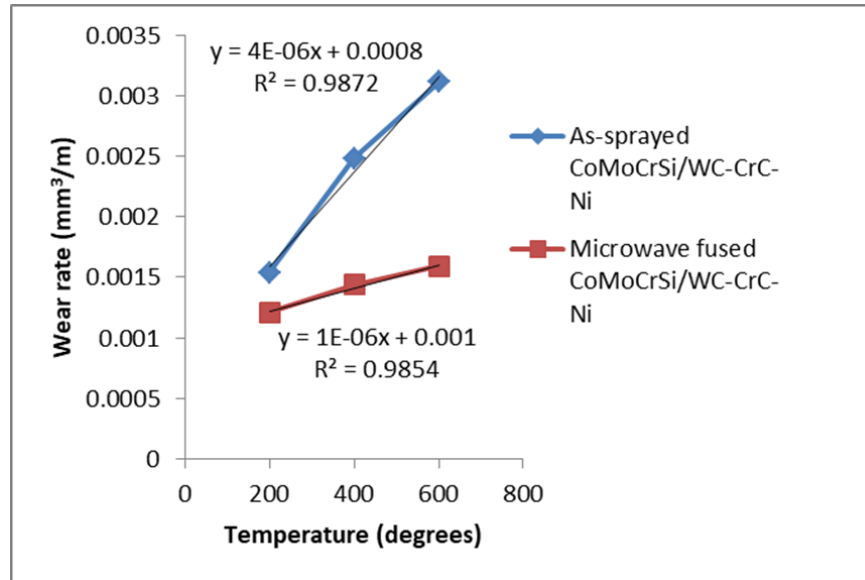


Figure 5.47 Wear rate coefficient k plot of flame sprayed and fused CoMoCrSi+WC-CrC-Ni composite coatings

5.8.2. Coefficient of Friction

The COF of flame sprayed and fused CoMoCrSi+WC-CrC-Ni composite coatings are shown in Figure 5.48 (a and b). The COF of the as-sprayed coating is significantly varying corresponding to the sliding distance. This is maybe due to contacted between coating sample and counter disc during sliding operation and presence uneven surface of the coating. The average COF of the as-sprayed coating under both test loads exhibits 0.65. The COF of the as-sprayed coating at 400 °C and 600 °C temperatures showed less value than 200°C temperature. This is due to the formation of oxides near the coating surface at elevated temperatures leads to a decrease in friction (Khameneh et al., 2006), (Hou et al., 2011). The fused coating tends to show lower COF of 0.51 which is better than as-sprayed coatings. Also, the fused coating displays steady friction at all test temperatures. The homogeneous structure and presence of intermetallics result in the smooth flow of friction. But under 20 N normal load (Figure 5.48b) both as-sprayed and fused coatings indicates more fluctuations of COF due to more applied force. Though at elevated temperatures fused coating subjected to severe oxidation results in a reduction in COF. The oxides films are formed at elevated temperatures cover the fused coating surface from breaking of material.

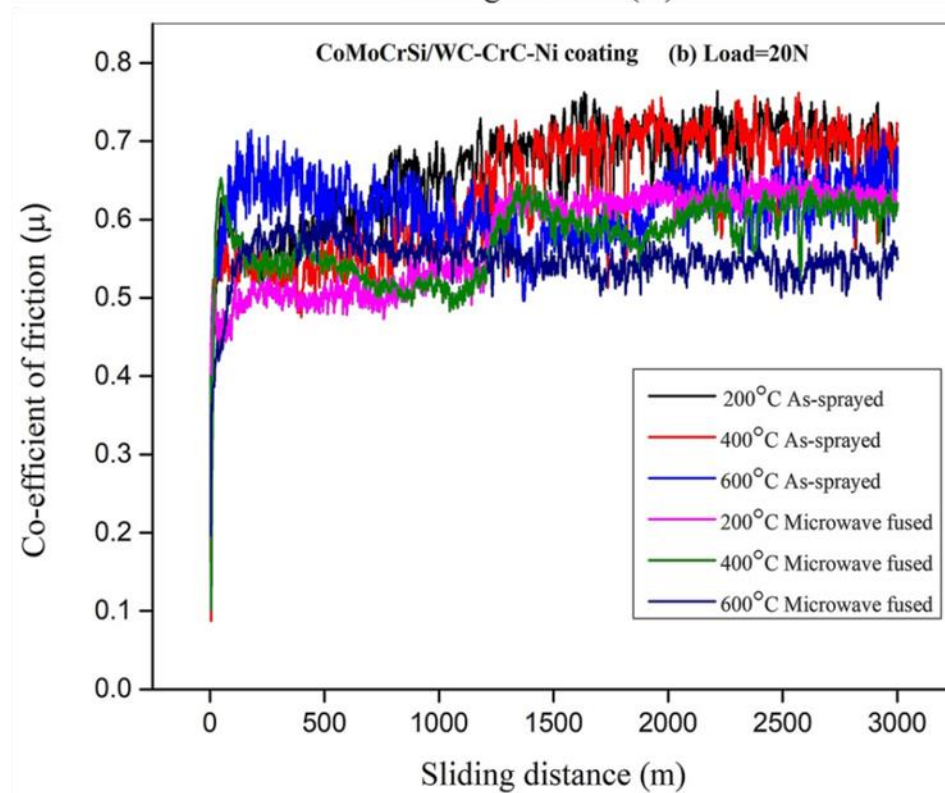
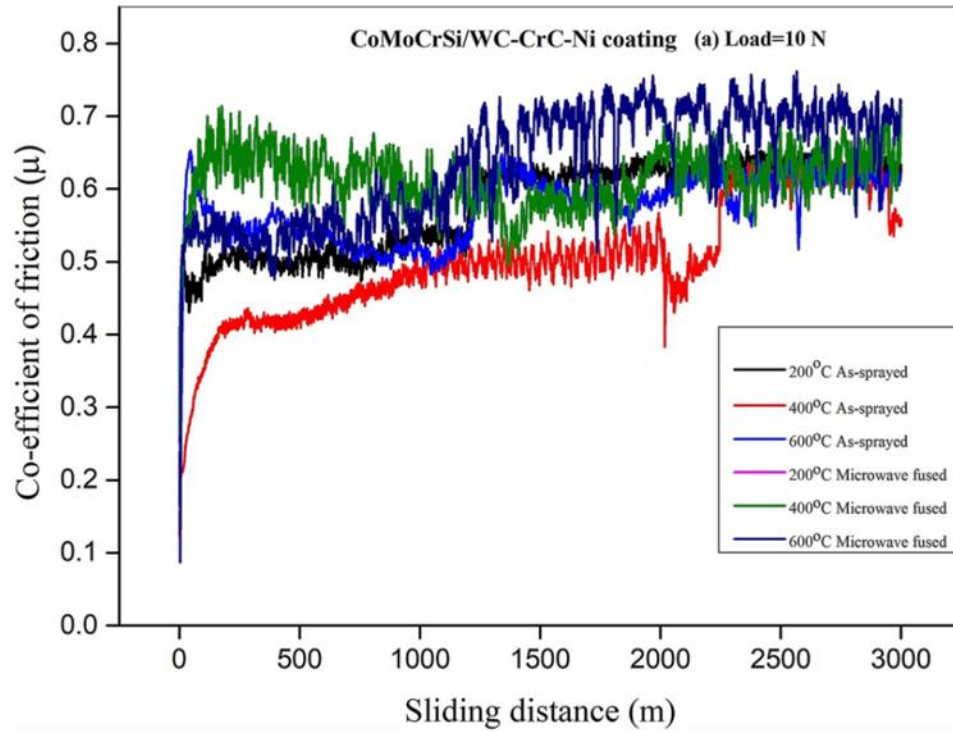


Figure 5.48 Friction coefficient of flame sprayed and microwave fused CoMoCrSi+WC-CrC-Ni composite coatings with respect to sliding distance (a) 10 N, (b) 20 N

5.8.3. X-Ray Diffraction analysis of Fused Coatings

The X-ray spectrum of microwave fused CoMoCrSi+WC-CrC-Ni worn coating is shown in Figure 5.49. The Co alloy is subjected to oxidation at elevated temperatures during siding test and oxides are easily formed at coating surfaces. In (Figure 5.49), observed Co_7Mo_6 and Co_3O_4 phases to be formed at 200°C and 400°C temperatures. At 400°C and 600°C test temperatures CoO , Cr_2O_3 phases to be found. The CoWo_4 and MoO_2 phases are noticed at 600°C. Nickel oxide and chromium oxide combined to form spinal NiCr_2O_4 phase is identified at 600°C shown in Figure 5.49. The fused coating exhibits less wear rate and COF because of oxides are actively formed leads to cover the exposed coating surface from adhesive wear mechanism.

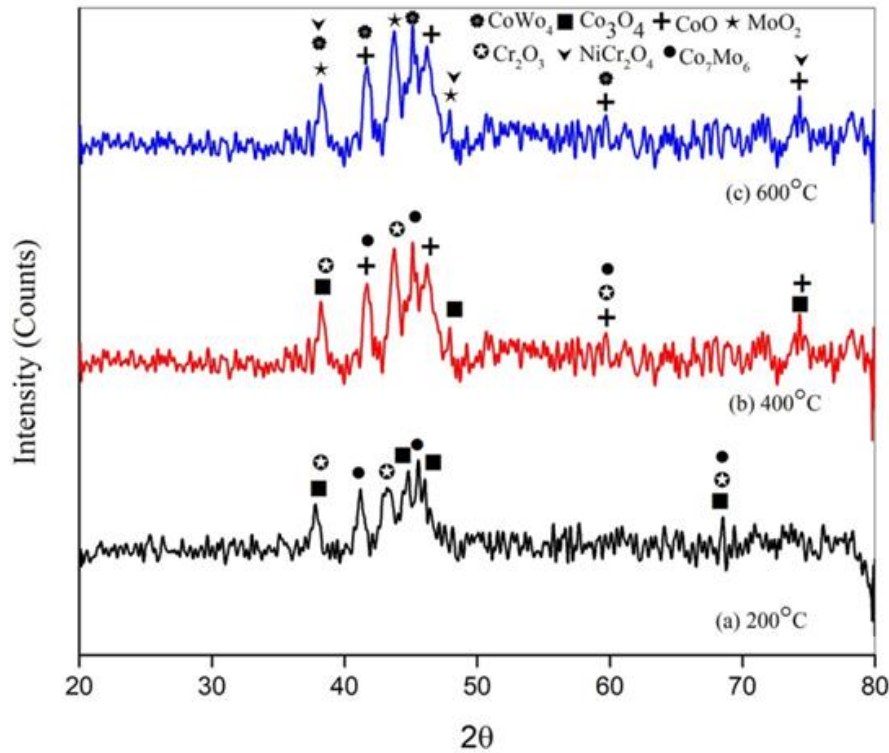


Figure 5.49 XRD pattern of microwave fused flame sprayed CoMoCrSi+WC-CrC-Ni composite coatings worn surfaces at all test temperatures

5.8.4. Worn Surface SEM and EDS analysis

The worn surfaces of flame sprayed CoMoCrSi+WC-CrC-Ni composite coating is investigated by SEM, to understand the wear phenomenon is shown in Figure 5.50 (a-f). The wear surfaces of as-sprayed coating samples at test temperatures under both test loads exhibit

short width wear tracks associated with the breaking of splats, the formation of large pits and underlying surface subjected to mild oxidation at elevated temperatures (Peat et al., 2016), (Karaoglanli et al., 2017). The presence of deep and short width wear tracks confirms transferring of counter disc material to wear surface. As noticed in (Figure 5.50 b and c) as-sprayed coating at 400°C and 600°C temperatures undergone more brittle fracture, this is caused due to the breaking of the oxide layer formed at these temperatures and allowed the surface to plough hardily. Also under 20 N normal load at 400°C and 600°C temperatures (Figure 5.50 e and f) produced large pits and more deformation has observed. This results in the as-sprayed coating produced adhesive wear mechanism. The EDS results of corresponding morphologies of the as-sprayed coating (Figure 5.50 a-f) indicates the presence of oxide and alumina content and its percentage is significantly increasing as a rise in test load and temperatures. These results depend on the increase in wear rate and higher friction, also other researchers have reported that indication of higher the surface roughness and lower microhardness results in a higher material loss (Asgari et al., 2017), (Xu et al., 2007).

The wear out surface morphology of fused CoMoCrSi+WC-CrC-Ni composite coating is shown in Figure 5.51 (a-f). There is no indication of the uneven surface of worn morphologies which is less rough and promotes to smoother sliding action. The homogeneous structure of fused coatings leads to protection of coating surfaces and these surfaces are subjected to the severe oxidational phenomenon (Zhang et al., 2009), (Fang et al., 2009). The higher microhardness of fused coating undergone fatigue spalling effect on wear tested samples. The fused coating at 200°C and 400°C temperatures under both test loads shown in (Figure 5.51 (a-b) and (d-e)) produced similar morphologies which are also confirmed by volume loss and wear rate plots shown similar values. At 600°C temperature under both test loads (Figure 5.51 (c) and (f)) due to more fatigue spalling effect, seen the few regions of coating surface are fractured. The percentage of alumina is less compared to as-sprayed coating and an increase in oxide content with an increase in test temperatures as noticed in EDS results of the respective fused coating shown in Figure 5.51 (a-f). The formation of tribo-oxide films on fused coating surfaces eliminates the adhesive wear mechanism and improves its wear and frictional resistance. The darker regions on fused coatings describe the protective shield of oxides to the underlying surface, which acts as

lubricants during sliding action (Kong and Zhao, 2017). Also no sign of detaching material and tearing of layers. The fused coating has the lower loss of volume, wear rate and COF, these results clearly understands that due to the change in microstructural features, enhances its tribological properties.

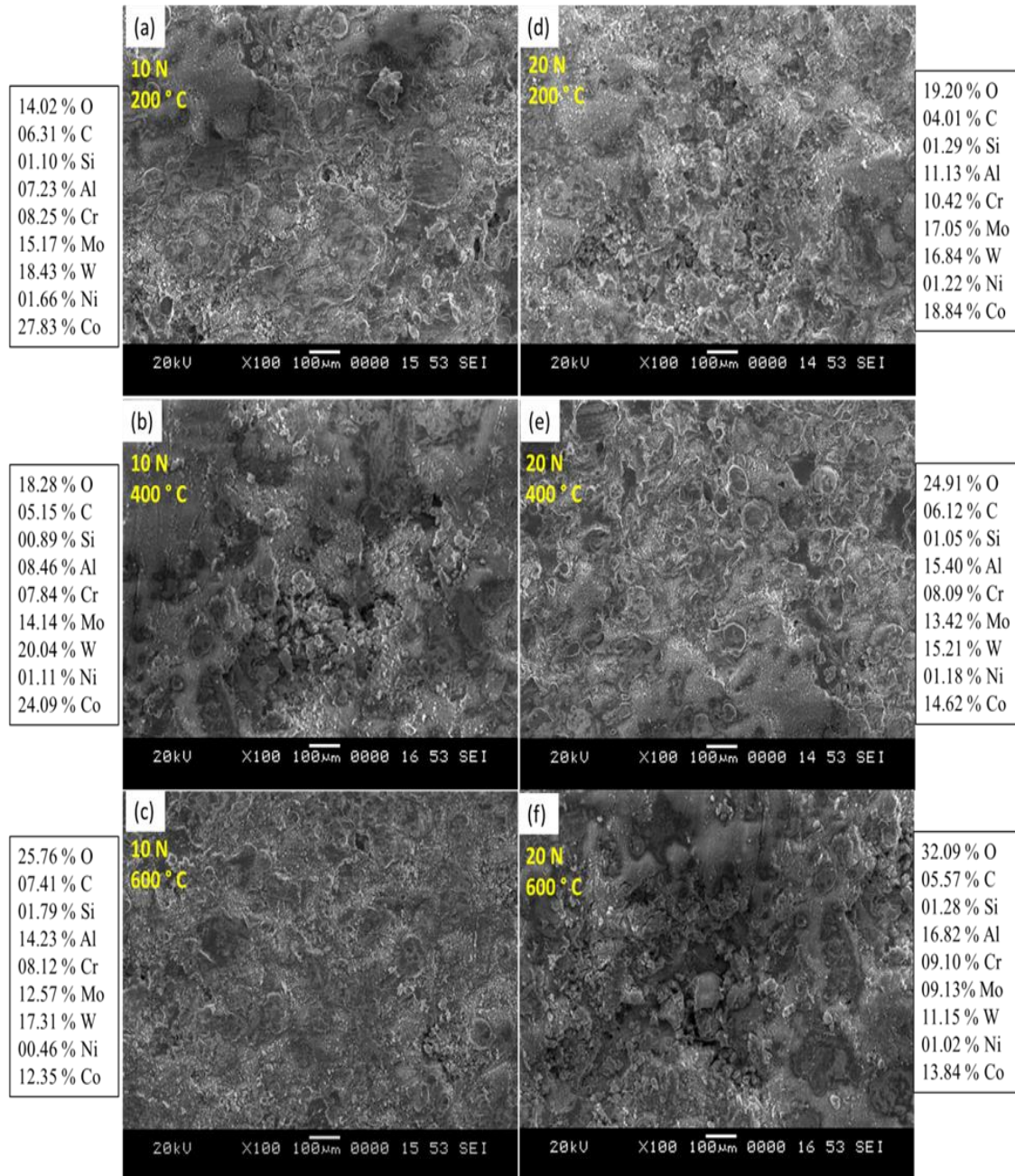


Figure 5.50 Morphology of flame sprayed CoMoCrSi+WC-CrC-Ni composite coating worn surfaces (a-c) under 10 N and (d-f) under 20 N at temperatures of 200°C, 400°C, 600°C

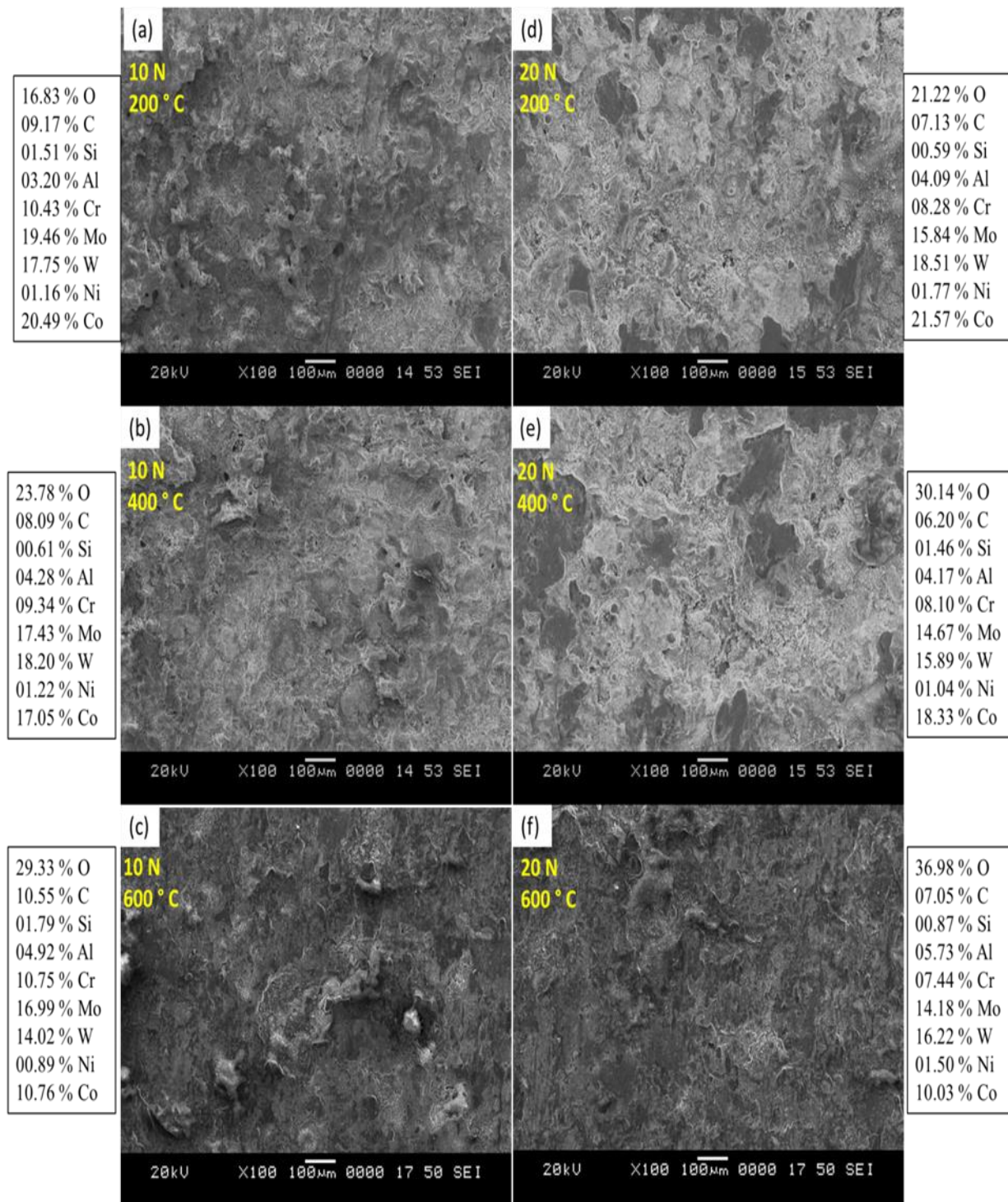


Figure 5.51 Morphology of microwave fused flame sprayed CoMoCrSi+WC-CrC-Ni composite coating worn surfaces (a-c) under 10 N and (d-f) under 20 N at temperatures of 200°C, 400°C, 600°C

5.9. WEAR STUDIES ON FLAME SPRAYED AND MICROWAVE FUSED CoMoCrSi+WC-12Co COMPOSITE COATINGS

5.9.1. Volume loss and Wear rate of Coatings

The loss of volume and wear rate of flame sprayed and microwave fused CoMoCrSi+WC-12Co composite coatings are shown in Figure 5.52 (a and b) and Figure 5.53 (a and b). The both as-sprayed and fused CoMoCrSi+WC-12Co composite coatings exhibit very lower volume loss and wear rate compared to the other three coatings. Since the CoMoCrSi+WC-12Co composite coating produced higher hardness and toughness leads to decreasing of material loss during wear test Figure 5.52 (a and b). The as-sprayed coating exhibits slight higher volume loss at 600 °C under both normal loads compared to fused coating Figure 5.52 (a and b). The fused coating shown the lower volume loss at all test temperatures under both loads, this is the clear evidence of the effect of microwave hybrid heating on coatings.

In CoMoCrSi+WC-12Co as-sprayed coating presents approximately 1-1.5 times higher wear rate than a fused coating for both applied loads shown in Figure 5.53 (a and b). Since the microhardness of CoMoCrSi+WC-12Co as-sprayed coating is higher than other coatings deposited by flame spray results in less rupture of material. The fused coating shown lower wear rate due to no significant loss of material and various oxide phases has generated which forms as a lubricant layer for coating surface. Some of the new hard phases $\text{Co}_6\text{W}_6\text{C}$, $\text{Co}_3\text{W}_9\text{C}$, and $\text{Co}_3\text{W}_3\text{C}$ generated in both as-sprayed and fused coatings this restricts the ploughing and plastic deformation of coating material. The post-treatment coating has a lower wear rate due to enhanced hardness by diffusion mechanism and obtained phases such as TiC, TiO_2 , are formed.

The plot of wear rate coefficient K value of flame sprayed and fused CoMoCrSi+WC-12Co composite coating is shown in Figure 5.54. The estimated values of flame sprayed and fused coatings are $3 \times 10^{-6} \text{ mm}^3/\text{N-m}$ and $8 \times 10^{-7} \text{ mm}^3/\text{N-m}$ respectively. After obtaining the K values of tested coatings, it is confirmed that the fused coating produced a lower wear rate than an as-sprayed coating.

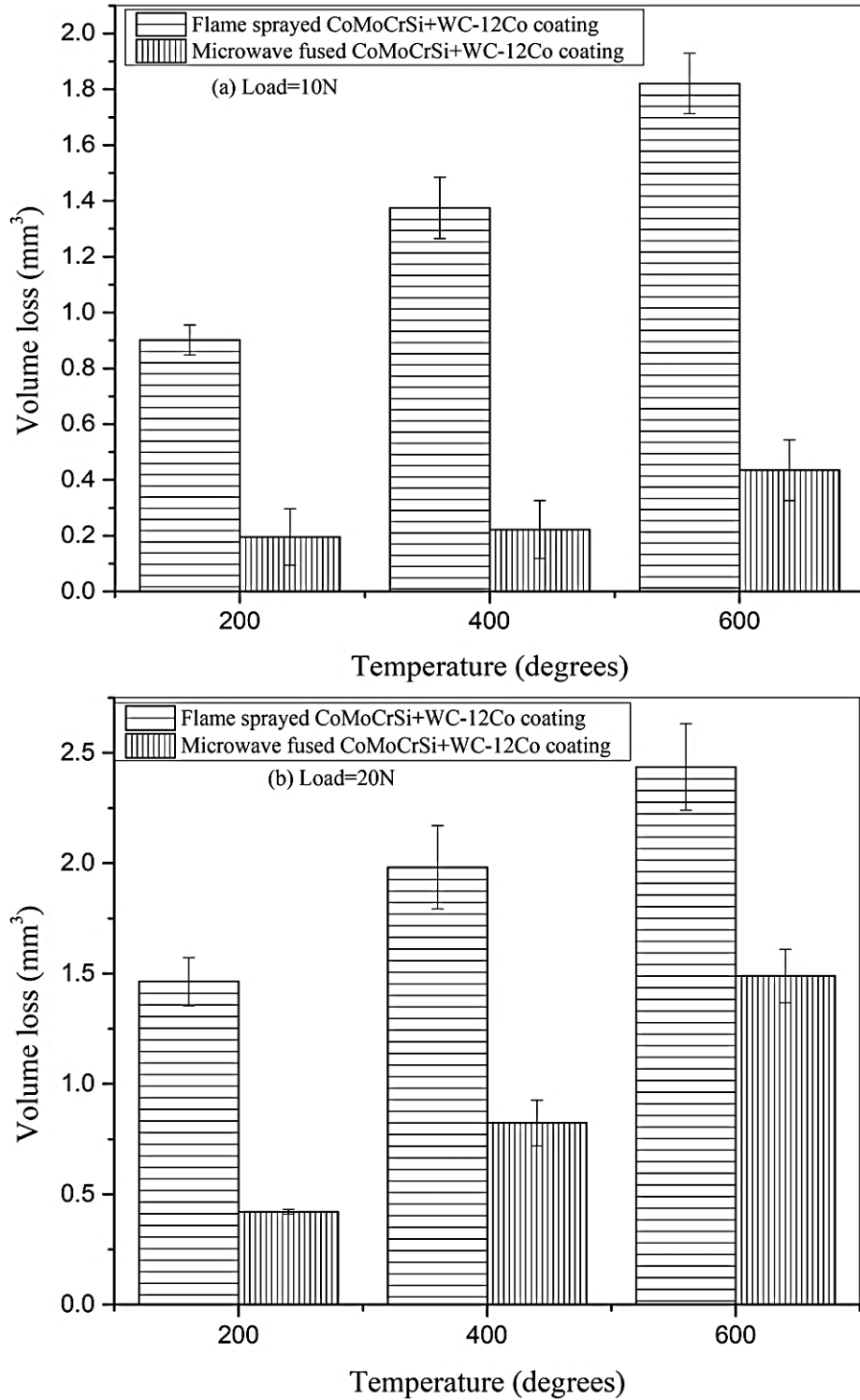


Figure 5.52 Wear volume loss of flame sprayed and microwave fused CoMoCrSi+WC-12Co composite coatings with respect to temperature (a) 10 N, (b) 20 N

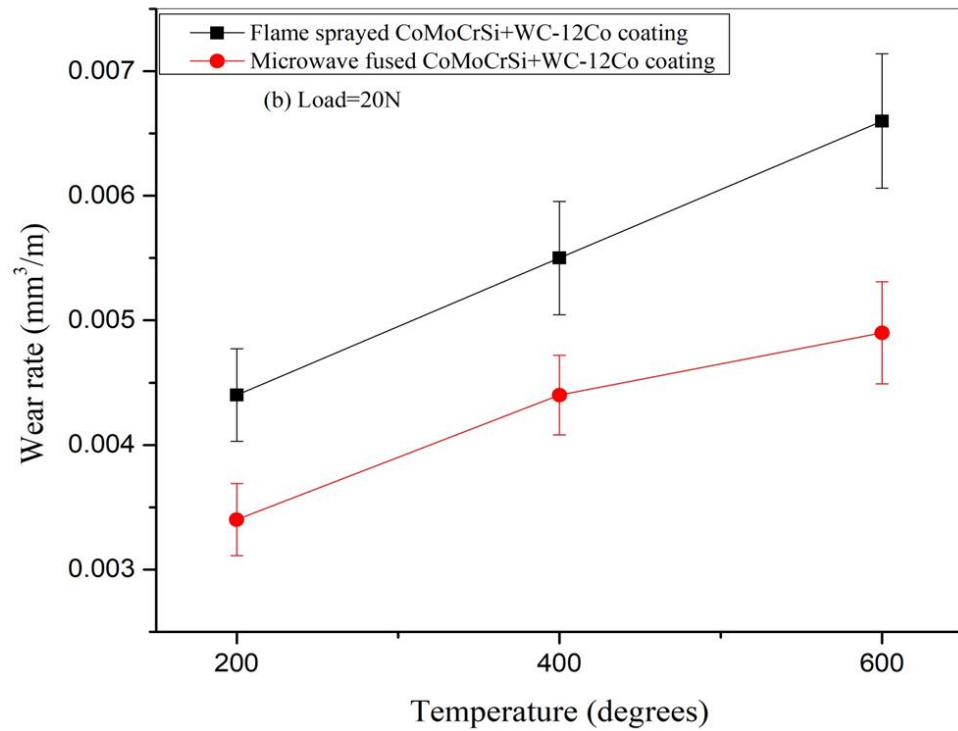
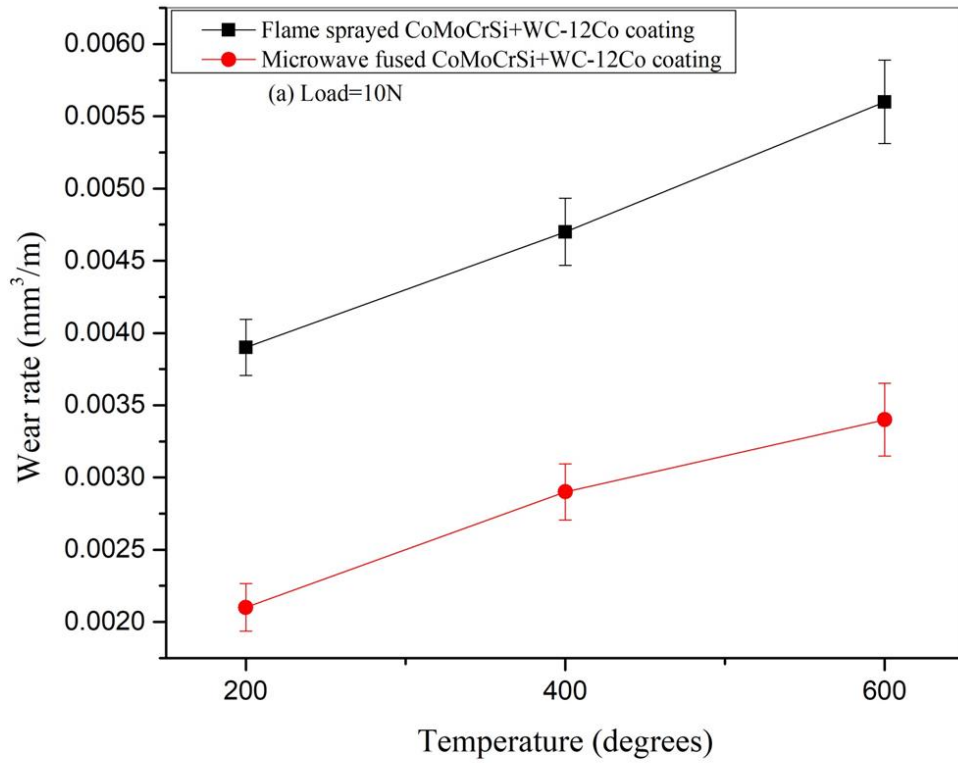


Figure 5.53 Wear rate plots of flame sprayed and microwave fused CoMoCrSi+WC-12Co composite coatings with respect to temperature (a) 10 N, (b) 20 N

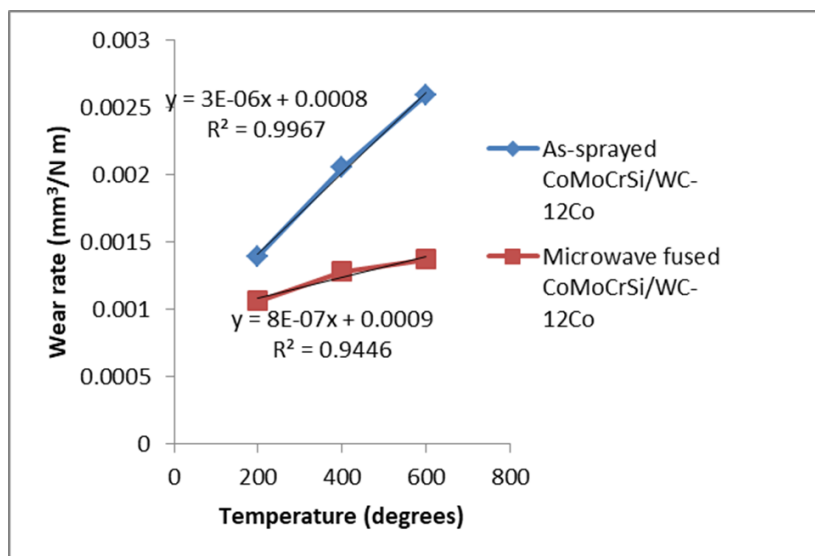


Figure 5.54 Wear rate coefficient k plot of flame sprayed and fused CoMoCrSi+WC-12Co composite coatings

5.9.2. Coefficient of Friction

The (Figure 5.55 (a and b)) presents the COF of flame sprayed and fused CoMoCrSi+WC-12Co composite coatings. The COF of the as-sprayed coating is unstable throughout the sliding action. The mean COF value of as-sprayed coating is 0.58, whereas fused coating exhibits a stable friction curve having an average COF is 0.42, this is lower than COF of as-sprayed coating.

During initial stage of test at 200°C temperature, the friction in as-sprayed and fused coatings showed slight higher value, later as test proceeds to 400°C and 600°C temperatures, produced lower COF. This is mainly due to the role of oxide layers formed near coating surface at 400 °C and 600 °C temperatures act as lubricants. Also noticed that compared to 10 N normal load, the COF of as-sprayed and fused coatings are varying significantly under 20 N normal load in Figure 5.55 (b). The increase in the contact force between sample and counter disc leads unstable in COF profiles.

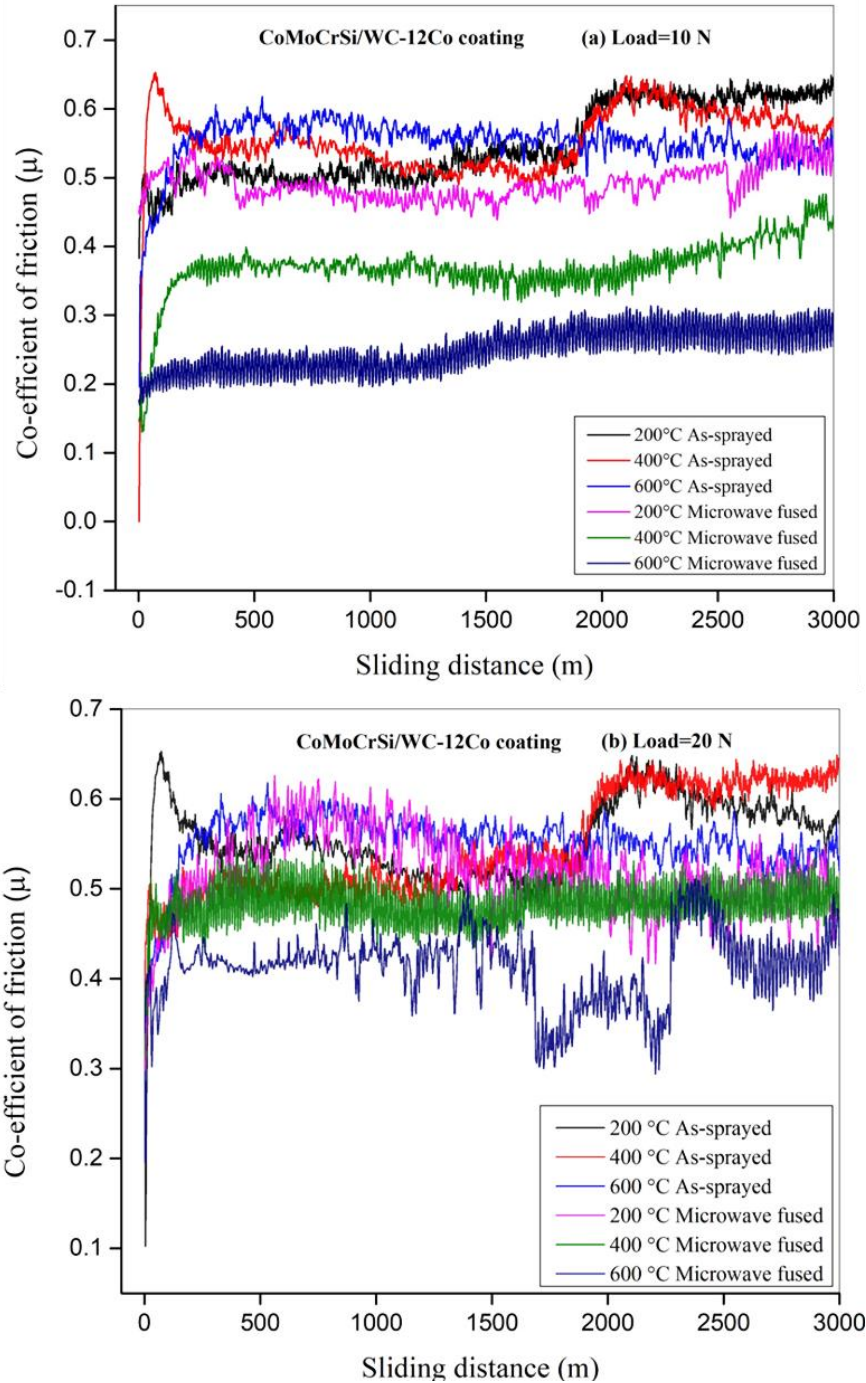


Figure 5.55 Friction coefficient of flame sprayed and microwave fused CoMoCrSi+WC-12Co composite coatings with respect to sliding distance (a) 10 N, (b) 20 N

5.9.3. X-Ray Diffraction analysis of Fused Coating

The oxide phases shown in (Figure 5.56) observed for fused CoMoCrSi+WC-12Co composite coating are similar phases obtained in CoMoCrSi+WC-CrC-Ni fused coating except for NiCr₂O₄ phase (Figure 5.49). The Co₇Mo₆ and Co₃O₄ phases have found at 200°C and 400°C temperatures respectively. At 400°C and 600°C CoO, and Cr₂O₃ phases are found. The CoWO₄ and MoO₂ phases are noticed at 600°C. These oxides performed a key role in decreasing the wear rate of fused coatings.

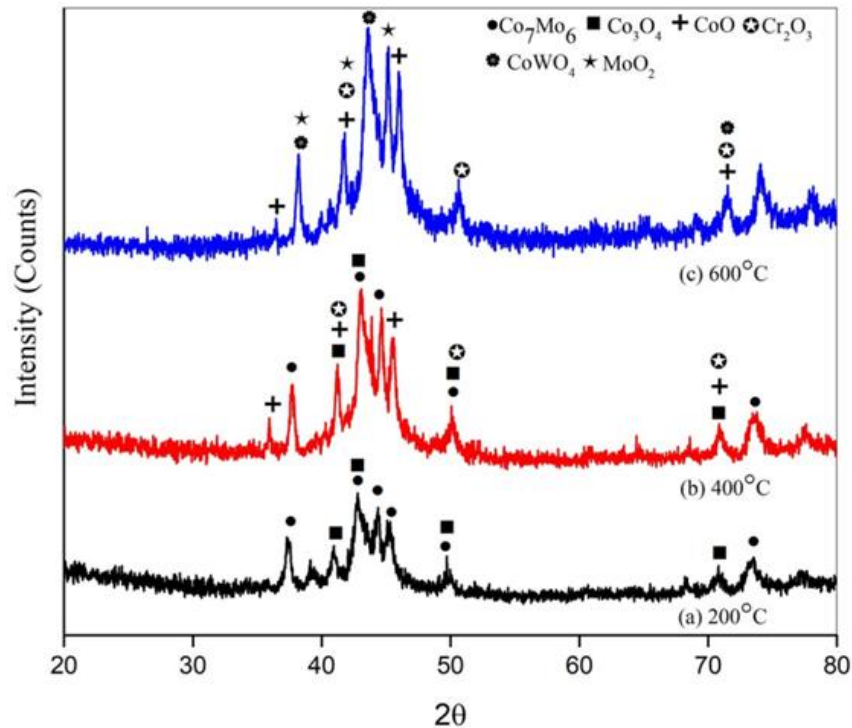


Figure 5.56 XRD pattern of microwave fused flame sprayed CoMoCrSi+WC-12Co composite coatings worn surfaces at all test temperatures

5.9.4. Worn Surface SEM and EDS analysis

The worn surface morphologies of flame sprayed CoMoCrSi+WC-12Co composite coating is shown in Figure 5.57 (a-f). At 200°C under 10 N and 20 N normal loads (Figure 5.57 (a and d)), observed microcracks, as well as the unmelted particles, are deformed plastically. As the rise in flash temperature to 400°C and 600°C under 10 N and 20 N normal loads, noticed delamination of coating surface due to constant heat supply and applied force Figure 5.57 (b-c) and (e-f). It results in detachment of splats in a higher rate and also surface is subjected to

oxidation. The wear track caused by adhesive phenomenon is observed at 600°C under 20 N normal load in Figure 5.57 (f).

The EDS results of as-sprayed coating (Figure 5.57 a-f) confirms the alumina content and oxide percentage also increased at 400°C and 600°C temperatures. As the increase in load and temperature, the alumina percentage also increased this indicates that the as-sprayed coating is severely exhibited adhesive wear mechanism by showing rough and shorter width wear scars.

The worn surface micrographs of fused CoMoCrSi+WC-12Co composite coating is shown in Figure 5.58 (a-f). After microwave fusing, the surface exhibits a homogeneous structure, it eliminates all the unmelted and semi-melted particles. This results in easy sliding of coating surface without causing damage. As observed in (Figure 5.58 a-c), fused worn surface reveals similar micrographs at 200°C, 400°C, and 600°C temperatures. The surface is very hard and also allows the counter disc to slide freely. During this operation, a tribo-oxide is initiated and as a rise in temperature, the oxide layers are covered by the fused coating surface which serves as lubricants. In the case of 20 N normal load at 400°, C and 600°C temperatures observed slight breaking of the surface due to fatigue spalling effect and also the formation of oxides is more show in Figure 5.58 (e-f).

The EDS analysis shown in (Figure 5.58 a-f), the alumina content is lower for fused coating compared to the as-sprayed coating. The oxide percentage is significantly higher at elevated temperatures of 400°C and 600°C. The formation of tribo oxide films on fused coating surfaces eliminates the adhesive wear mechanism and improves its wear and frictional resistance.

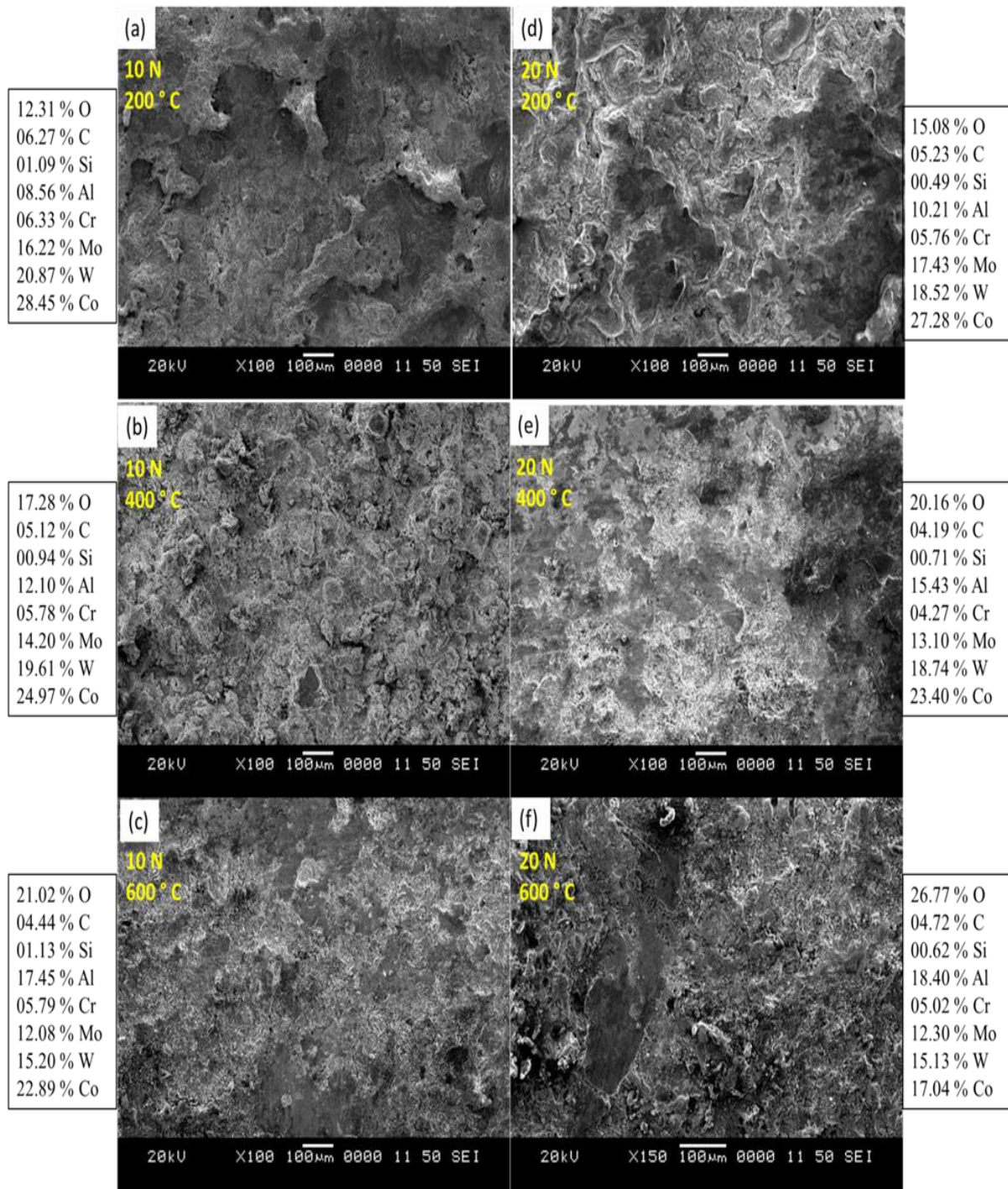


Figure 5.57 Morphology of flame sprayed CoMoCrSi+WC-12Co composite coating worn surfaces (a-c) under 10 N and (d-f) under 20 N at temperatures of 200°C, 400°C, 600°C

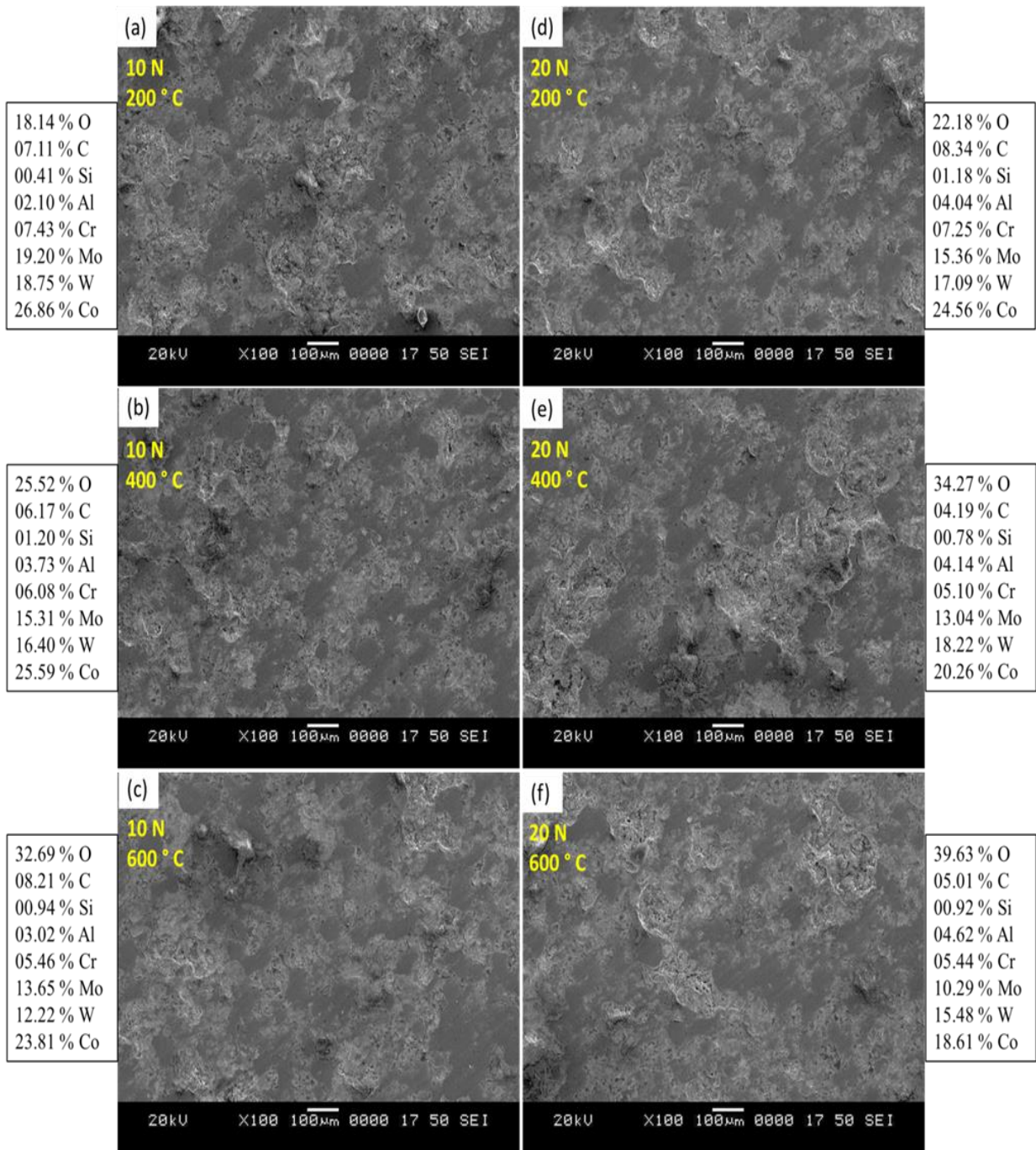


Figure 5.58 Morphology of microwave fused flame sprayed CoMoCrSi+WC-12Co composite coating worn surfaces (a-c) under 10 N and (d-f) under 20 N at temperatures of 200°C, 400°C, 600°C

5.10. COMPARATIVE DISCUSSION OF FLAME SPRAYED AND FUSED COATINGS SUBJECTED TO WEAR

The loss of volume and wear rate of flame sprayed and microwave fused four types of composite coatings are shown in Figure 5.59 (a and b) and Figure 5.60 (a and b). The flame sprayed coatings are having many unmelted and semi-melted particles which create brittle fracture of material by splats detachments have observed. This results in a significant increase in its loss of volume and wear rate under both test loads (Figure 5.59 a and b) and (Figure 5.60 a and b). Based on the tested results, the ascending order of volume loss and wear rate of flame sprayed coatings CoMoCrSi+WC-12Co, CoMoCrSi+WC-CrC-Ni, CoMoCrSi+Cr₃C₂ and CoMoCrSi. The CoMoCrSi and CoMoCrSi+Cr₃C₂ coatings possess higher porosity and exhibit many surface defects lead to the heterogeneous structure. The coatings with heterogeneous structure are responsible for severe material degradation. The volume loss of CoMoCrSi and CoMoCrSi+Cr₃C₂ coatings are increased with respect to increases in temperature. These coatings also show the higher value of COF values with significant variations. The worn surface morphologies of CoMoCrSi and CoMoCrSi+Cr₃C₂ flame sprayed coatings (Figure 5.36 and Figure 5.43) present the large pitting of surface due to subsurface defects and also inclusions of oxides along the grain boundaries which reduces its strength with increase in temperature and loads. The EDS analysis of worn samples confirms the percentage of alumina increases due to increase in load to 20 N at all test temperatures; this is the clear evidence of adhesive wear mechanism experienced by as-sprayed coatings.

The fused coatings have a significant reduction in the volume loss and wear rate due to the presence of a homogeneous structure, higher microhardness and stable oxides act as lubricants at 400°C and 600°C temperatures under both test loads. The fused CoMoCrSi+WC-12Co and CoMoCrSi+WC-CrC-Ni composite coatings produced lower volume loss, less than 1 mm³ and wear rate less than 0.01 mm³/m compared to fused CoMoCrSi and CoMoCrSi+Cr₃C₂ coatings. The fused CoMoCrSi+WC-12Co and CoMoCrSi+WC-CrC-Ni composite coatings exhibit new hard phases Co₆W₆C, Co₃W₉C, and Co₃W₃C, these carbides produces high strength to withstand the higher loads at high temperatures and significantly reduces the coating deformation during sliding action. Fused

coatings experienced fatigue spalling effect results in irregular cavities have observed on worn surface morphologies. EDS results show a higher percentage of oxides as an increase in test temperature.

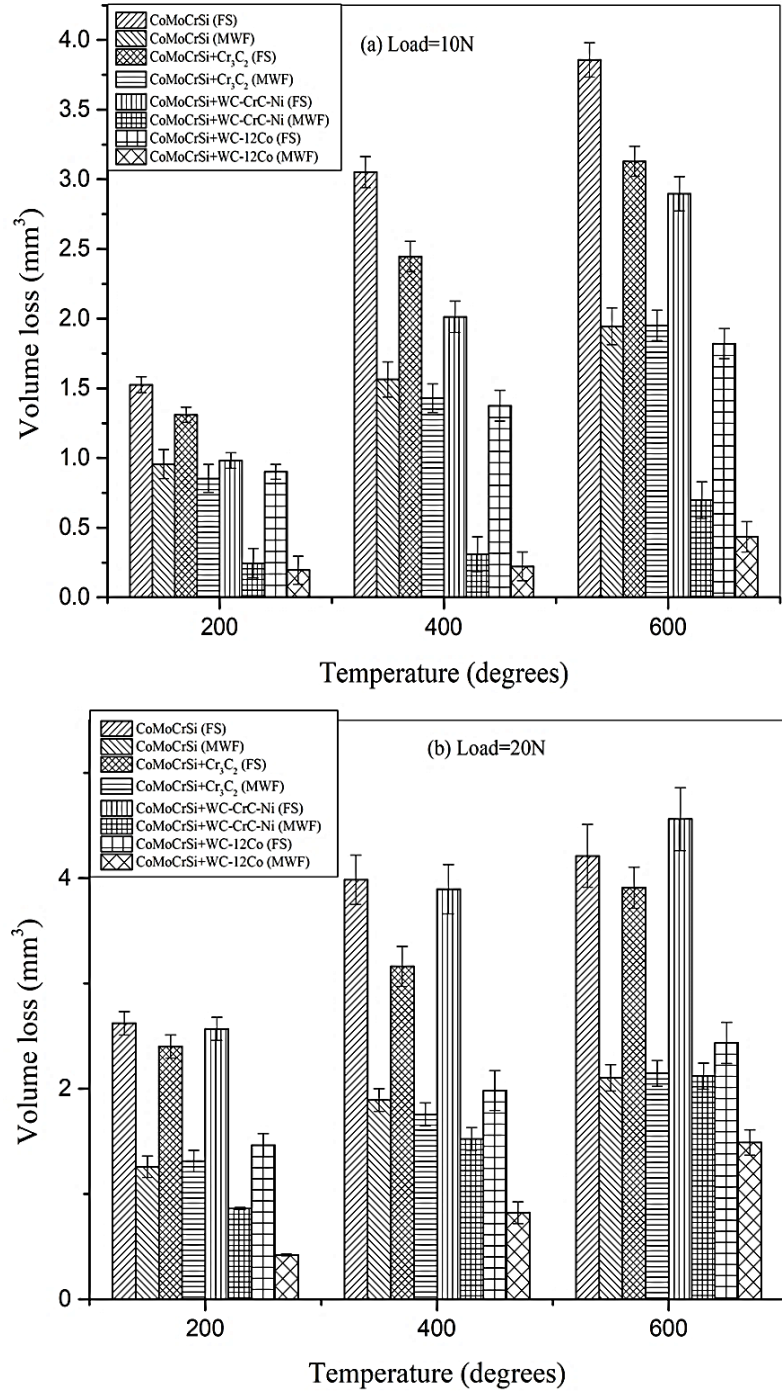


Figure 5.59 Wear volume loss of flame sprayed and microwave fused of four different coatings with respect to temperature (a) 10 N, (b) 20 N

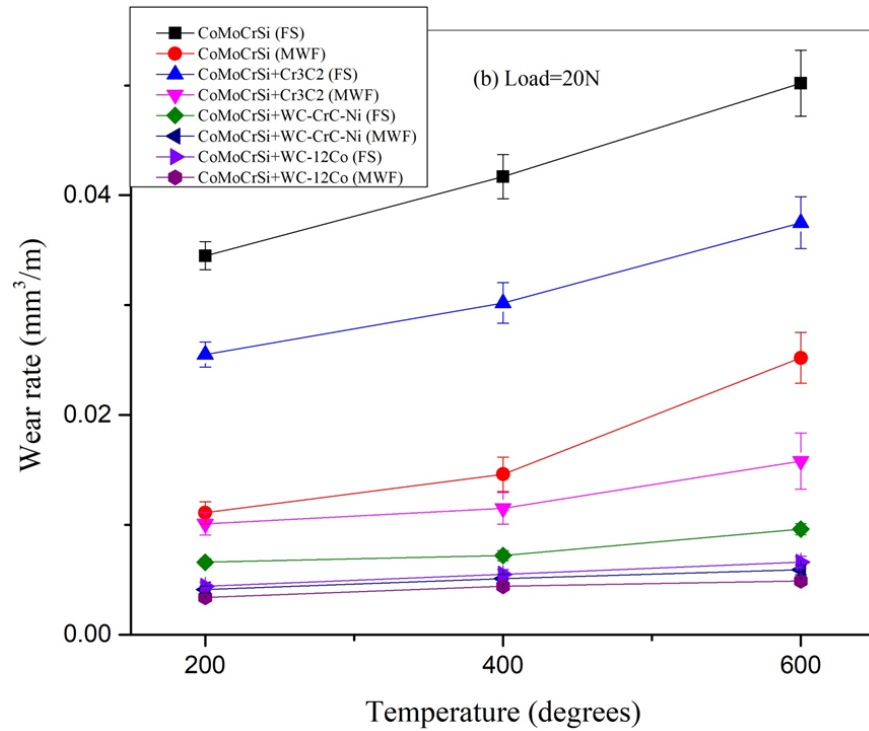
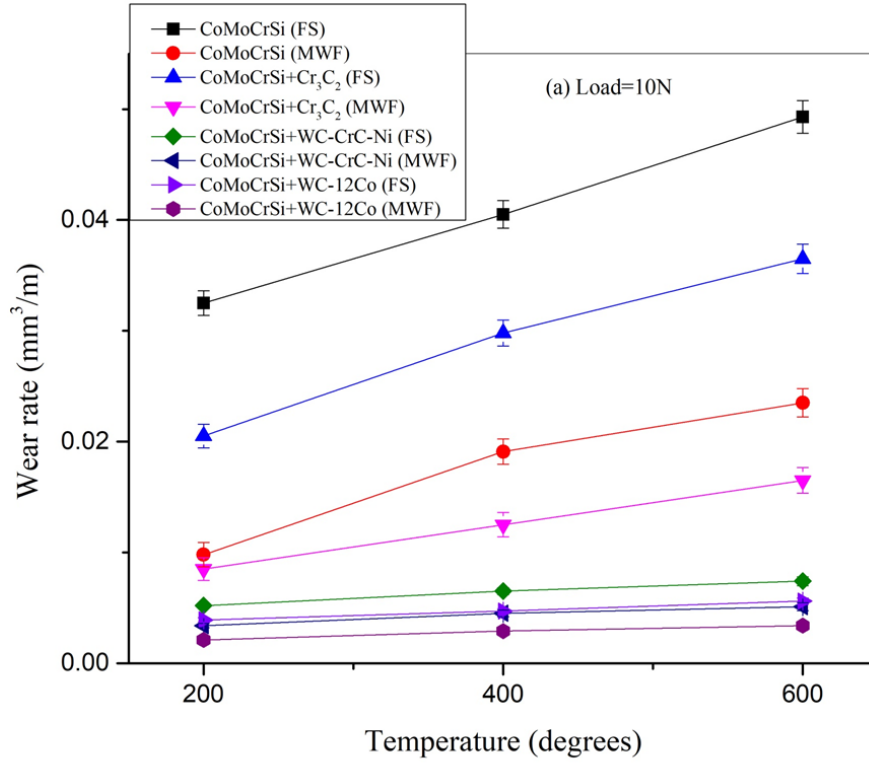


Figure 5.60 Wear rate plots of flame sprayed and microwave fused of four different coatings with respect to temperature (a) 10 N, (b) 20 N

5.11. WEAR STUDIES ON SUBSTRATE

5.11.1. Volume loss and Wear rate Substrate

The loss of volume and wear rate of the substrate is shown in Figure 5.61 and Figure 5.62. The volume loss and wear rate increase with an increase in the test temperature and applied load. It is observed that the substrate volume loss and wear rate is higher than all four coatings. High volume loss and wear rate of the substrate is observed at 600°C under 20 N as seen in Figure 5.61 and Figure 5.62. Generally, the bulk hardness of titanium is less with the increase in temperature leads to excessive loss of material. At elevated temperatures, the oxide film is formed on the substrate it lacks combat sliding action which leads to the splitting of the oxide film (delamination). This results in the increase in volume loss and wear rate with increment in test temperatures. The computed wear rate coefficient k of the substrate is $9 \times 10^{-6} \text{ mm}^3/\text{N}\cdot\text{m}$.

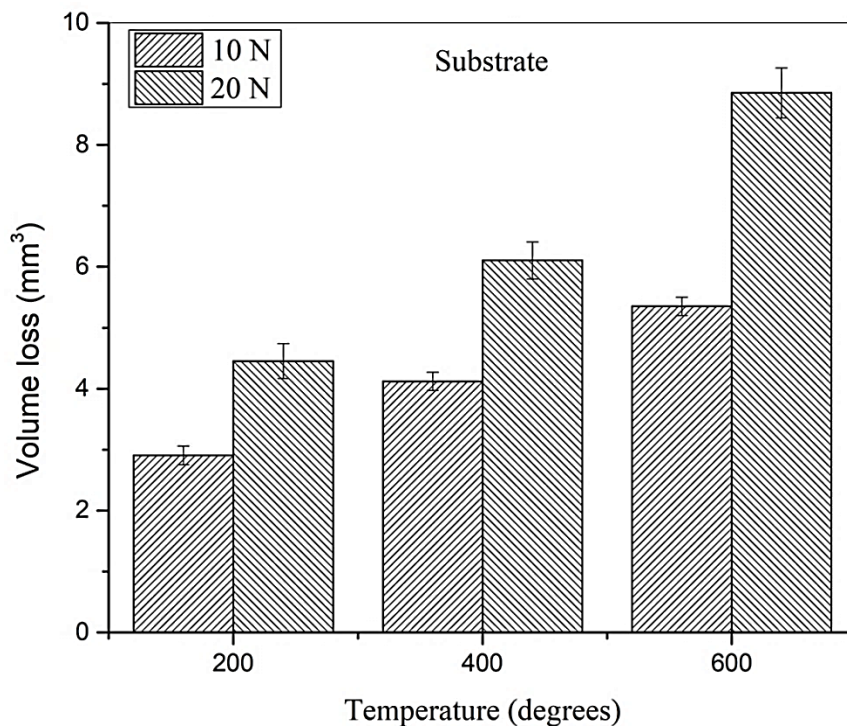


Figure 5.61 Wear volume loss of substrate with respect to temperature (a) 10 N, (b) 20 N

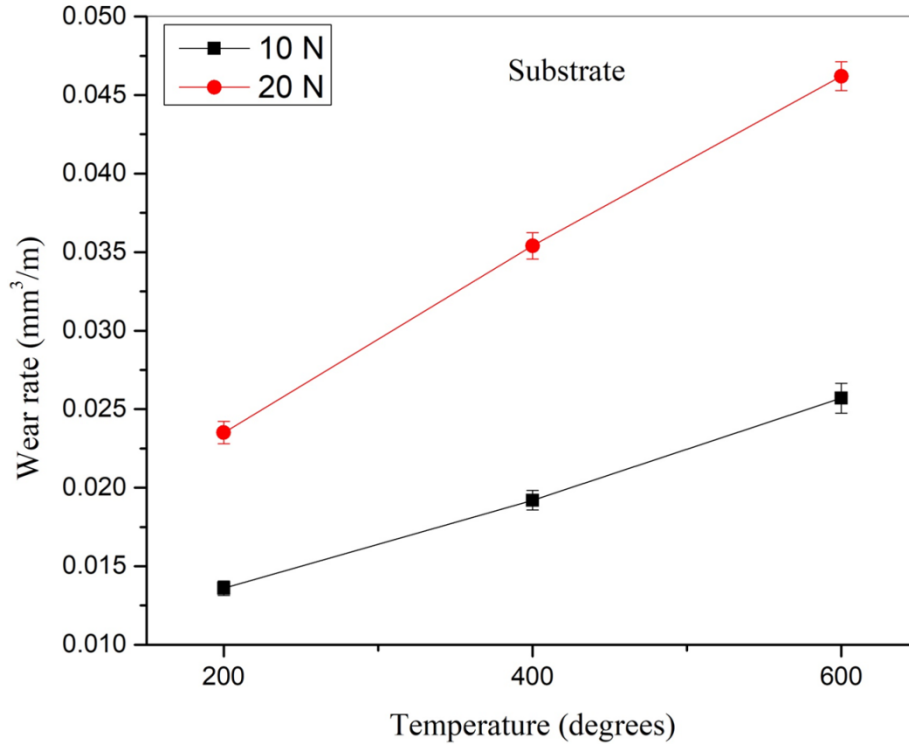


Figure 5.62 Wear rate plots of substrate with respect to temperature (a) 10 N, (b) 20 N

5.11.2. Coefficient of Friction

The COF profiles of the substrate under 10 N and 20 N is shown in Figure 5.63 (a and b). The COF of the substrate shows an increasing trend as an increase in test temperatures. As observed in Figure 5.63 (a), the COF of the substrate at 200°C is initiated at 0.55 and risen to 0.76 later it remains constant at particular COF value, also significant variations in COF is noticed by curves. At 400°C and 600°C temperatures, the COF is increased drastically to 0.85-0.90 range; this is caused due to lower microhardness of the substrate at a higher temperature.

The average COF value of substrate under 10 N is 0.76. Similarly, the substrate under 20 N experienced a higher COF value, as observed in Figure 5.63 (b). The substrate experienced rough and deep scars leads to adhesive wear, it results in a higher COF of 0.88 to 0.96 at 400°C and 600°C temperatures. The average COF value of substrate under 20 N is 0.85.

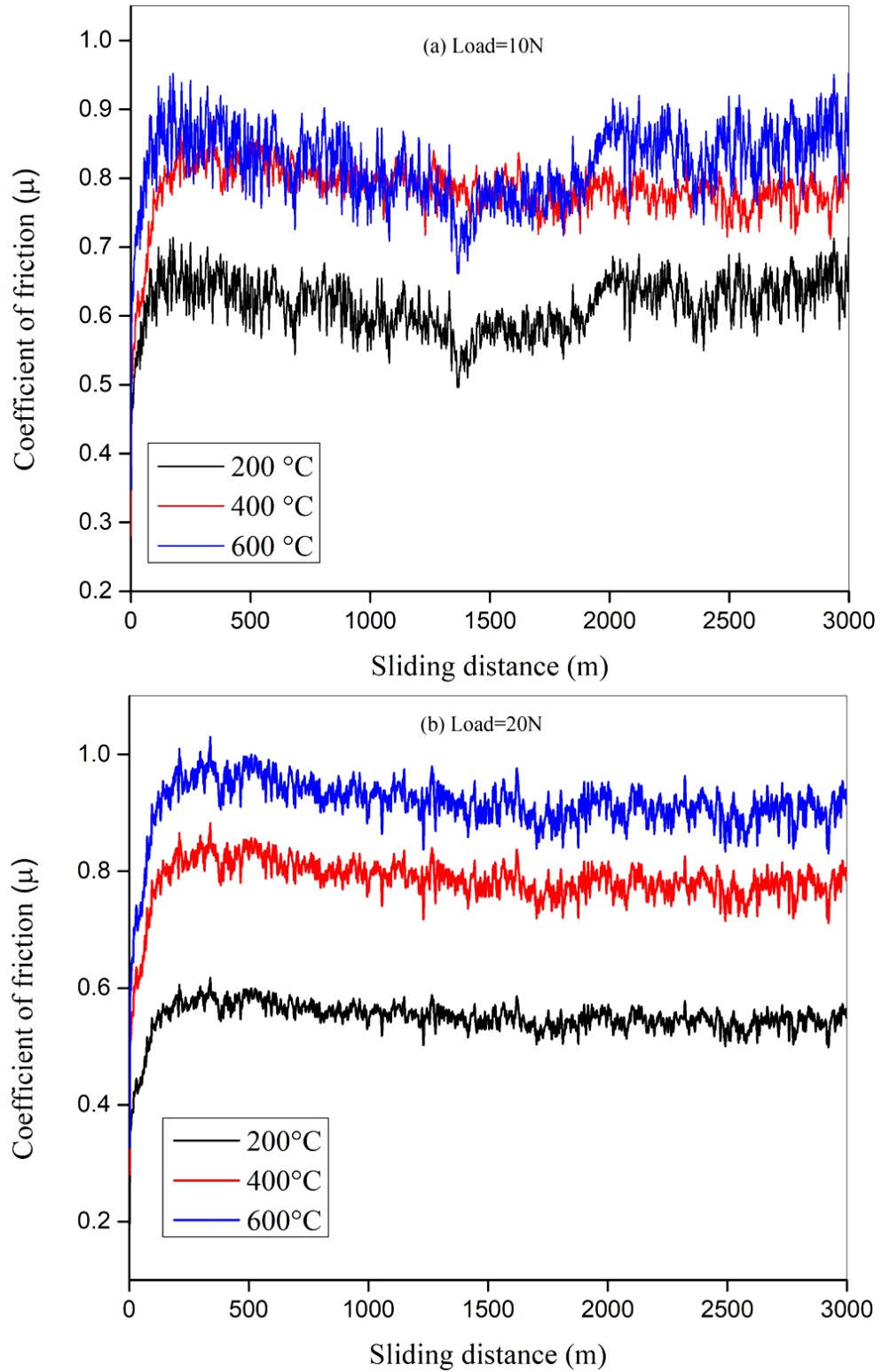


Figure 5.63 Friction coefficient of substrate with respect to sliding distance

(a) 10 N, (b) 20 N

5.11.3. Worn Surface SEM Micrographs

The worn surface morphologies of the substrate corresponding to all test temperatures and the load are depicted in Figure 5.64 (a-f). The worn surface of the substrate has ploughing features such as rough and breaking oxide layer leads to local plastic deformation is observed in Figure 5.64 (a-b) and (d-e). However, the substrate exhibits severe deformation with large pits and deep grooves at 600 °C under both test loads. This is mainly due to the low hardness and strength of titanium results in severe adhesive wear and also a large amount of material removal at 600 °C is observed in Figure 5.64 (c and f).

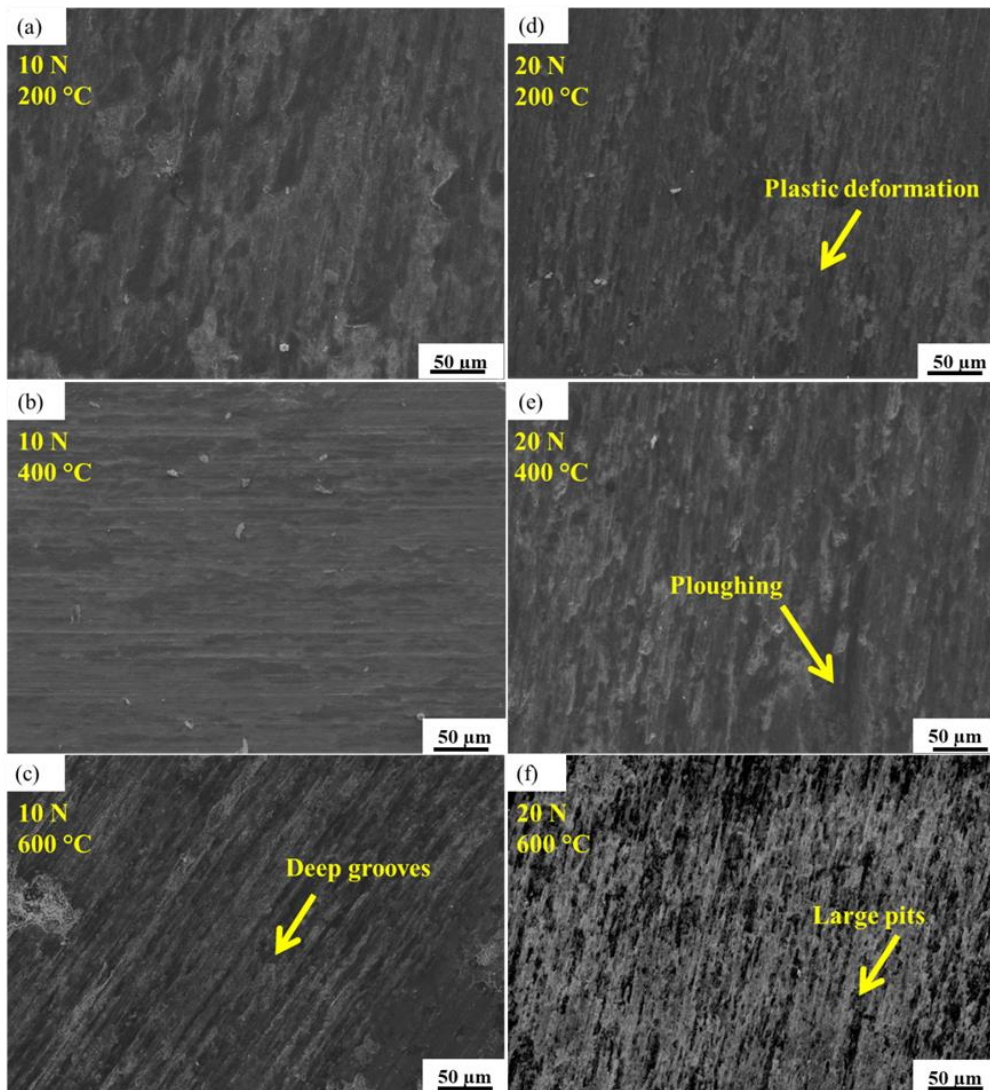


Figure 5.64 Morphology of substrate worn surfaces (a-c) under 10 N and (d-f) under 20 N at temperatures of 200°C, 400°C, 600°C

5.12. SUMMARY

The HVOF and flame sprayed CoMoCrSi coatings exhibited higher volume loss and wear rate compared to other three CoMoCrSi+WC-12Co, CoMoCrSi+WC-CrC-Ni, and CoMoCrSi+Cr₃C₂ as-sprayed composite coatings. Since the CoMoCrSi as-sprayed coatings registered lower microhardness due to the absence of carbides results in lower wear resistance.

The hard phase reinforced CoMoCrSi+WC-12Co, CoMoCrSi+WC-CrC-Ni and CoMoCrSi+Cr₃C₂ composite coatings shown excellent wear resistance because of the presence of intermetallic laves phases and carbides which imparts high strength to the underlying surface during sliding action. In the present investigation of sliding wear, all four coatings deposited by HVOF process exhibited lower loss of volume, wear rate compared with substrate and flame sprayed coatings is shown in Figure 5.29 and Figure 5.30. The coatings deposited by flame spray process reveal lower density, leads to lower cohesive strength in between splats and also the presence of porosity in coatings is almost 10 times higher than all HVOF sprayed coatings, these results in a decrease in microhardness of flame sprayed coatings. The worn morphologies of flame sprayed coatings clearly shown that the material loss occurred due to brittle fracture and splats detachment. Its EDS results confirm the presence of alumina and oxides is more at higher temperatures under 20 N normal load.

The higher density of coatings deposited by HVOF process exhibited higher microhardness results in higher wear resistance. The worn morphologies of all HVOF sprayed coatings confirm the material removed by nucleation of crack, propagation in the surface, and splats detachment. Both HVOF and flame sprayed coatings reveal that, the surface damage caused by adhesive wear phenomenon.

The post-treated coatings by microwave hybrid heating technique exhibited lower volume loss, wear rate and COF compared to the substrate, HVOF sprayed and flame sprayed coatings is shown in Figure 5.29, Figure 5.30, Figure 5.59 and Figure 5.60. This lower wear rate and COF is mainly influenced by higher microhardness of all fused coatings. The worn morphologies of all the fused coatings presented smooth wear scars and a tribo-oxide layer is

formed which protects the underlying surface from the counter disc at high temperature and high speed. Also at higher temperatures, fused coatings exhibited some stable oxides like CoO, Co₃O₄, MoO₂, MoO₃, and Cr₂O₃. These oxide phases act as lubricants at higher temperature conditions by protecting the underlying surface.

All the as-sprayed and fused coatings showed lower volume loss, wear rate and COF, compared with pure titanium grade-2 substrate. The lower microhardness of substrate is the main reason for the significant loss of volume and wear rate at all test temperatures and normal loads are shown in Figure 5.61 and Figure 5.62. Its SEM micrographs confirm the material loss caused by plastic deformation is presented in Figure 5.63.

Based on the wear rate data, the relative wear resistance of the pure titanium grade-2 substrate and coatings under dry sliding conditions are arranged in the following sequence:
(CoMoCrSi+WC-12Co) > (CoMoCrSi+WC-CrC-Ni) > (CoMoCrSi+Cr₃C₂) > (CoMoCrSi) > (Pure titanium grade-2 substrate).

Higher wear resistance of CoMoCrSi+WC-12Co coatings is attributed to the higher hardness of CoMoCrSi obtained by intermetallic laves phases.

CHAPTER 6

CONCLUSIONS

The salient conclusions from the experimental results are summarized as follows:

1. CoMoCrSi feedstock has been successfully processed using HEBM method. $\text{Co}_3\text{Mo}_2\text{Si}$, Co_7Mo_6 , Mo_3Si , Co_3Mo , Co_2Mo_3 , are the intermetallic laves phases generated in feedstock with an average particle size of $60.12\ \mu\text{m}$. The XRD pattern of CoMoCrSi milled powder at 5 hr confirms the formation of the amorphous structure by showing a broadening of peaks.
2. The hard phase carbides such as Cr_3C_2 , WC-CrC-Ni, and WC-12Co are successfully reinforced into milled CoMoCrSi feedstock with a mass fraction of 70%:30% using HEBM process. The composite feedstock reveals the retaining of its original phases after blending.
3. All the HVOF sprayed coatings exhibited flat lamellar structure with a uniform thickness in the range of $150\text{-}250\ \mu\text{m}$ having lesser than 2% porosity and flame sprayed coatings exhibited elongated splats with a uniform thickness in the range of $170\text{-}270\ \mu\text{m}$ having more than 10% porosity.
4. Microwave fused HVOF coatings exhibited less than 1% porosity and microwave fused flame sprayed coatings having less than 5% porosity. The 50% reduction in porosity is observed in fused coatings.
5. The HVOF and Flame sprayed coatings exhibits heterogeneous structure with higher surface roughness and microwave fused coatings exhibits homogeneous structure with lower surface roughness.
6. All the HVOF sprayed and flame sprayed coatings have almost retained their phases as observed in powders with minor oxidation of Co and decarburization of WC and

Cr₃C₂ carbides at high processing temperature. The oxidized and carburized phase have been observed and indexed to minor peaks. Fused coatings retain the similar phases as obtained by as-sprayed coatings and also few oxide phases have formed.

7. All the coatings exhibited higher hardness as compared to pure titanium grade-2 substrate due to the intermetallic laves phases. CoMoCrSi+WC-12Co coatings deposited by HVOF and Flame spray displayed higher hardness of 1290 ± 35 and 1050 ± 10 respectively.
8. All the HVOF sprayed coatings exhibited the higher adhesion strength in the range of 55 to 75 MPa, and the coatings deposited by flame spray shows the adhesion strength range of 25 to 35 Mpa. CoMoCrSi+WC-12Co coating deposited by HVOF and Flame spray displayed higher adhesion strength of 64.22 MPa and 35.49 MPa respectively.
9. Fractured surface of HVOF sprayed coatings reveals the adhesive failure of the coatings, whereas flame sprayed coatings reveals the cohesive failure of coatings which is due to lower impact force of low-density coatings formed during deposition of particles.
10. All the fused coatings reveal the formation of metallurgical bonding due to inter-diffusion of substrate elements towards the coating which is confirmed by elemental X-ray mapping results.
11. Microwave fused coatings represent less volume loss, wear rate and COF compare to the substrate and as-sprayed coatings for all test temperatures and normal loads. This is due to higher microhardness and higher cohesive strength between splats of the coatings.
12. At all test temperatures, the HVOF sprayed coatings exhibited nucleation of crack, propagation into surface and breaking of splats have observed, whereas all the flame

sprayed coatings exhibited plastic deformation and brittle fracture of splats is observed under 20 N normal load.

13. All the HVOF sprayed coatings registered lower volume loss, wear rate and COF as compared to all the flame sprayed coatings. This is due to lower porosity, higher microhardness, and density of coatings.
14. At higher temperatures, fused coating produces some stable oxides like CoO, Co₃O₄, MoO₂, MoO₃, and Cr₂O₃. These oxide phases act as lubricants at higher temperature conditions by protecting the underlying surface. Fused coating exhibits increased width and smooth wear scars due to fatigue spalling mechanism.
15. The relative wear resistances of the coatings under dry sliding conditions are arranged from minimum to maximum value in the following sequence: (CoMoCrSi+WC-12Co) > (CoMoCrSi+WC-CrC-Ni) > (CoMoCrSi+Cr₃C₂) > (CoMoCrSi).
16. Higher wear resistance of CoMoCrSi+WC-12Co coatings is attributed to the presence of intermetallic laves phases and carbides, which imparts high strength to underlying surface during sliding action.

SCOPE OF FUTURE WORK

In the current studies, intermetallic laves phases and microwave hybrid heating have influenced significantly on coatings for improving sliding wear resistance. Some of the recommendations for future work are as follows:

1. Coatings with hard phase carbides exhibited higher microhardness, adhesion strength and wear resistance, this can be further improved by developing coatings with a combination of hard phase carbides and solid lubricants in different tribological environments like erosion and abrasion.
2. These coatings having chromium content should be explored in tribo-corrosion conditions where components are operating in a combination of wear and corrosive environments.
3. The different hard phase carbides with varying its percentage for sliding wear resistance may also be studied.
4. High-temperature oxidation and hot corrosion behavior of these coatings may also be studied.
5. Attempts can be made to predict the useful life of these coated materials by extrapolation of the laboratory data by mathematical modeling.
6. The cladding can be developed for these powder combinations using microwave cladding in order to understand the wear behavior compare to coatings.

REFERENCES

- Bahbou M F, Nylen P and Wigren J (2004). "Effect of grit blasting and spraying angle on the adhesion strength of a plasma-sprayed coating." *Journal of Thermal Spray Technology*. 13, 508–14.
- Bakhsheshi, E. Hamzah, A.F. Ismail, M. Daroonparvar, M.A.M. Yajid, M. Medraj. (2016). "Preparation and characterization of NiCrAlY/nano-YSZ/PCL composite coatings obtained by a combination of atmospheric plasma spraying and dip coating on Mg-Ca alloy." *Journal of Alloys and Compounds*, 658, 440-452.
- Bemporad, M. Sebastiani, F. Casadei, F. Carassiti. (2007). "Modelling, production, and characterization of duplex coatings (HVOF and PVD) on Ti–6Al–4V substrate for specific mechanical applications." *Surface & Coatings Technology*, 201, 7652–7662.
- Bemporad, M. Sebastiani, M.H. Staia, E. Puchi Cabrera. (2008). "Tribological studies on PVD/HVOF duplex coatings on Ti6Al4V substrate." *Surface & Coatings Technology*, 203 566-571.
- Betteridge (1982), "Cobalt and Its Alloys", *Halsted Press*, Chichester. John Wiley & Sons, 159 pages.
- Bolelli and Lusvarghi. (2006). "Heat Treatment Effects on the Tribological Performance of HVOF Sprayed Co-Mo-Cr-Si Coating." *Journal of Thermal Spray Technology*, 802, 15 (4).
- Bolelli G and Lusvarghi L. (2007). "Tribological properties of HVOF as-sprayed and heat treated Co–Mo–Cr–Si coatings." *Tribol. Lett.* 25, 43–54.
- Bolelli G, Cannillo V, Lusvarghi L and Ricco S. (2006). "Mechanical and tribological properties of electrolytic hard chrome and HVOF sprayed coatings." *Surface & Coatings Technology* 200, 2995–3009.
- C Durga Prasad, Sharnappa Joladarashi, M R Ramesh, M S Srinath and B H Channabasappa. (2018). "Influence of microwave hybrid heating on the sliding wear behaviour of HVOF sprayed CoMoCrSi coating." *Materials Research Express* 5, 086519.

Cameron, R. A. Hoffman, and R.W. Poskitt. (1975). "Tribaloy Intermetallic Alloy Compositions-New Materials or Additives for Wear Resistant Applications." *Progress in Powder Metallurgy*, 31, 41-51.

Cho J Y, Zhang S H, Cho T Y, Yoon J H, Joo Y K and Hur S K. (2009). "The processing optimization and property evaluations of HVOF Co base alloy T800 coating." *J. Mater. Sci.* 44, 6348–55.

Cinca N, Roberto C, Lima C and Guilemany J M. (2013). "An overview of intermetallics research and application: status of thermal spray coatings." *J. Mater. Res. Technol.* 2, 75–86.

Davis. (2000). "Nickel, Cobalt, and their Alloys." ASM International, Materials Park, OH. Pages 442, ISBN: 978-0-87170-685-0.

Dejun K and Tianyuan S. (2017). "Wear behaviors of HVOF sprayed WC-12Co coatings by laser remelting under lubricated condition." *Optics & Laser Technology* 89 86–91.

Fauchais P. (2015). "2 - Current status and future directions of thermal spray coatings and techniques."

Fernandez E, Cadenas M, Gonzalez R, Navas C, Fernandez R and de Damborenea J. (2005). "Wear behavior of laser clad NiCrBSi coating." *Wear* 259, 870–5.

Franklin S E and Dijkman J.A. (1995). *Wear*, 181-183, 1-10.

Gao F, Liua R and WuXJ. (2010). "Tribological behavior of T-401/tin-bronze composite coating deposited by HVOF on the bushing of planet journals." *Wear*, 269, 724–32.

Gao, R. Liu, X.J. Wu. (2011). "Tribaloy alloy reinforced tin-bronze composite coating for journal bearing applications." *Thin Solid Films*, 519 4809–4817.

García, M.Cadenas, M.R.Fernández, A.Noriega. (2013). "Tribological effects of the geometrical properties of plasma spray coatings partially melted by a laser." *Wear*, 305, 1–7.

Giovanni Bolelli, Lutz-Michael Berger, Matteo Bonetti, and Luca Lusvarghi. (2014). "Comparative study of the dry sliding wear behavior of HVOF-sprayed WC-(W, Cr) 2C-Ni and WC-CoCr hard metal coatings." *Wear* 309, 96–111.

Gupta and Sharma. (2011). "Development and microstructural characterization of microwave cladding on austenitic steel." *Surface and Coatings Technology*, 205, 5147–5155.

Gupta and Sharma. (2011). "Investigation on sliding wear performance of WC10Co2Ni cladding developed through microwave irradiation." *Wear*, 271, 1642–1650.

Gupta, Prabhakar M. Bhovi, Apurbba Kumar Sharma, and Sushanta Dutta. (2012). "Development and characterization of microwave composite cladding." *Journal of Manufacturing Processes*, 14, 243–249.

H. Kim, S. Hwang, C. Lee, and P. Juvanon. (2003). "Assesment of wear performance of flame sprayed and fused Ni-based coatings, *Surface & Coatings Technology*, 172, 262–269.

Halstead and Rawlings. (1984). "Structure and hardness of Co-Mo-Cr-Si wear resistant alloys (Triballoys)." *Metal Science*, 18 (10), 491-500.

Halstead and Rawlings. (1985). "Effect of iron additions on the microstructure and properties of the Tribaloy Co-Mo-Cr-Si wear resistant alloys." *Journal of Materials Science*. 20 (5), 1693-1704.

Halstead and Rawlings. (1985). "Fracture behavior of two Co-Mo-Cr-Si wear resistant alloys (Triballoys)." *Journal of Materials Science*, 20 (4). 1248-1256.

Hebbale and Srinath. (2016). "Microstructural investigation of Ni-based cladding developed on austenitic SS-304 through microwave irradiation." *Journal of material research and Technology*, 5 (4), 293–301.

Hebbale and Srinath. (2017) "Taguchi analysis on erosive wear behavior of cobalt based microwave cladding on stainless steel AISI-420." *Measurement*, 99, 98–107.

Holmberg K, A. Matthews, and H. Ronkainen. (1993). "Wear mechanisms of coated sliding surfaces." *Thin Films in Tribology*. D. Dowson et al., Eds. In: Proceedings of the 19th Leeds-Lyon Symp. on Tribology, Elsevier Tribology Series, 25, 399-407.

Holmberg K, H. Ronkainen, and A. Matthews. (2000). "Tribology of thin coatings." *Ceramics International* 26, 787-795.

- Holmberg K. (1992). *Surface and Coatings Technology*, 56 10.
- Hong S, WuY, Wang B, Zhang J, Zheng Y and Qiao L. (2017). “The effect of temperature on the dry sliding wear behavior of HVOF sprayed nanostructured WC-CoCr coatings.” *Ceramics. International*. 43, 458–62.
- Hong, Yuping Wu, Bo Wang, Yugui Zheng, Wenwen Gao, and Gaiye Li. (2014). “High-velocity oxygen-fuel spray parameter optimization of nanostructured WC–10Co–4Cr coatings and sliding wear behavior of the optimized coating.” *Materials and Design*, 55, 286–291.
- Huang, M. Samandi, and M. Brandt. (2004). “Abrasive wear performance and microstructure of laser clad WC/Ni layers.” *Wear*, 256, 1095–1105.
- I D Utua, and G. Marginean. (2017), “Effect of electron beam remelting on the characteristics of HVOFsprayed Al₂O₃-TiO₂coatings deposited on titanium substrate.” *Colloids and Surfaces A: Physicochem. Eng. Aspects* 526, 70–75.
- Jianfeng Li, Hanlin Liao, and Christian Coddet. (2002). “Friction and wear behavior of flame-sprayed PEEK coatings.” *Wear* 252, 824–831.
- Kaiming W, Yulong L, Hanguang F, Yongping L, Zhenqing S and Pengfei M. (2018). “A study of laser cladding NiCrBSi/Mocomposite coatings.” *Surface Engineering*. 34, 267–75.
- Kandeva M, Grozdanova T, Karastoyanov D and Assenova E. (2017). “Wear resistance of WC/Co HVOF-coatings and galvanic Cr coatings modified by diamond nanoparticles.” *Mater. Sci. Eng.* 174 012060.
- Kandeva M, Ivanova B, Karastoyanov D, Grozdanova T and Assenova E. (2017). “Abrasive wear of high velocity oxygen fuel (HVOF) superalloy coatings under vibration load.” *Material Science Engineering*. 174 012010.
- Khor, H. Li, and P. Cheang. (2004). “Significance of melt-fraction in HVOF sprayed hydroxyapatite particles, splats, and coatings.” *Biomaterials*, 25, 1177–1186.

Khun, A.W.Y. Tan, K.J.W. Bi, and E. Liu. (2016). “Effects of working gas on wear and corrosion resistance of cold sprayed Ti-6Al-4V coatings.” *Surface & Coatings Technology* 302, 1-12.

Kong Dejuna, and Sheng Tianyuan. (2017). “Wear behaviors of HVOF sprayed WC-12Co coatings by laser remelting under the lubricated condition.” *Optics & Laser Technology* 89, 86–91.

Kumar S, Selvarajan V, Padmanabhan PVA and Sreekumar K P. (2006). “Characterization and comparison between ball milled and plasma processed iron-aluminium thermal spray coatings” *Surface & Coatings Technology* 201 1267–75.

Kumara and Sharma, S.K. Goel. (2016). “Erosion behavior of WC–10Co–4Cr coating on 23-8-N nitronic steel HVOF thermal spraying.” *Applied Surface Science*, 370 418–426.

Kumari, K. Anand, Michelangelo Bellacci, and Massimo Giannozzi. (2010). “Effect of microstructure on abrasive wear behavior of thermally sprayed WC–10Co–4Cr coatings.” *Wear* 268, 1309–1319.

Kuroda S, Kawakita J, Watanabe M and Katanoda H. (2008). “Warm spraying a novel coating process based on the high-velocity impact of solid particles.” *Sci. Technol. Adv. Mater.* 9 03300.

Li, Xiufang Cui, Guo Jin, Zhaobing Cai, Na Tana, Bingwen Lu, and Zonghong Gao. (2017). “Interfacial bonding properties between cobalt-based plasma cladding layer and substrate under tensile conditions.” *Materials and Design*, 123, 54–63.

Lin W C and Chen C. (2006). “Characteristics of thin surface layers of cobalt-based alloys deposited by laser cladding.” *Surface & Coatings Technology* 200 4557–63

Lin, Shih-Hung Yen, and Cherng-Yuh Su. (2016). “Measurement and optimization of atmospheric plasma sprayed CoMoCrSi coatings parameters on Ti-6Al-4V substrates affecting microstructural and properties using hybrid abductor induction mechanism.” *Measurement*, 94, 157-167.

Liu Y, Chen H, Gou G and Tu M. (2010). “Research on dynamic wear behavior at an elevated temperature of HVOF sprayed nanostructured WC-17Co coating.” *J. Phys.: Conf. Ser.* 240 012165.

Maestracci, A. Sova, M. Jeandin, J.M. Malhaire, I. Movchan, Ph. Bertrand, and I. Smurov. (2016). “Deposition of composite coatings by cold spray using stainless steel 316L, copper, and Tribaloy T-700 powder mixtures.” *Surface & Coatings Technology*, 287, 1–8.

Manne B, Bontha S, Ramesh M R, Krishna M and Balla V K. (2017). “Solid state amorphization of Mg-Zn-Ca system via mechanical alloying and characterization.” *Advanced Powder Technology* 28 223–9.

Manojkumar P A, Gandhi A S, Kamaraj M and Tyagi A K. (2014). “Sliding wear behavior of alumina coatings prepared from mechanically milled powders.” *Wear* 313 11–8.

Mathapati M, Ramesh M R and Doddamani M. (2017). “High temperature erosion behavior of plasma sprayed NiCrAlY/WC-Co/ cenosphere coating.” *Surface & Coatings Technology* 325, 98–106.

Matikainen V, Bolelli G, Koivuluoto H, Sassatelli P, Lusvarghi L and Vuoristo P. (2017). Sliding wear behaviour of HVOF and HVAF sprayed Cr₃C₂-based coatings.” *Wear* 388–389 57–71.

Matthews S, James B and Hyland M. (2009), “High temperature erosion of Cr₃C₂-NiCr thermal spray coatings the role of phase microstructure.” *Surface & Coatings Technology*, 203, 1144-1153. 92.

Matthews S, James B and Hyland M. (2010). “The Effect of Heat Treatment on the Oxidation Mechanism of Blended Powder Cr₃C₂-NiCr Coatings.” *Journal of Thermal Spray Technology*, 19, 119-127.

Mishra R R and Sharma A K. (2016). “Microwave–material interaction phenomena: heating mechanisms, challenges, and opportunities in material processing.” *Composites A* 81 78–97.

Mitra Akhtari Zavareh, Ahmed Aly Dia Mohammed Sarhan, Parisa Akhtari Zavareh, Wan Jeffrey Basirun. (2016). “Electrochemical corrosion behavior of carbon steel pipes coated

with a protective ceramic layer using plasma and HVOF thermal spray techniques for oil and gas”. *Ceramics International*, 42 3397–3406.

Movahedi. (2013). “Fracture toughness and wear behavior of NiAl-based nano composite HVOF coatings.” *Surface and Coatings Technology* 235, (25), 212–219.

Murugan K, Ragupathy A, Balasubramanian V and Sridhar K. (2014). “Optimizing HVOF spray process parameters to attain minimum porosity and maximum hardness in WC–10Co–4Cr coatings.” *Surface & Coatings Technology* 247 90–102.

Ortiz, A. García, M. Cadenas, M. R. Fernández, and J. M. Cueto. (2017). “WC particles distribution model in the cross-section of laser cladding NiCrBSi + WC coatings for different wt% WC.” *Surface & Coatings Technology*, 324, 298–306.

Ozdemir I, Ogawa K and Sato K. (2014). “Iron boron based powders sprayed by high velocity spray processes.” *Surface & Coatings Technology* 240 373–9.

P.D. Wood, H.E. Evans, and C.B. Ponton. (2010). “Investigation into the wear behavior of Tribaloy 400C during rotation as an unlubricated bearing at 600 °C.” *Wear* 269, 763–769.

Peat, Alexander M. Galloway, Athanasios I. Toumpis, David Harvey. (2016). “Evaluation of the synergistic erosion-corrosion behavior of HVOF thermal spray coatings.” *Surface & Coatings Technology*, 299 37–48.

Pukasiewicz AGM, de Boer H E, Sucharski G B, Vaz R F and Procopiak LA J. (2017). “The influence of HVOF spraying parameters on the microstructure, residual stress and cavitation resistance of FeMnCrSi coatings.” *Surface & Coatings Technology* 327, 158–66.

Qun Wang A, Chen Z, Li L and Yang G. (2012). “The parameters optimization and abrasion wear mechanism of liquid fuel HVOF sprayed bimodal WC–12Co coating.” *Surface & Coatings Technology* 206 2233–41.

R. Gonzalez, M. Cadenas, R. Fernandez, J.L. Cortizo, and E. Rodriguez. (2007). “Wear behaviour of flame sprayed NiCrBSi coating remelted by flame or by laser.” *Wear* 262, 301–307.

- Ramesh M R, Prakash S, Nath S K, Sapra P K and Venkataraman B. (2010). "Solid particle erosion of HVOF sprayed WC-Co/NiCrFeSiB coatings." *Wear* 269, 197–205.
- Ramesh M R, S. Prakash, S.K. Nath, Pawan Kumar Sapra, and N. Krishnamurthy. (2011). "Evaluation of thermocyclic oxidation behavior of HVOF-sprayed NiCrFeSiB coatings on boiler tube steels." *Journal of Thermal Spray Technology*, 992, 20 (5).
- S. Harsha, D.K. Dwivedi, and A. Agrawal. (2007). "Influence of WC addition in Co–Cr–W–Ni–C flame sprayed coatings on microstructure, microhardness and wear behavior." *Surface & Coatings Technology* 201, 5766–5775.
- Sadri and Ashrafizade. (2013). "Structural characterization and mechanical properties of plasma sprayed nanostructured Cr₂O₃-Ag composite coatings." *Surface & Coatings Technology*, 236 91–101.
- Sahariah B J, Vashishtha N and Sapate S G. (2018). "Effect of abrasive particle size on friction and wear behaviour of HVOF sprayed WC-10Co-4Cr coating." *Mater. Res. Express* 5 066424.
- Sahraoui T, FeraounHI, Fenineche N, Montavon G, Aourag H and Coddet C (2004). "HVOF-sprayed Tribaloy-400: microstructure and first principle calculations." *Mater. Lett.* 58, 2433–6
- Sarka Houdkov, Eva Smazalov, Marek Vostrak, and Jan Schubert. (2014). "Properties of NiCrBSi coating, as sprayed and remelted by different technologies." *Surface & Coatings Technology* 253, 14–26.
- Sathiyamoorthy, K. Shanmugam, and V. Balasubramanian. (2014). "Dry sliding wear behavior of SiC reinforced Titania coating deposited by HVOF", *Procedia Materials Science* 5 648-655.
- Sh. Khameneh Asl, M. Heydarzadeh Sohi, K. Hokamoto, and M. Uemura. (2006). "Effect of heat treatment on wear behavior of HVOF thermally sprayed WC-Co coatings." *Wear* 260, 1203–1208.

Sharma and Gupta. (2010). "Method of cladding/coating of metallic and non-metallic powders on metallic substrates by microwave Irradiation." Indian Patent 2010, Application No. 527.

Sharma and Gupta. (2012). "On microstructure and flexural strength of metal–ceramic composite cladding developed through microwave heating." *Applied Surface Science*, 258, 5583– 5592.

Shashank M Lingappa, M S Srinath, and H J Amarendra. (2017). "An experimental investigation to find the critical (coupling) temperature in microwave hybrid heating of bulk metallic materials." *Materials Research Express* 4, 106521.

Sidhu B.S. and Prakash, S. (2006). "Studies on the behavior of stellite-6 as plasma sprayed and laser remelted coatings in the molten salt environment at 900 °C under cyclic conditions." *Journal of Material Process Technology*, 172, 52-63.

Srinath, Apurbba Kumar Sharma, Pradeep Kumar. (2011). "A new approach to joining of bulk copper using microwave energy." *Materials and design*, 2685–2694.

Susila, Praveen, J. Sarangan, S. Suresh, and B.H. Channabasappa. (2016). "Optimization and erosion wear response of NiCrSiB/WC–Co HVOF coating using Taguchi method." *Ceramics International*, 1094–1104.

Tahari M, Shamanian M and Salehi M. (2015). "The effect of heat treatment and thermal spray processes on the grain growth of nanostructured composite CoNiCrAlY/YSZ powders." *Journal of Alloys and Compounds*. 646, 372–9.

Torres B, M. Campo, M. Lieblich, and J. Rams. (2013). "Oxy-acetylene flame thermal sprayed coatings of aluminium matrix composites reinforced with MoSi₂ intermetallic particles." *Surface & Coatings Technology* 236, 274–283.

Utu, G. Marginean, I. Hulka, V.A. Serban, and D. Cristea. (2015). "Properties of the thermally sprayed Al₂O₃-TiO₂ coatings deposited on a titanium substrate." *Int. Journal of Refractory Metals and Hard Materials*, 51, 118-123.

- V. Matikainen, G. Bolelli, H. Koivuluoto, P. Sassatelli, L. Lusvarghi, and P. Vuoristo. (2017). "Sliding wear behaviour of HVOF and HVAF sprayed Cr_3C_2 -based coatings." *Wear*, 388–389, 57–71.
- Verdon C, Karimi A and Martin J. (1998). "A study of high velocity oxy-fuel thermally sprayed tungsten carbide-based coatings." *Part I: microstructures Mater. Sci. Eng. A* 246, 11–24.
- Wang Y, Liu JW, Kang N, Darut G, Poirier T, Stella J, Liao H and Planche M P (2016) "Cavitation erosion of plasma-sprayed CoMoCrSi coatings." *Tribology International* 102, 429–35.
- Weng, Huijun Yu, Chuanzhong Chen, Jianli Liu, Longjie Zhao, Jingjie Dai, and Zhihuan Zhao. (2017). "Effect of process parameters on the microstructure evolution and wear property of the laser cladding coatings on Ti-6Al-4V alloy." *Journal of Alloys and Compounds*, 692, 989–996.
- Zafar and Sharma. (2014). "Development and characterizations of WC–12Co microwave clad." *Materials. Characterisation*, 96, 241–248.
- Zhang H, Hu Y, Hou G, An Y and Liu G. (2014). "The effect of high-velocity oxy-fuel spraying parameters on microstructure, corrosion and wear resistance of Fe-based metallic glass coatings" *J. Non-Cryst. Solids* 406, 37–44.
- Zhao G, Xia L, Zhong B, Wen G, Song L and Wang X. (2014). "Effect of milling conditions on the properties of HA/Ti feedstock powders and plasma-sprayed coatings." *Surface & Coatings Technology* 251, 38–47.
- Zhou W, Zhou K, Li Y, Deng C and Zeng K. (2017). "High temperature wear performance of HVOF-sprayed Cr_3C_2 -WC-NiCoCrMo and Cr_3C_2 -NiCr hard metal coatings." *Appl. Surf. Sci.* 416, 33–44.
- Zhou, X. Zeng, Q. Hu, and Y. Huang. (2008). "Analysis of crack behavior for Ni-based WC composite coatings by laser cladding and crack-free realization." *Applied Surface Science*, 255, 1646–1653.

List of Publications based on PhD Research Work

Sl. No.	Title of the paper	Authors (in the same order as in the paper. Underline the Research Scholar's name)	Name of the Journal/ Conference, Vol., No., Pages	Month, Year of Publication	Category*
1.	Influence of Microwave Hybrid Heating on the Sliding Wear Behaviour of HVOF Sprayed CoMoCrSi Coating	<u>C Durga Prasad</u> , Sharnappa Joladarashi, M R. Ramesh, M S Srinath, B H Channabasappa	Materials Research. Express 5 (2018):086519	July 2018	1
2.	Microstructure and Tribological Behavior of Flame Sprayed and Microwave Fused CoMoCrSi/CoMoCrSi-Cr ₃ C ₂ Coatings.	<u>C Durga Prasad</u> , Sharnappa Joladarashi, M R. Ramesh, M S Srinath, B H Channabasappa	Materials Research. Express 6 (2019):026512.	November 2018	1
3.	Development and Sliding Wear Behavior of Co-Mo-Cr-Si Cladding through Microwave Heating	<u>C Durga Prasad</u> , Sharnappa Joladarashi, M R. Ramesh, M S Srinath, B H Channabasappa	Silicon, (Springer) https://doi.org/10.1007/s12633-019-0084-5 .	January 2019	1
4.	Effect of Microwave Heating on Microstructure and Elevated Temperature Adhesive Wear Behavior of HVOF Deposited CoMoCrSi-Cr ₃ C ₂ Composite Coating	<u>C Durga Prasad</u> , Sharnappa Joladarashi, M R. Ramesh, M S Srinath, B H Channabasappa	Surface and Coatings Technology	Revised Manuscript submitted	1
5.	Comparison of High Temperature Wear Behavior of Microwave Assisted HVOF Sprayed CoMoCrSi-WC-CrC-Ni/WC-12Co Composite Coatings	<u>C Durga Prasad</u> , Sharnappa Joladarashi, M R. Ramesh, M S Srinath, B H Channabasappa	Surface and Coatings Technology	Revised Manuscript submitted	1

6.	High Temperature Sliding Wear Resistance of Flame Sprayed CoMoCrSi/WC-CrC-Ni and CoMoCrSi/WC-12Co Composite Coatings Remelted by Microwave Hybrid Heating.	C Durga Prasad , Sharnappa Joladarashi, M R. Ramesh, M S Srinath, B H Channabasappa	Journal of Materials Engineering and Performance (Springer)	Under review	1
7.	Effect of Intermetallic Laves Phases on Elevated Temperature Wear Behavior of HVOF Sprayed Co-Mo-Cr-Si Coating	C D Prasad , Sharnappa Joladarashi, M R Ramesh, B H Channabasappa.	TACT2017 International Thin Films Conference, National Dong Hwa University, Hualien, Taiwan.	Oct. 15–18, 2017	3
8.	Development of Tribaloy Co-Mo-Cr-Si Cladding through Microwave Heating and its Characterization	Durga Prasad C , Sharnappa J, Ramesh M R, Srinath M S Channabasappa B H	International Conference on Advances in Materials & Processing: Challenges & Opportunities (AMPCO 2017), IIT Roorkee, India.	Nov. 29-Dec 2, 2017	3
9	High Temperature Gradient Cobalt based Clad Developed Using Microwave Hybrid Heating	C Durga Prasad , Sharnappa Joladarashi, M. R Ramesh, Anunoy Sarkar	International Conference on Design, Materials and Manufacture (Icdem 2018), NITK Surathkal, Karnataka, India.	Jan. 29-31, 2018	3

* Category: 1: Journal paper, full paper reviewed 2: Journal paper, Abstract reviews 3: Conference/Symposium paper, full paper reviewed
4: Conference/Symposium paper, abstract reviewed 5: others (including papers in Workshops, NITK Research Bulletins, Short notes etc.)

Durga Prasad C
Research Scholar
Department of Mech. Engg
NITK Surathkal

Dr Sharnappa Joladarashi
Research Guide
Department of Mech. Engg
NITK Surathkal

Dr Ramesh M R
Research Guide
Department of Mech. Engg
NITK Surathkal

BIO-DATA

Name: Durga Prasad C
Father's Name: Channabasavaiah
Date of Birth: 31-07-1991
Nationality: Indian
Marital Status: Unmarried



Address:

Permanent Address

S/o. **Channabasavaiah**
Shivakrupa,
7th Cross Vidyanagar
Tumakuru, Karnataka, India

Mobile Number: +919538005639

E-mail id: durgapras71@gmail.com

Present Address

Department of Mechanical Engineering
National Institute of Technology Karnataka
Surathkal-575025, Srinivasanagar,
Mangaluru, Karnataka, India.

Educational Qualification:

Qualification	College/school	University/Board	Year of Passing	Performance
Ph.D. Mechanical Engineering	National Institute of Technology Karnataka	NITK, Surathkal	Pursuing	8.85 (CGPA) (Coursework)
M. Tech Manufacturing Engineering	Siddaganga Institute of Technology Tumakuru	VTU, Belagavi	2015	9.27 (CGPA)
B. Tech. Mechanical Engineering	HMS Institute of Technology Tumakuru	VTU, Belagavi	2013	74.25%
DIPLOMA Mechanical Engineering	Siddaganga Polytechnic Tumakuru	BTE, Bengaluru	2010	69.65%

Publication Details

Papers Published	Under Review	Conference	Workshops/ Symposium	Awards and Recognitions
3	3	3	15	<ul style="list-style-type: none">• MHRD Scholarship for pursuing Ph.D

I declare that the above information is true and correct to best of my knowledge.

(DURGA PRASAD C)